PARAMETRIC DESIGN OF NON-CONVENTIONAL DIAGRID SYSTEMS FOR TALL BUILDINGS

PERFORMANCE OF STRUCTURAL GRIDS INSPIRED IN HISTORICAL GEOMETRIC ISLAMIC ORNAMENTAL ART

DOC I. MAIN REPORT

CARLOS A. MERI CELMA

MASTER THESIS // MAY 2020

TU Delft Delft University of Technology

MATER THESIS
STRUCTURAL ENGINEERING // STRUCTURAL MECHANICS
TU DELFT // FACULTY OF CIVIL ENGINEERING (CiTG)

AUTHOR

Carlos A. Meri Celma
carlosmericelma@gmail.com

GRADUATION COMMITTEE

Prof.dr.ir. Jan Rots (Chair)	TU DELFT - CiTG // Materials, Mechanics, Management & Design – Structural Mechanics
Dr. ir. Carlos Lázaro (Supervisor)	UPV (Spain) - ETSICCP // Continuous Medium Mechanics and Theory of Structures
Dr. ir. Max Hendriks	TU DELFT - CiTG // Materials, Mechanics, Management & Design – Structural Mechanics
Ir. Lennert van der Linden	TU DELFT - CiTG // Materials, Mechanics, Management & Design – Structural Design

A project in cooperation with:

Faculty of Civil Engineering and Geoscience (CiTG)

Department of Continuous Medium Mechanics and Theory of Structures

AKNOWLEDGEMENTS.

I would like to express my gratitude to the members of my thesis committee Jan Rots, Max Hendriks and Lennert van der Linden for their flexibility, for the freedom they granted me during this time and their valuable suggestions. I would also like to express my gratitude to Carlos Lazaro and David Gallardo, both from the Universitat Politècnica de Valéncia, for welcoming me as a research student. Carlos Lazaro, as my daily supervisor, has provided me great guidance and support and David has helped me with the analysis automation. Without David´s support, this project could never have reached this level of insight.

In my thoughts are above all my parents, Eduardo Meri and Mari Carmen Celma, who relentless encouraged me to follow my dreams and achieve all my goals. And my brother Jose Luis who has always been my closest friend.

This document is designed to be printed in A4 on. both sides, adjusting the scale to printer margins.

ABSTRACT

Geometric patterns inspired in historical Islamic ornamental art have attracted the attention of contemporary designers worldwide. The large variety of shapes, symmetries and combinations is a source of inspiration, but at the same time makes it difficult to provide general rules when used in a technological application. Structural small-scale applications have been object of research, but there are potential applications at larger scales that deserved attention. In view of some recent proposals of Islamic patterns as structural grids for tall building skins, the question of their structural efficiency, especially compared to conventional grids, arises.

The purpose of this research is to assess the performance of structural grids based on geometric Islamic patterns as outer skins of tall buildings. For this purpose, several historic patterns have been classified. An equivalent meta-material has been defined for each pattern, based on the homogenization method for a series of saturations or beam sizes. Their response in different orientations has been studied to identify their structural behaviour based on the pattern geometry. Their relative performance has been assessed for all patterns against themselves and against the conventional diagrid system. All this process has been collected and summarized in a predesign tool made of graphs, pictures and tables Finally, the predesign tool accuracy has been assessed and applied to three tall buildings. All those steps have been structured in three distinctive levels:

At the method level, the conclusion is that the developed predesign tool is a success as it provides a higher level of accuracy than modelling all the beams. It is also faster and easier to implement, than modelling all the beam elements, to compare alternatives in early stages as the complexity of modelling the patterns is postponed to later stages. As the saturation decreases and the effective beam length influence in the beam model results diminishes, the beam model will become more reliable than the predesign tool and vice versa.

At the pattern level, the most interesting finding is that the patterns with square symmetry (symmetry directions at 90º) display a perpendicular isotropic behaviour, whereas the patterns with pentagonal symmetry (symmetry directions at 72ª) display an orthotropic behaviour, and the patterns with hexagonal symmetry (symmetry directions at 60ª) display an isotropic behaviour. It has also been studied the effect that would have filling the stars as an alternative to building the patterns as an assembly of beams.

At the building level, it has been found a few geometric Islamic patterns that could be suitable alternatives to the conventional diagrid systems, a pattern with a similar performance and even a pattern with a higher structural performance than the conventional diagrids. This highly performing pattern is currently been used for some architects such as Shigeru Ban in their parametric designs. In this regard, it can be concluded that the objective of finding suitable alternatives to conventional diagrid systems has also been a success and it can affect some designers engineering judgement. The homogenization process obtained an equivalent ideal material corresponding to a plane infinite panel that will not correspond with the built structural grid. The use of complex geometries and its application to tall buildings introduce effects not considered in the homogenization that will disrupt the expected structural performance. Those effects are minimized in the case of other shells structures such as domes but can be important in the case of tall buildings. It is not advisable to account for the squeezing effect by adapting the saturation with the change of the modulus size in the x-direction as the relative beam depth has a greater impact in the overall stiffness than the change of geometry due to the squeezing effect. The distortion effect cannot be accounted for directly and it depends on the angle of the distortion and the pattern. However, in the studied case it has been found a required correction factor of 1.2-1.3, in line with other uncertainty factors used in practice. Finally, the intermediate supports can have a great influence in the final drift. It depends on the pattern used and the number of diaphragms inside the module. Nevertheless, the use of intermediate supports is always beneficial and not considering them will always lead to more conservative solutions.

In conclusion, this document successfully bridges the knowledge gap regarding the structural behaviour of historic Islamic patterns, with comparative tables. It identifies the best performing patterns and their best orientation, and it provides a useful tool for the decision making in the design process of in-plane bearing geometric Islamic patterns.

TABLE OF CONTENTS

LIST OF SYMBOLS

Greek symbols

ε_{ij}	Strain in plane normal to i in j direction. Used for normal stresses ($i = j$)	$-$
γ_{ij}	Strain in plane normal to i in j direction. Used for tangential stresses ($i \neq j$)	$-$
σ_{ij}	Stress in plane normal to i in j direction. Used for normal stresses ($i = j$)	N/mm^2
τ_{ij}	Stress in plane normal to i in j direction. Used for tangential stresses ($i \neq j$)	N/mm^2
ν_{ij}	Poisson's ratio in plane normal to i in j direction.	$-$
$\nu_{h,ij}$	Homogenized Poisson's ratio in plane normal to i in j direction.	$-$
θ	Contact angle in Hankin method	º
η	Number of crossings in Hankin method	$-$
Δl	Imposed deformation	mm

Symbols

A	Area	m^2
$C_{2D\_E_i}$	Membrane correction factor for the modulus of elasticity in i direction.	-
C_{2D_G}	Membrane correction factor for the shear modulus.	-
$C_{2D\_\nu_{ij}}$	Membrane correction factor for the Poisson ratio.	-
$C_{R\alpha\_E_i}$	Rotation factor for the modulus of elasticity in i direction, with rotation of α degrees	-
$C_{R\alpha\_G}$	Rotation factor for the shear modulus, with rotation of α degrees	-
$C_{R\alpha\_\nu_{ij}}$	Rotation factor for the Poisson ratio, with rotation of α degrees	-
D	Relative distance between of the application of the contact angles in Hankin method	%
d/n	Mesh size such that n elements fit in the d beam depth	-
d_i	Imposed displacement in i direction	m
E_i	Modulus of elasticity in i direction	N/m^2
E_{base}	Modulus of elasticity of the base material	N/m^2
$E_{h,i}$	Homogenized modulus of elasticity in I direction normalized as percentage of E_{base}	%
EI	Bending stiffness	Nm^2
G	Shear modulus	N/m^2
G_h	Homogenized shear modulus normalized as percentage of E_{base}	N/m^2
GA_s	Shear rigidity	N
H	Building height	m
I	Moment of inertia	m^4
L	Relative pentagon side respect to the module size in Rosette transform	%
L_i	Length of the panel in the i direction	m
m_i	Number of modules in the i direction	-
N_{ij}	Panel reaction in plane normal to i in j direction.	N
N_{ih}	Panel reaction in i direction for horizontal imposed displacement	kN
N_{ih}	Panel reaction in i direction for vertical imposed displacement	kN
Q_{ij}	Coefficient $[i, j]$ in the constitutive matrix	N/mm^2
q_w	Distributed wind loading	N/m
$u_x(y)$	Maximum horizontal displacement at height y	m
x	In-plane horizontal direction	-
y	In-plane vertical direction	-
z	Out-of-plane direction	-

Contractions

$Diff.$	Difference. Change in the results between steps in mesh refinement.	%
rbd	Relative beam depth. Beam depth as percentage of the module size in x-direction.	%
$Rot.$	Rotation. The pattern is rotated this angle.	º
$Sat.$	Saturation. Percentage of the surface occupied by the structure.	%

LIST OF PICTURES

1. INTRODUCTION

1.1. RESEARCH MOTIVATION.

According to the United Nations Department of Economic and Social Affairs (UN DESA)[2.] during the next 30 years there will be a mass exodus of population from the rural areas to the cities. Among them, 90% in the regions of Africa and Asia. This process will lead to ever-growing megalopolis with a high density of population. From a social and environmental point of view, it is essential to research into different constructive and structural alternatives that integrated with their social environment make an efficient use of the resources. In that sense, the Bending Rigidity Index defined by Le Messurier[3] shows how a perimeter array of the bearing elements is generally more efficient regarding the material use. The tube system has been widely employed regardless being less efficient than the braced systems, since its elements work in bending to withstand the wind action. Within the braced systems, the mega-frame system has been so far the most commonly used. However, it still presents the problem of relative displacement between floors inside each module and it strongly constrains the designer when it comes to irregular building shapes. Finally, diagrids systems use has been quite limited due to its aesthetic impact and its nodes high construction costs. However, currently diagrid systems are living a new golden age due to its adaptability to complex and organic building shapes, due to the new software that simplifies its analysis and manufacture reducing costs, and due to its aesthetic possibilities with the apparition of non-conventional designs. Examples of non-conventional diagrid systems:

FIG 1.1 Surnrise Tower[4]

FIG 1.2. Sino-Steel Tower[2]

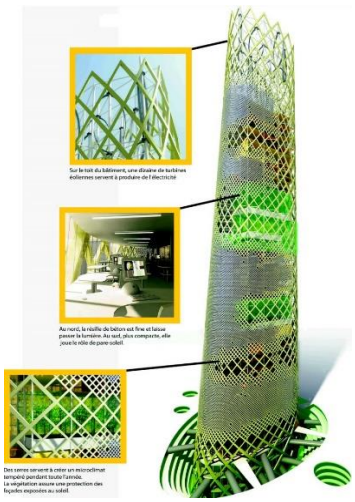

FIG 1.3. Hypergreen Tower[3]

FIG 1.4 Citic Financial Centre[4]

A literature review shows recent researches about the structural optimization of conventional diagrid systems (Moon et al 2007)[4.] about other simple geometries such as pentagrids (Taranath et al 2014)[5] and hexagrids (Montuori et al 2015)[6.] and a method for the preliminary design of irregular diagrids based on Voronoi's tessellation (Angelucci and Mollaioli 2018)[7]. However, other geometries which are more complex, open to prefabrication and widely present on the regions where most of the tall buildings will be erected, such as the Arabic, have not been researched. That is the reason behind this master thesis focus in this research area. An area that is under development, that has practical applicability in the coming years and that in case of being applied will have social, environmental and economic effects. Examples of Arabic patterns in conceptual design of modern architecture:

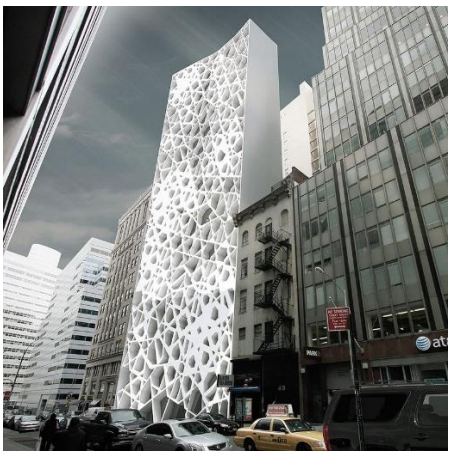

FIG 1.5. Park51[12]

FIG 1.6. Algerian Parliament[13]

FIG 1.7. Nomad Inception[14]

1.2. RESEARCH OBJECTIVE.

The main **objective of this thesis is to provide insight into the structural behaviour and design of geometric Islamic patterns as alternative to conventional diagrid systems for tall buildings**. In other words, to fill that knowledge gap, to assist future designers by providing insight into the geometric Islamic patterns in-plane behaviour, their relative structural performance, their design and their feasibility as alternative to conventional diagrid systems for tall buildings. This research objective is articulated at three levels:

METHOD LEVEL:
Development of a simple tool for the predesign of surface structures with geometric Islamic patterns

PATTERN LEVEL:
Determination of the **structural behaviour and performance comparison** of surface structures with geometric Islamic patterns loaded in their plane

BUILDING LEVEL:
Feasibility of the adoption of geometric Islamic patterns **as an alternative to conventional diagrid systems**.

1.3. RESEARCH QUESTIONS.

The research questions are enunciated so their answers will provide the knowledge sought by the research objectives. Therefore, three main research questions are required, matching the three knowledge levels (method, pattern and building) distinguished when laying out the research objectives.

METHOD LEVEL:
Can a simple tool be developed for the predesign of geometric Islamic patterns as a non-conventional diagrid system?

PATTERN LEVEL:
How do geometric Islamic patterns behave and compare when loaded in their plane?

BUILDING LEVEL:
Can Islamic inspired patterns become a feasible alternative to traditional **diagrid systems for tall buildings**?

1.4. METHODOLOGY

Each research question is approached by a series of stepping stones in order to reach a satisfactory answer:

METHOD LEVEL:
Can a simple tool be developed for the predesign of geometric Islamic patterns as a non-conventional diagrid system?

- Method chosen and methodology for its adoption
- Development of a pre-design tool.
- Assessment of the developed tool

PATTERN LEVEL:
How do geometric Islamic patterns behave and compare when loaded in their plane?

- Selection of historic Islamic patterns and their parametric variations
- Characterization of the patterns' structural behaviour
- Performance comparison of the different patterns
- Proposals for their improvement

BUILDING LEVEL:
Can Islamic inspired patterns become a feasible alternative to traditional diagrid systems for tall buildings?

- Performance comparison of the different patterns and the conventional diagrids
- Overview practical applications of best performing patterns
- Special cases in tall buildings

1.5. SCOPE

This study is limited to the in-plane structural behaviour of geometric Islamic patterns under linear elastic response. The research will account for the Representative Volume Element effects and mesh size during the homogenization process. It has been considered that 20 widespread historic Islamic patterns will be comprehensive enough to assess their structural behaviour and performance. It has been proposed a series of parametric variations of each historic pattern to show the designer the variation possibilities of this method and provide them with a basis to come up with their own designs. Once the structural behaviour and performance of the selected historic patterns is obtained, they are compared against each other and against a conventional diagrid system to evaluate their suitability for practical application. The tables, graphs and figures are collected in a compendium as a pre-design tool, whose accuracy is assessed.

The homogenization process requires of 4 tests (two elongations and two distortions). As the relative beam depth affects the grid response, each pattern is tested for an average of 9 different relative beam depths. The historic patterns and their 6 proposed parametric variations are test for 3 different panel sizes with beam elements (1x1, 2x2 and 4x4). Just the historic patterns are tested for 2 different mesh sizes (D/6 and D/12). All of this makes a total of 16,560 tests. Including the stars filling, study cases and other tests, the total amount of tests in SAP2000 done for the development of this research are near to 20,000.

1.6. DOCUMENT OUTLINE

This report is structured as a direct transposition of the outlined methodology, with extra chapters to account for the conclusions and preliminary sections.

PRELIMINARIES	-	Introduction	Ch 1
	-	Literature review	Ch 2
	-	Geometric Islamic patterns	Ch 3
RQ1. METHOD LEVEL	-	Method adopted	Ch 4.1
	-	Homogenization methodology	Ch 4.2
	-	Representative Element Volume (REV)	Ch 4.3
	-	FEM Beam elements	Ch 4.4
	-	FEM Membrane elements	Ch 4.5
	-	Mesh refinement	Ch 4.6
	-	Membrane correction factor (C2D)	Ch 4.7
	-	Ideal homogenized mechanical properties	Ch 4.8
RQ2. PATTERN LEVEL	-	Directional mechanical properties.	Ch 5.1
	-	Wire patterns performance	Ch 5.2
	-	Star filling	Ch 5.3
	-	Filled patterns performance	Ch 5.4
	-	From wire to filled patterns	Ch 5.5
RQ3. BUILDING LEVEL	-	Conventional diagrids	Ch 6.1
	-	Diagrids vs historic patterns performance	Ch 6.2
	-	Overview of best performing patterns	Ch 6.3
	-	Accuracy assessment	Ch 6.4
	-	Special cases in tall buildings	Ch 6.5
CONCLUSIONS	-	Research Question 1. Method level	Ch 7.1
	-	Research Question 2. Pattern level	Ch 7.2
	-	Research Question 3. Building level	Ch 7.3
ANNEX	-	Design Guide	Appendix I
	-	Numerical results	Appendix II

2. LITERATURE REVIEW

2.1. PREVIOUS RESEARCH ON THE STRUCTURAL USE OF GEOMETRIC ISLAMIC PATTERNS

Traditionally, the geometric Islamic patterns have had a mere decorative application as carved, cladded or painted. Nowadays architects are showing their wish to use them for other functions such as light control or structural bearing. The available literature on the structural use of geometric Islamic pattern is:

- N. Emami, A. Khodadadi and P.V. Buelow, (2014)[8]. Design of shading screens inspired by Persian geometric patterns: An integrated structural and daylight performance evaluation. IASS-SLTE Symposium: Parametric study of a patterned wall based on the dynamic shading of Al Bahr Tower. The structural analysis concludes that "these are not appropriate configurations to choose as a self-standing wall, even though their daylight performance is acceptable. Different structural system needs to be designed to use these configurations"

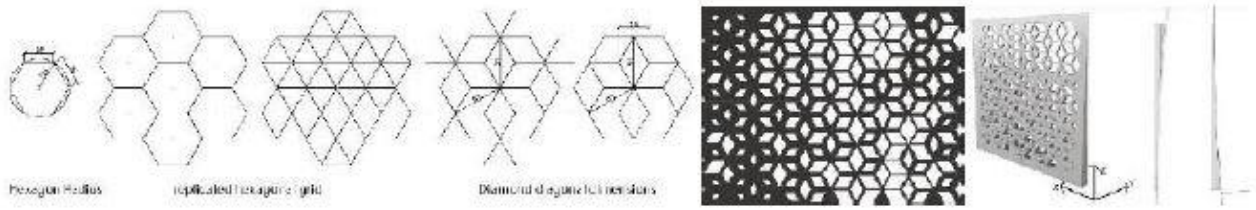

FIG 2.1. Shading screens inspired by Persian geometric patterns

- N. K. Khouri (2017)[9]. Structural Grid Shell Design with Islamic Pattern Topologies. Master thesis Massachusetts Institute of Technology: Parametric optimization of the pattern 4.8.8. by modifying the contact angle, for the use on funicular shells. Master thesis focus primarily in form finding and parametric optimization.

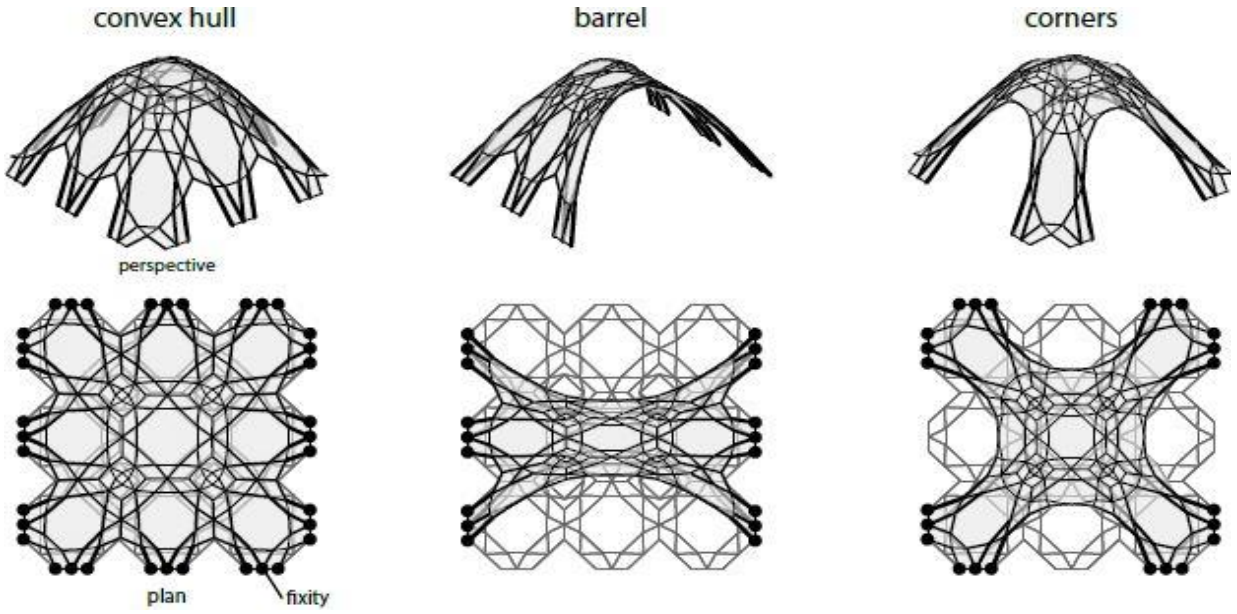

FIG 2.2..Hankin method on pattern 4.8.8.mapped into funicular shells

From the existing literature on the structural use of geometric Islamic patterns, it is concluded that:

- There is no previous literature on the in-plane structural behaviour and structural characterization of the most important historic geometric Islamic patterns.
- There is no previous literature on the structural performance comparative between the most important historic geometric Islamic patterns.
- There is no previous literature on the structural performance comparative of the most important historic geometric Islamic patterns with regard other conventional structural systems.
- There is no previous literature on the effects of the rotation in the in-plane structural behaviour of the most important historic geometric Islamic patterns.
- There is no existing tool or guide for the predesign of historic geometric Islamic patterns
- The only parametric study on the structural behaviour of Islamic patterns is limited to the tessellation 4.8.8.

2.2. DIAGRID SYSTEMS

A diagrid is a regular assembly of diagonally intersecting beams that creates a planar rigid structure. Its name is the acronym for diamond grid as the resulting pattern is a rhomboid tessellation. The diagrid system has been experiencing an evolution of its topology during the last decades, leading to the following possible classification:

First generation: The first conceptual proposals were presented in 1953 at the Illinois Institute of Technology by Myron Goldsmith[10]. He designed three triangulated structures for tall buildings, namely a variable-density diagrid, a regular narrow diagrid and a mega-diagonal solution.

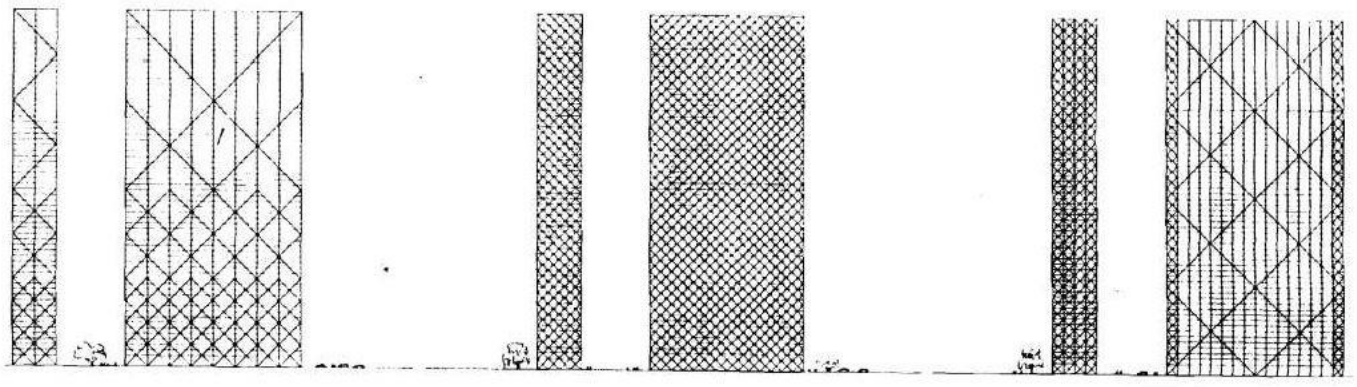

FIG 2.3. Diagrid systems proposed by Goldsmith

Under this first generation are those "diagrid systems" currently better known as "braced frames". A clear example of these early applications was the Hancock tower built in Chicago in 1965. This typology keeps the beams and columns leaving the diagonals the role of bracing against horizontal loads. This provides a high bending stiffness proving to be suitable for very slender buildings. In his drawings, Goldsmith represented this solution with right-angled triangles, but it does not have to be always the case.

Second generation: Under this generation are those diagrid systems currently referred as conventional diagrids. As the columns are removed, the diagonals have to work for gravitational as well as horizontal loads, making the structure more efficient in terms of material use. When this typology is applied to a building, all the nodes at the same level are normally tied with a horizontal beam to triangulate the structure improving greatly its stiffness.

The widespread use of Computer Aided Design software in the construction field has pushed the boundaries of architecture into more geometrically complex designs. In this regard, conventional diagrids are the natural result of faceting organic shapes and as result, they have found a new re-awaken as the best feasible solution for complex buildings such as the Museum of the future[18] in Dubai or 30st Mary Axe[19] in London. The characteristic module of the second generation is the equilateral triangle.

FIG 2.4. Museum of the future[18]

FIG 2.5. 30st Mary Axe[19]

FIG 2.6. Hearst Tower[20]

Third generation: As the acceptance of this structural typology increases, the interest in its practical application catalyses the search of more optimal diagrid systems. The third generation is characterized by diagrids whose triangles are distorted in order to obtain better mechanical properties. A representative example is the Hearst Tower[20] in New York, where a parametric study of the diagrid angle allowed to save 20% of the material in comparison with a conventional diagrid.

In his article "Material-Saving Design Strategies for Tall Building Structures", Professor Kyoung Sun Moon[11] states regarding the optimal diagrid angle: "Thus, the optimal angle of diagonal is highly dependent upon the building height. Since the optimal angle of the columns for maximum bending rigidity is 90 degrees and that of the diagonals for maximum shear rigidity is about 35 degrees, it is expected that the optimal angle of diagonal members for diagrid structures will fall between these angles and as the building height increases, the optimal angle also increases." So there is not an optimal angle a priori, it will ultimately derive from the height and slenderness of the building under study.

Fourth generation: New patterns are arising for aesthetic and structural reason which deviate from the original diamond shape that gives name to the diagrid system. They are better known as unconventional diagrid systems and a few different mainstreams can be identified:

- **Michell truss**: In 1904 G. A. Michell[12] defined analytically the optimal structure to withstand a point load for continuum, giving name to this specific typology. Due to W. Prager contribution for the application on discrete trusses on recent years, this typology is sometimes referred to as Prager truss as well for his contributions[13]. The main objective of this typology is to obtained the most efficient structure in terms of material consumption so its shape derives directly from the building shape and the loads considered. A recent example is the Citic Financial Centre[4] in Shenzhen. The design can be obtained analytically as proposed by Michell, iteratively with a genetic algorithm in a parametric design, or by means of topology optimization.

- **Organicist**: Variations of the diagrid system to get an aesthetic that evokes the nature. An example is the unbuilt Sunrise Tower[1] designed for Kuala Lumpur. However, the most extreme case is the use of Voronoi tessellation that is wide spread in the nature. Angelucci and Mollaioli (2018)[7] have recently proposed a method for the preliminary design of non-conventional diagrids based on Voronoi's tessellation.

- **Hexagrids:** Other simple geometries different to triangles have recently been studied as alternatives to conventional diagrid systems for their aesthetic interest. It is the case of pentagrids (Taranath et al 2014)[5] whose module is the pentagon or the case of hexagrids (Montuori et al 2015)[6] whose module is the hexagon. An example is the Sino-Steel Tower[2] currently under construction in Tianjin.


FIG 2.7. Surnrise Tower[1]


FIG 2.8. Sino-Steel Tower[2]


FIG 2.9. Hypergreen Tower[3]


FIG 2.10 Financial Centre

- **Geometric Islamic Patterns**: Based on the historic geometric Islamic patterns across the Muslim world. Examples of Arabic patterns in conceptual design of modern architecture are the Park51[5] proposed for New York, the project for the Algerian Parliament[6] or the façade solutions offered by Nomad Inception[7].

FIG 2.11. Park51[5]

FIG 2.12. Algerian Parliament[6]

FIG 2.13. Nomad Inception[7]

2.3. STIFNESS-BASED DESIGN.

In tall buildings the most critical loads are the lateral loads, specially the wind loads. If the wind load is simplified to its equivalent constant distributed load, the shear distribution will be linear (h^1), the bending distribution parabolic (h^2), the rotations distribution cubic (h^3) and deformations will have a distribution directly proportional to the building's height at the power of four (h^4). The mechanical properties that have to withstand the bending force are related to the inertia of the bearing system. As the external tube is approximately a hollow section, according to Steiner's rule, the inertia is directly proportional to the area of the structural element times the distance to the neutral axis squared $(b/2)^2$. In other words, as the building slenderness increases, the displacement limitations at the top become more critical than the resistance limitations at the base. Generally speaking, it can be stated that in tall buildings, fulfilling the global Service Limit State limitations indirectly leads to the fulfilment of the Ultimate Limit State limitations as they tend to be more restrictive. This premise is valid only for the predesign and all the limitations must be later verified, especially those concerning the global stability of the building overturning as a rigid body

The stiffness-based design approach is derived from the above premise. The structural elements are disposed and sized so the overall stiffness of the structure is enough to fulfil the required displacement limitation. This approach is widely used for the preliminary design of tall buildings and is applied by Moon[11] for his diagrid optimization:

"Tall building structures can be modelled as vertical cantilever beams on the ground. Then, the deflection at the top is given by:

$$u_x(H) = \gamma^* H + \frac{\chi^* H^2}{2} \qquad (1.1)$$

$\gamma^* H$ is the contribution from shear deformation and

$\chi^* H^2/2$ is the contribution from bending"

Then, the dimensionless 's' factor equal to the ratio of the displacement at the top of the structure due to bending and the displacement due to shear is introduced. The optimization study will find the appropriate ´s´ for the most economic design.

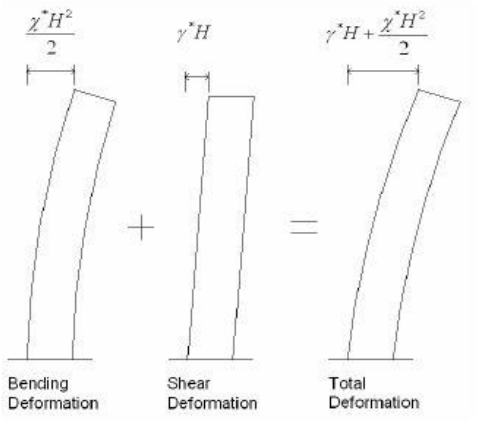

FIG 2.14.Stiffness based design

Applying Timoshenko beam theory to a prismatic cantilever beam under uniform distributed load:

$$u_x(H) = \frac{q_w H^4}{8EI} + \frac{q_w H^2}{2GA_s} \leq u_x(H)_{max} \qquad (1.2)$$

The top displacement is compared with the drift limitation and the mechanical properties chosen to meet it.

2.4. HOMOGENIZATION METHOD.

This method was first developed for the theory of materials, to simulate the macroscale behaviour of porous materials without the need of modelling its constitutive microscale elements. The main idea is to get analytically or numerically the 'equivalent' or 'homogenized' mechanical properties of a continuous metamaterial that represents the periodic structure that forms it. In the context of non-conventional diagrids, the diagrid would be substituted by an equivalent homogenized material whose homogenized mechanical properties would lead to the same displacements with stiffness-based design equations.

G.M. Montuori[14] uses this method in his hexagrid structural assessment research: "(…) the idea is to idealize whichever grid as a continuous depleted medium, characterized by penalized mechanical properties, according to the classical micromechanical approach based on homogenization methods. In fact a plane periodic structure made up of an isotropic linearly elastic material and possessing a certain degree of symmetry behaves macroscopically as an isotropic material; the macroscopic properties of the structure are called the effective properties, and depend on both the mechanical properties of the solid matrix and on the microstructural features of the grid, namely topology, density and orientation."

Module: "The module is the frame shape, i.e. the geometrical arrangement of the structural members giving a visual representation of the pattern (hexagon for hexagrid and triangle for diagrid), anyway the replication of the module gives rise to overlaps of the edges, so that the overall geometry cannot be obtained by simply copying the module."

Unit cell: "Defined as the geometric unity that through replication allows to obtain the overall geometrical pattern without overlaps or gaps".

Representative Volume Element (RVE): "While the unit cells represent the repetitive unit from the geometric point of view, the RVE represents the structural idealization of the unit cell, that only can be established by anticipating the deformation modes and internal forces arising in the unit cell as a part of the global grid ".

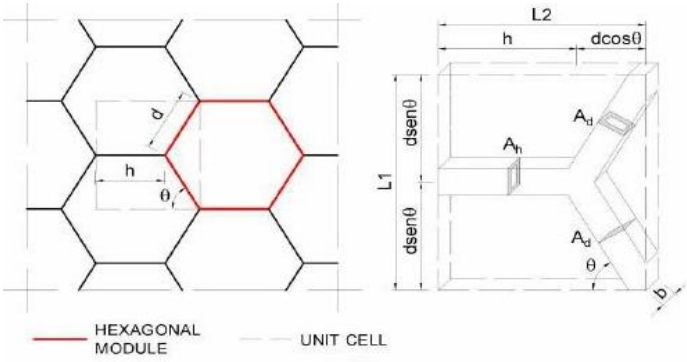

FIG 2.15. Unit cell definition

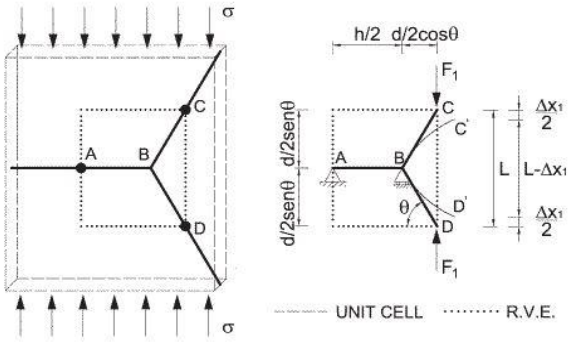

FIG 2.16. Representative Volume Element definition

This document diverges from the above definitions provided by G.M. Montuori[14]. The modules do not overlap, the unit cells are not the minimum possible unit and the representative volume elements are the direct structural idealization of the unit cells. For simplicity of the proposed design method, only the terminology "module" is employed to refer to the three of them, that in all cases have the exact same geometry. Their geometric definition is derived from the minimum rectangle standing in the x- and y-axis, whose replication leads to the complete pattern. These definitions are applied to Great Mosque of Damascus pattern in the following pictures:

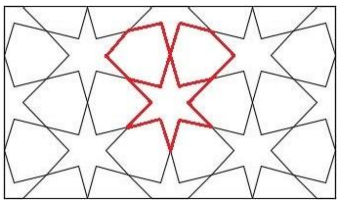

FIG 2.17. Module as per Montuori

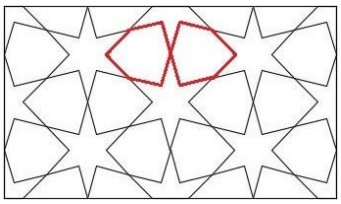

FIG 2.18. Unit cell as per Montuori

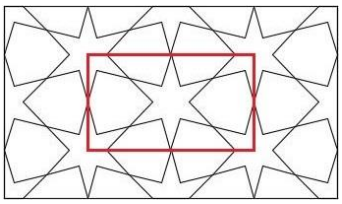

FIG 2.19. Module edges in this doc.

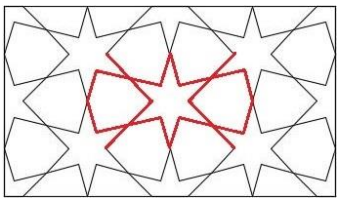

FIG 2.20.Unit cell and RVE in this doc.

The unit cell is exploded to fit into the module`s defining rectangle so the results are expected to have a great dependency on the applied boundary conditions and a Representative Volume Element refinement will be necessary.

2.5. PERIODIC BOUNDARY CONDITIONS

Historic geometric Islamic patterns can present three main geometric symmetries, namely square, pentagonal and hexagonal symmetries. Each generating symmetry will lead to a different orientation and number of axis of symmetry corresponding to the pattern's principal directions. For simplicity and to allow the automation of the analysis, a rectangular module is chosen for all patterns for the homogenization process. The unit cell is exploded in order to fit into the module's defining rectangle, leading ultimately to distortions in the results that need to be account for with a Representative Volume Element refinement.

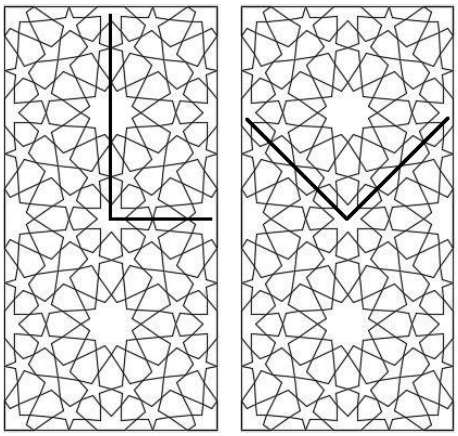

FIG 2.21. 90º. Square symmetry

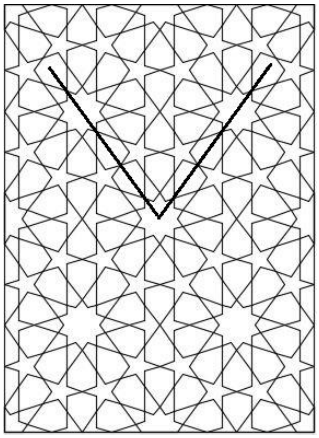

FIG 2.22.72º. Pentagonal symmetry

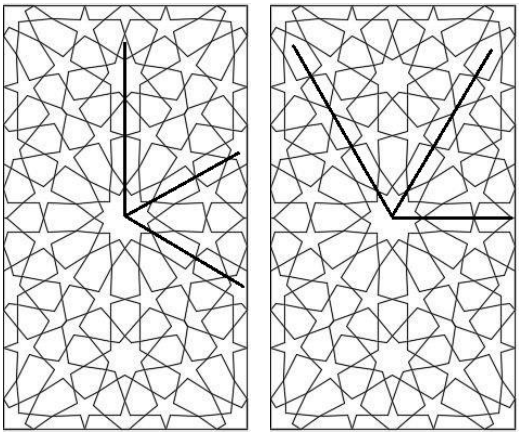

FIG 2.23. 60º. Hexagonal symmetry

A similar phenomenon is found when the cracking formation in concrete is studied a with Finite Element Analysis. The orthogonality of the element discretization does not correspond with the diverse orientations in which the cracking can occur. This difference in the cracking and finite element orientation can affect the crack generation derived from the different concentration of strains. A possible solution would be to repeat the tests changing the orientation of the square finite elements inside the volume under study, leading to a periodic boundary condition in its perimeter.

A brief introduction is extracted from A.T. Slobbe, M.A.N. Hendriks and J.G. Rots[15] paper on periodic boundary conditions applied to crack band model:

"The test uses the concept of periodicity in the field of strain localization analysis. Due to inclusion of periodic boundary conditions, different mesh alignments of element orientations with respect to the loading direction can be adopted. In contrary to standard tests this can be done without disturbance of the localization process by the model boundaries and without loss of mess uniformity. (…) The proposed systematic testing procedure could be applied on different constitutive models. In this paper it is done for the crack band approach, which is (in a qualitative sense) known from literature to suffer from mesh-induced directional bias".

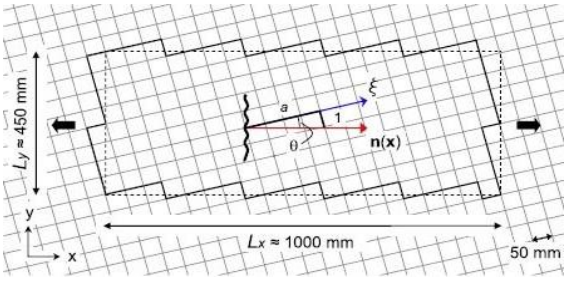

FIG 2.24. Periodic boundary conditions from the mesh rotation

For the 2D situation, the formulation can be expressed as:

$u_{j2.i} = 1.0 \cdot u_{j1.i} + 1.0 \cdot u_{\Delta ji}$, for $i = x, y$ and j= x, y (1.3)

$u_{c2.x} = 1.0 \cdot u_{c1.x} + 1.0 \cdot u_{\Delta xx} - 1.0 \cdot u_{\Delta yx}$ (1.4)

$u_{c2.y} = 1.0 \cdot u_{c1.y} + 1.0 \cdot u_{\Delta yy} + 1.0 \cdot u_{\Delta xy}$ (1.5)

In which $u_{j1.i}$, $u_{c1.x}$, and $u_{c1.y}$ are the master nodal displacements components and $u_{j2.i}$, $u_{c2.x}$, and $u_{c2.y}$their coupled slave nodal displacement components. The parameter $u_{\Delta ji}$ is the master nodal dof that represents the constant displacement difference Δji

Periodic boundary conditions address mesh-induced directional bias on continuous materials. It could a direct application in this project if the tests were performed to the homogenized equivalent material. However, the test are carried out to the discontinuous, heterogeneous and periodic patterns, so their application is not that obvious or direct as desired.

For the sake of finding a method that is directly applicable to all patterns and easy to automate, continuous boundary conditions are finally chosen over periodic boundary conditions in this research. More details on the boundary conditions can be found in Ch4. Homogenization process.

2.6. CONSTITUTIVE MATRIX FOR 2D ORTHOTROPIC BEHAVIOUR

The scope of this research is limited to the in-plane structural behaviour of the geometric Islamic patterns. A priori it is not possible to know if the equivalent metamaterial will have an isotropic, orthotropic or anisotropic behaviour. The most sensible approach would be to address it as an isotropic material and determine the actual behaviour by the obtained results. However, considering an isotropic behaviour would be too simplistic and an anisotropic behaviour would be excessive as one of the main objectives of this research is to develop an easy to use tool for the predesign of non-conventional diagrid systems based on geometric Islamic patterns. Therefore, in this research, the behaviour of the geometric Islamic patterns has been assumed a priori as orthotropic and the homogenization process has been designed in a manner to better provide the required input for such characterization.

The following formulation of the constitutive equations of 2D orthotropic materials is extracted from the course on Composite Materials and Structures from the Aerospace Department of the IIT Madras (NPTEL)[16].

Starting with the generalized Hooke's law for an anisotropic material, after applying the stress symmetry $\sigma_{ij} = \sigma_{ji}$ and the strain symmetry $\varepsilon_{ij} = \varepsilon_{ij}$ conditions, we can write Hooke's law in a contract form as:

$$\sigma_i = C_{ij}\varepsilon_j \quad (i,j = 1.2. \dots ,6) \tag{1.6}$$

Or in its better-known form:

$$\varepsilon_{11} = \frac{\sigma_{11}}{E_1} - \frac{\nu_{21}}{E_2}\sigma_{22} - \frac{\nu_{31}}{E_3}\sigma_{33} \tag{1.7}$$

$$\varepsilon_{22} = -\frac{\nu_{12}}{E_1}\sigma_{11} + \frac{\sigma_{22}}{E_2} - \frac{\nu_{32}}{E_3}\sigma_{33} \tag{1.8}$$

$$\varepsilon_{33} = -\frac{\nu_{13}}{E_1}\sigma_{11} - \frac{\nu_{23}}{E_2}\sigma_{22} + \frac{\sigma_{33}}{E_3} \tag{1.9}$$

Whereas the engineering shear strain components are given as:

$$\gamma_{12} = \frac{\tau_{12}}{G_{12}}, \quad \gamma_{13} = \frac{\tau_{13}}{G_{13}}, \quad \gamma_{23} = \frac{\tau_{23}}{G_{23}} \tag{1.10}$$

E_i represents the Young's moduli, G_{ij} the shear moduli and ν_{ij} the Poisson's ratio. For the 2D case, the terms ε_{33}, γ_{13} and γ_{23} are zero. Written in matrix form it is known as the compliance form:

$$\begin{Bmatrix} \varepsilon_{11} \\ \varepsilon_{22} \\ \gamma_{12} \end{Bmatrix} = \begin{bmatrix} \frac{1}{E_1} & \frac{-\nu_{21}}{E_2} & 0 \\ \frac{-\nu_{12}}{E_1} & \frac{1}{E_2} & 0 \\ 0 & 0 & \frac{1}{G_{12}} \end{bmatrix} \begin{Bmatrix} \sigma_{11} \\ \sigma_{22} \\ \tau_{12} \end{Bmatrix} \tag{1.11}$$

Finally, the stiffness matrix is the inverse of the compliance matrix:

$$\begin{Bmatrix} \sigma_{11} \\ \sigma_{22} \\ \tau_{12} \end{Bmatrix} = \begin{bmatrix} \frac{E_1}{1-\nu_{12}\nu_{21}} & \frac{\nu_{12}\,E_2}{1-\nu_{12}\nu_{21}} & 0 \\ \frac{\nu_{yx}\,E_x}{1-\nu_{12}\nu_{21}} & \frac{E_y}{1-\nu_{12}\nu_{12}} & 0 \\ 0 & 0 & G_{12} \end{bmatrix} \begin{Bmatrix} \varepsilon_{11} \\ \varepsilon_{22} \\ \gamma_{12} \end{Bmatrix} \tag{1.12}$$

This formulation has been derived for the material's principal direction. However, the principal directions of the geometric Islamic patterns under study are unknown. As the assumption and steps taken stand for other orthogonal directions, the principal directions are replaced by the x- and y-directions.

Stiffness matrix used in the homogenization process:

$$\begin{Bmatrix} \sigma_{xx} \\ \sigma_{yy} \\ \tau_{xy} \end{Bmatrix} = \begin{bmatrix} \frac{E_x}{1-\nu_{xy}\nu_{yx}} & \frac{\nu_{xy}\,E_y}{1-\nu_{xy}\nu_{yx}} & 0 \\ \frac{\nu_{yx}\,E_x}{1-\nu_{xy}\nu_{yx}} & \frac{E_y}{1-\nu_{xy}\nu_{yx}} & 0 \\ 0 & 0 & G \end{bmatrix} \begin{Bmatrix} \varepsilon_{xx} \\ \varepsilon_{yy} \\ \gamma_{xy} \end{Bmatrix} \tag{1.13}$$

2.7. ROTATION OF THE CONSTITUTIVE MATRIX.

The formulation included in this chapter has been obtained from the course on Composite Materials and Structures from the Aerospace Department of the IIT Madras (NPTEL)[16].

The rotation matrix around the x_3 axis is well-known:

$$a_{ij} = \begin{bmatrix} \cos(\alpha) & -\sin(\alpha) & 0 \\ \sin(\alpha) & \cos(\alpha) & 0 \\ 0 & 0 & 1 \end{bmatrix} \tag{1.14}$$

The direction cosines are used to transform a vector, a second order tensor or a fourth order tensor, and are given by the following relation:

$$a_{ji} = \frac{\partial x'_i}{\partial x_j} \tag{1.15}$$

Applied to a vector P_j such that the rotated coordinate system is given in terms of components in unrotated system:

$$P_i = a_{ji}P_j = a_{1i}P_x + a_{2i}P_y + a_{3i}P_z \tag{1.16}$$

$$P_1 = \cos(\alpha)\,P_x + \sin(\alpha)\,P_y \tag{1.17}$$

$$P_2 = -\sin(\alpha)\,P_x + \cos(\alpha)\,P_y \tag{1.18}$$

$$P_3 = P_z \tag{1.19}$$

Applied to a second order tensor σ_{kl}:

$$\sigma_{ij} = a_{ki}\,a_{lj}\,\sigma_{kl} \tag{1.20}$$

$$\begin{aligned}\sigma_{ij} = {} & a_{1i}\,a_{1j}\,\sigma_{xx} + a_{1i}\,a_{2j}\,\sigma_{xy} + a_{1i}\,a_{3j}\,\sigma_{xz} + a_{2i}\,a_{1j}\,\sigma_{yx} + a_{2i}\,a_{2j}\,\sigma_{yy} + \\ & + a_{2i}\,a_{3j}\,\sigma_{yz} + a_{3i}\,a_{1j}\,\sigma_{zx} + a_{3i}\,a_{j2}\,\sigma_{zy} + a_{3i}\,a_{3j}\,\sigma_{zz}\end{aligned} \tag{1.21}$$

$$\begin{aligned}\sigma_{11} = {} & a_{11}\,a_{11}\,\sigma_{xx} + a_{11}\,a_{21}\,\sigma_{xy} + a_{11}\,a_{31}\,\sigma_{xz} + a_{21}\,a_{11}\,\sigma_{yx} + a_{21}\,a_{21}\,\sigma_{yy} + \\ & + a_{21}\,a_{31}\,\sigma_{yz} + a_{31}\,a_{11}\,\sigma_{zx} + a_{31}\,a_{12}\,\sigma_{zy} + a_{31}\,a_{31}\,\sigma_{zz}\end{aligned} \tag{1.22}$$

$$\sigma_{11} = \cos^2(\alpha)\,\sigma_{xx} + 2\cos(\alpha)\sin(\alpha)\,\sigma_{xy} + \sin^2(\alpha)\,\sigma_{yy} \tag{1.23}$$

The remaining five stress terms are also obtained in a similar way using stress symmetry ($\sigma_{xy} = \sigma_{xy}$). The transformation matrix for stress tensor $[T_1]$ is given using short forms for $\cos(\alpha) = m$ and $\sin(\alpha) = n$.

$$\begin{Bmatrix} \sigma_{11} \\ \sigma_{22} \\ \tau_{12} \end{Bmatrix} = \begin{bmatrix} m^2 & n^2 & 2mn \\ n^2 & m^2 & -2mn \\ -mn & mn & m^2-n^2 \end{bmatrix} \begin{Bmatrix} \sigma_{xx} \\ \sigma_{yy} \\ \tau_{xy} \end{Bmatrix} \tag{1.24}$$

Similarly, the strain transformation matrix $[T_2]$

$$\begin{Bmatrix} \varepsilon_{11} \\ \varepsilon_{22} \\ \gamma_{12} \end{Bmatrix} = \begin{bmatrix} m^2 & n^2 & mn \\ n^2 & m^2 & -mn \\ -2mn & 2mn & m^2-n^2 \end{bmatrix} \begin{Bmatrix} \varepsilon_{xx} \\ \varepsilon_{yy} \\ \gamma_{xy} \end{Bmatrix} \tag{1.25}$$

Note that the transformation matrices $[T_1]$ and $[T_2]$ are not symmetric. There is a difference of factor 2 in two entries of the matrices. The transformation matrices $[T_1]$ and $[T_2]$ can be inverted using the following relation:

$$[T_i(\alpha)]^{-1} = [T_i(-\alpha)] \qquad i = 1.2 \tag{1.26}$$

Regarding the structural behaviour, the in-plane stress orthotropic reduced constitutive equation using stiffness matrix:

$$\begin{Bmatrix} \sigma_{xx} \\ \sigma_{yy} \\ \tau_{xy} \end{Bmatrix} = \begin{bmatrix} Q_{11} & Q_{12} & 0 \\ Q_{12} & Q_{22} & 0 \\ 0 & 0 & Q_{33} \end{bmatrix} \begin{Bmatrix} \varepsilon_{xx} \\ \varepsilon_{yy} \\ \gamma_{xy} \end{Bmatrix} \tag{1.27}$$

Where the Q_{ij} terms can be written using index notation as follows:

$$Q_{ij} = C_{ij} - \frac{C_{i3}\, C_{3j}}{C_{33}} \quad (i,j = 1.2) \tag{1.28}$$

Being C_{ij} the terms of the 3D constitutive equation using stiffness matrix in principal material directions. Since reduced stiffness matrix is symmetric, Q_{21} has been directly written as Q_{12}. Substitution of the terms leads to the known formulation previously adopted.

The plane stress constitutive equation in principal material coordinates is

$$\{\sigma\}_{123} = [Q]\{\varepsilon\}_{123} \tag{1.29}$$

The above equation can be re-written to give stresses in global coordinates as

$$\{\sigma\}_{xyz} = [T_1]^{-1}[Q][T_2]\{\varepsilon\}_{xyz} \tag{1.30}$$

Introducing the definition of the plane stress transformed reduced stiffness matrix $[\bar{Q}]$

$$[\bar{Q}] = [T_1]^{-1}[Q][T_2] \tag{1.31}$$

$$\{\sigma\}_{xyz} = [\bar{Q}]\{\varepsilon\}_{xyz} \tag{1.32}$$

$[\bar{Q}]$ is a symmetric matrix. Further, it is a fully populated matrix with non-zero $\bar{\boldsymbol{Q}}_{\boldsymbol{13}}$, $\bar{\boldsymbol{Q}}_{\boldsymbol{23}}$ coefficients, as they define the coupling between the in-plane normal and shear responses. However, in this research they are going to be assumed as zero so the results are coherent with the homogenization employed so far. It will inevitably lead to errors for pattern orientations deviating from the principal directions. The importance of those errors will be assessed by tests.

$$\bar{Q}_{11} = Q_{11}m^4 + 2(Q_{12} + 2Q_{33})m^2n^2 + Q_{22}n^4 \tag{1.33}$$

$$\bar{Q}_{12} = (Q_{11} + Q_{22} - 4Q_{33})m^2n^2 + Q_{12}(n^4 + m^4) = \bar{Q}_{21} \tag{1.34}$$

$$\bar{Q}_{13} = (Q_{11} - Q_{12} - 2Q_{33})m^3n + (Q_{12} - Q_{22} + 2Q_{33})n^3m = \bar{Q}_{31} \to 0 \tag{1.35}$$

$$\bar{Q}_{22} = Q_{11}n^4 + 2(Q_{12} + 2Q_{33})m^2n^2 + Q_{22}m^4 \tag{1.36}$$

$$\bar{Q}_{23} = (Q_{11} - Q_{12} - 2Q_{33})mn^3n + (Q_{12} - Q_{22} + 2Q_{33})nm^3 = \bar{Q}_{32} \to 0 \tag{1.37}$$

$$\bar{Q}_{33} = (Q_{11} + Q_{22} - 2Q_{12} - 2Q_{33})m^2n^2 + Q_{33}(n^4 + m^4) \tag{1.38}$$

Theoretical exact result obtained from derivation:

$$\begin{Bmatrix} \sigma_{xx} \\ \sigma_{yy} \\ \tau_{xy} \end{Bmatrix} = \begin{bmatrix} \bar{Q}_{11} & \bar{Q}_{12} & \bar{Q}_{13} \\ \bar{Q}_{21} & \bar{Q}_{22} & \bar{Q}_{23} \\ \bar{Q}_{31} & \bar{Q}_{32} & \bar{Q}_{33} \end{bmatrix} \begin{Bmatrix} \varepsilon_{xx} \\ \varepsilon_{yy} \\ \gamma_{xy} \end{Bmatrix} \tag{1.39}$$

Approximation used for practical purposes:

$$\begin{Bmatrix} \sigma_{xx} \\ \sigma_{yy} \\ \tau_{xy} \end{Bmatrix} = \begin{bmatrix} \bar{Q}_{11} & \bar{Q}_{12} & 0 \\ \bar{Q}_{21} & \bar{Q}_{22} & 0 \\ 0 & 0 & \bar{Q}_{33} \end{bmatrix} \begin{Bmatrix} \varepsilon_{xx} \\ \varepsilon_{yy} \\ \gamma_{xy} \end{Bmatrix} \tag{1.40}$$

3. GEOMETRIC ISLAMIC PATTERNS

3.1. HISTORY OF THE GEOMETRIC ISLAMIC PATTERNS

Many studies have been done in the field of geometric Islamic patterns (GIP) from different perspectives such as mathematical description, artistic implications and historic evolution. The information and pictures provided in this introduction about the history of the geometric Islamic patterns is extracted from Y. Abdullahi and M. R. Bin Embi article Evolution of geometric Islamic patterns[17]

"The expansion and development of geometry through Islamic art and architecture can be related to the significant growth of science and technology in the Middle East, Iran, and Central Asia during the 8th and 9th centuries (…) History of Islamic geometrical ornaments is characterized by a gap of nearly three centuries – from the rise of Islam in the early 7th century to the late 9th century, when the earliest example of geometrical decorations can be traced from the surviving buildings of the Muslim world"

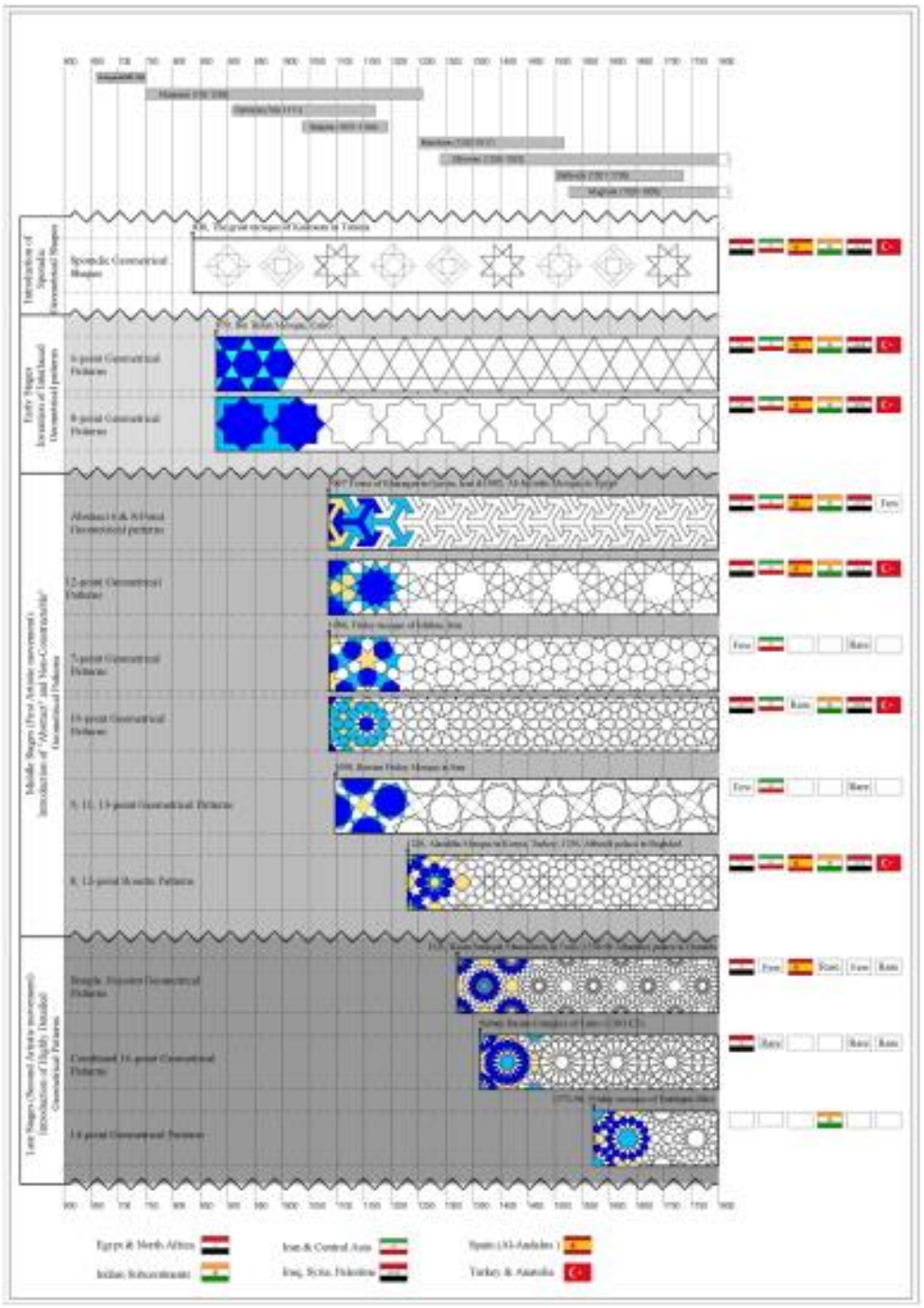

FIG 3.1. Time chart of the evolution of GIPs throughout history elaborated by Y. Abdullahi and M. R. Bin Embi[17]

Umayyad architecture (660-750 CE): By the end of the 7th and early 8th centuries, vegetal and floral patterns derived Sassanid and Byzantine architecture became common in Islamic architecture. In 705CE, substantial parts of the Damascus Christian Temple were converted into the Great Mosque of Damascus

Abbasids architecture (750-1258 CE): The ornaments of the Great Mosque of Kairouan (originally built in 670 CE and rebuilt in 836CE) are designed primarily with vegetal and floral motifs, but some elementary geometrical shapes are also observed. The Mosque of Ibn-Tulun is considered a milestone in terms of its introduction of geometrical patterns to Islmaic architecture. By the late 8th and early 9th centuries, geometrical shapes were introduced to surface decoration. However, woven geometrical patterns (6- and 8- patterns) began dominating Islamic architecture only during the late 9th century.

Fatimids architecture (909-1171 CE): Al-Azhar Mosque (970-972 CE), Al-Juyushi Mosque (1085 CE), Aqnar Mosque (1125 CE) and Mosque of Al-Salih-Tala'i (1160 CE) belong to this stage with mixed vegetal, calligraphic and geometrical decorations. Early Fatimid decorative ornaments are commonly in the form of isolated elements, rather than entire surface-covering patterns. Geometrical patterns became prevalent because of the heavy influence of Seljuk in the late Fatimid era.

Seljuk architecture (1038-1194 CE): First artistic movement. The Seljuks exerted tremendous efforts in transforming their ornaments from floral and figural into geometrical decorations, and their architecture is strongly characterized by geometrical patterns. The Friday Mosque of Isfaharan introduced highly complex and sophisticated 10-point geometrical patterns as well and abstract 6- and 8- point geometrical patterns. This movement continued on the Barsian Friday Mosque (1098 CE), to the early 13th century when unique 7-, 9-, 11- and 13- point patterns were used.

Mamluk architecture (1250 – 1517 CE): second artistic movement. Architectural movement taking place in Cairo and characterized by 6-, 8-, 10- and 12- point patterns in early buildings such as Mosque of Baybar (1267 CE) OR THE Qalawun Complex (1283 – 1285 CE). Later, 16-point patterns would become very popular amid Mamluk architects and artisans as shown in Muayyad Mosque (1415 – 1475 CE), the Amir Qijmas Al-Ishaqi Mosque (1480-1481 CE) or Wikala of Al-Ghori (1505-1515 CE).

Ottoman architecture (1290-1923 CE). Geometrical ornaments are generally only secondary decorative elements in Ottoman buildings such as the Yesli Mosque of Bursa (1421 CE), the Rustam Pasha Mosque (1560 – 1563 CE) orr the Selimiye Complex (1568 – 1575 CE). In general, Ottoman architects favored floral and vegetal patterns over geometrical decorations, whose use was limited to door and Minbar panels. Ottoman architects and artisans preferred 6-, 5-, and eventually 10- and 12- point patterns over the 8- and 16- point geometrical patterns that were very popular among Mamluk artisans.

Safavid architecture (1501-1736 CE). Safavid architects used geometrical ornaments in both religious and secular buildings. Artisans preferred 8- and 10- point geometrical patterns, mixing them with calligraphic inscriptions in religious buildings as in Hakim Mosque of Isfahan (1656-1662 CE) and filling them with vegetal motifs in secular buildings as in the Ali-Qapu Palace (1598 CE).

Mughal architecture (1526-1737 CE). In Mughal architecture, red sandstone, white marble and polychromatic tiles are the main cladding and decorative materials. Used in both secular and religious buildings, , Mughal architects avoided highly detailed geometrical arrangements such as 12- and 16- point patterns. Instead, they exerted great effort to create accurate and perfect proportions of shapes and angles. Nonetheless, the rarest 14- point geometrical patterns can be found in some Mughal buildings. Examples of this era are the Mausoleum of Humayun in Delhi (1566 CE) or the Etimad-ud-Daulah Tomb in Agra (1628 CE).

Muslims of Spain. Important surviving buildings are the Great Mosque of Cordoba (785-987 CE), Aljaferia Palace in Zaragoza (mid 11th century), the Great Mosque of Seville (1182 CE) and the Alhambra Palace (1338-1390 CE). Almost all the surfaces are richly decorated with the finest floral and geometrical motifs. Although geometrical ornaments were extensively used with profusely colored and intricate renders, highly complex patterns such as 7-, 9-, and 14-point patterns are missing.

3.2. DRAWING OF GEOMETRIC ISLAMIC PATTERNS

There are two main approaches for drawing geometric Islamic patterns:

STEP BY STEP METHOD: It is the approach taught by the School of Islamic Geometric Design[18] and collected by Eric Broug[19] in its book *Islamic Geometric Patterns* that will serve as reference in this document to identify different historic patterns. It consists in a series of steps that must be followed to draw a specific pattern. It is as a recipe and the rules change for each pattern. As an example, the Lahore Fort Complex pattern is drawing is shown in 8 simple steps.

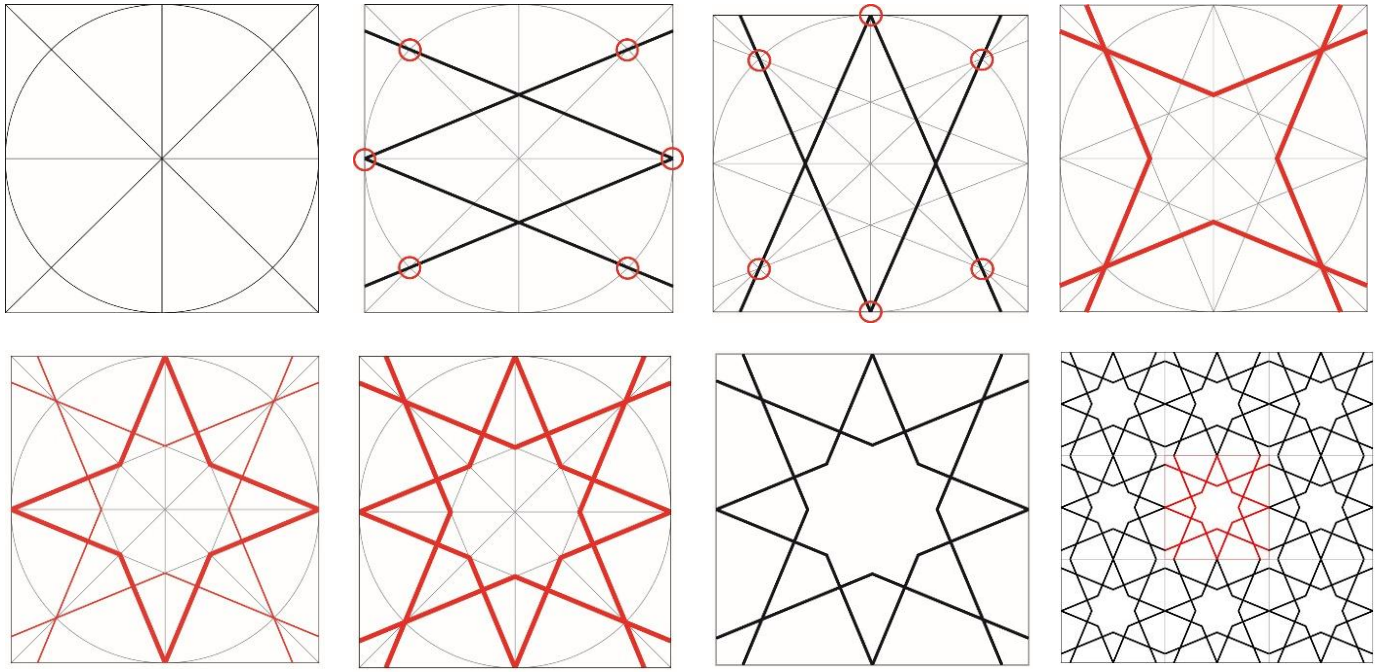

FIG 3.2. Step by step method for Great Mosque of Damascus pattern.

HANKIN METHOD: Proposed in 1925 by E.H. Hankin[20] and recently popularized by C.S. Kaplan[31], it is a method that allows to generate Islamic inspired starred patterns from a generating geometric tessellation. It consists of a simple algorithm or set of steps as the previous method, that depending on the generating generation that it is applied to and the values of the parameters inputted, will generate an Islamic inspired pattern. To an actual historic pattern, the designer must choose the appropriate tessellation and the matching values of the parameters. The advantage of this method is that it simplifies the automation of the generation process for mathematical analysis and computational design, it allows the creation of parametric variations and it gives more freedom to the designer to create his own pattern. In Hankin's words, the method would be described as follows:

"In making such patterns, it is first necessary to cover the surface to be decorated with a network consisting of polygons in contact. Then through the centre of each side of each polygon two lines are drawn. These lines cross each other like a letter X and are continued till they meet other lines of similar origin. This completes the pattern. The original construction lines are then deleted and the pattern remains without any visible clue to the method by which it was drawn" (8. p.4)

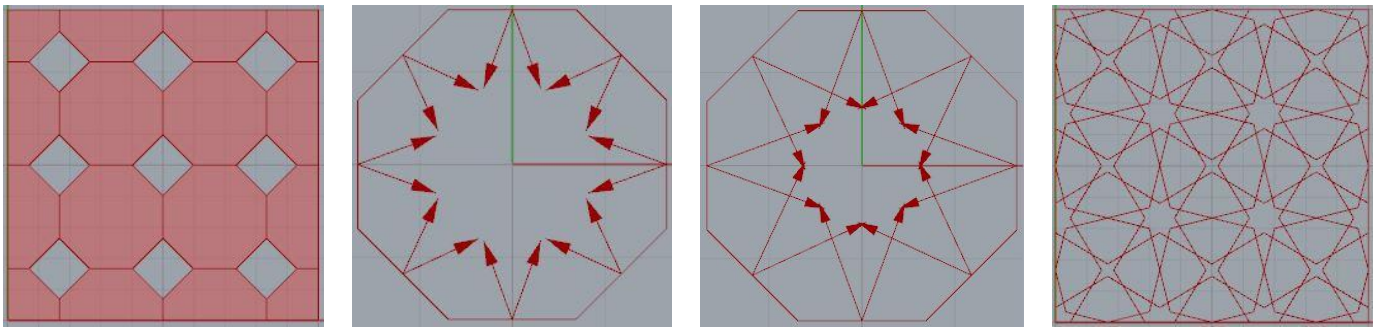

1. Tessellation 4.8.8. 2. Contact angle θ = 67.5º 3. N. of crossings η = 1 4. Complete pattern

FIG 3.3. Hankin method for Great Mosque of Damascus pattern.

A tessellation of a flat surface is the tilling of a plane using one or more geometric shapes with no overlaps and no gaps. The tessellations included in this document are Euclidean plane edge-to-edge polygon tilling, implying that the sides of a polygon in the tessellation matches in length and position to the edge of the next polygon adjacent to it. In this disposition, two polygons in contact share a common vertex that is used as reference for the nomenclature.

The tessellations label corresponds to the enumeration of the number of sides of the polygons found around a common vertex. Regardless of the vertex chosen as reference, the polygons found are always the same. Finally, the polygons are enumerated counter-clockwise starting by the lowest value. Following those rules, the tessellation below is called 4.8.8. Note that it is commonly used a more compact form with superscripts indicating that the same polygon appears more than once in a row, in this case, this tessellation could be called 4.8^2.

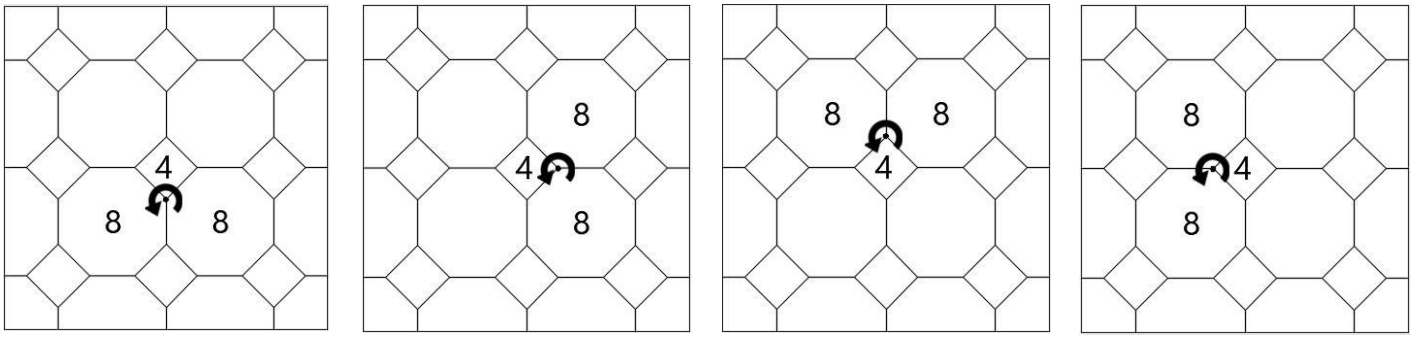

FIG 3.4. polygons found from different vertices for tessellation 4.8.8.

The Lahore Fort Complex pattern shown in the step by step method, can be obtained from the tessellation 4.8.8. with contact angle θ = 67.5º and number of crossings η = 1 with the Hankin method. Finally, the following pictures extracted from Islamic Star Patterns from Polygons in Contact will serve clarify the concept of contact angle.

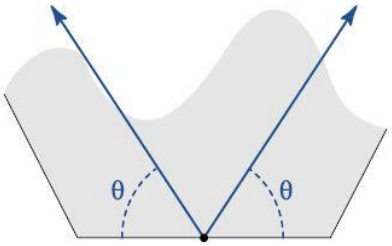

FIG 3.5. Contact angle. Kaplan[21]

The contact angle is drawn from the centre of each side of all polygons constituting the tessellation. The value of the angle can vary between 0º and 90º. A contact angle of 0º corresponds to the vectors superposing with the original polygon sides and a contact angle of 90º to the vectors being perpendicular to them. The vectors generated are symmetric with respect a plane perpendicular to the polygon sides and when the same contact angle is applied to all polygons, the vectors are symmetric with respect the polygons sides as well.

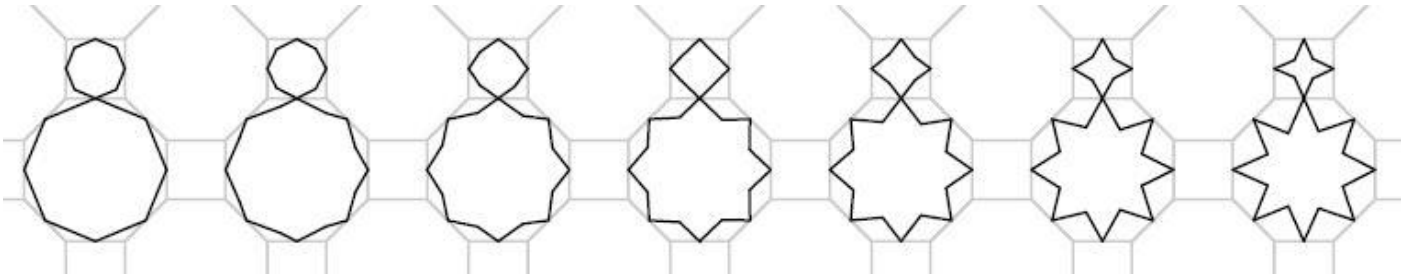

FIG 3.6. Increasing contact angle in tessellation 4.8.8.with number of crossings equal to zero η = 0. Kaplan[21]

For this research several patterns have been chosen to have a comprehensive view of the structural behaviour of the Islamic inspired star patterns and to provide a wide range of possibilities to the future designer. The number of solutions grows exponentially with the freedom given to the different parameters involved in the design. To better delimit the space of solutions around the desired ones, the parameters have been treated as follows:

Tessellation: The first step is to choose the tessellation to which apply the Hankin method. First the wished historic patterns have been chosen and then the tessellation leading to those specific patterns have been identified.

Contact angle (θ): A parametric study is carried out with this variable, constraining its range around the wished solution. It has been done with the aim of leaving some freedom of design to the future designer, of being able to identify new appealing innovative patterns and to assess the efficiency of the chosen solutions.

Number of crossings (η): The number of crossings is not specified for the whole tessellation but for each of the polygons that form it, in accordance to the following table. A reduced number of crossings for high-order polygons lead to inefficient patterns from the structural point of view, as the inner beams of those polygons barely work. A higher number of crossings than specified for all polygons lead to small openings, which difficult its construction and massifies its visual perception. However, the main reason is historical, as this table has been developed in accordance to the observed the historical geometric Islamic patterns.

n. points star	3	4	5	6	7	8	9	10	11	12	>12
η = 0	x	x	x	x							
η = 1					x	x	x	x	x	x	
η = 2											x

TABLE 3.1. Maximum number of crossings for each star based on the observation of historical geometric Islamic patterns

Others: In specific cases some other parameters arise which are not directly derived from the Hankin method. It is the case of the "Sabz Pushan", where the generating vectors do not part from the centre of the polygons' sides. It is also the case of many of the historic patterns where the pentagons can be filled up either with "stars", "arrows" or "Bayezid" type. This shows the great amount of design possibilities and will only be treated punctually in those patterns that require it.

3.3. SELECTION OF HISTORIC GEOMETRIC ISLAMIC PATTERNS

A first selection was originally carried out with the help of the book *Islamic Geometric Patterns*[19], but a closer look on showed that many of the most spread patterns were not included in that book and pictures of some of the patterns from the book were not easily available on the internet (as pattern L. Ben Yusuf madrasa). The final selection comes from browsing thousands of pictures on the internet and choosing those that seemed the most representative. The names are given after the location where the attached picture was taken, not meaning that that is the only or first place where that pattern was used. It is worth noting that some of the patterns in this document have different names than the ones from the book *Islamic Geometric Patterns*[19] due to the pictures' availability (as E. Palace of the Shirvanshahs or H. Generalife). The variations are the result of changing one of the parameters involved in the implementation of the Hankin method. A total of 20 different historic geometric Islamic patterns are studied and presented in growing complexity, together with 6 parametric variations.

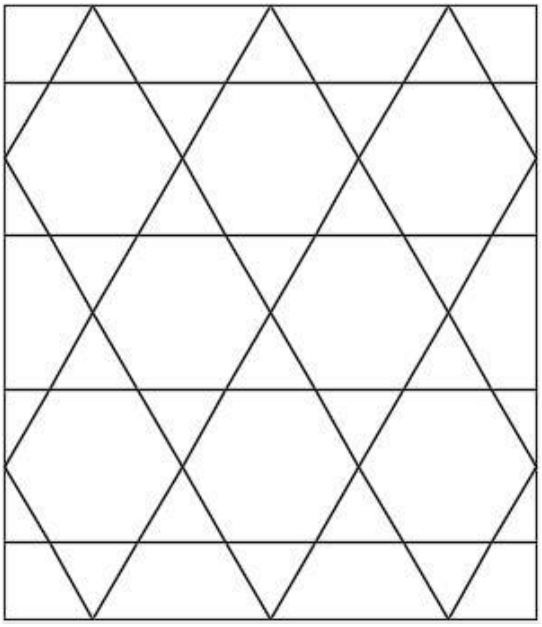

A) YESLI MOSQUE

FIG 3.7. Bursa, Turkey (AD 1421/ AH 823)[11]

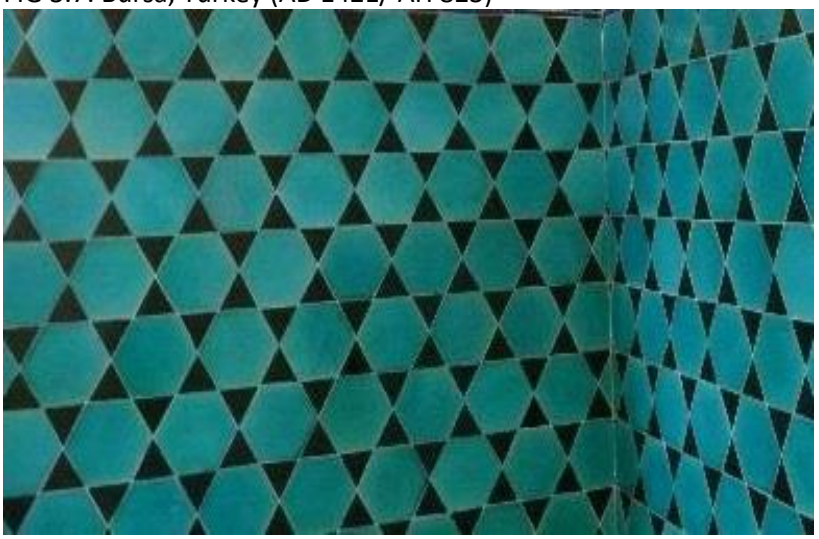

FIG 3.8. Tessellation **3.6.3.6.** directly (no variations)

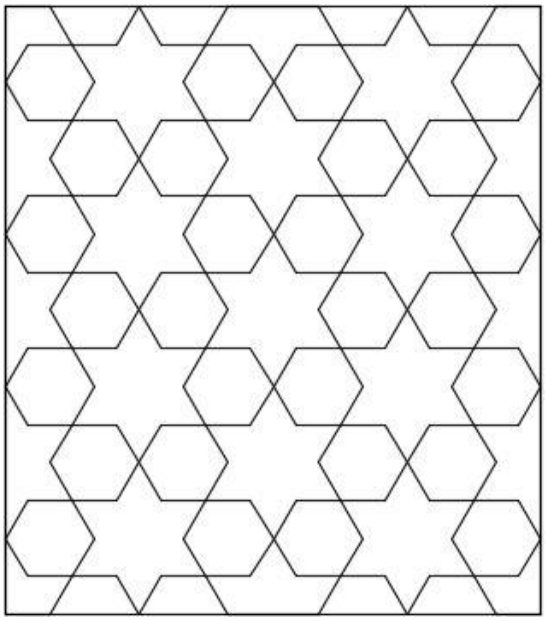

B) GREAT MOSQUE OF DAMASCUS

FIG 3.9 Damascus, Syria (AD 709 / AH 90)[12]

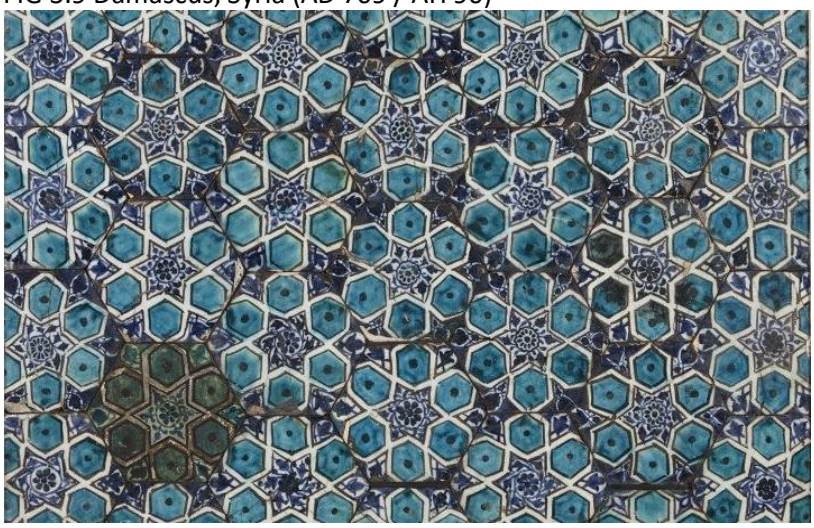

FIG…3.10. Tessellation **6.6.6.** θ =60º

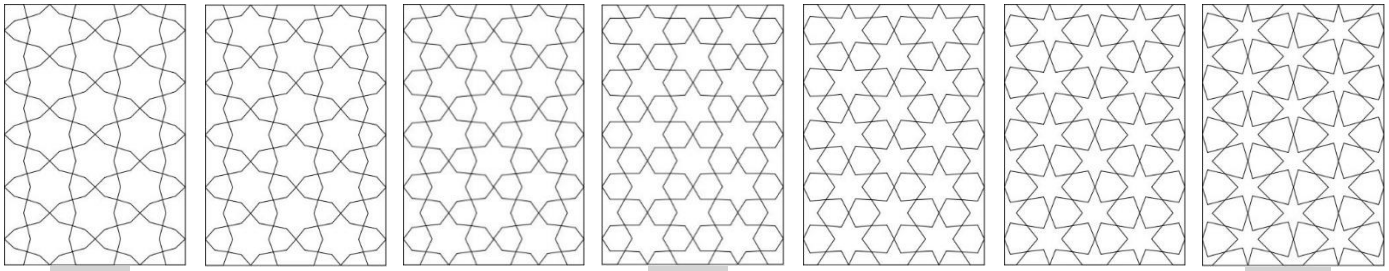

θ= 45º θ= 50º θ= 55º **θ= 60º** θ = 65º θ = 70º θ = 75º

FIG 3.11. Tessellation 6.6.6. parametric variations

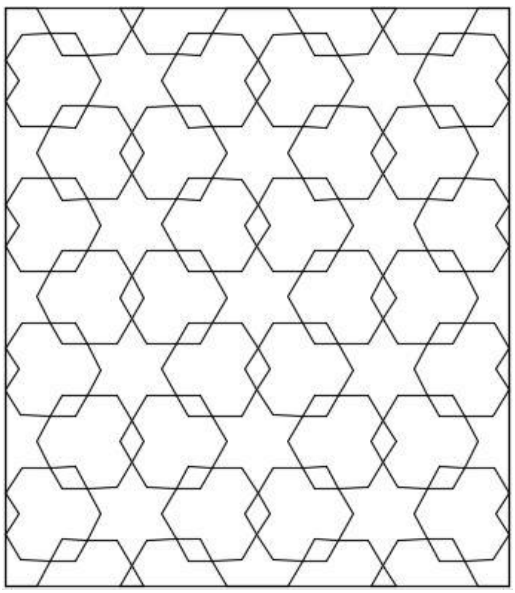

C) SABZ PUSHAN

FIG 3.12. Nishapur, Iran (AD 960 / AH 348)[13]

FIG 3.13. Tessellation **6.6.6** θ =60º, opening distance 35%

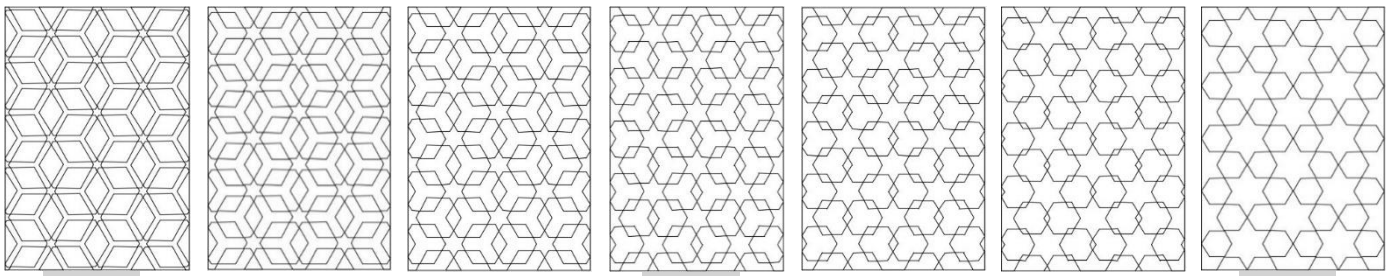

D = 20% D = 25% D = 30% **D = 35%** D = 40% D = 45% D = 50%

FIG 3.14. Tessellation 6.6.6. parametric variations

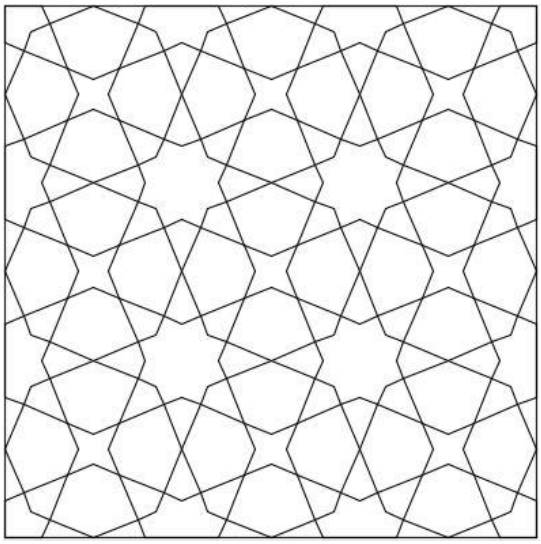

D) LAHORE FORT COMPLEX

FIG 3.15. Punjab, Pakistan (AD 1566 / AH 973)[14]

FIG 3.16. Tessellation **4.8.8.** θ =67.5º

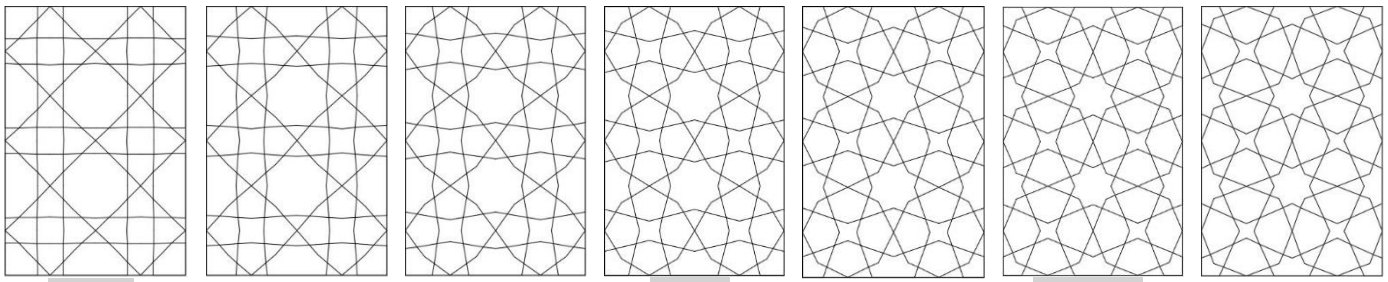

θ = 45º | θ = 50º | θ = 55º | θ =60º | θ = 65º | **θ = 67.5º** | θ = 70º

FIG 3.17. Tessellation 4.8.8. parametric variations

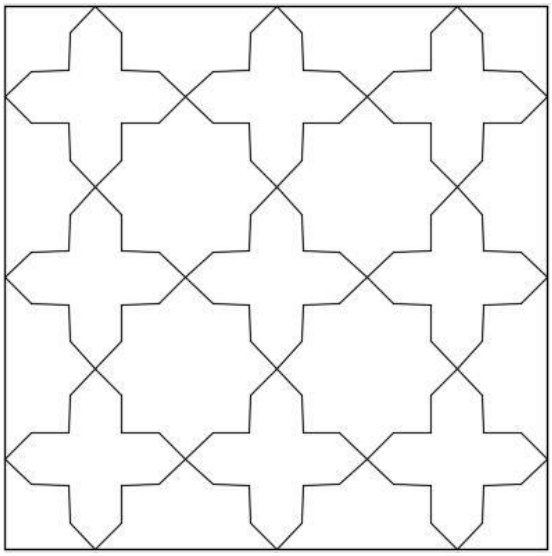

E) PALACE OF THE SHIRVANSHAHS

FIG 3.18. Baku, Azerbaijan (AD 845 / AH 230)[15]

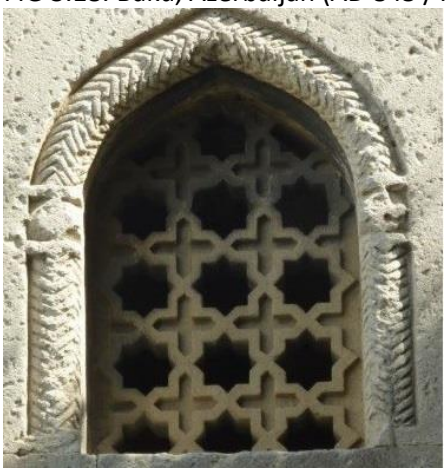

FIG 3.19. Tessellation **4.8.8.** θ =45º, with number of crossings = 0

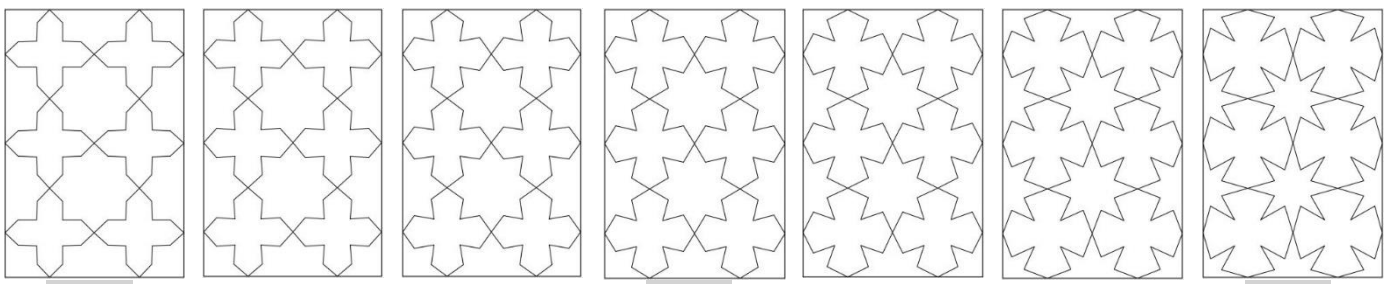

θ = 45º | θ = 50º | θ = 55º | θ = 60º | θ = 65º | θ = 70º | θ = 75º

FIG 3.20. Tessellation 4.8.8.. parametric variations

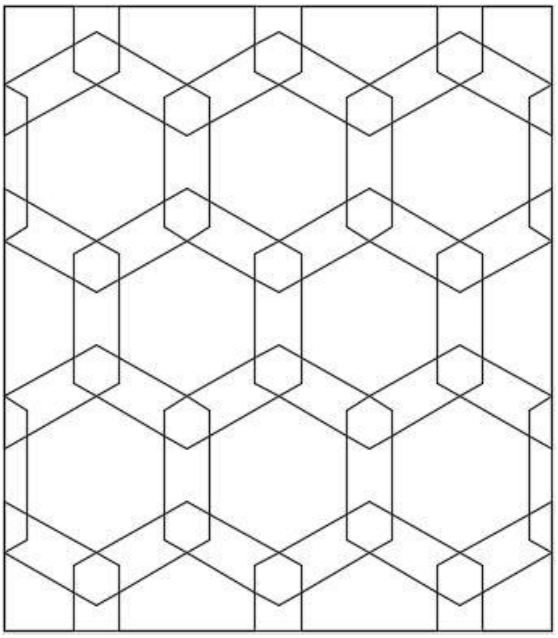

F) MUSTANSIRIYA MADRASA

FIG 3.21. Baghdad, Iraq (AD 1227/ AH 624)[16]

FIG 3.22. Tessellation **3.6.3.6.** θ =30º

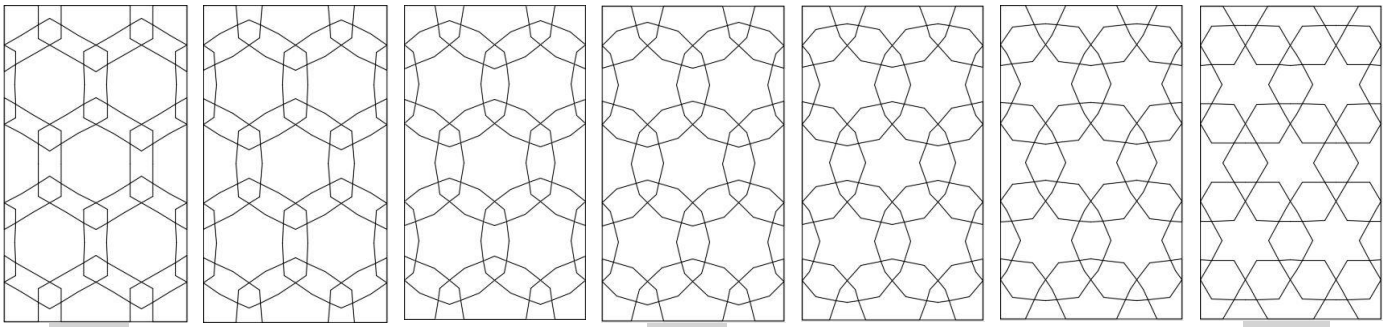

θ= 30º θ= 35º θ= 40º θ= 45º θ = 50º θ = 55º **θ = 60º**

FIG 3.23. Tessellation 3.6.3.6. parametric variations

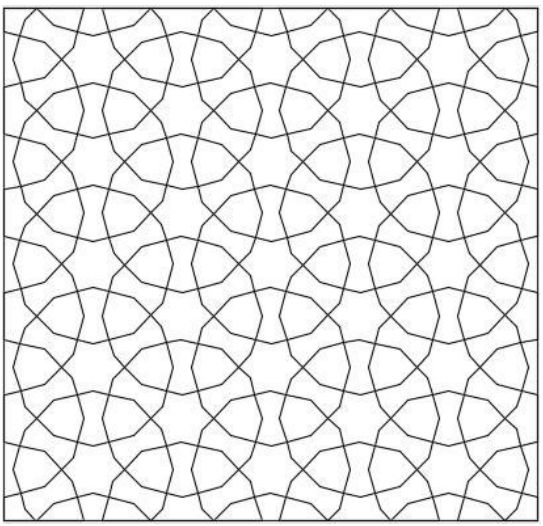

G) TOMB OF SALIM CHISHTI

FIG 3.24. Agra, India (AD 1580 / AH 974)[17]

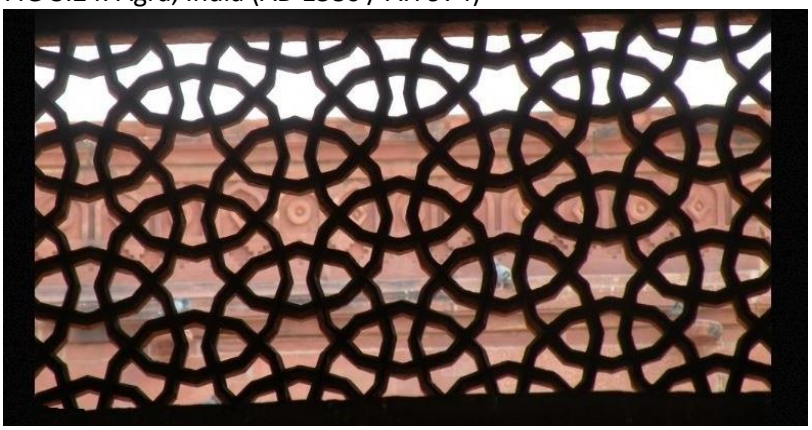

FIG 3.25. Tessellation **6.6.6.** D = 65%, θ =75º

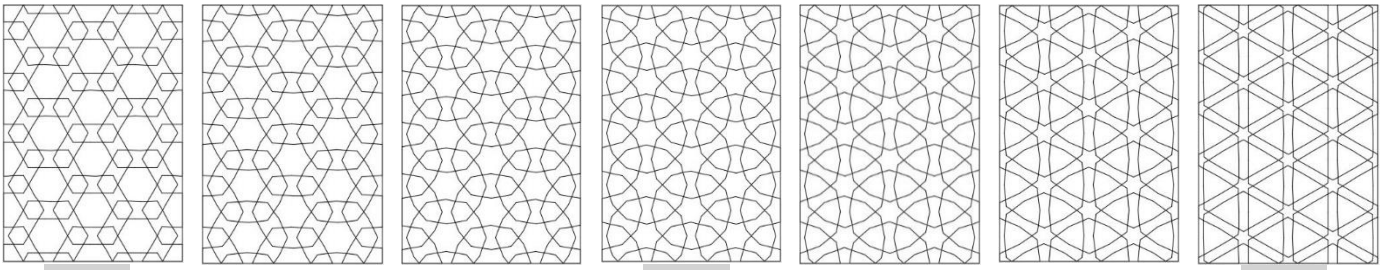

θ = 60º θ = 65º θ = 70º **θ = 75º** θ = 80º θ = 85º θ = 90º

FIG 3.26. Tessellation 6.6.6. D=75%.. parametric variations

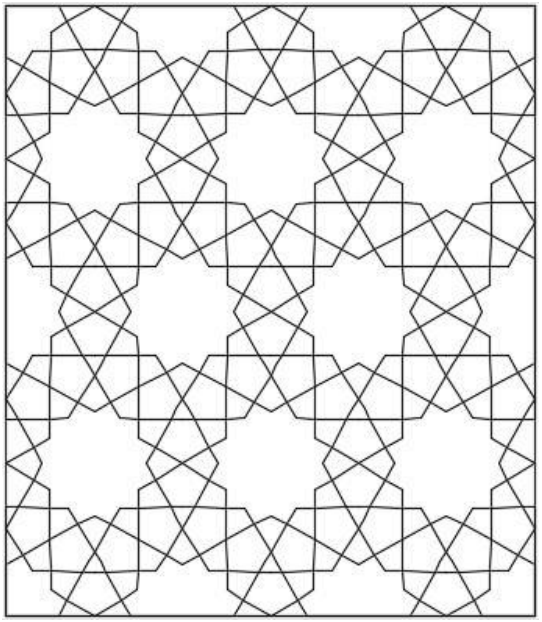

H) GENERALIFE

FIG 3.27. Granada, Spain (AD 1200 / AH 596)[18]

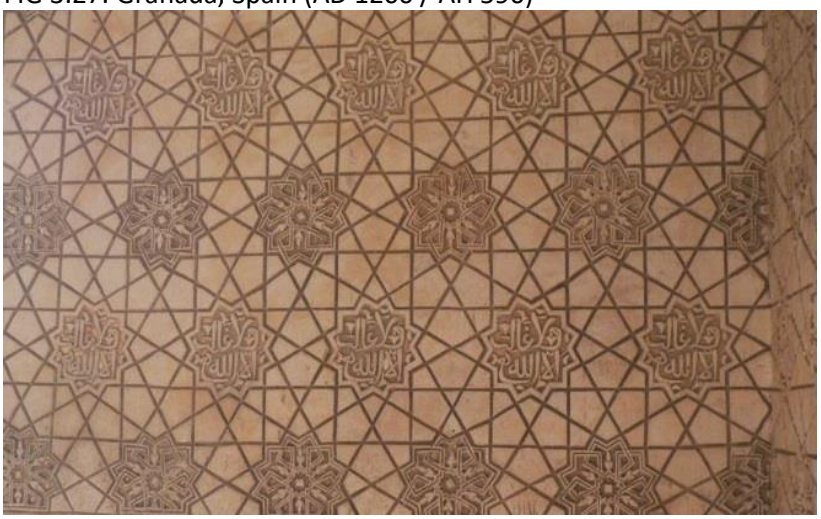

FIG 3.28. Tessellation **3.12.12.** θ =60º

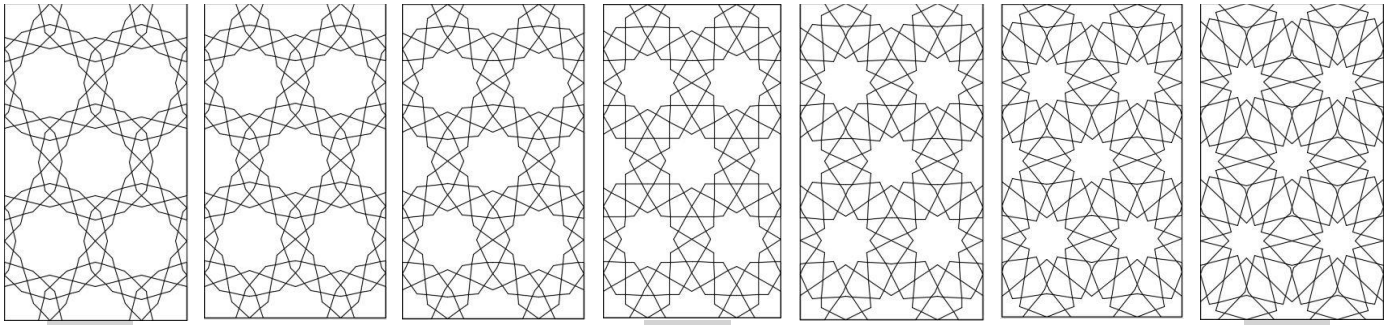

θ = 45º | θ = 50º | θ = 55º | **θ = 60º** | θ = 65º | θ = 70º | θ = 75º

FIG 3.29. Tessellation 3.12.12. parametric variations

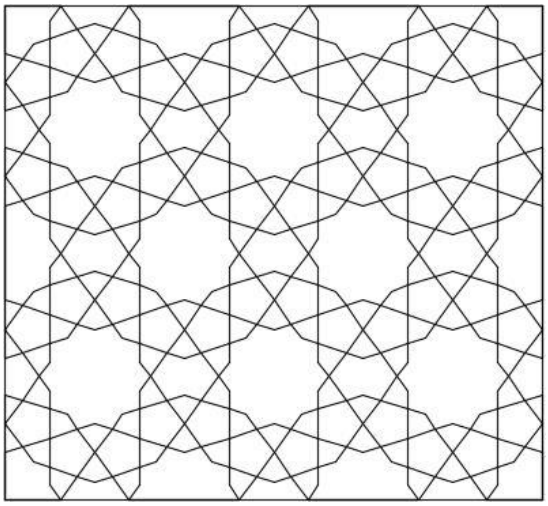

I) HASHT BEHESHT

FIG 3.30. Safavid, Iran (AD 1660 / AH 1054)[19]

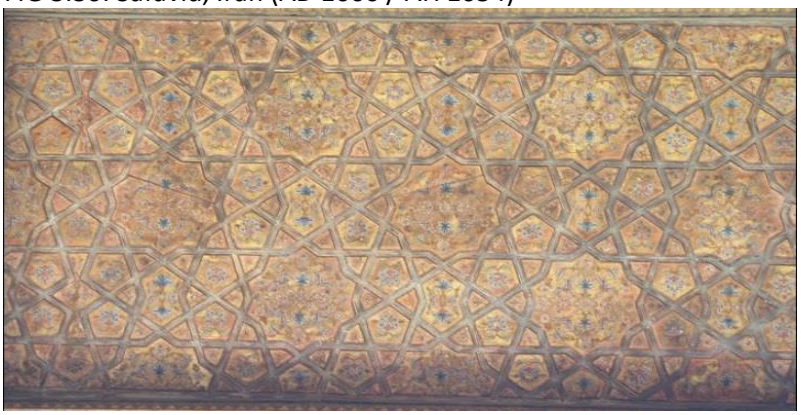

FIG 3.31. Tessellation **I-6.10.10.** θ =54º

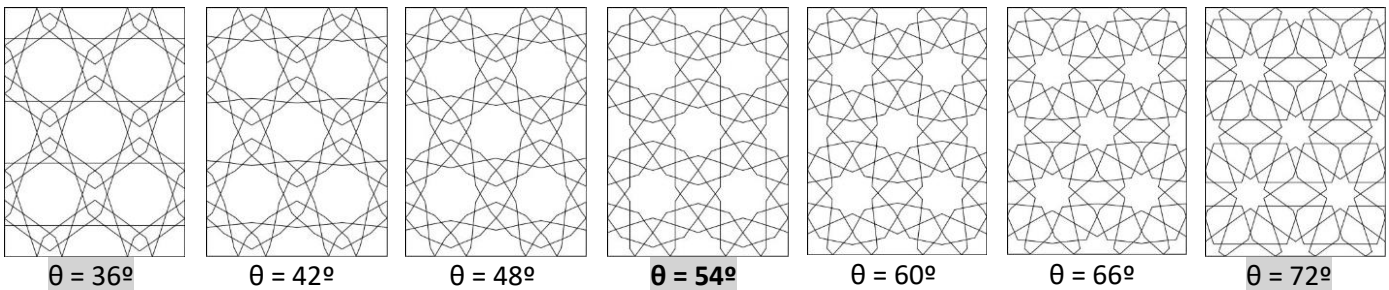

θ = 36º | θ = 42º | θ = 48º | **θ = 54º** | θ = 60º | θ = 66º | θ = 72º

FIG 3.32. Tessellation I-6.101.10. parametric variations

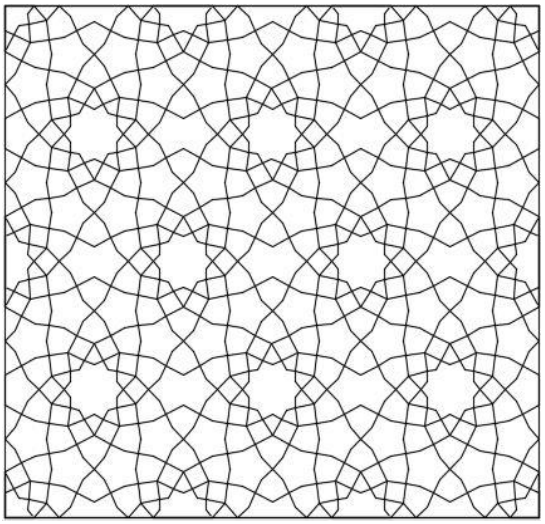

J) MODARI-KHAN MADRASH

FIG 3.33. Bukhara, Uzbekistan (AD 1567 / AH 948)[20]

FIG 3.34. Tessellation **ROS-I-6.10.10.** $\theta_1 = 45º$, $\theta_2 = 60º$, type Star

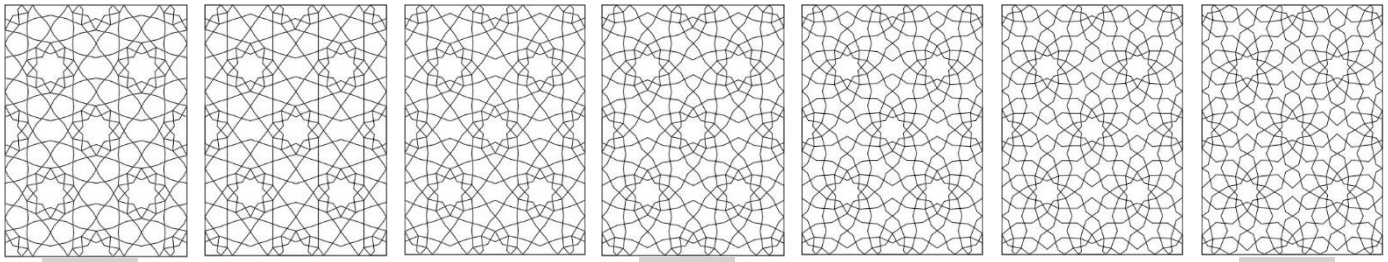

$\theta_1 = 30º$ $\theta_1 = 35º$ $\theta_1 = 40º$ **$\theta_1 = 45º$** $\theta_1 = 50º$ $\theta_1 = 55º$ $\theta_1 = 60º$

FIG 3.35. Tessellation ROS-I-6.10.10. parametric variations

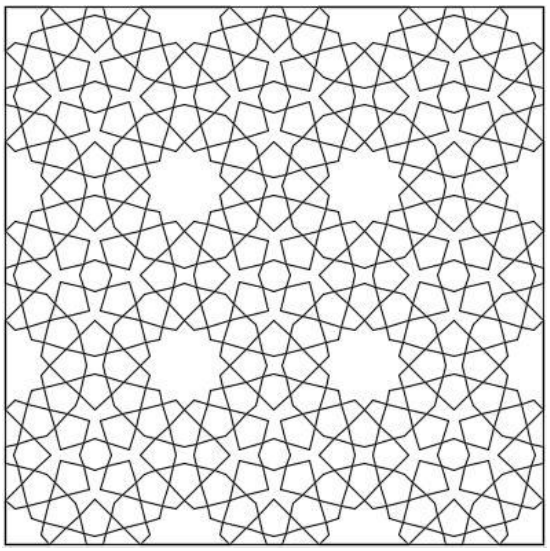

K) COMPLEX OF SULTAN BAYEZID II

FIG 3.36. Edirne, Turkey (AD 1488 / AH 893)[21]

FIG 3.37. Tessellation **ROS-3.4.3.12_3.12.12.** θ =60º, type Bayezid

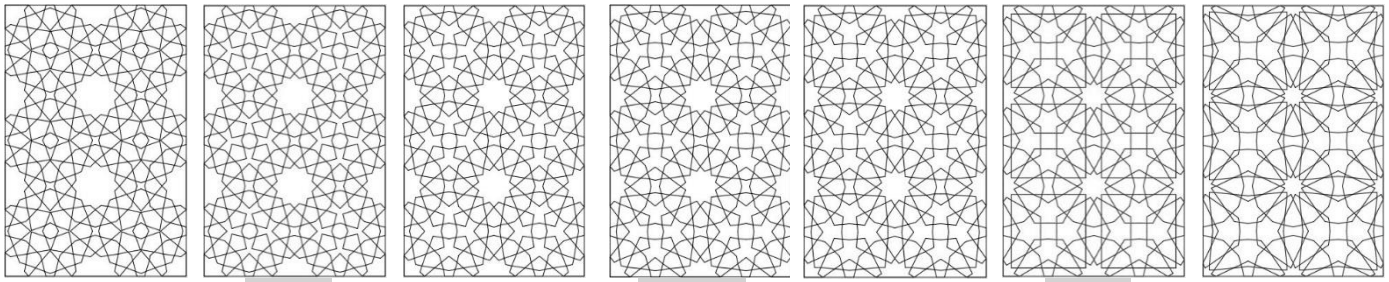

θ = 55º **θ = 60º** θ = 65º θ = 67.5º θ = 70º θ = 75º θ = 80º

FIG 3.38. Tessellation ROS-3.4.3.12_3.12.12. parametric variations

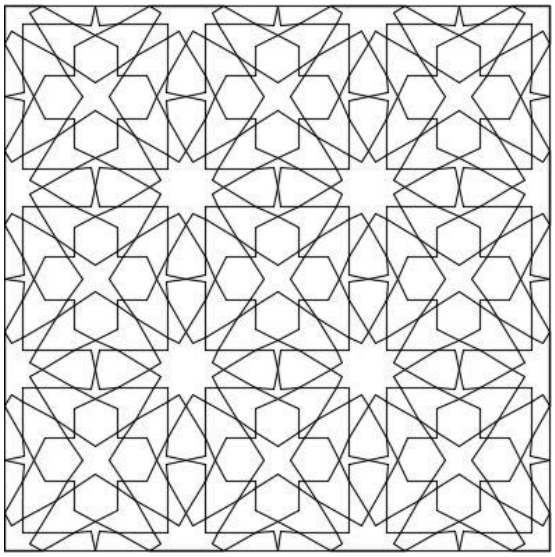

L) BEN YUSUF MADRASA

FIG 3.39. Marrakesh, Morocco (AD 1564 / AH 971)[22]

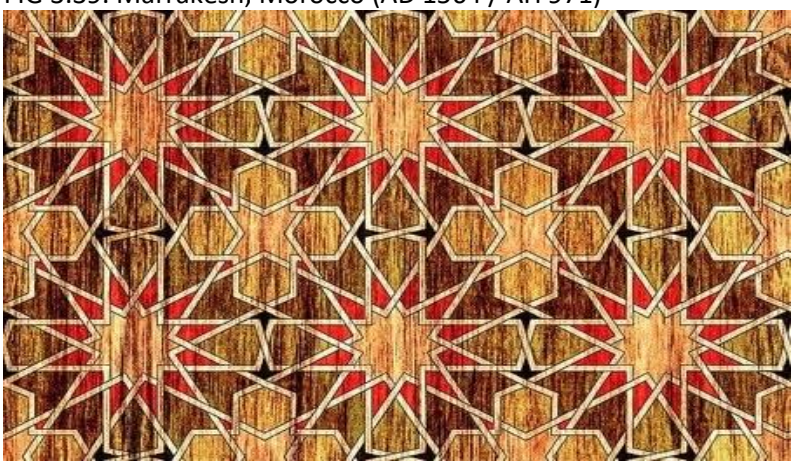

FIG 3.40. Tessellation **ROS-3.4.3.12_3.12.12.** θ_1 =78.5º, type Arrow

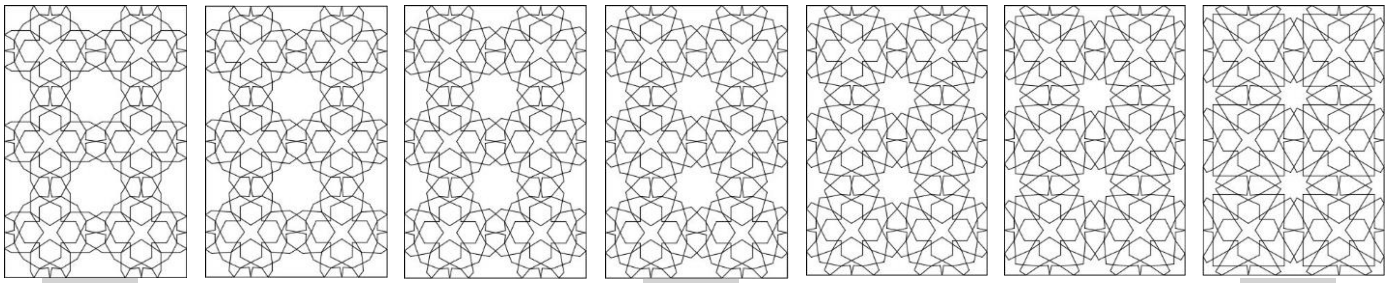

θ_2 = 45º | θ_2 = 50º | θ_2 = 55º | θ_2 = 60º | θ_2 = 65º | θ_2 = 70º | **θ_2 = 75º**

FIG 3.41. Tessellation ROS-3.4.3.12_3.12.12. parametric variations

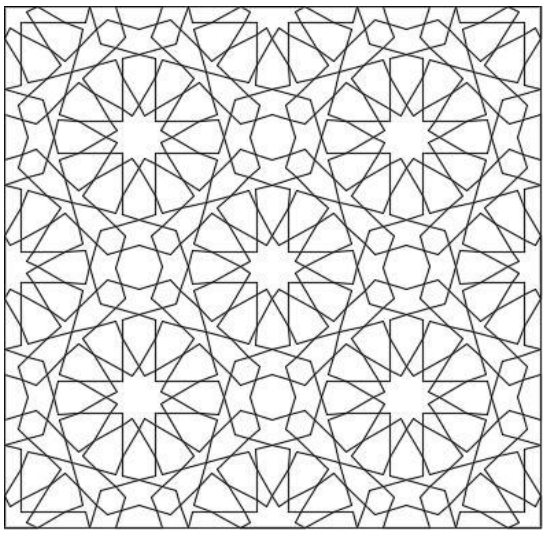

M) MOSQUE OF AL-NASIR MUHAMMAD'S MINBAR

FIG 3.42. Cairo, Egypt (AD 1318 / AH 717)[23]

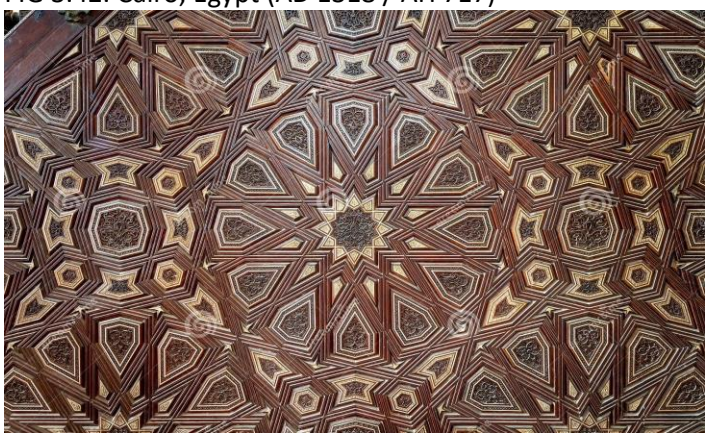

FIG 3.43. Tessellation **ROS-I-6.12.8.12.** θ =75º, L =20%, type Arrow

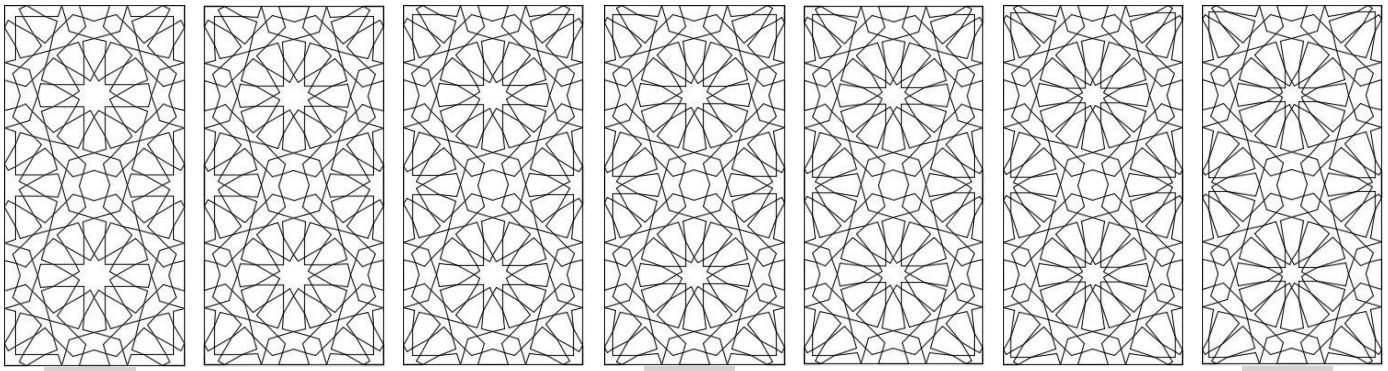

L = 20% | L = 25% | L = 30% | L = 35% | L = 40% | L = 45% | L = 50%

FIG 3.44. Tessellation ROS-I-6.12.8.12. parametric variations

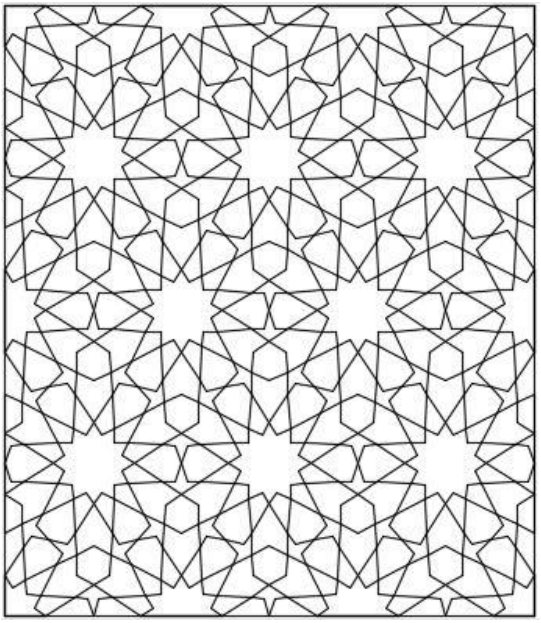

N) MOSQUE OF AL-NASIR MUHAMMAD

FIG 3.45. Cairo, Egypt (AD 1318 / AH 717)[24]

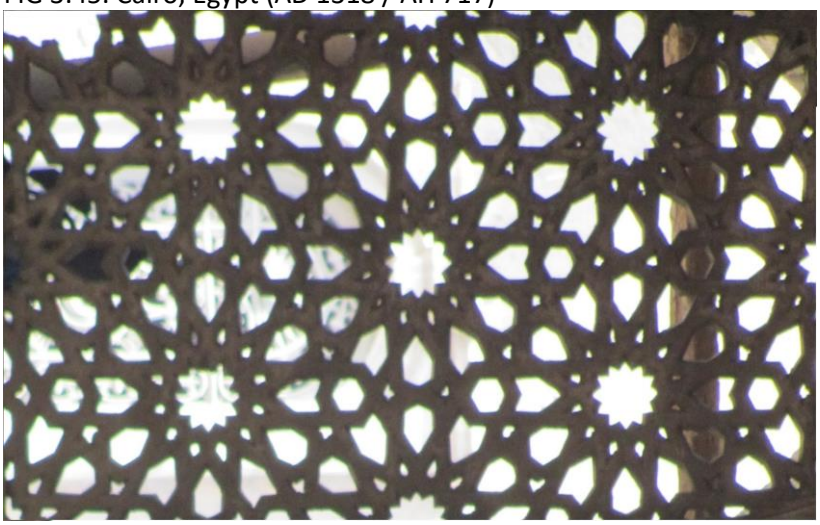

FIG 3.46. Tessellation **ROS-3.12.12.** θ =75º, type Arrow

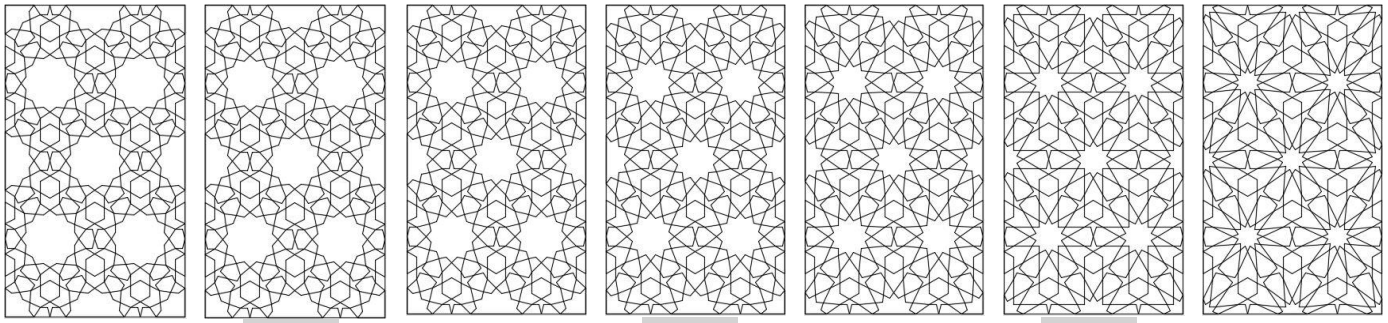

θ_2 = 50º | θ_2 = 55º | θ_2 = 60º | θ_2 = 65º | θ_2 = 70º | **θ_2 = 75º** | θ_2 = 80º

FIG 3.47. Tessellation ROS-3.12.12 parametric variations

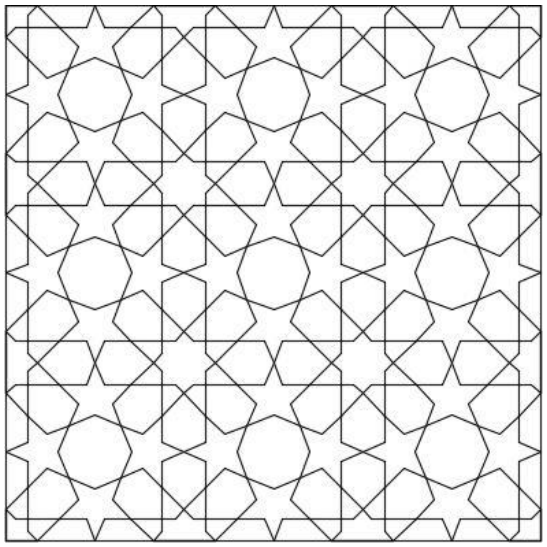

O) GREAT MOSQUE OF HERAT

FIG 3.48. Herat, Afghanistan (AD 1200 / AH 596)[25]

FIG 3.49. Tessellation **ROS-4.8.8.** θ =67.5º, L =30%

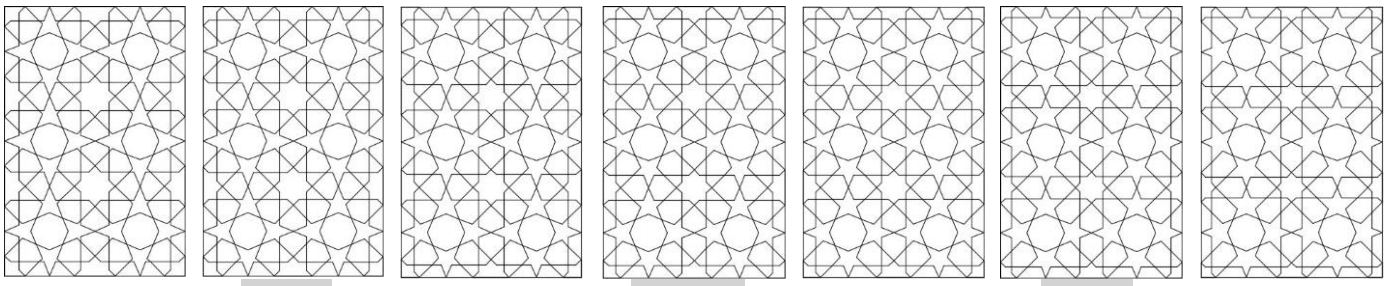

L = 10% | L = 15% | L = 20% | L = 22.5% | L = 25% | **L = 30%** | L = 35%

FIG 3.50. Tessellation ROS-4.8.8. parametric variations

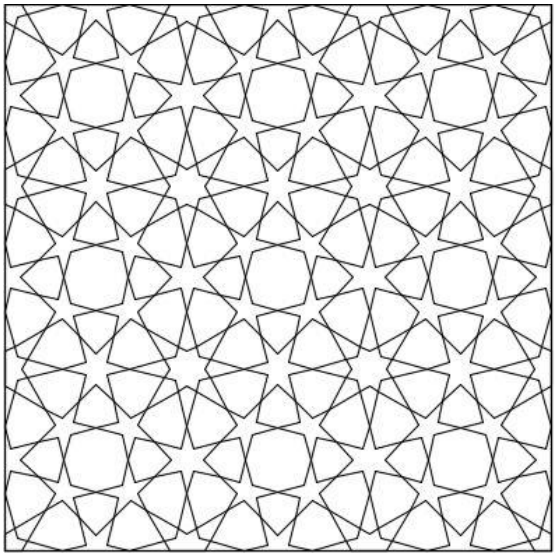

P) MOSQUE OF AL-SALIH TALA'I FIG 3.51. Cairo (AD 1160/AH 554)[26]

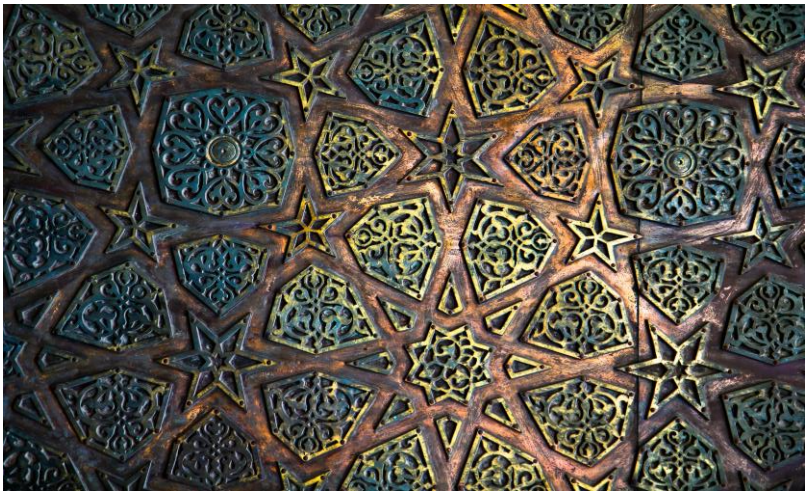

FIG 3.52. Tessellation **ROS-3.4.3.8_3.8.8.** θ =75º, L = 25% type Star

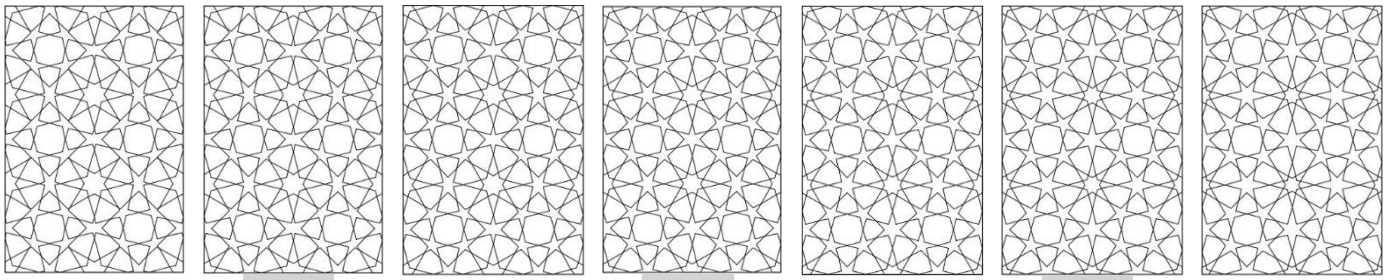

L = 10% | L = 15% | L = 20% | **L = 25%** | L = 30% | L = 35% | L = 40%

FIG 3.53.Tessellation ROS-3.4.3.8_3.8.8. parametric variations

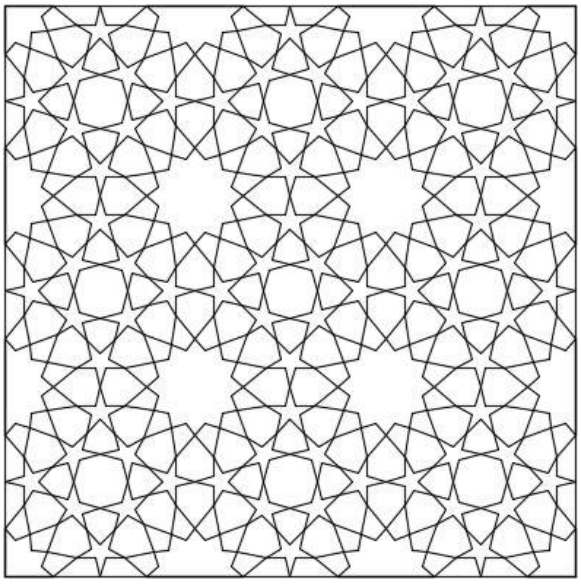

Q) MOSQUE OF IBN TULUN FIG 3.54. Egypt (AD 884/AH 278)[27]

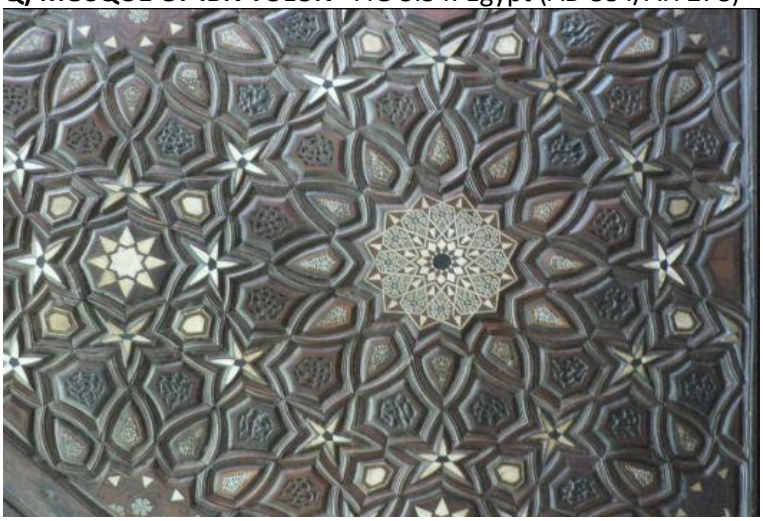

FIG 3.55. Tessellation **ROS-3.4.3.12_3.12.12.** θ_1=75º, θ_2=65º, Star

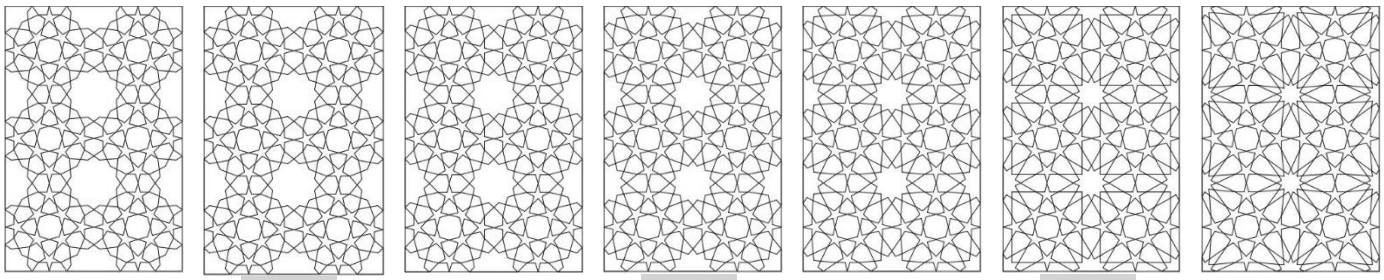

θ_2 = 50º | θ_2 = 55º | θ_2 = 60º | **θ_2 = 65º** | θ_2 = 70º | θ_2 = 75º | θ_2 = 80º

FIG 3.56. Tessellation ROS-3.4.3.12_3.12.12. parametric variations

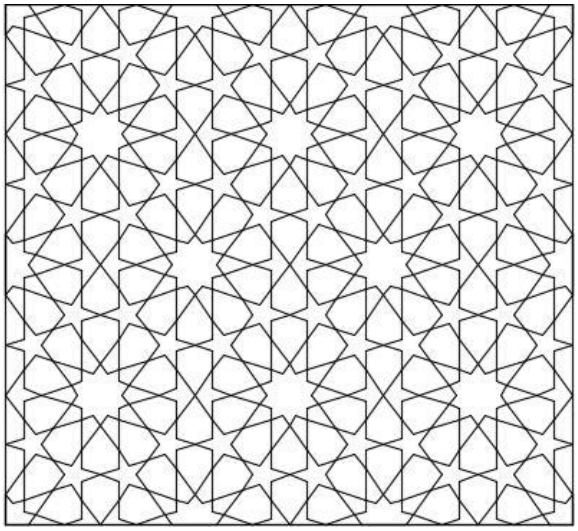

R) FATEHPUR SIKRI COMPLEX

FIG 3.57. Agra, India (AD 1580 / AH 974)[28]

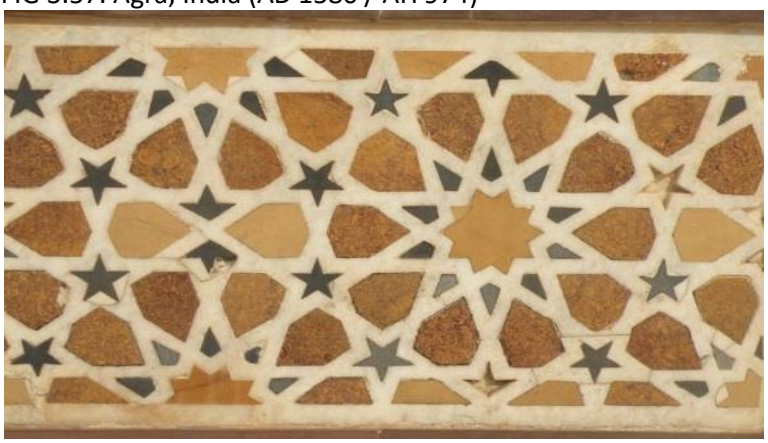

FIG 3.58. Tessellation **ROS-I-6.10.10.** θ =72º type Star

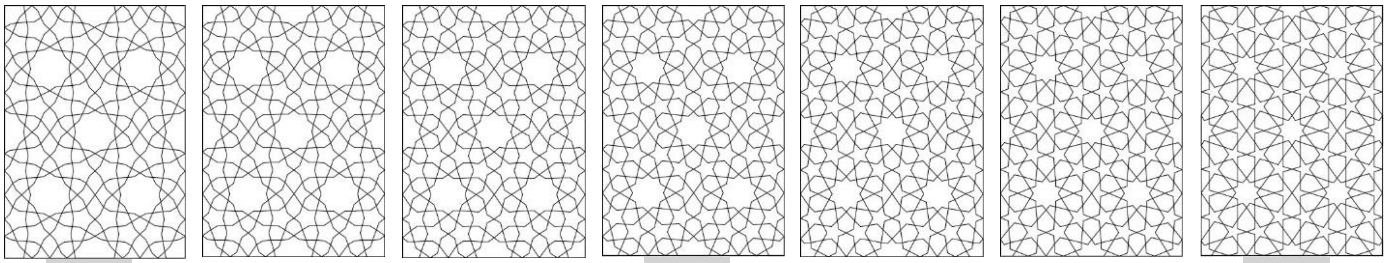

θ = 48º θ = 52º θ = 56º θ = 60º θ = 64º θ = 68º **θ = 72º**

FIG 3.59. Tessellation ROS-I-6.10.10. parametric variations

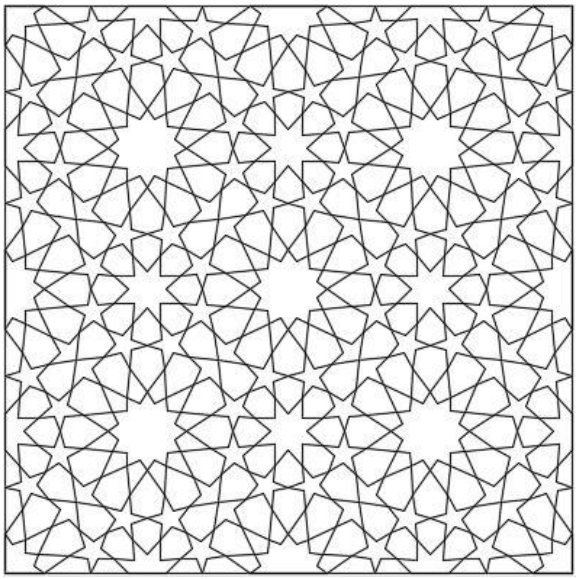

S) JAMEH MOSQUE

FIG 3.60. Yazd, Iran (AD 1324 / AH 729)[29]

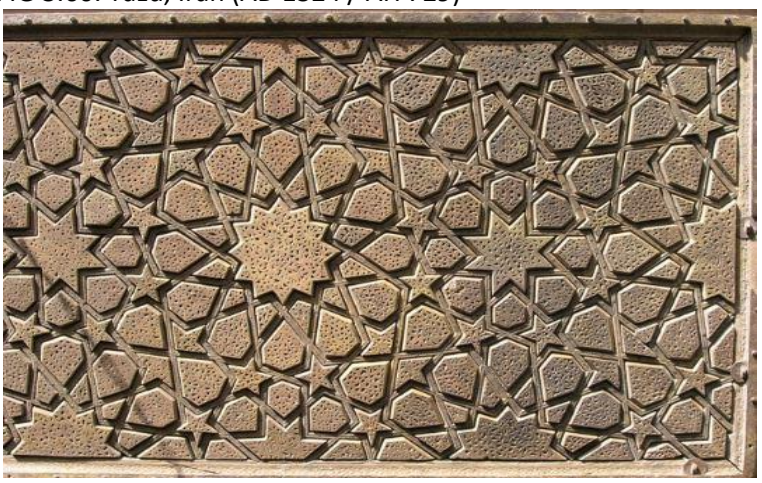

FIG 3.61. Tessellation **ROS-I-6.12.8.12.** θ=67.5º, L=20%, Type Star

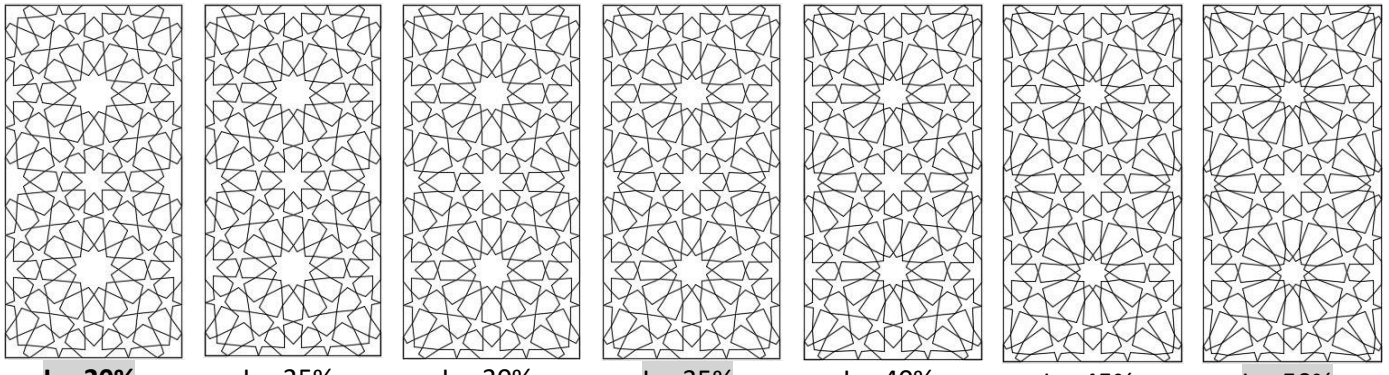

L = 20% L = 25% L = 30% L = 35% L = 40% L = 45% L = 50%

FIG 3.62. Tessellation ROS-I-6.12.8.12. parametric variations

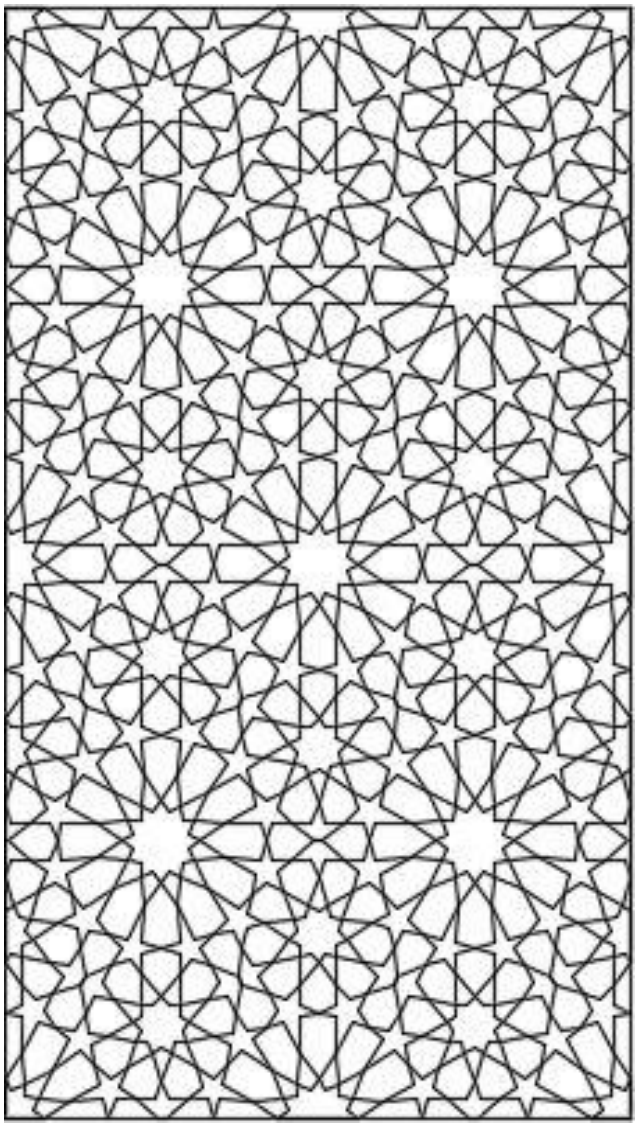

T) ALHAMBRA

FIG 3.63. Granada, Spain (AD 889 / AH 284)[30]

FIG 3.64. **Alhambra.** Tessellation **ROS-I-6.9.12.9.**θ=70º, L=35%

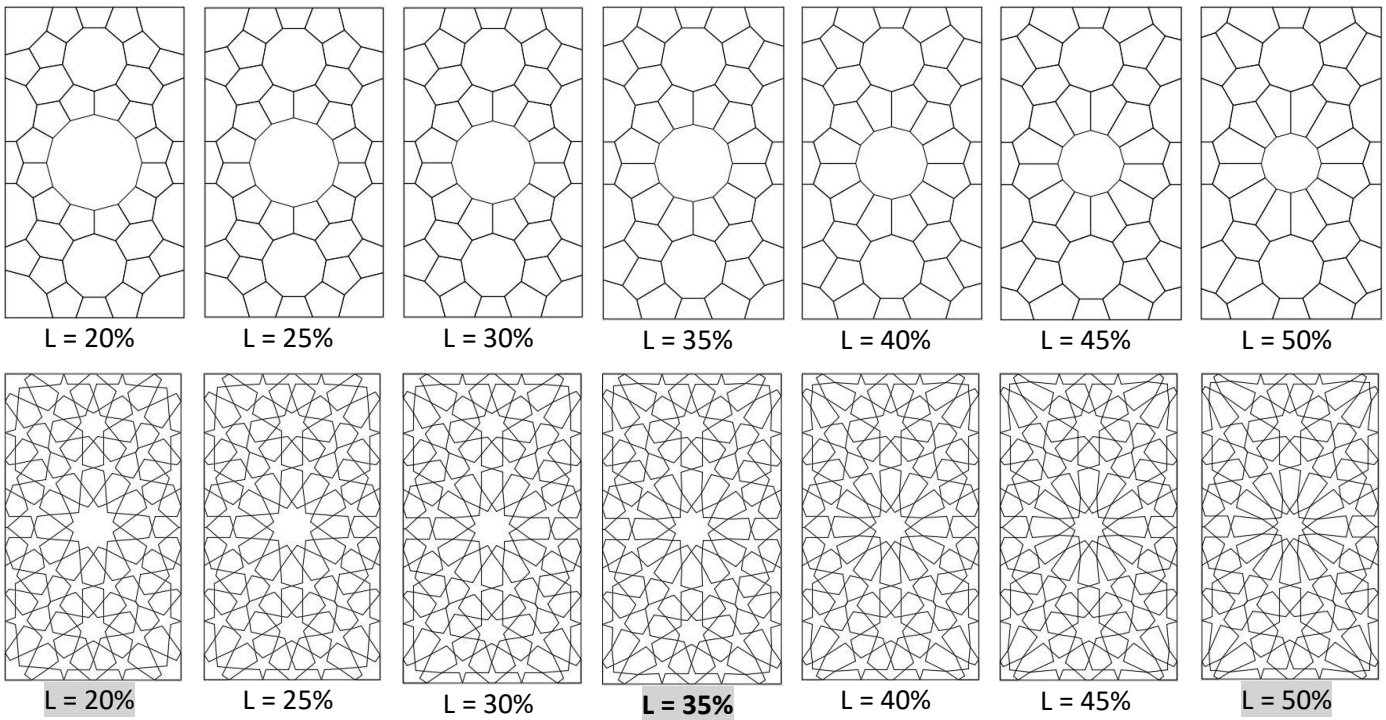

FIG 3.65. Tessellation ROS-I-6.9.12.9. parametric variations

3.4. TESSELLATION DEFINITION AND APPLICATION

Regular tiling: The tessellations in this group are characterized by being composed of only one regular polygon that is repeated symmetrically edge-to-edge to fill the plane. There must be six equilateral triangles, four squares or three regular hexagons at a vertex. In this document only the tessellation 6.6.6. is used for the patterns Great Mosque of Damascus variation (B75), Sabz Pushan (C) and Tomb of Salim Chishti (N).

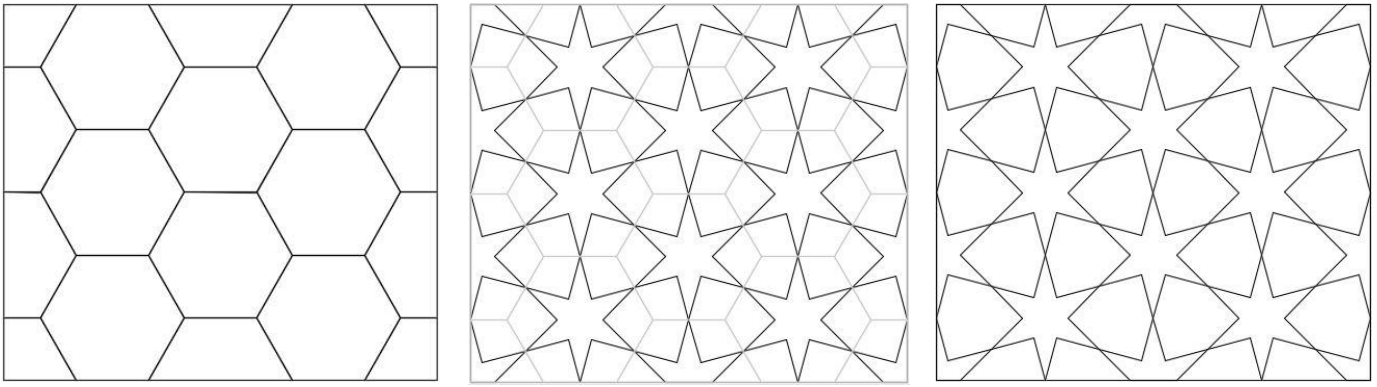

FIG 3.66. Tessellation 6.6.6. for Great Mosque of Damascus (B)

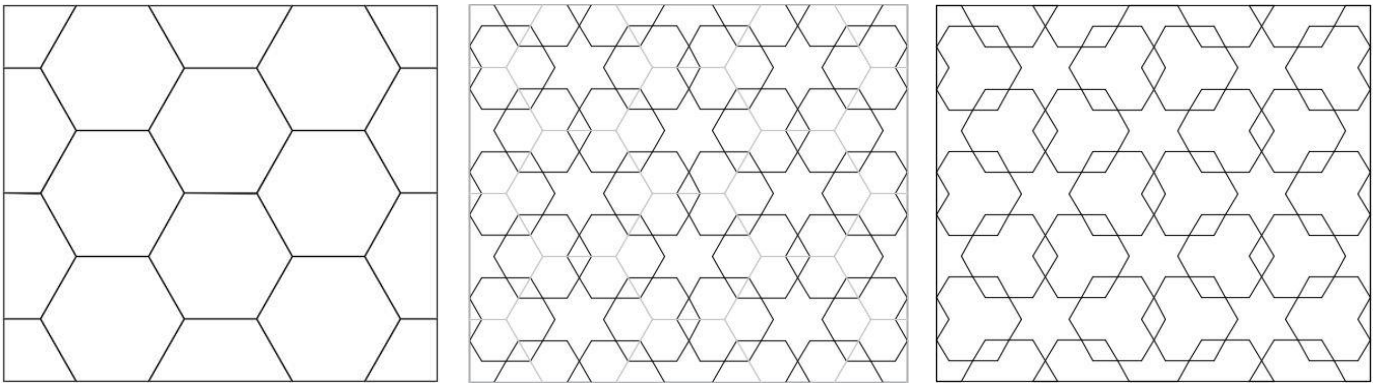

FIG 3.67. Tessellation 6.6.6. for Sabz Pushan (C)

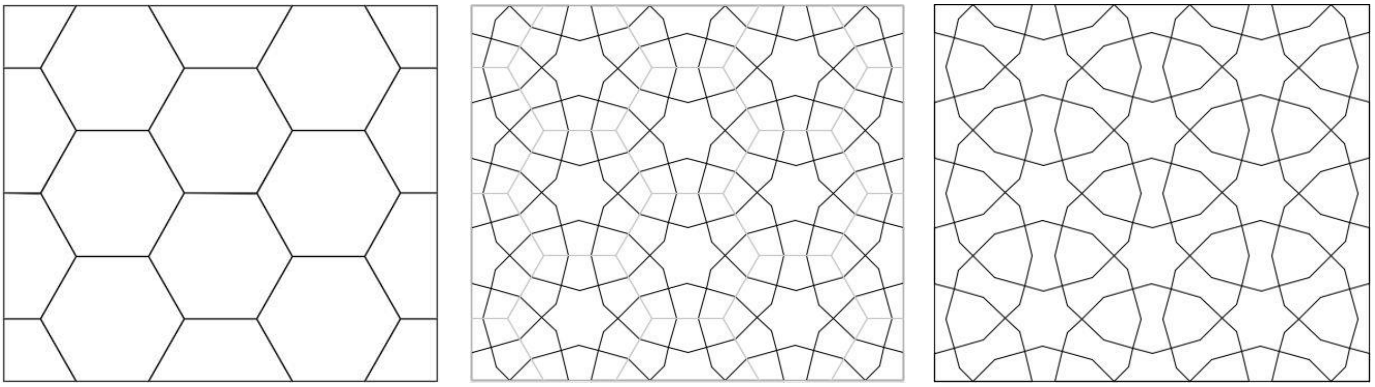

FIG 3.68. Tessellation 6.6.6. for Tomb of Salim Chishi (N)

See that the patterns Sabz Pushan (C) and Tomb of Salim Chisthi (N) are obtained from the tessellation 6.6.6. applying a variation of the Hankin method in which the opening angle is not applied at the same point in the centre of the polygon sides but with a gap.

Semiregular tiling: The tessellations in this group are characterized by being composed of more than one regular polygon that are disposed around a common vertex. There are 8 different semiregular tiling, but in this document it is only used the tessellations 3.6.3.6. for the pattern Mustansiriya Madrasa (F), the tessellation 3.12.12. for the tessellation Generalife (H) pattern and 4.8.8. for Lahore Fort Complex (D) and Palace of the Shirvanshahs (E) patterns. See that Palace of the Shirvanshahs (E) pattern uses a variation of the Hankin method in which not all the polygons (in this case the squares) are filled.

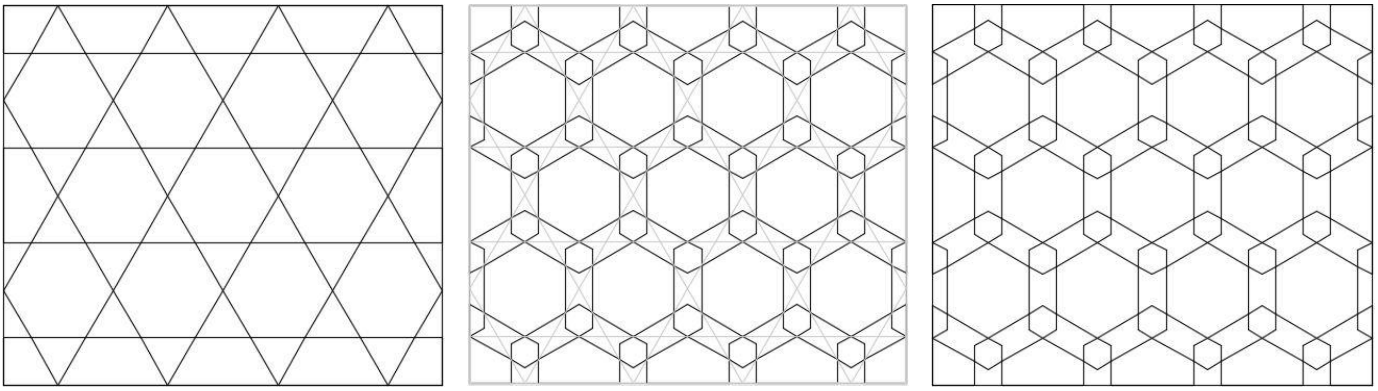

FIG 3.69. Tessellation 3.6.3.6. for Mustansiriya Madrasa (F)

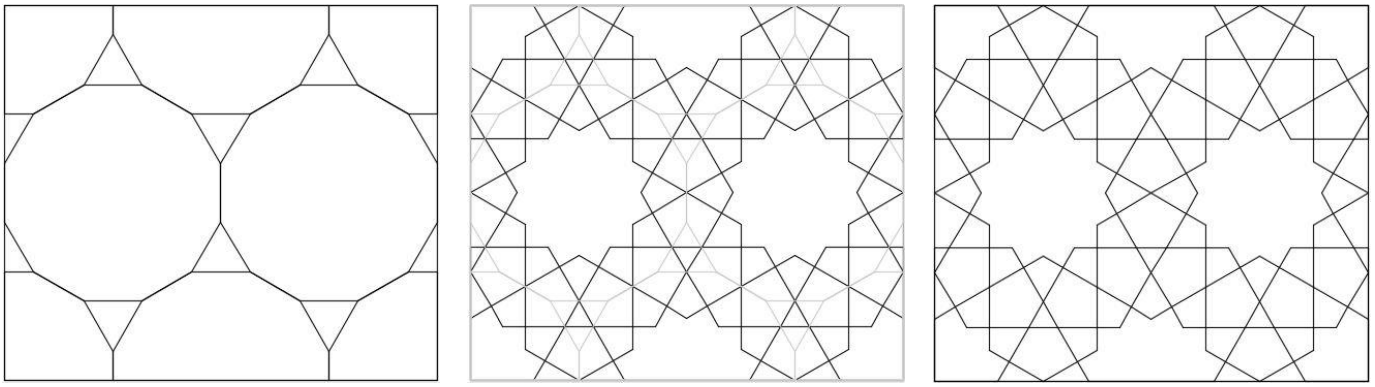

FIG 3.70. Tessellation 3.12.12. for Generalife (H)

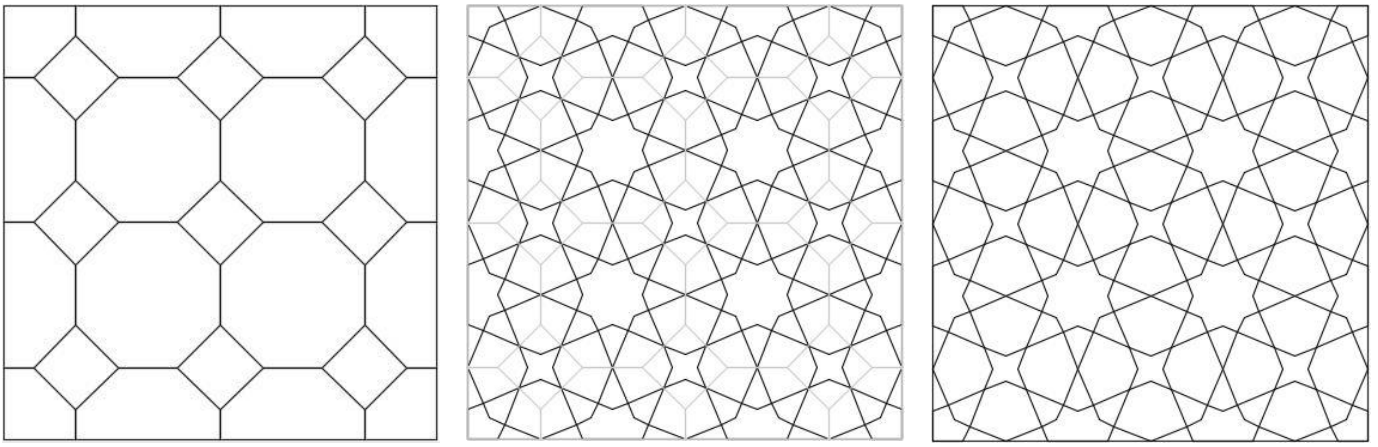

FIG 3.71. Tessellation 4.8.8. for Lahore Fort Complex (D)

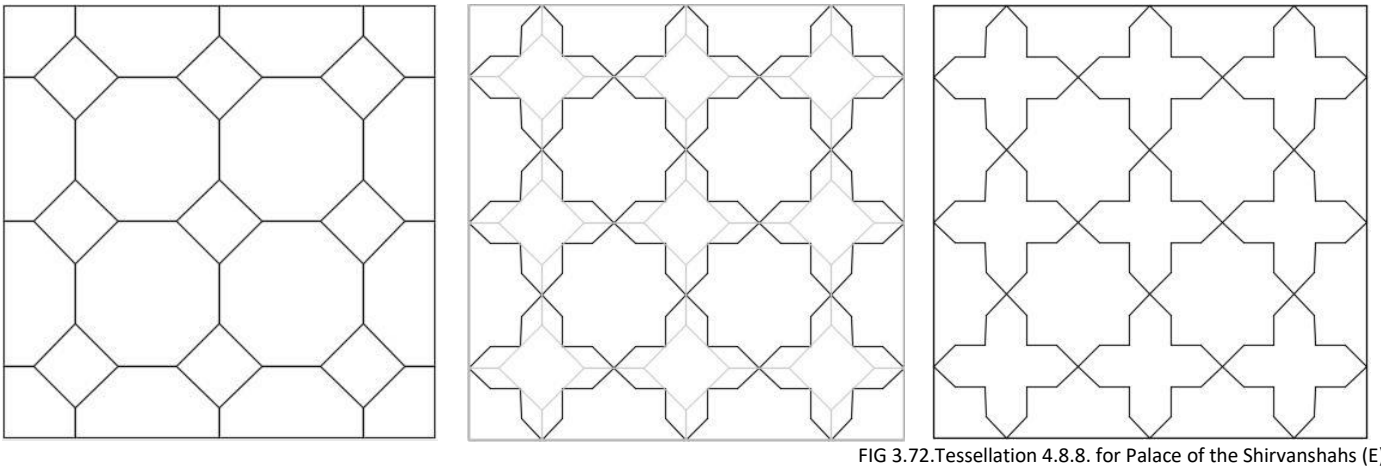

FIG 3.72.Tessellation 4.8.8. for Palace of the Shirvanshahs (E)

Irregular tiling: Characterized by one or more irregular polygons disposed around a common vertex. Only tessellations with regular polygons combined with concave hexagons have been studied. Several irregular tessellations are used indirectly with Rosette transforms, but only the tessellation I-6.10.10 is used unaltered for Hasht Behesht (I) pattern. The prefix "I-" in the tessellation's name is introduced to indicate that it contains irregular polygons.

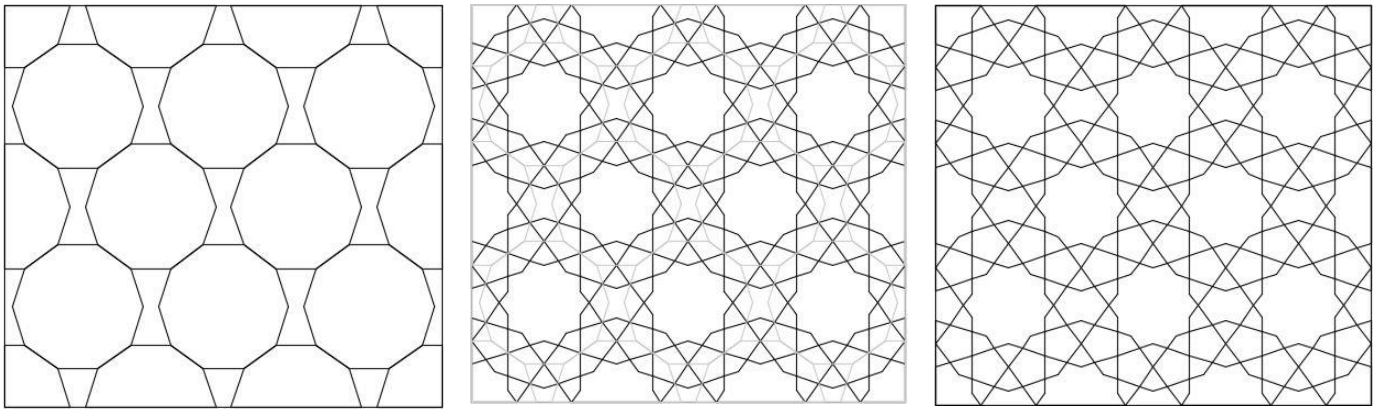

FIG 3.73. Tessellation I-6.10.10. for Hasht Behesht (I)

Periodic tiling: characterized by regular polygons whose disposition varies depending on the vertex under consideration. In this document such tilings are not directly applied but are used in conjunction with the Rosette transform to obtain other higher order tessellations. The periodic tilings employed are 1-orbit periodic, meaning that the polygons disposition is repeated in alternative vertices. Depending on the considered vertex, there are two possible names for the given tessellation. Both possibilities are included in the complete name, as in P-3.4.3.8_3.8.8. and P-3.4.3.12_3.12.12. The prefix "P-" is introduced to indicate that it is a periodic tessellation.

Rosette transform: It is an algorithm applied to other tessellations in order to modify them and generate new tessellations. The transformation consists on adding pentagons or hexagons in the perimeter of the polygons to create a higher order tessellation. The following pictures show the application of the rosette transform to the tessellations 3.12.12. 4.8.8., I-6.9.12.9., I-6.10.10. I-6.12.8.12., P-3.4.3.8_3.8.8. and P-3.4.3.12_3.12.12.

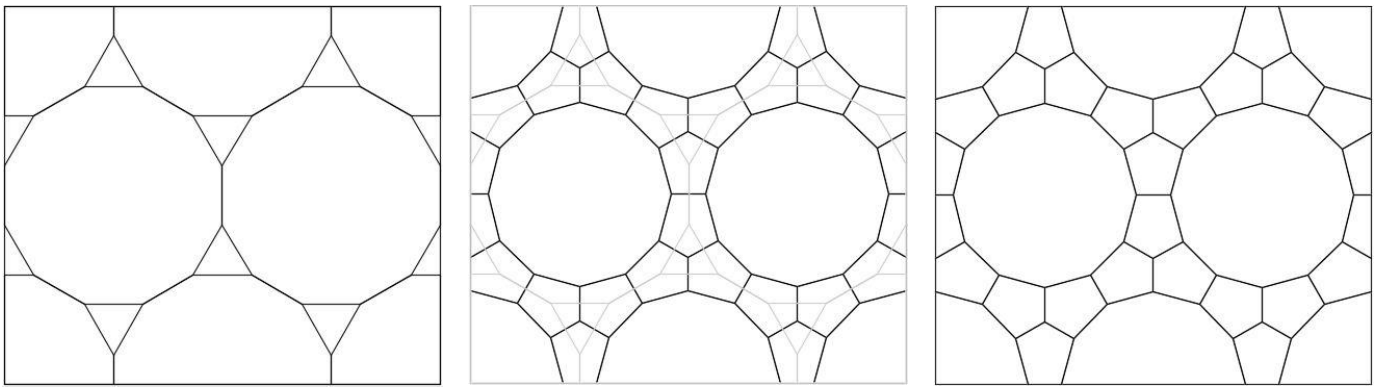

FIG 3.74. Rosette transform applied to tessellation 3.12.12.

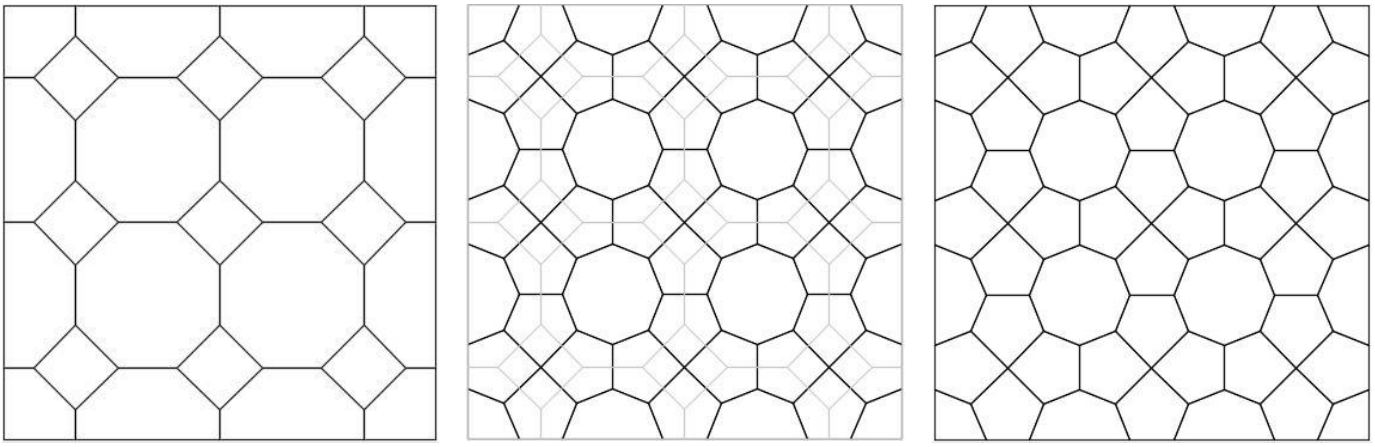

FIG 3.75. Rosette transform applied to tessellation 4.8.8.

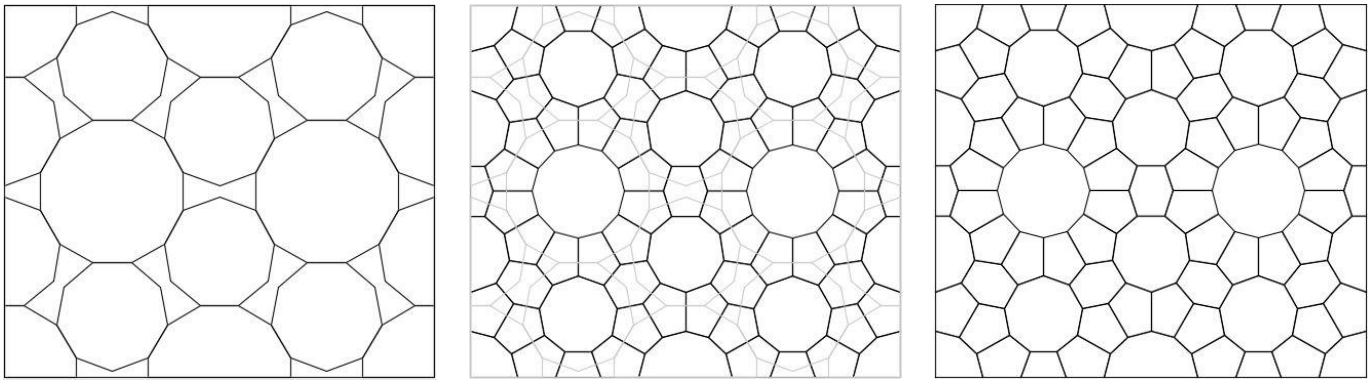

FIG 3.76. Rosette transform applied to tessellation I-6.9.12.9.

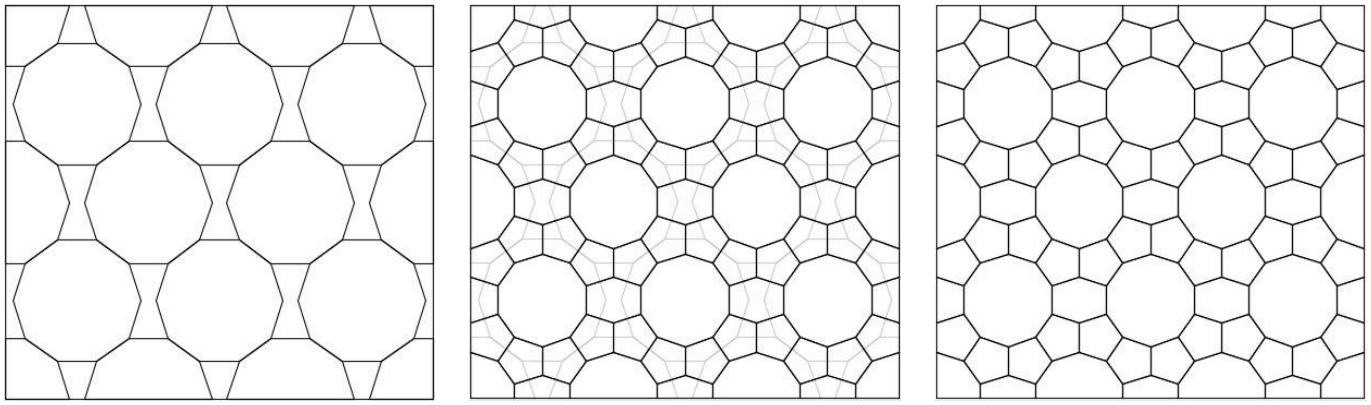

FIG 3.77. Rosette transform applied to tessellation I-6.10.10.

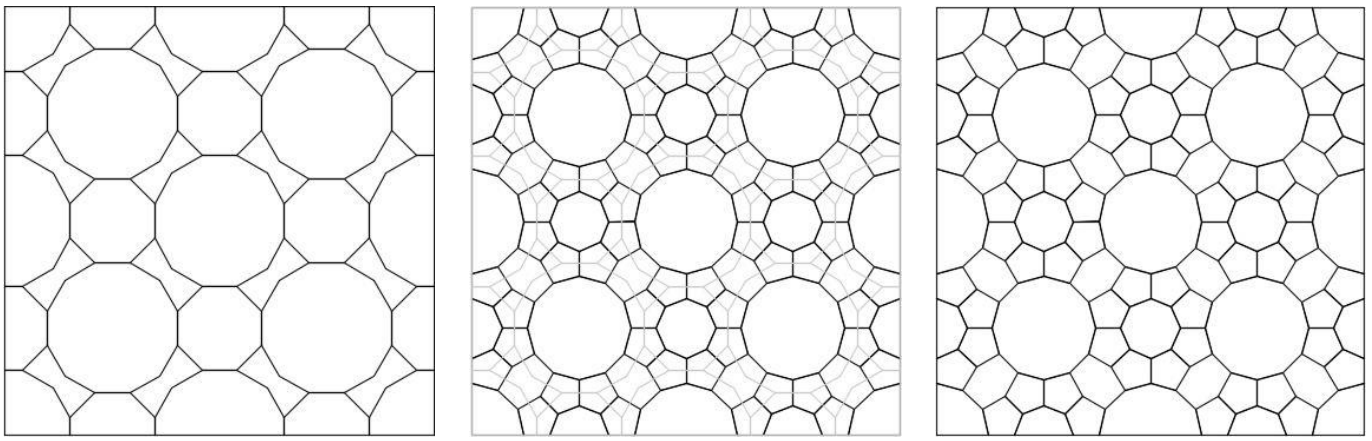

FIG 3.78. Rosette transform applied to tessellation I-6.12.8.12.

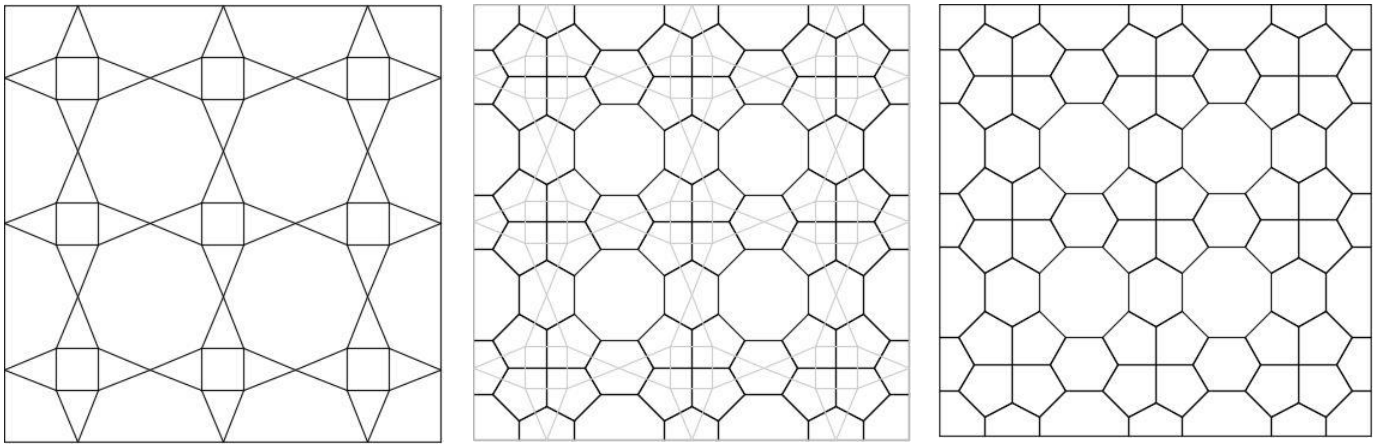

FIG 3.79.Rosette transform applied to tessellation P-3.4.3.8_3.8.8.

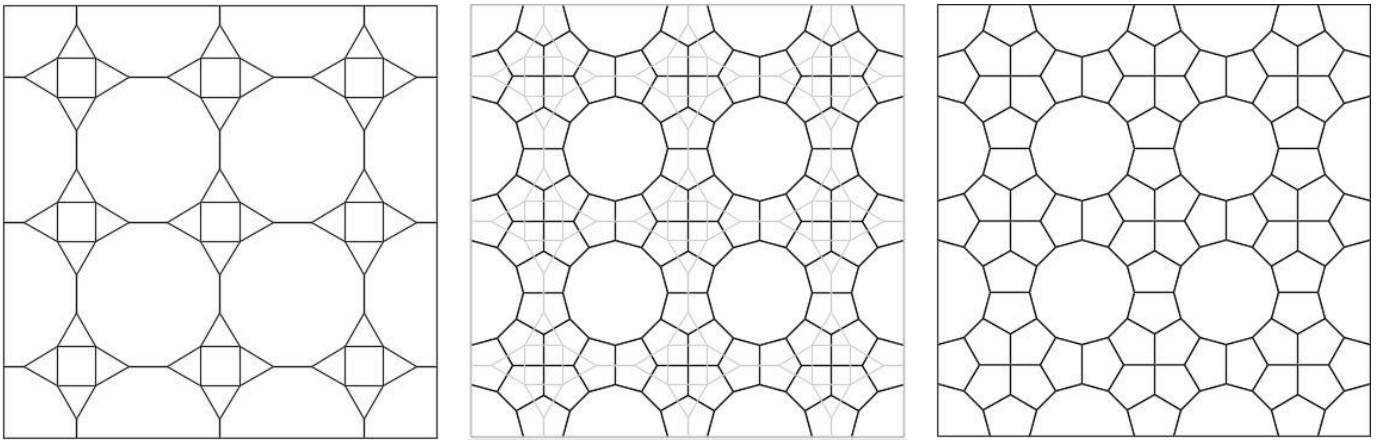

FIG 3.80. Rosette transform applied to tessellation P-3.4.3.12_3.12.12.

ROS-3.12.12. for Mosque of Al-Nasir Muhammad (N), ROS-4.8.8. for Great Mosque of Herat (O), ROS-I-6.9.12.9. for Alhambra (T), ROS-I-6.10.10 for Modari-Khan Madrash (J) and Fatehpur Sikri(R), ROS-I-6.12.8.12. for Al-Nasir Muhammad's Minbar (M) and Jameh Mosque (S), ROS-P3.4.3.8_3.8.8. for Mosque of Al-Salih Tala'I (P), ROS-P3.4.3.12_3.12.12. for Sultan Bayezid II (K), Ben Yusuf Madrasa (L) and Mosque of Ibn Tulun (Q).

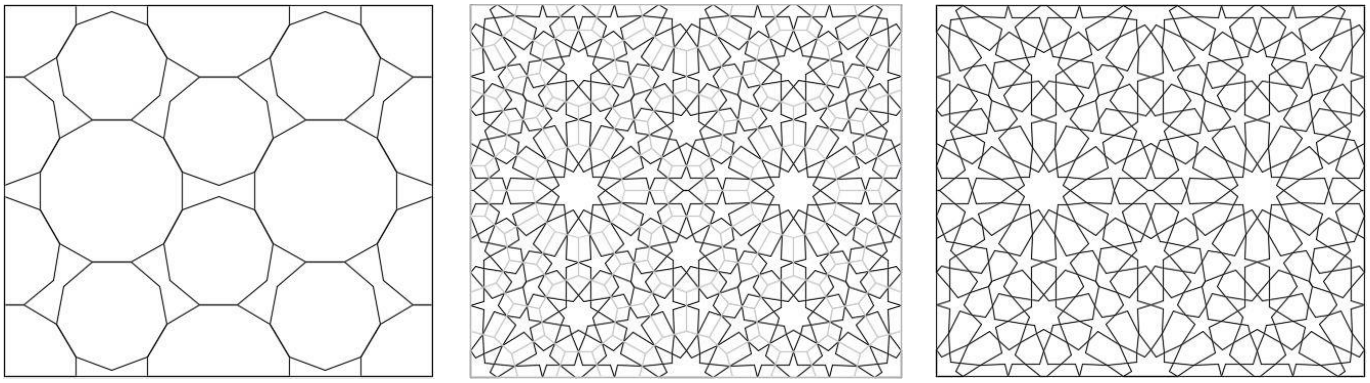

FIG 3.81. ROS- I-6.9.12.9. for Alhambra (T)

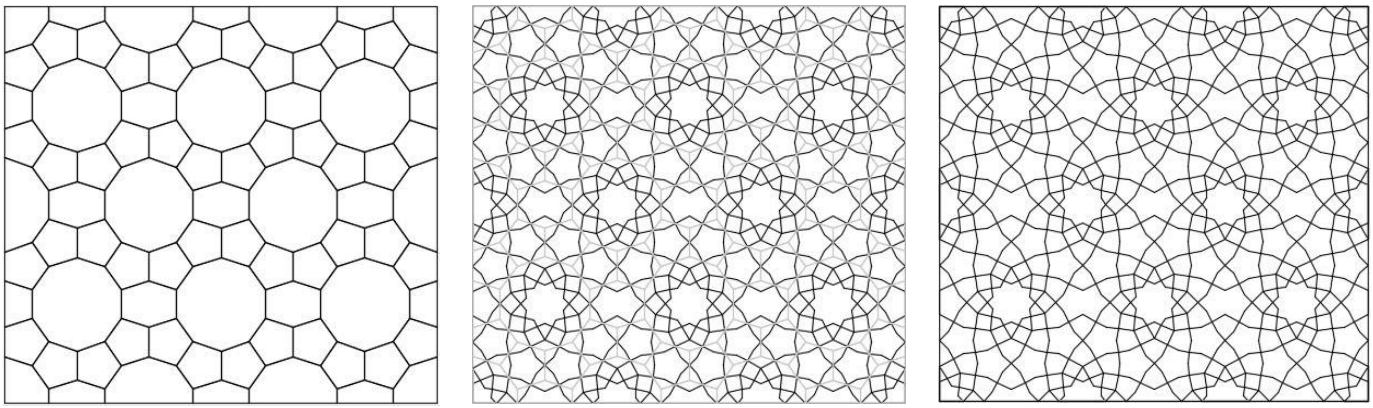

FIG 3.82. ROS- I-6.10.10. for Modari-Khan Madrash (J)

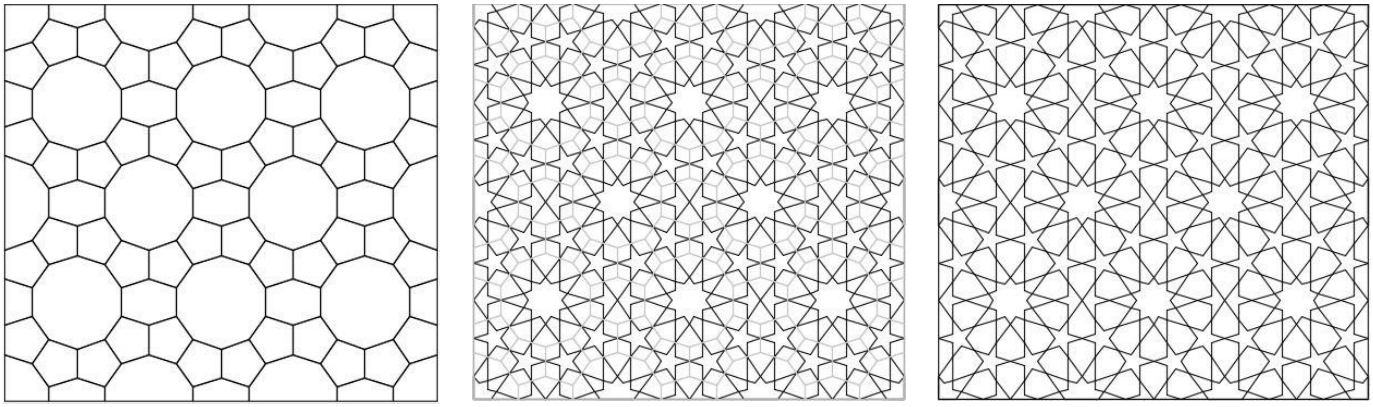

FIG 3.83. ROS- I-6.10.10. for Fatehpur Sikri (R)

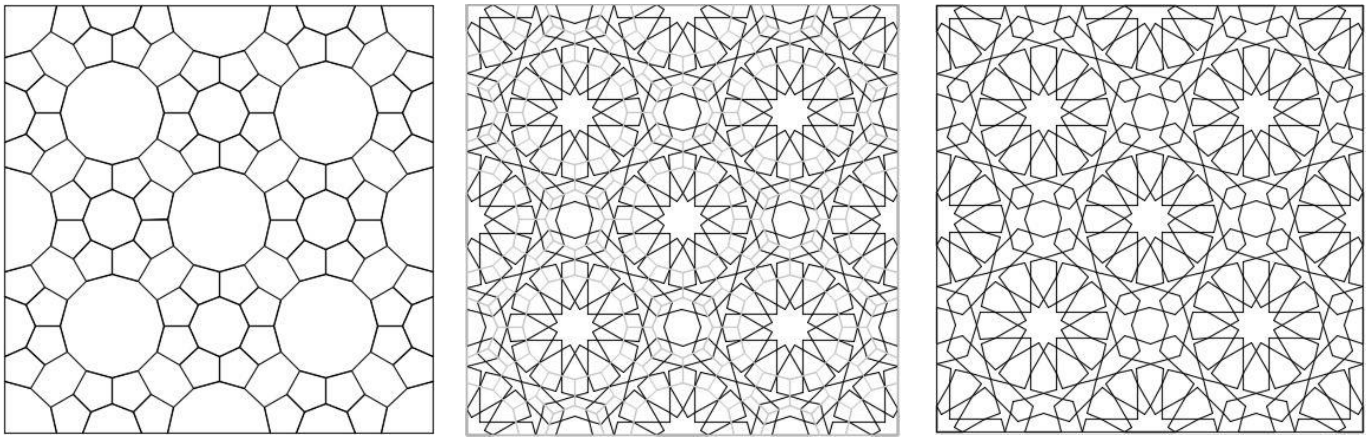

FIG 3.84. ROS- I-6.12.8.12. for Al-Nasir Muhammad's minbar (M)

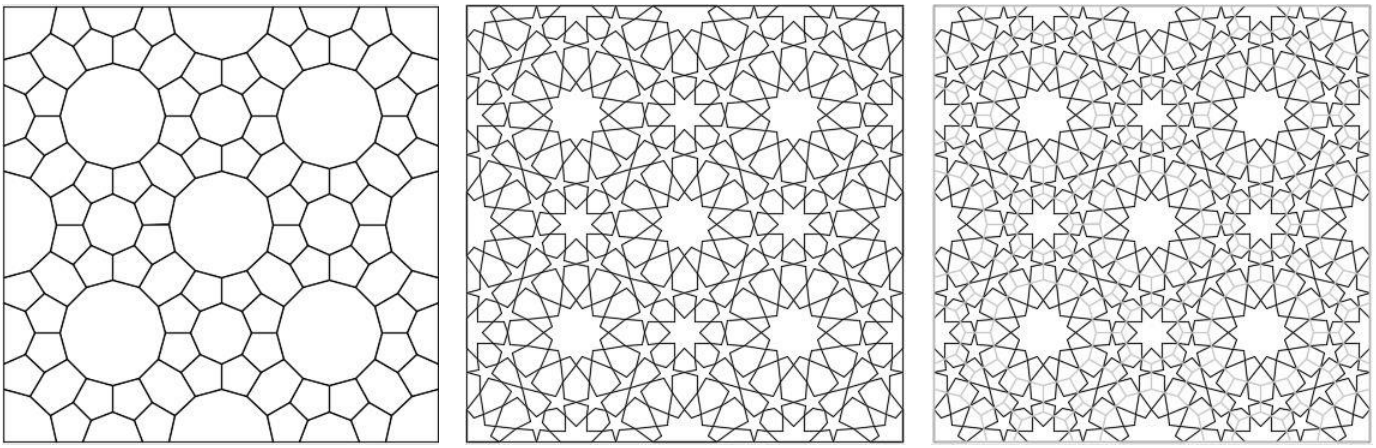

FIG 3.85. ROS- I-6.12.8.12. for Jameh Mosque (S)

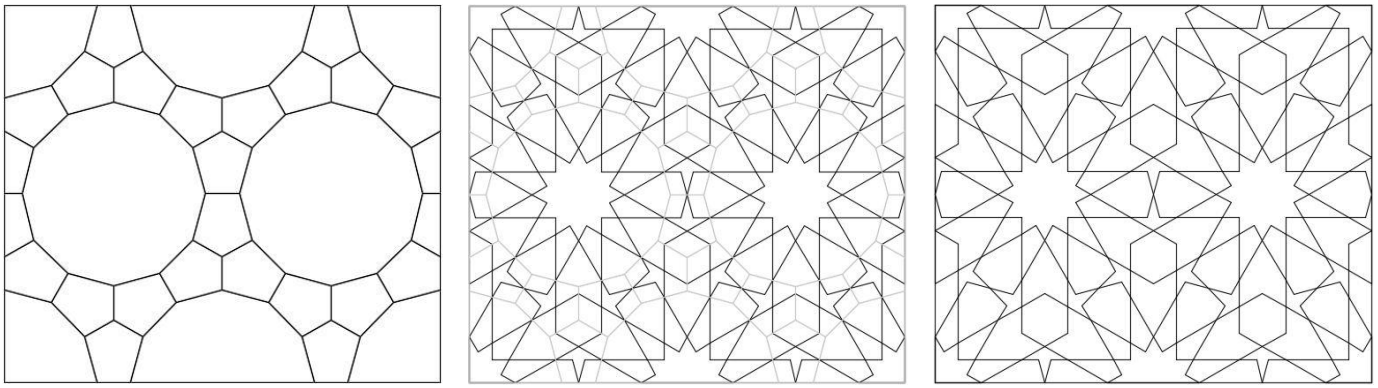

FIG 3.86. ROS-3.12.12. for Mosque of Al-Nasir Muhammad (N)

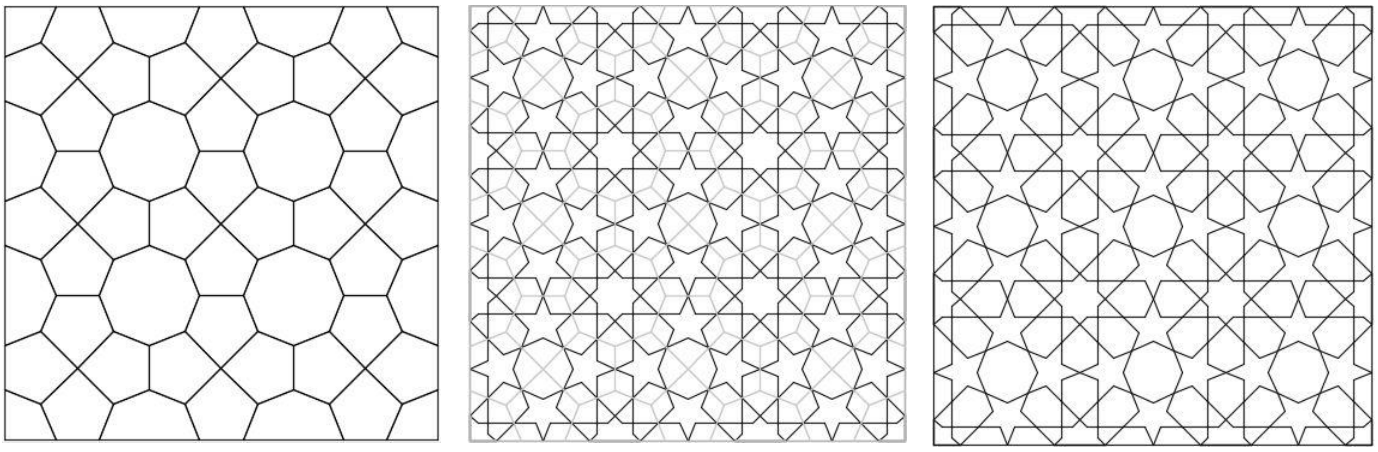

FIG 3.87. ROS-4.8.8. for Great Mosque of Herat (O)

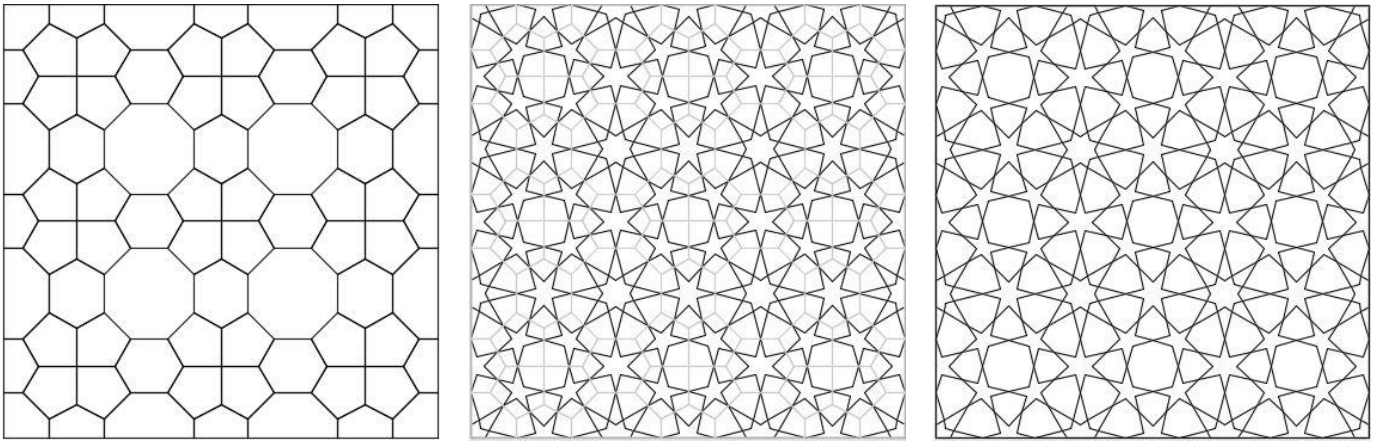

FIG 3.88. ROS-P-3.4.3.8_3.8.8. for Mosque of Al-Salih Tala'i (P)

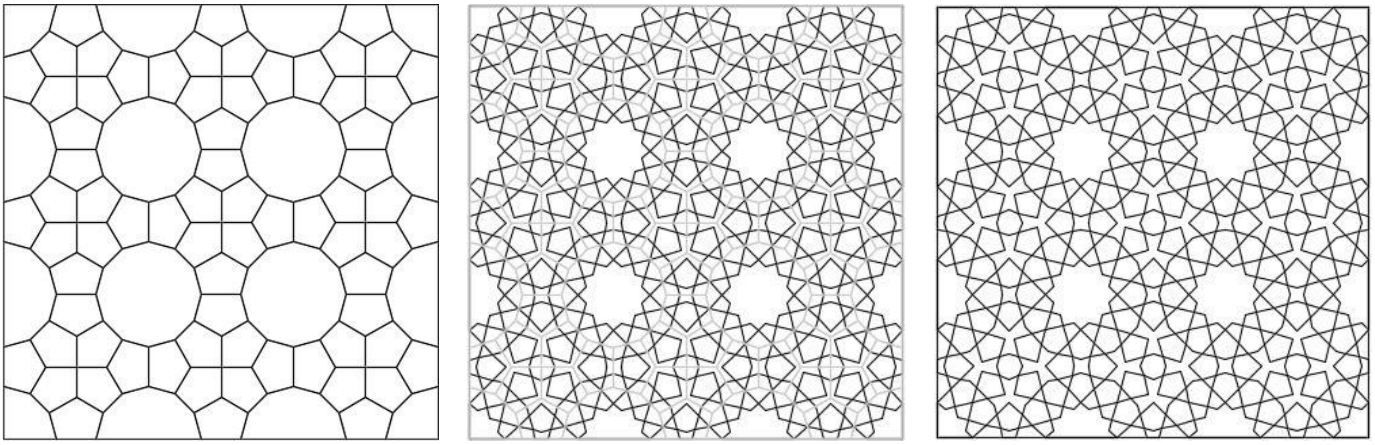

FIG 3.89. ROS-P-3.4.3.12_3.12.12. for Sultan Bayezid II (K)

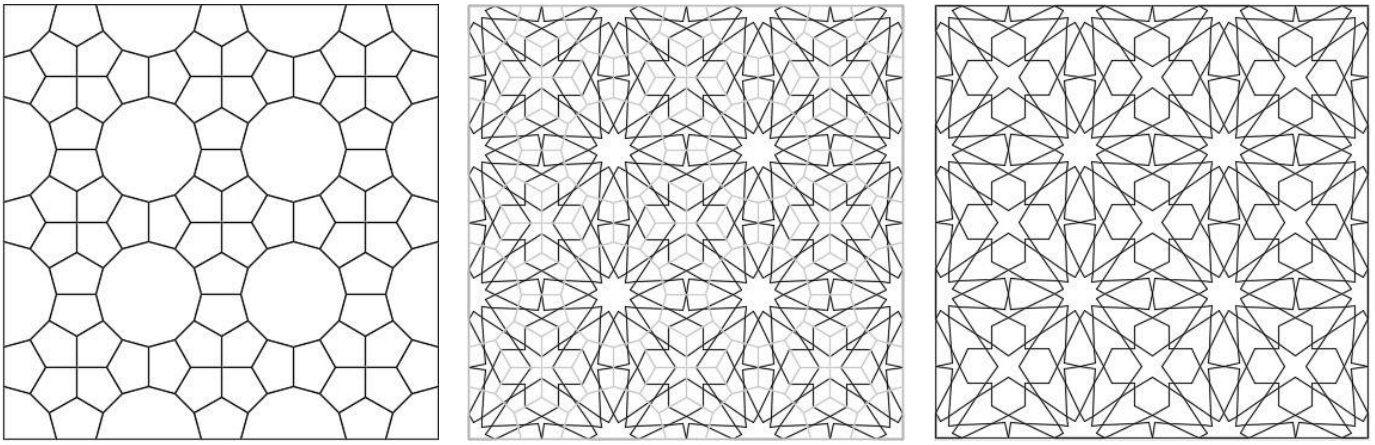

FIG 3.90. ROS-P-3.4.3.12_3.12.12. for Ben Yusuf Madrasa (L)

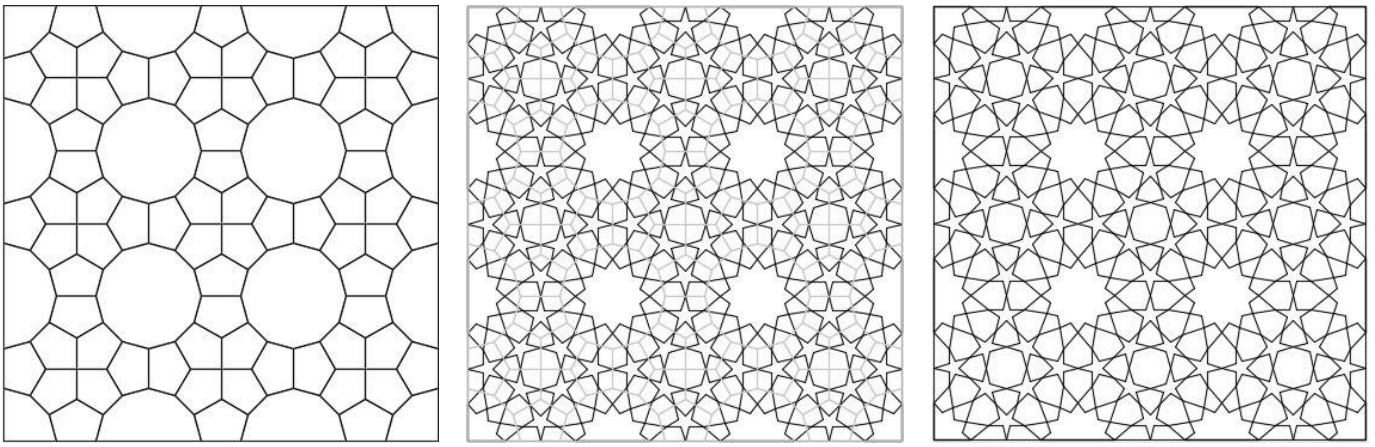

FIG 3.91. ROS-P-3.4.3.12_3.12.12. for Mosque of Ibn Tulun (Q)

3.5. SATURATION AND RELATIVE BEAM DEPTH.

As the beam depth increases, the façade becomes opaquer and more material is used. It is an important parameter in the design stage that will affect the solar gain in the interior spaces, the overall appearance of the building, the mechanical properties obtained and the amount of material employed. However, the information regarding the beam depth is only representative when it is expressed in relative terms with respect the module size. A beam depth of 1m can be either big or small depending on the module size and the specific pattern. To address this and provide a benchmark for comparison of the different pattern, the following concepts are introduced:

- **Saturation (Sat.):** it is defined as the **percentage of the panel surface that is covered by the structure.** This concept leads a more accurate comparison of the relative performance of the different patterns, as the equivalent mechanical properties will be compared for the same amount of material. The saturation times the façade surface, times its thickness, results in the volume of material employed. It is very useful for the pretended design tables, as the designer will have a tool to rapidly estimate the amount of material required and will know visually the final appearance.

- **Relative beam depth (rbd): it** is defined as the **relation between the beam depth and the module size in the x-direction** (horizontal direction for the pattern oriented as *in Chapter 3.3. Selection of historic geometric Islamic patterns*). A specific relative beam depth always leads to the same grade of saturation for a given variation independently of the panel size.

- **Module:** it corresponds to the **minimum rectangular module** that can reproduce the whole pattern by its orthogonal repetition. As mentioned in the literature review, in this document there is not a geometric difference between module, unit cell and representative volume element (RVE) as it is customary for the homogenization process. Instead, for easiness of use of the results and automation of the analysis process, the minimum rectangular module is defined as "the module" for all cases. To prevent misunderstandings, a panel with a clear identification of the module will be provided for each pattern.

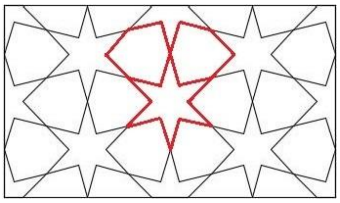
FIG 3.92. Module as per Montuori

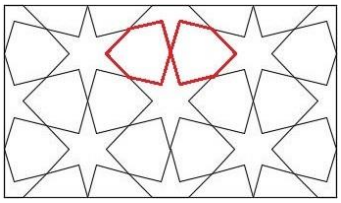
FIG 3.93. Unit cell as per Montuori

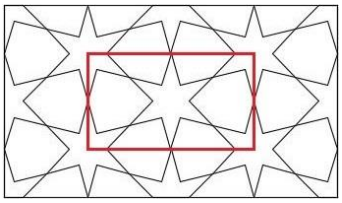
FIG 3.94. Module edges in this doc.

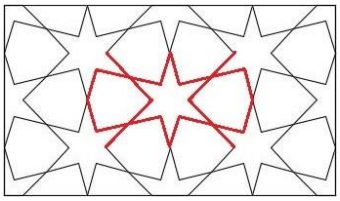
FIG 3.95.Unit cell and RVE in this doc.

3.5.1. HOW TO USE THE SATURATION TABLES.

As an example, imagine a square tall building with a height of 200m and a base of 25m, for which the Lahore Fort Complex pattern has been chosen (tessellation 4.8.8. θ=67.5º). Applying the predesign method developed in this document, required equivalent mechanical properties are needed to meet the target displacement at the top floor. There are three parameters that can be adjusted for that purpose, namely the base material, the façade (panel) thickness and the saturation. After adjusting those parameters and taking into consideration other aspects such as desired opacity and aesthetic appearance, a conclusion could be for instance that the desired saturation is 25%.

Making use of the already linearly extrapolated saturation tables, for that specific pattern a saturation of 25% corresponds to a relative beam depth of 3.69%.

The last step would be to choose the number of modules composing the panel (the whole façade). As this precise pattern is square, the façade can be populated by 5x40 modules of 5m, by 2x16 modules of 12.5m, by 1x8 modules of 25m, etc. If a module size in the x-direction of 5m is chosen (5x40 modules), the equivalent beam depth would be 18.45cm (5m,3.69/100 = 0.1845m).

This is a predesign method to have an order of magnitude of the expected results and a starting cross-section for the analysis. Later, it will be proven that this predesign method provide more accurate results than modelling the pattern with beam elements.

3.5.2. SATURATION TABLES.

Appendix I. Design Guide: It includes the following information regarding the historic Islamic patterns under study as well as two of their parametric variations for each case:

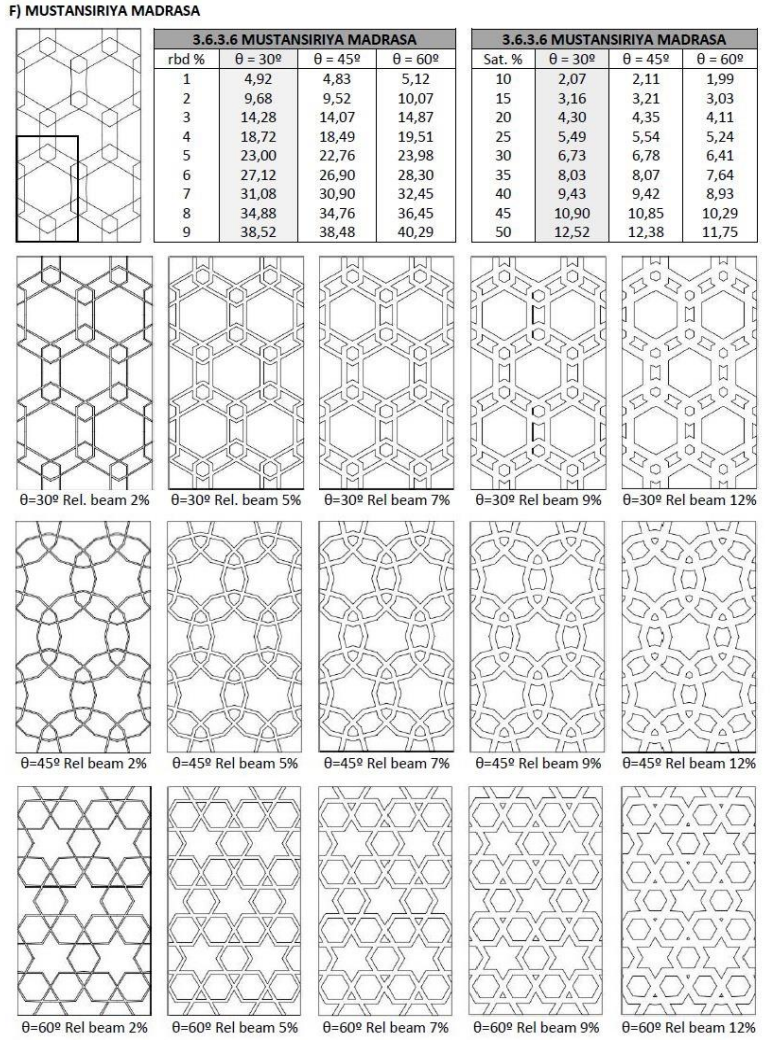

FIG 3.96.Typical saturation table in Appendix I. Design guide

Module identification: This picture allows the designer to easily identify what is the pattern module as its length in the x-direction is required to get the absolute beam depth from the relative beam depth in the tables.

Saturation table: The saturation values are obtained varying the beams depth in Grasshopper and retrieving the saturation value. This table gives the corresponding saturation (Sat. %) for a given relative beam depth (rbd %).

Linearly interpolated saturation table; To facilitate the comparison between patterns and in order to give more tools to the designer, the saturation table's values are linearly interpolated. This table gives the corresponding relative beam depth (rbd %) for a given saturation (Sat. %). Note that the values in this table are less accurate.

Extruded patterns: Those pictures display how the pattern and saturation would look like for different relative beam depths. It is intended to help the designer visualize the resulting appearance in order to take informed decisions and limit the range of the desired relative beam depth (rbd) or saturation (Sat)

In this chapter just the historical patterns are displayed for 15%, 25%, 35% and 45% saturations:

A) YESLI MOSQUE

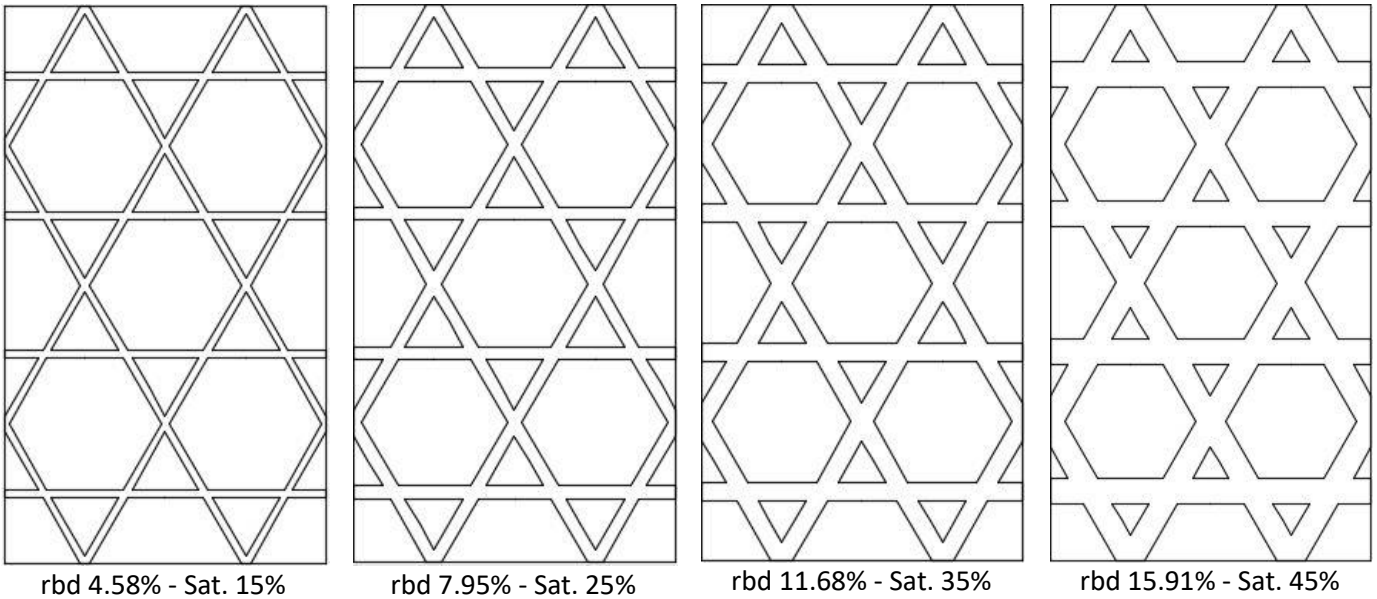

FIG 3.97. A) Yesli Mosque pattern with 15%, 25%, 35% and 45% saturations

B) GREAT MOSQUE OF DAMASCUS

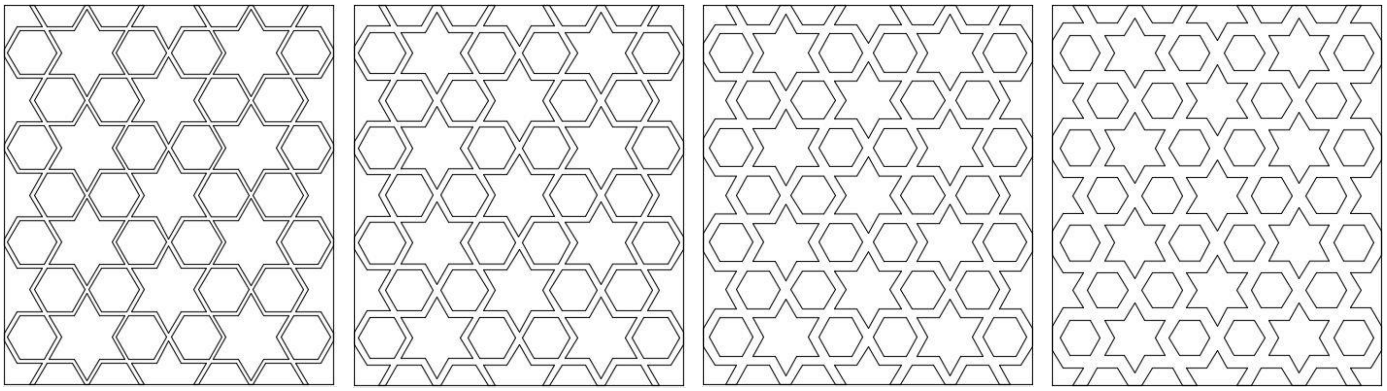

rbd 2.26% - Sat. 15% rbd 3.87% - Sat. 25% rbd 5.60% - Sat. 35% rbd 7.46% - Sat. 45%

FIG 3.98. B) Great Mosque of Damascus pattern with 15%, 25%, 35% and 45% saturations

C) SABZ PUSHAN

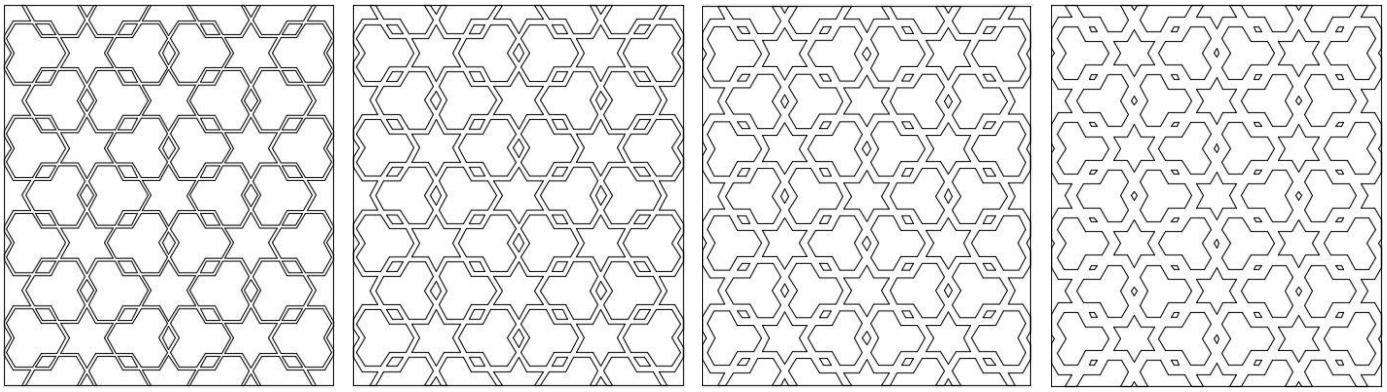

rbd 1.75% - Sat. 15% rbd 3.02% - Sat. 25% rbd 4.41% - Sat. 35% rbd 5.93% - Sat. 45%

FIG 3.99. C) Sabz Pushan pattern with 15%, 25%, 35% and 45% saturations

D) LAHORE FORT COMPLEX

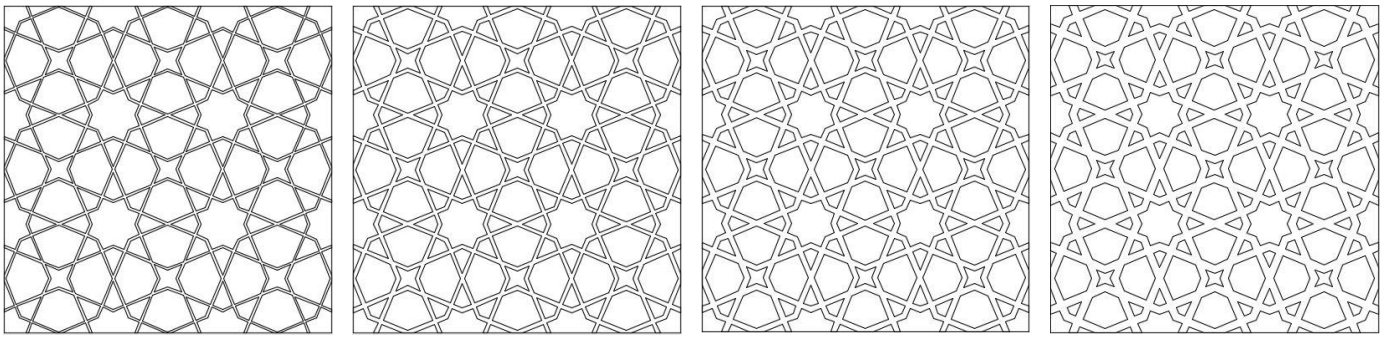

rbd 2.13% - Sat. 15% rbd 3.69% - Sat. 25% rbd 5.39% - Sat. 35% rbd 7.27% - Sat. 45%

FIG 3.100. D) Lahore Fort complex pattern with 15%, 25%, 35% and 45% saturations

E) PALACE OF THE SHIRVANSHAHS

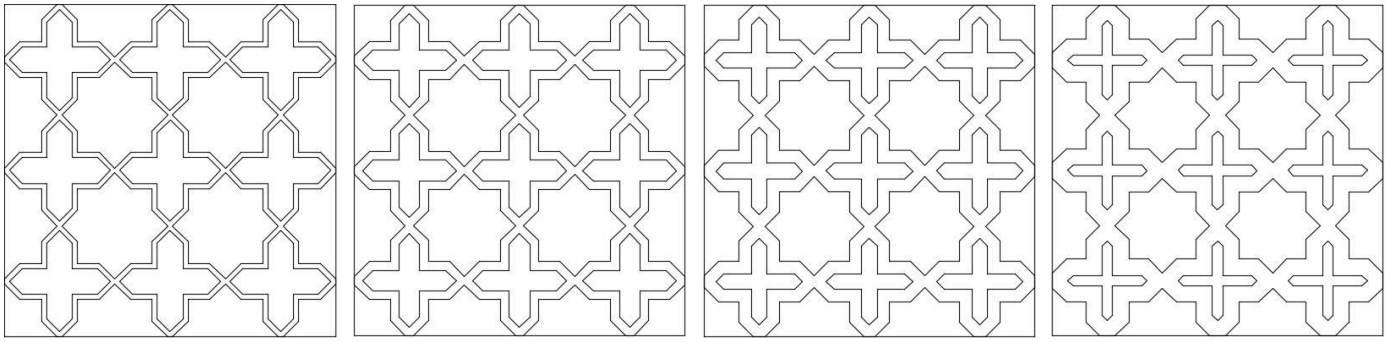

rbd 3.11% - Sat. 15% rbd 5.28% - Sat. 25% rbd 7.56% - Sat. 35% rbd 9.95% - Sat. 45%

FIG 3.101. E) Palace of the Shirvanshahs pattern with 15%, 25%, 35% and 45% saturations

F) MUSTANSIRIYA MADRASA

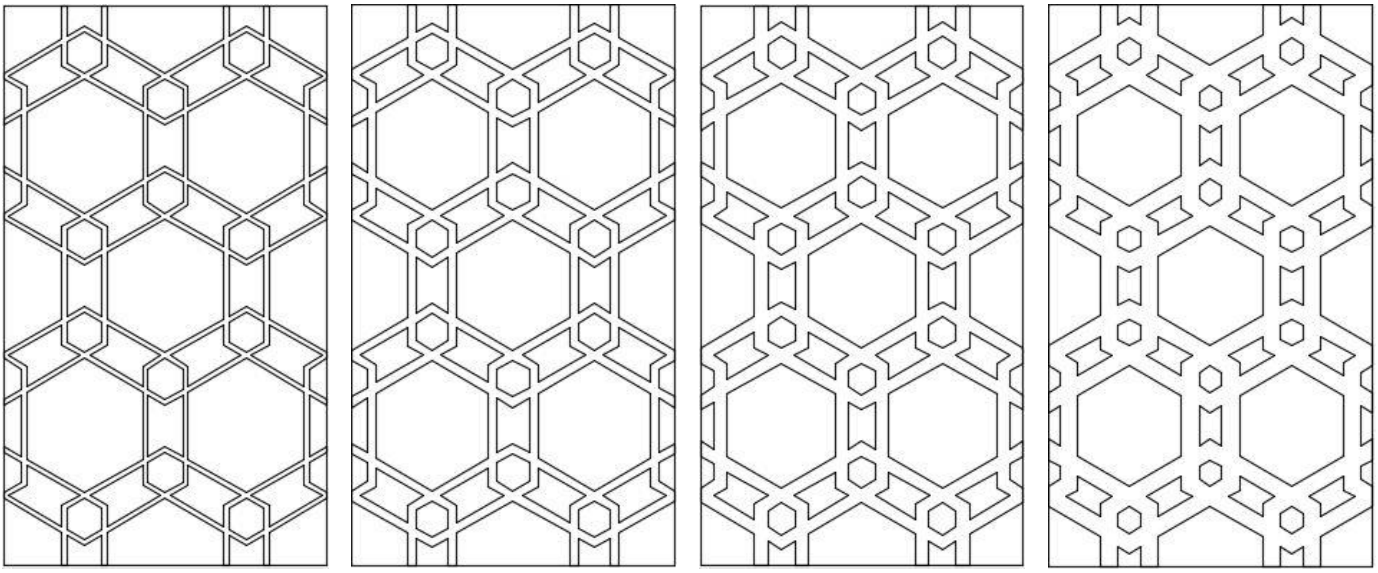

rbd 3.16% - Sat. 15% rbd 5.49% - Sat. 25% rbd 8.03% - Sat. 35% rbd 10.90% - Sat. 45%

FIG 3.102. F) Mustansiriya madrasa pattern with 15%, 25%, 35% and 45% saturations

G) TOMB OF SALIM CHISHTI

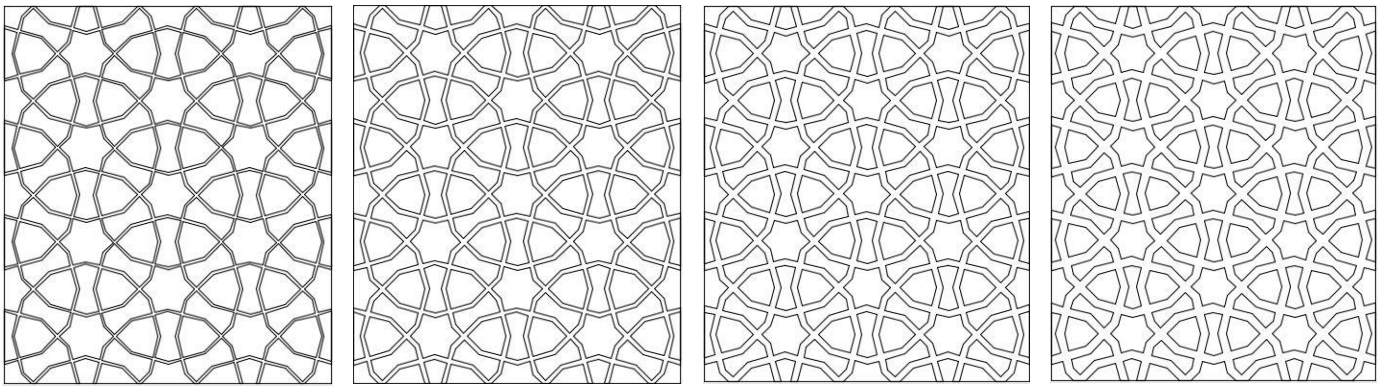

rbd 1.61% - Sat. 15% rbd 2.76% - Sat. 25% rbd 3.96% - Sat. 35% rbd 5.26% - Sat. 45%

FIG 3.103. G) Tomb of Salim Chisthi pattern with 15%, 25%, 35% and 45% saturations

H) GENERALIFE

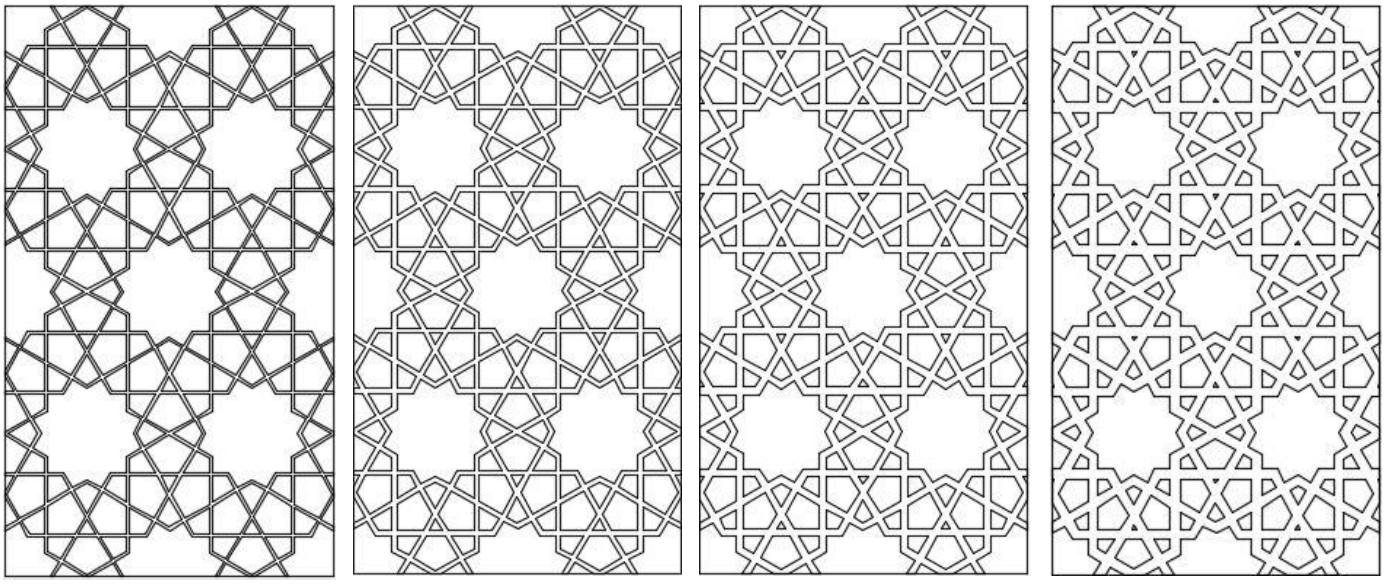

rbd 1.78% - Sat. 15% rbd 3.08% - Sat. 25% rbd 4.52% - Sat. 35% rbd 6.13% - Sat. 45%

FIG 3.104. H) Generalife pattern with 15%, 25%, 35% and 45% saturations

I) HASHT BEHESHT

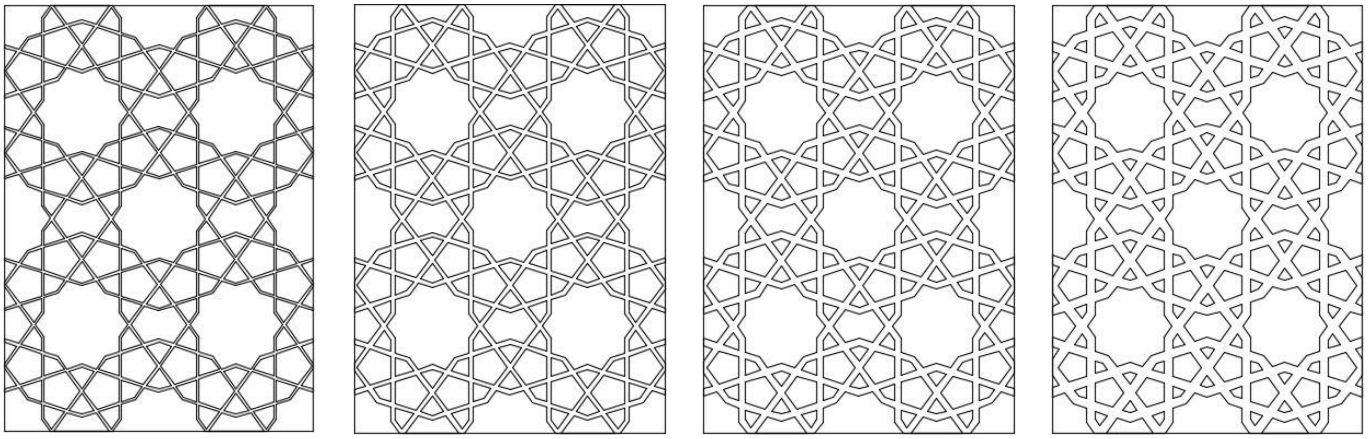

rbd 1.73% - Sat. 15% | rbd 3.00% - Sat. 25% | rbd 4.41% - Sat. 35% | rbd 5.98% - Sat. 45%

FIG 3.105. I) Hasht Behesht pattern with 15%, 25%, 35% and 45% saturations

J) MODARI-KHAN MADRASH

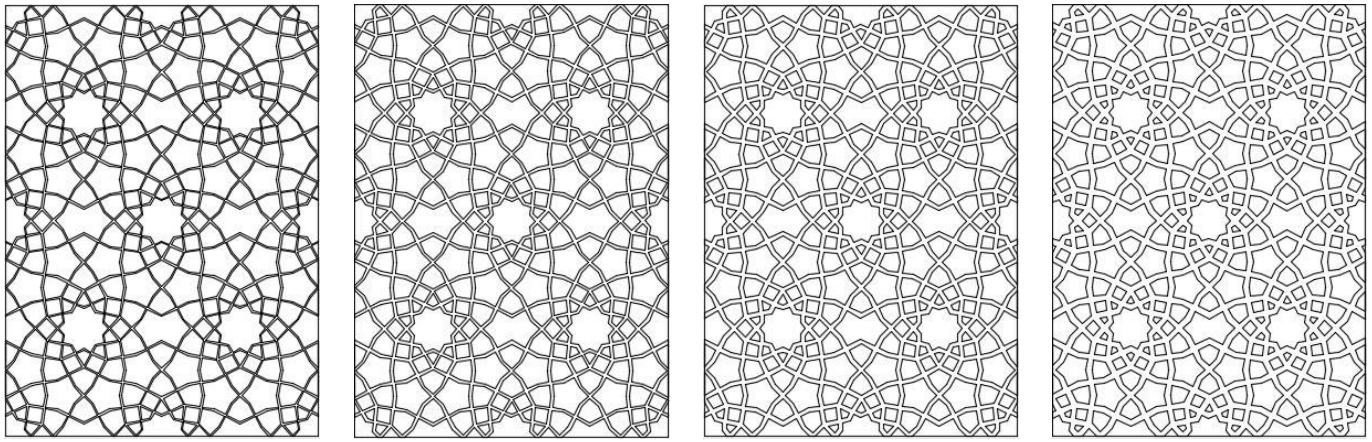

rbd 1.12% - Sat. 15% | rbd 1.93% - Sat. 25% | rbd 2.81% - Sat. 35% | rbd 3.78% - Sat. 45%

FIG 3.106. J) Modari-Khan madrash pattern with 15%, 25%, 35% and 45% saturations

K) COMPLEX OF SULTAN BAYEZID II

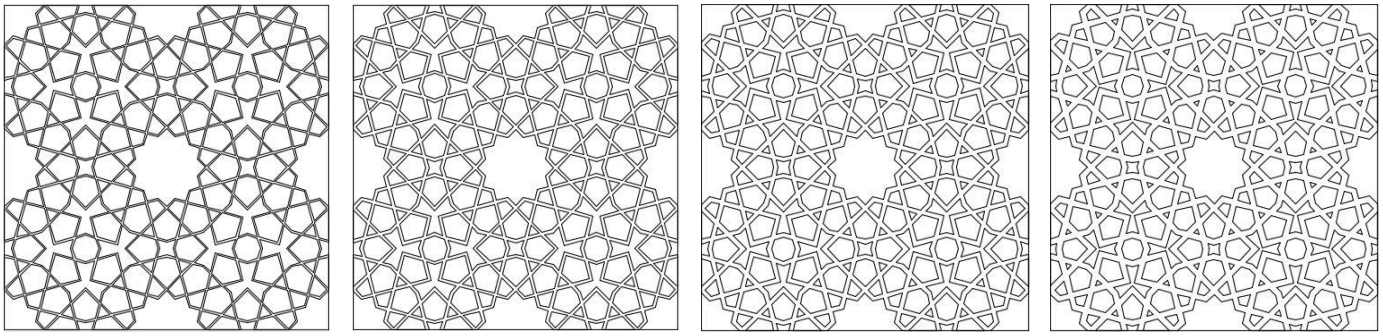

rbd 1.10% - Sat. 15% | rbd 1.90% - Sat. 25% | rbd 2.77% - Sat. 35% | rbd 3.73% - Sat. 45%

FIG 3.107. K) Complex of Sultan Bayezid II pattern with 15%, 25%, 35% and 45% saturations

L) BEN YUSUF MADRASA

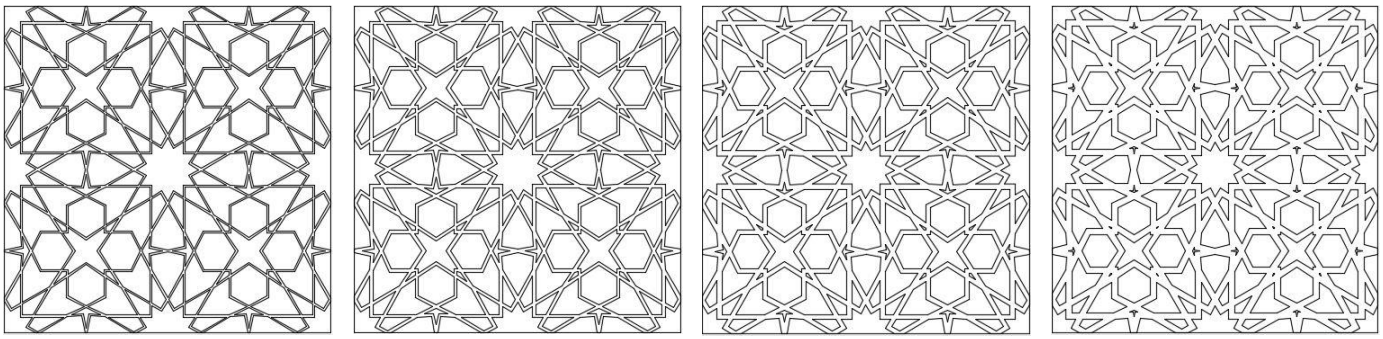

rbd 1.14% - Sat. 15% | rbd 1.97% - Sat. 25% | rbd 2.89% - Sat. 35% | rbd 3.91% - Sat. 45%

FIG 3.108. L) Ben Yusuf madrasa pattern with 15%, 25%, 35% and 45% saturations

M) AL-NASIR MUHAMMAD'S MINBAR

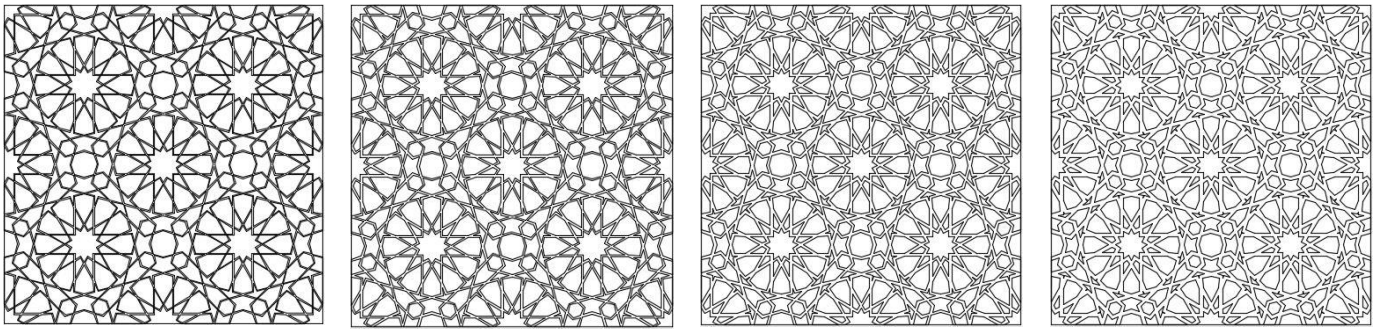

rbd 0.69% - Sat. 15% rbd 1.19% - Sat. 25% rbd 1.74% - Sat. 35% rbd 2.35% - Sat. 45%

FIG 3.109. M) Al-Nasir Muhammad´s minbar pattern with 15%, 25%, 35% and 45% saturations

N) MOSQUE OF AL-NASIR MUHAMMAD

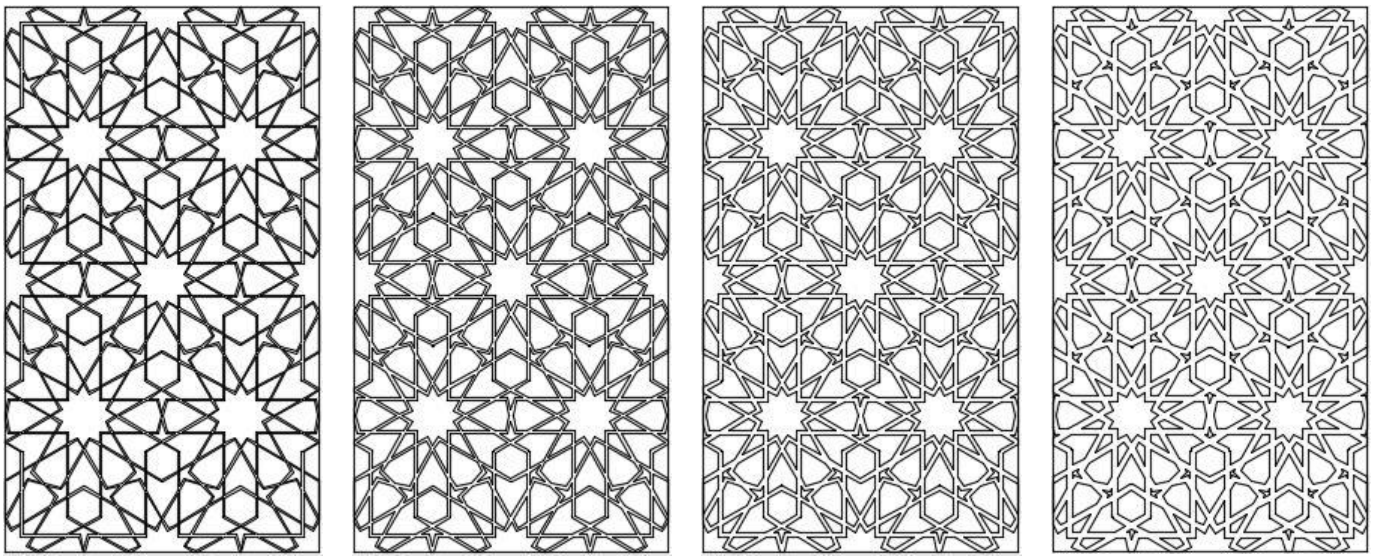

rbd 1.13% - Sat. 15% rbd 1.95% - Sat. 25% rbd 2.85% - Sat. 35% rbd 3.84% - Sat. 45%

FIG 3.110. N) Mosque of Al-Nasir Muhammad pattern with 15%, 25%, 35% and 45% saturations

O) GREAT MOSQUE OF HERAT

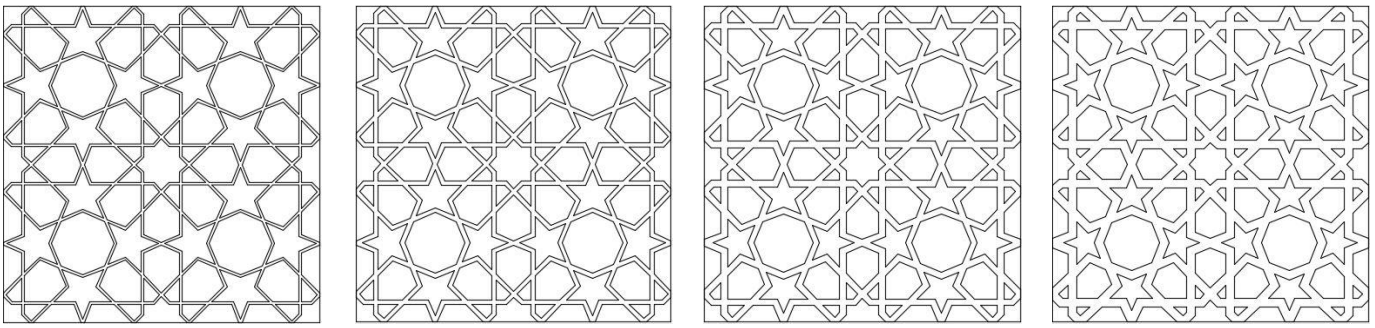

rbd 1.62% - Sat. 15% rbd 2.79% - Sat. 25% rbd 4.05% - Sat. 35% rbd 5.47% - Sat. 45%

FIG 3.111. O) Great Mosque of Herat pattern with 15%, 25%, 35% and 45% saturations

P) MOSQUE OF AL-SALIH TALA'I

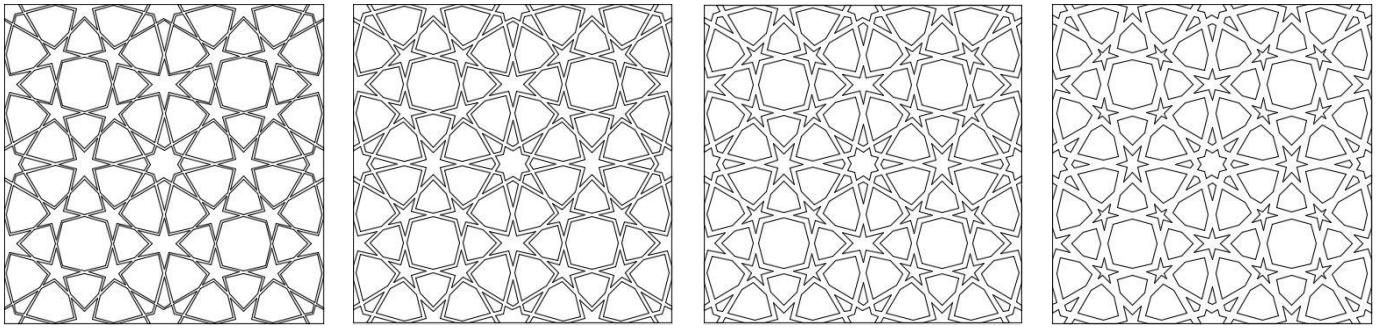

rbd 1.28% - Sat. 15% rbd 2.21% - Sat. 25% rbd 3.23% - Sat. 35% rbd 4.38% - Sat. 45%

FIG 3.112. P) Mosque of Al-Salih Tala'i pattern with 15%, 25%, 35% and 45% saturations

Q) MOSQUE OF IBN TULUN

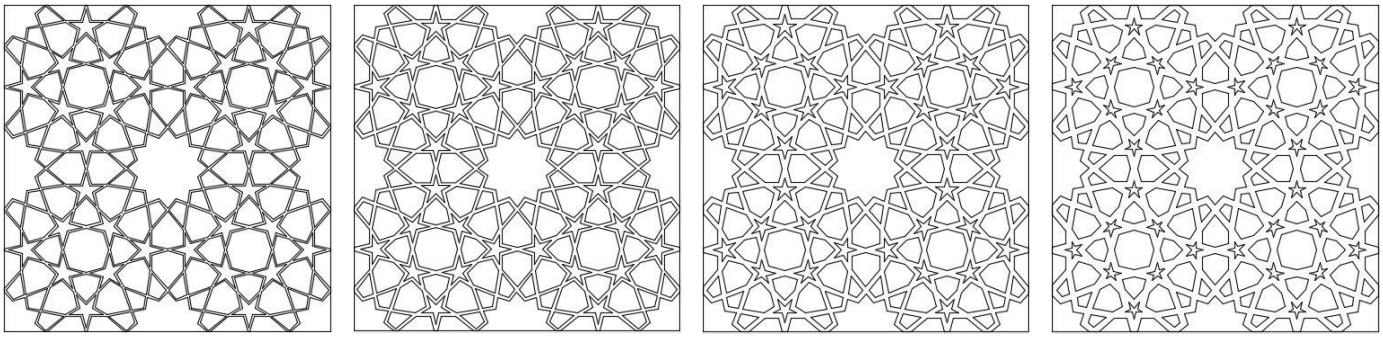

rbd 1.16% - Sat. 15% rbd 2.00% - Sat. 25% rbd 2.93% - Sat. 35% rbd 3.98% - Sat. 45%

FIG 3.113. Q) Mosque of Ibn Tulun pattern with 15%, 25%, 35% and 45% saturations

R) FATEHPUR SIKRI

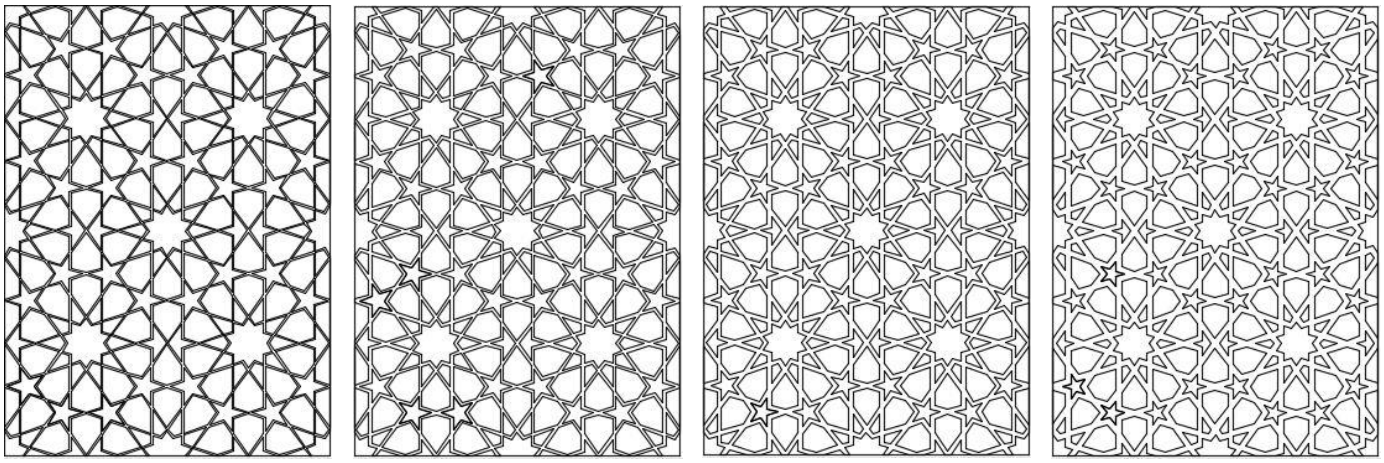

rbd 1.09% - Sat. 15% rbd 1.88% - Sat. 25% rbd 2.75% - Sat. 35% rbd 3.70% - Sat. 45%

FIG 3.114. R) Fatehpur Sikri pattern with 15%, 25%, 35% and 45% saturations

S) JAMEH MOSQUE

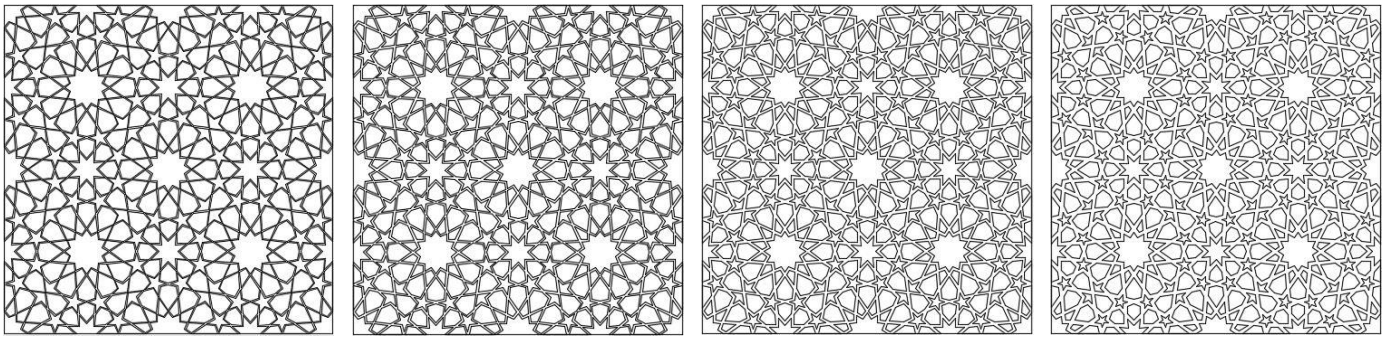

rbd 0.70% - Sat. 15% rbd 1.20% - Sat. 25% rbd 1.75% - Sat. 35% rbd 2.35% - Sat. 45%

FIG 3.115. S) Jameh Mosque pattern with 15%, 25%, 35% and 45% saturations

T) ALHAMBRA

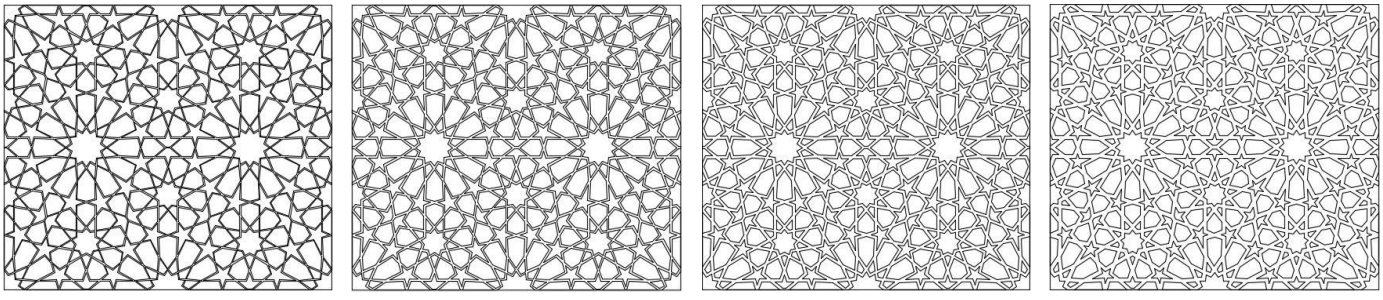

rbd 0.71% - Sat. 15% rbd 1.23% - Sat. 25% rbd 1.79% - Sat. 35% rbd 2.40% - Sat. 45%

FIG 3.116. T) Alhambra pattern with 15%, 25%, 35% and 45% saturations

4. RESEARCH QUESTION 1. METHOD LEVEL

The main objective of this thesis is to provide insight into the structural behaviour and design of geometric Islamic patterns as alternative to conventional diagrid systems for tall buildings. This research objective is articulated at three levels: method level, pattern level and building level.

Each of the three research questions addresses one of those levels and they are further developed in a series of sub-questions described in the following document structure:

METHOD LEVEL:

Can a simple tool be developed for the design of geometric Islamic patterns as a non-conventional diagrid system?

- **Method chosen and methodology for its adoption**
- **Development of a pre-design tool.**
- **Assessment of the developed tool**

PATTERN LEVEL:

How do geometric Islamic patterns behave and compare when loaded in their plane?

- Selection of historic Islamic patterns and their parametric variations
- Characterization of the patterns' structural behaviour
- Performance comparison of the different patterns
- Proposals for their improvement

BUILDING LEVEL:

Can Islamic inspired patterns become a feasible alternative to traditional diagrid systems for tall buildings?

- Performance comparison of the different patterns and the conventional diagrids
- Overview practical applications of best performing patterns
- Special cases in tall buildings

4.1. METHOD ADOPTED

4.1.1. HOMOGENIZATION METHOD

Generally speaking, it can be stated that in tall buildings, fulfilling the global Service Limit State limitations indirectly leads to the fulfilment of the Ultimate Limit State limitations as they tend to be more restrictive. This premise is valid only for the predesign and all the limitations must be later verified, especially those concerning the global stability of the building overturning as a rigid body In the **stiffness-based design approach**, the structural elements are disposed and sized so the overall stiffness of the structure is enough to fulfil the required displacement limitation. This approach is widely used for the preliminary design of tall buildings and is applied by Moon[11] for his diagrid optimization. Applying Timoshenko beam theory to a prismatic cantilever beam under uniform distributed load:

$$u_x(H) = \frac{q_w H^4}{8EI} + \frac{q_w H^2}{2GA_s} \leq u_x(H)_{max} \qquad (1.2)$$

The top displacement is compared with the drift limitation and the mechanical properties chosen to meet that limitation.

In the case of geometric Islamic patterns, we do not have mechanical properties properly speaking as the pattern is not a material but a framed structure. The **homogenization method** finds analytically or numerically the 'equivalent' or 'homogenized' mechanical properties of a continuous metamaterial that represents the periodic structure that conforms it. In the context of non-conventional diagrids, the diagrid would be substituted by an equivalent homogenized material whose homogenized mechanical properties would lead to the same displacements with stiffness-based design equations.

G.M. Montuori[14] uses this method in his hexagrid structural assessment research: "(…) the idea is to idealize whichever grid as a continuous depleted medium, characterized by penalized mechanical properties, according to the classical micromechanical approach based on homogenization methods. In fact a plane periodic structure made up of an

isotropic linearly elastic material and possessing a certain degree of symmetry behaves macroscopically as an isotropic material; the macroscopic properties of the structure are called the effective properties, and depend on both the mechanical properties of the solid matrix and on the microstructural features of the grid, namely topology, density and orientation."

This document diverges from the above definitions provided by G.M. Montuori[14]. The modules do not overlap, the unit cells are not the minimum possible unit and the representative volume elements are the direct structural idealization of the unit cells. For simplicity of the proposed design method and systematization of the analysis, only the terminology "module" is employed to refer to the three of them, that in all cases have the exact same geometry. Their geometric definition is derived from the minimum rectangle standing in the x- and y-axis, whose replication leads to the complete pattern. These definitions are applied to Great Mosque of Damascus pattern in the following pictures:

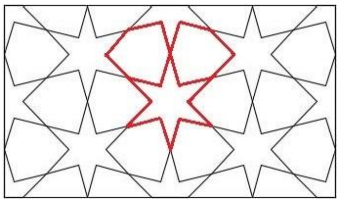
FIG 4.1. Module as per Montuori

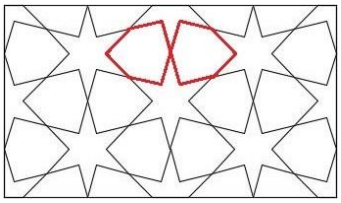
FIG 4.2. Unit cell as per Montuori

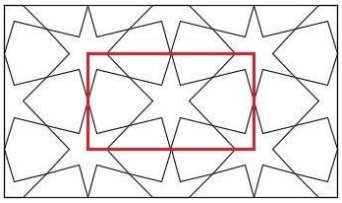
FIG 4.3. Module edges here

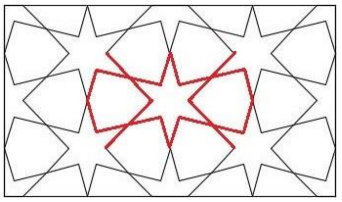
FIG 4.4. Unit cell and RVE here

The choice of these methodology is based on their extended use in other similar papers and their clear applicability for this study. The method proposed consists in the determination of an equivalent metamaterial for any of the chosen historic mechanical properties. The saturation serves as representation of the amount of material employed in each case and the homogenized mechanical show its structural performance. The predesign tool consist on a series of tables, graphs and pictures that show and compare the aesthetic image, the structural mechanical properties and amount of material employed for different beams sizes in each pattern.

4.1.2. PLANE-STRESS ANALYSIS

Geometric Islamic patterns can be applied to shell structures such as domes, where the mechanical out-of-plane properties are at least as relevant as the mechanical in-plane properties. Nevertheless, other shell structures such as hypars are designed so the out-of-plane stresses are minimal and their in-plane mechanical properties are enough to properly define the overall performance of the structure. This is the case of diagrid systems in tall buildings, where the structure can be approximated as a thin-shell cantilever beam. In this research only the in-plane structural behaviour is studied, leaving the further out-of-plane characterization to future studies.

4.1.3. BEAM SIZE EFFECTS

As with Vierendeel trusses, the bars' layout is not triangular and modelling the nodes as pinned would lead to a mechanism. Thus, the bars are modelled clamped to each other in fully bending-resisting nodes. As the bars are no longer subjected just to axial forces but also to bending moments, their size and shape affect the overall response. The homogenized mechanical properties are not directly proportional to the beam sizes or the saturation of the panel, so a full range of different beam sizes must be tested for each pattern.

4.1.4. ORTHOTROPIC BEHAVIOUR

In his study about the structural performance of hexagrids, Montuori et al in 2015[6] characterize the hexagrid in-plane structural behaviour as isotropic and then some empirical coefficients are included to calibrate the analytical expected values with the actual results obtained with a FEM analysis.

A priori it is not possible to know how the chosen historic Islamic patterns will behave when loaded in their plane as there is not previous research into that. While considering them as isotropic is an over simplification, considering them

as anisotropic introduces a series of complications that go against the systematization of the analysis and the simple use of the predesign tool. Finally, it is decided to study the patterns behaviour considering them as orthotropic. This allows to systematize the analysis by using rectangular panels in all cases for the tests and it simplifies the design tool by providing just the homogenized mechanical properties in two orthogonal directions.

The results will later prove that the pattern actual behaviour comes from the planes of symmetry of its geometry. It will be further discussed in *Chapter 5.1. Directional mechanical properties*.

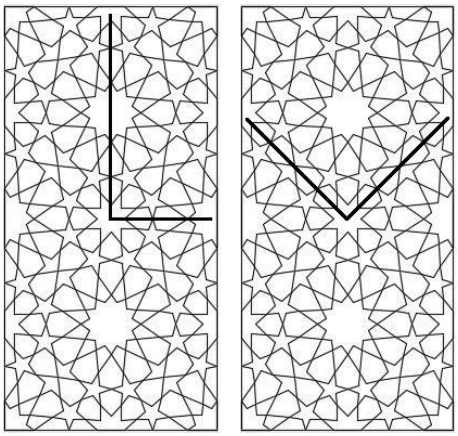

FIG 4.5. 90º. Square symmetry

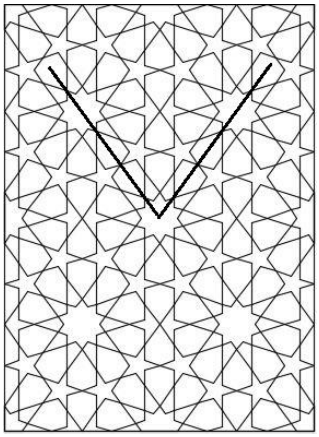

FIG 4.6.72º. Pentagonal symmetry

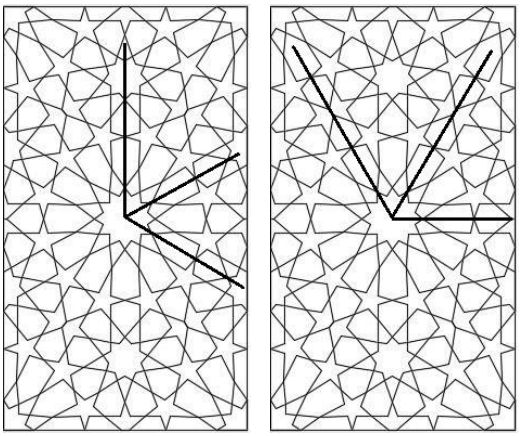

FIG 4.7. 60º. Hexagonal symmetry

Symmetry	Square	Pentagonal	Hexagonal
Pattern	D, E, K, L, M, O, P, Q, S	I, J, R	A, B, C, F, G, H, N, T

- Square symmetry: Perpendicular isotropy. Symmetry directions form 90ª.
- Pentagonal symmetry: Orthotropic Symmetry directions form 72º
- Hexagonal symmetry: Pure isotropic. Symmetry directions form 60º

The formulation of the constitutive matrix of 2D orthotopic behaviour is detailed in the literature review, specifically in *Chapter 2.6. Constitutive matrix for 2D orthotropic behaviour* and it is as follows:

$$\begin{Bmatrix} \sigma_{xx} \\ \sigma_{yy} \\ \tau_{xy} \end{Bmatrix} = \begin{bmatrix} \frac{E_x}{1-\nu_{xy}\nu_{yx}} & \frac{\nu_{xy}\,E_y}{1-\nu_{xy}\nu_{yx}} & 0 \\ \frac{\nu_{yx}\,E_x}{1-\nu_{xy}\nu_{yx}} & \frac{E_y}{1-\nu_{xy}\nu_{yx}} & 0 \\ 0 & 0 & G \end{bmatrix} \begin{Bmatrix} \varepsilon_{xx} \\ \varepsilon_{yy} \\ \gamma_{xy} \end{Bmatrix} \tag{1.13}$$

4.1.5. HOMOGENIZATION PROCESS

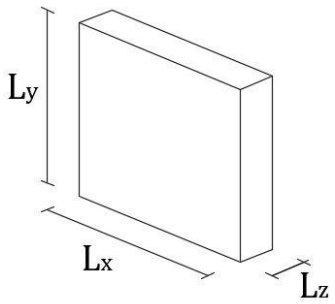

FIG 4.8. Panel geometry

The length of the panel in the x-direction is called L_x and its height L_y. As the in-plane behaviour of the panel with respect to its thickness L_z will be linear, a unitary value has been assigned in all cases for the tests.

Strains are indirectly imposed, in the sense that in the FEM what are actually assigned to the nodes are displacements not strains. The magnitude of the assigned displacement does not play any role in this chapter as the analysis carried out is linear elastic and hereby it will be referred to as Δl.

As aforementioned, the imposed strains are not assigned directly but derived from the specified imposed displacement:

$$\varepsilon_{xx}^{h} = \Delta l/L_x \qquad \varepsilon_{yy}^{v} = \Delta l/L_y \qquad \gamma_{xy} = \Delta l/L_x \qquad \gamma_{yx} = \Delta l/L_y \tag{4.01}$$

In the notation used, when there are two indexes (N_{xy}), the first index (x) corresponds to the axis normal to the plane in which the force is applied and the second (y) to the positive direction in which that force is acting. In this particular case (N_{xy}), the force is acting in a vertical edge (normal to x-direction) with positive values in the positive y-direction (vertical force, follows the y-direction). When only one index is used, that means that it is no longer referred to a vector. In such cases, the index corresponds to the axis in which directions that value is measured (L_x is the length of the panel in the x-direction).

Forces are directly measured in the nodes belonging to the same edge with the structural software and added up. Here it is emphasized that the nodes belong to the same edge, because in some case the forces in opposite edges compensate each other to keep the equilibrium (such as N_{yy}^{h}). Equilibrium is the first requisite when verifying the accuracy and applicability of the test.

The geometric Islamic patterns are considered orthotropic in their plane, for which the previous constitutive matrix stands. Nevertheless, as the values obtained in the FEM model are forces instead of stresses, so the matrix is modified to simplify its writing (coefficients Q instead of rational expressions) and to allow the input of the values retrieved from the FEM analysis.:

$$\begin{Bmatrix} \sigma_{xx} \\ \sigma_{yy} \\ \tau_{xy} \end{Bmatrix} = \begin{Bmatrix} N_{xx}/(L_y \cdot L_z) \\ N_{yy}/(L_x \cdot L_z) \\ N_{xy}/(L_y \cdot L_z) \end{Bmatrix} = \begin{bmatrix} Q_{11} & Q_{12} & 0 \\ Q_{21} & Q_{22} & 0 \\ 0 & 0 & Q_{33} \end{bmatrix} \begin{Bmatrix} \varepsilon_{xx} \\ \varepsilon_{yy} \\ \gamma_{xy} \end{Bmatrix} \tag{4.02}$$

The Poisson ratios cannot be directly obtained from the tests. As the material is not homogeneous, leaving one or two edges free and then measuring the transversal displacement would lead to different values depending on the node chosen. Even measuring the transversal displacement in all nodes and getting the average value would lead to incoherencies with the results obtained with other methods. Therefore, the test proposed in this research only allows a displacement (strain) at the time, getting directly an element of the constitutive matrix. The homogenized mechanical properties will later be derived from their equations.

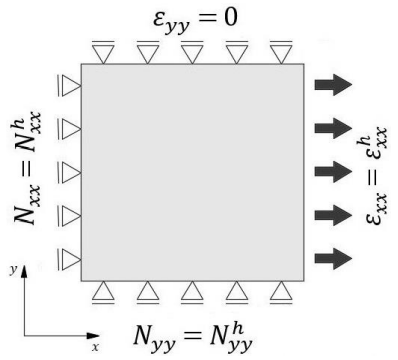

IMPOSED HORIZONTAL STRAIN.

$$\begin{Bmatrix} \sigma_{xx}^{h} \\ \sigma_{yy}^{h} \\ \tau_{xy}^{h} \end{Bmatrix} = \begin{Bmatrix} N_{xx}^{h}/(L_y \cdot L_z) \\ N_{yy}^{h}/(L_x \cdot L_z) \\ N_{xy}^{h}/(L_y \cdot L_z) \end{Bmatrix} = \begin{bmatrix} Q_{11} & Q_{12} & 0 \\ Q_{21} & Q_{22} & 0 \\ 0 & 0 & Q_{33} \end{bmatrix} \begin{Bmatrix} \varepsilon_{xx}^{h} \\ 0 \\ 0 \end{Bmatrix}$$

$$\sigma_{xx}^{h} = Q_{11} \cdot \varepsilon_{xx}^{h} \rightarrow Q_{11} = N_{xx}^{h} \cdot L_x/(L_y \cdot L_z \cdot \Delta l) \tag{4.03}$$

$$\sigma_{yy}^{h} = Q_{21} \cdot \varepsilon_{xx}^{h} \rightarrow Q_{21} = N_{yy}^{h}/(L_z \cdot \Delta l) \tag{4.04}$$

FIG 4.9. Imposed horizontal strain

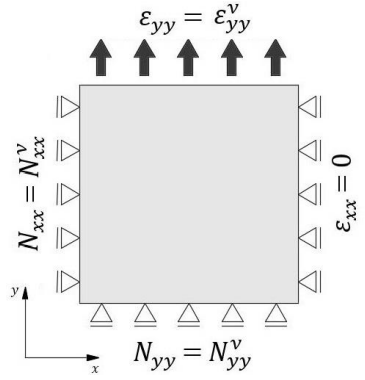

IMPOSED VERTICAL STRAIN.

$$\begin{Bmatrix} \sigma_{xx}^{v} \\ \sigma_{yy}^{v} \\ \tau_{xy}^{v} \end{Bmatrix} = \begin{Bmatrix} N_{xx}^{v}/(L_y \cdot L_z) \\ N_{yy}^{v}/(L_x \cdot L_z) \\ N_{xy}^{v}/(L_y \cdot L_z) \end{Bmatrix} = \begin{bmatrix} Q_{11} & Q_{12} & 0 \\ Q_{21} & Q_{22} & 0 \\ 0 & 0 & Q_{33} \end{bmatrix} \begin{Bmatrix} 0 \\ \varepsilon_{yy}^{v} \\ 0 \end{Bmatrix}$$

$$\sigma_{xx}^{v} = Q_{12} \cdot \varepsilon_{yy}^{v} \rightarrow Q_{12} = N_{xx}^{v}/(L_z \cdot \Delta l) \tag{4.05}$$

$$\sigma_{yy}^{v} = Q_{22} \cdot \varepsilon_{yy}^{v} \rightarrow Q_{22} = N_{yy}^{v} \cdot L_y/(L_x \cdot L_z \cdot \Delta l) \tag{4.06}$$

FIG 4.10. Imposed vertical strain

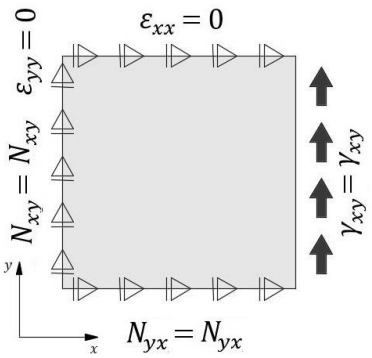

IMPOSED TRANSVERSE VERTICAL STRAIN.

$$\begin{Bmatrix} \sigma_{xx} \\ \sigma_{yy} \\ \tau_{xy} \end{Bmatrix} = \begin{Bmatrix} N_{xx}/(L_y \cdot L_z) \\ N_{yy}/(L_x \cdot L_z) \\ N_{xy}/(L_y \cdot L_z) \end{Bmatrix} = \begin{bmatrix} Q_{11} & Q_{12} & 0 \\ Q_{21} & Q_{22} & 0 \\ 0 & 0 & Q_{33} \end{bmatrix} \begin{Bmatrix} 0 \\ 0 \\ \gamma_{xy} \end{Bmatrix}$$

$$\tau_{xy} = Q_{33} \cdot \gamma_{xy} \;\rightarrow\; Q_{33} = N_{xy} \cdot L_x/(L_y \cdot L_z \cdot \Delta l) \quad (4.07)$$

FIG 4.11. Imposed transverse vertical strain

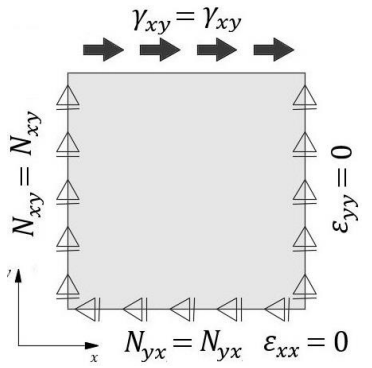

IMPOSED TRANSVERSE HORIZONTAL STRAIN.

$$\begin{Bmatrix} \sigma_{xx} \\ \sigma_{yy} \\ \tau_{yx} \end{Bmatrix} = \begin{Bmatrix} N_{xx}/(L_y \cdot L_z) \\ N_{yy}/(L_x \cdot L_z) \\ N_{yx}/(L_x \cdot L_z) \end{Bmatrix} = \begin{bmatrix} Q_{11} & Q_{12} & 0 \\ Q_{21} & Q_{22} & 0 \\ 0 & 0 & Q_{33} \end{bmatrix} \begin{Bmatrix} 0 \\ 0 \\ \gamma_{yx} \end{Bmatrix}$$

$$\tau_{yx} = Q_{33} \cdot \gamma_{yx} \;\rightarrow\; Q_{33} = N_{yx} \cdot L_y/(L_x \cdot L_z \cdot \Delta l) \quad (4.08)$$

FIG 4.12. Imposed transverse horizontal strain

The angular distortion is applied by means of a transverse strain in one of the edges, called here imposed transverse vertical or horizontal strain. In each case, Q_{33} can be obtained after retrieving the reactions N_{xy} or N_{yx}, according to Cauchy $\tau_{xy} = \tau_{yx}$ resulting to the same Q_{33} independently of the one chosen. AS long as N_{xy} in the imposed transverse vertical strain is equal to N_{yx} in the imposed transverse horizontal strain, the two tests will lead to the same result as well. To test the integrity of the experiment, Q_{33} is calculated in those four different ways and in all cases the results are equivalent. The homogenized mechanical properties follow the system of equations:

$$\begin{bmatrix} Q_{11} = \dfrac{E_x}{1 - \nu_{xy}\nu_{yx}} & Q_{12} = \dfrac{\nu_{xy}E_y}{1 - \nu_{xy}\nu_{yx}} & 0 \\ Q_{21} = \dfrac{\nu_{yx}E_x}{1 - \nu_{xy}\nu_{yx}} & Q_{22} = \dfrac{E_y}{1 - \nu_{xy}\nu_{yx}} & 0 \\ 0 & 0 & Q_{33} = G \end{bmatrix} \quad (4.09)$$

$$E_x = E_x \rightarrow\; Q_{11} \cdot (1 - \nu_{xy}\nu_{yx}) = Q_{21} \cdot (1 - \nu_{xy}\nu_{yx})/\nu_{yx} \;\rightarrow\; \nu_{yx} = Q_{21}/Q_{11} \quad (4.10)$$

$$E_y = E_y \rightarrow\; Q_{22} \cdot (1 - \nu_{xy}\nu_{yx}) = Q_{12} \cdot (1 - \nu_{xy}\nu_{yx})/\nu_{xy} \;\rightarrow\; \nu_{xy} = Q_{12}/Q_{22} \quad (4.11)$$

$$E_x = Q_{11} \cdot (1 - \nu_{xy}\nu_{yx}) \rightarrow\; E_x = Q_{11} - Q_{21} \cdot Q_{12}/Q_{22} \quad (4.12)$$

$$E_y = Q_{22} \cdot (1 - \nu_{xy}\nu_{yx}) \rightarrow\; E_y = Q_{22} - Q_{21} \cdot Q_{12}/Q_{11} \quad (4.13)$$

$$G = Q_{33} \quad (4.14)$$

As final step, those results are normalized diving them by the modulus of elasticity of the base material (E_b). The tables will present the results as percentages. A percentage of 20% indicates that the homogenized modulus of elasticity is a fifth of the modulus of elasticity of the base material.

4.1.6. BOUDARY CONSTRAINS REGARDING ROTATION

Those boundary conditions refer to the displacement degrees of freedom but nothing has been stated regarding the rotation degree of freedom of the beam elements on the panel perimeter as that parameter is decoupled in the constitutive matrix. There are two possibilities regarding the rotation in the z-direction of the bars end in the panel perimeter, **they can be either be pinned or fixed.** The moments distribution changes slightly:

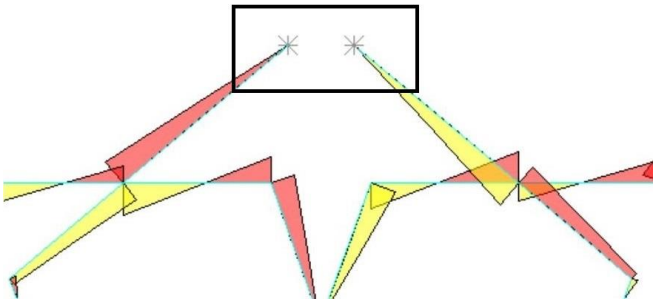

FIG 4.13. Bars pinned in the perimeter

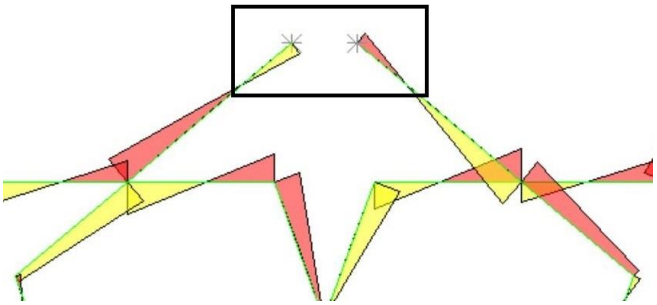

FIG 4.14. Bars fixed in the perimeter

The reactions obtained in both cases are different as the corresponding homogenized mechanical properties. This local effect has less influence in the global homogenized mechanical properties as the number of modules in the panel increases. A panel of infinite modules will have ideal homogenized mechanical properties regardless of the rotation constrain in the perimeter. That phenomenon is called **Representative Element Volume effect** and it will be further studied with a sensitivity assessment. In all cases, constraining the bars rotation at the perimeter provide exact results for all mechanical properties exept for the shear modulus, while the opposite is true when the tests are done with the rotation dof left free. In other words, symmetric boundary conditions provide the ideal vaues for the symmetric mechanical properties, while antisymmetric boundary conditions provide the ideal vaues for the antisymmetric mechanical properties:

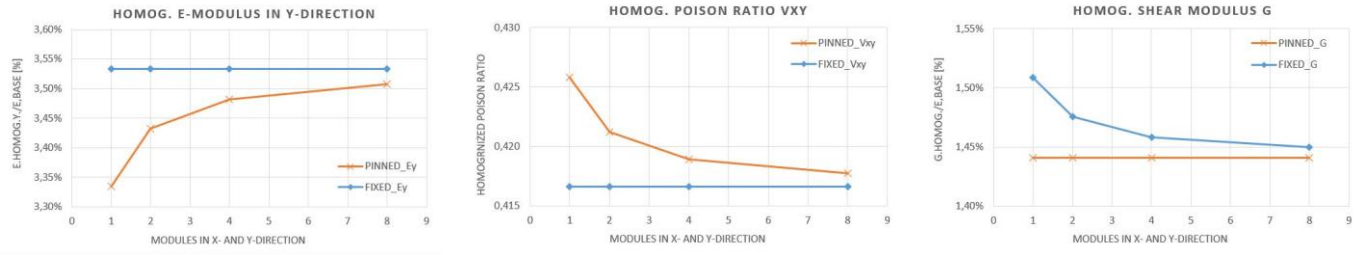

FIG 4.15. Homogenized mechanical properties obtained with symmetric (blue) and antisymmetric (orange) boundary conditions for different panel sizes

Symmetric boundary conditions (rotation constrained) result in ideal values for the symmetric homogenized mechanical properties (homogenized moduli of elasticity and Poisson ratios):

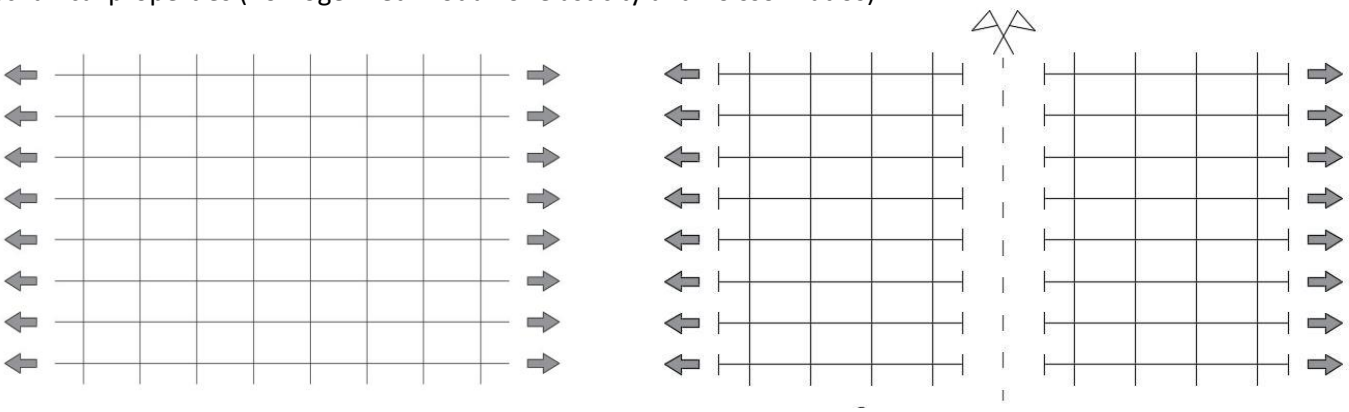

FIG 4.16. Symmetric boundary conditions

Antisymmetric boundary conditions (rotation free) result in ideal values for the antisymmetric homogenized mechanical properties (shear modulus):

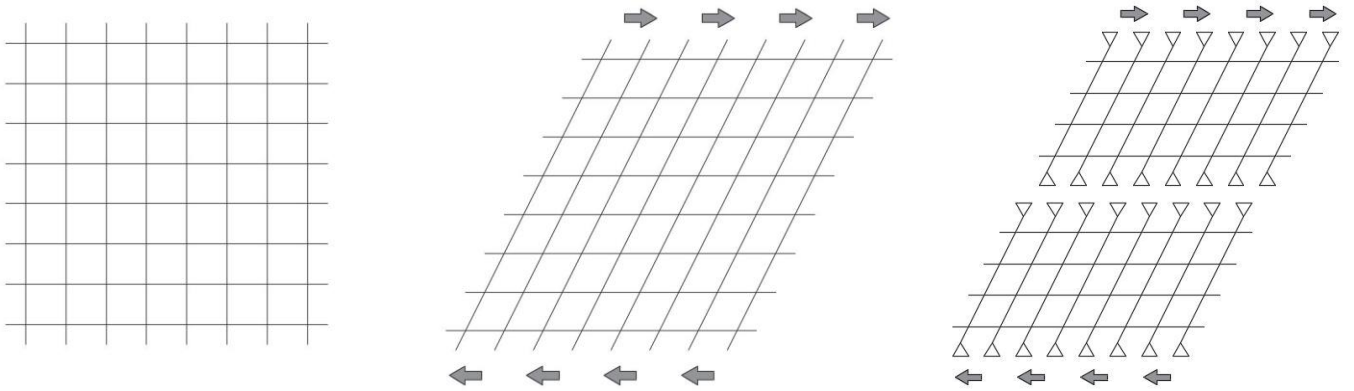

FIG 4.17. Antisymmetric boundary conditions

The least cost-effective approach would be to automate the process so the panel is tested with the rotation dof constrained to retrieve the reactions for the Poisson ratios and moduli of elasticity. Then, automatically release the rotation dof in the supports so the panel can be tested again to retrieve the reactions for the shear modulus. This approach provides directly ideal results and it keeps at minimum the number of models to be exported and tested.

However, this is only suitable for the tests done with beam elements that are, on the other hand, done very fast. When analyzing the patterns with membrane elements, the rotation dof at the supports is indirectly restrained as the imposed displacements are the same at different points of the beam depth.

One of the objectives is to systematize the analysis, to do so, in all cases the rotation dofs at the supports are restrained and a Representative Element Volume refinement is done to take into account that effect. The use of identical boundary conditions for the beam and membrane elements analyses will allow to obtain the 2D correction factors by analyzing panels of just 1x1 modules.

The possibility of using periodic boundary conditions to obtain directly the ideal homogenized mechanical properties analyzing just one size panel has been discarded in *Chapter 2.5. Periodic boundary conditions* due to its complexity of implementation as a systematic analysis in patterns with different generating symmetries.

4.2. HOMOGENIZATION METHODOLOGY

The homogenization of the chosen historic geometric Islamic patterns is performed in accordance with the procedure and formulation described in *Chapter 4.1.5. Homogenization process*. There are, nevertheless, three important phenomena that must be taken into account in order to have an accurate homogenization:

- Representative Element Volume: Difference in the homogenized mechanical properties due to the size of the sample. In this case, difference in the results due to the number of modules that compose the panel. It is directly related to the effect that the boundaries have in the global behaviour. As the number of modules used increases, the effect of the boundary conditions diminishes. A Representative Element Volume refinement is done with the beam elements to get the ideal behaviour of an infinite by infinite modules panel. The result of this exercise is the pattern 1D ideal behaviour.

- Mesh refinement: In the case of the geometric Islamic patterns, it is found that the results are very sensitive to the mesh size probably because they are full of sharp openings leading to numerous concentrations of stresses. The result of this refinement is the 2D ideal behaviour of a 1x1 panel.

- Membrane correction factor: As the beam depth increases and the slenderness of the beams decreases, the beam theory ceases to be applicable. It will also lead to overlapping and other effects that are not included when modelling with beam elements. An analysis with membrane elements is necessary to take into account those effects that have a great importance in all the geometric Islamic patterns. The result of this exercise is the membrane correction factors.

All those effects are addressed for each chosen historic geometric Islamic pattern and for different beam sizes. At the end, approximately 10 000 analyses have been necessary to define all the homogenized mechanical properties of all the patterns and beam sizes, in accordance with the following scheme:

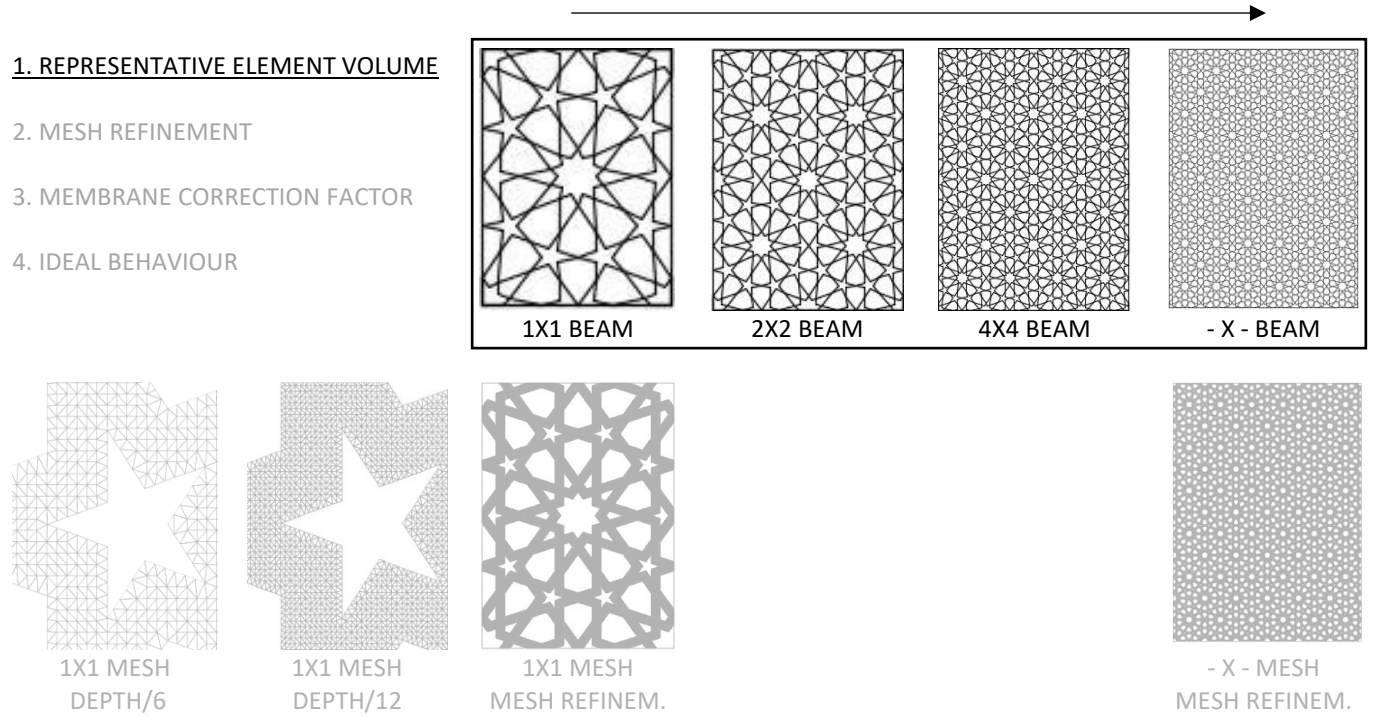

FIG 4.18. Homogenization methodology. Step 1

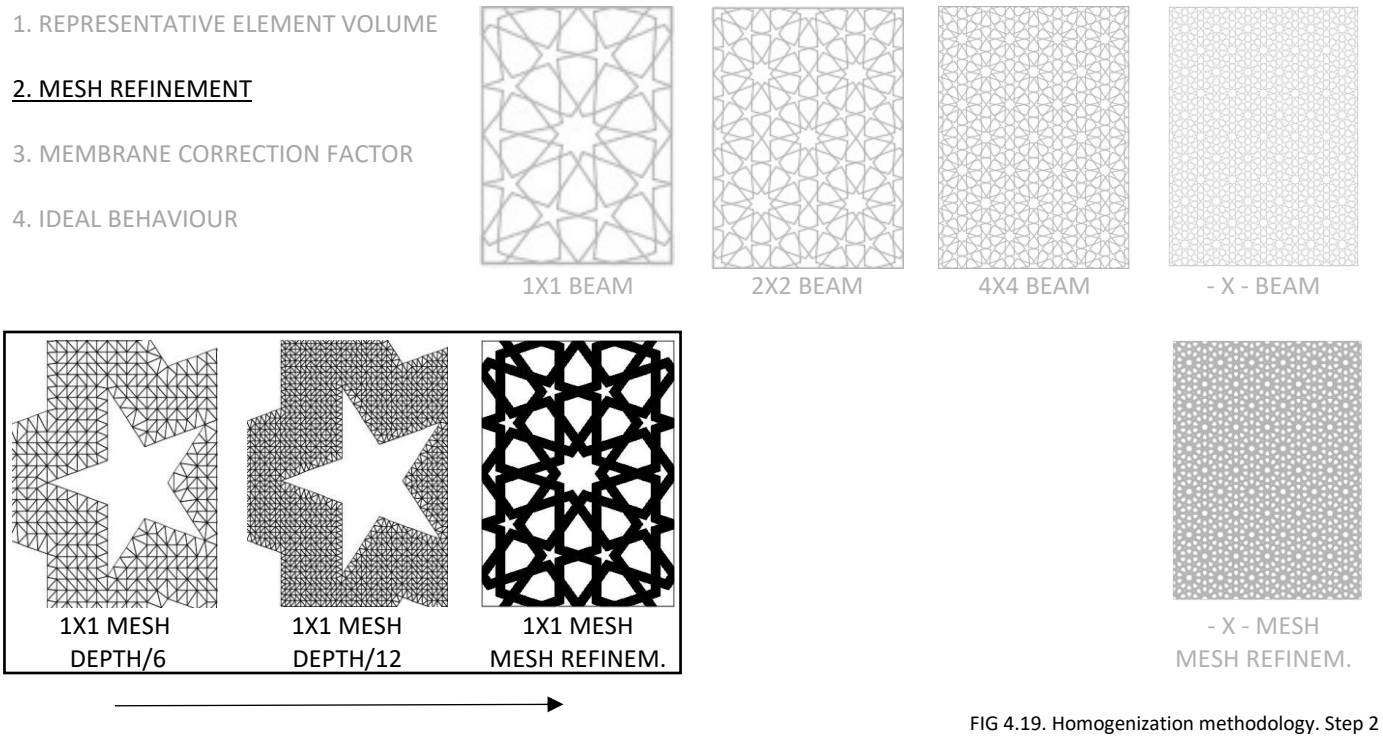

FIG 4.19. Homogenization methodology. Step 2

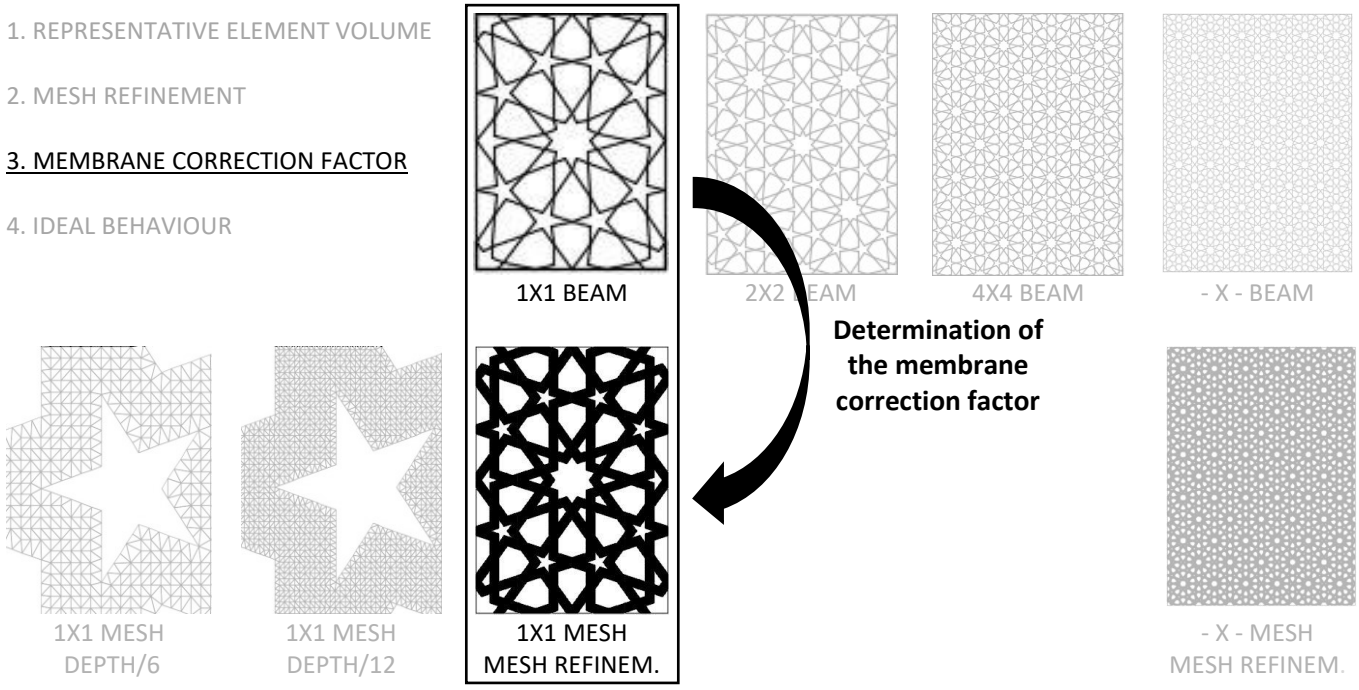

FIG 4.20. Homogenization methodology. Step 3

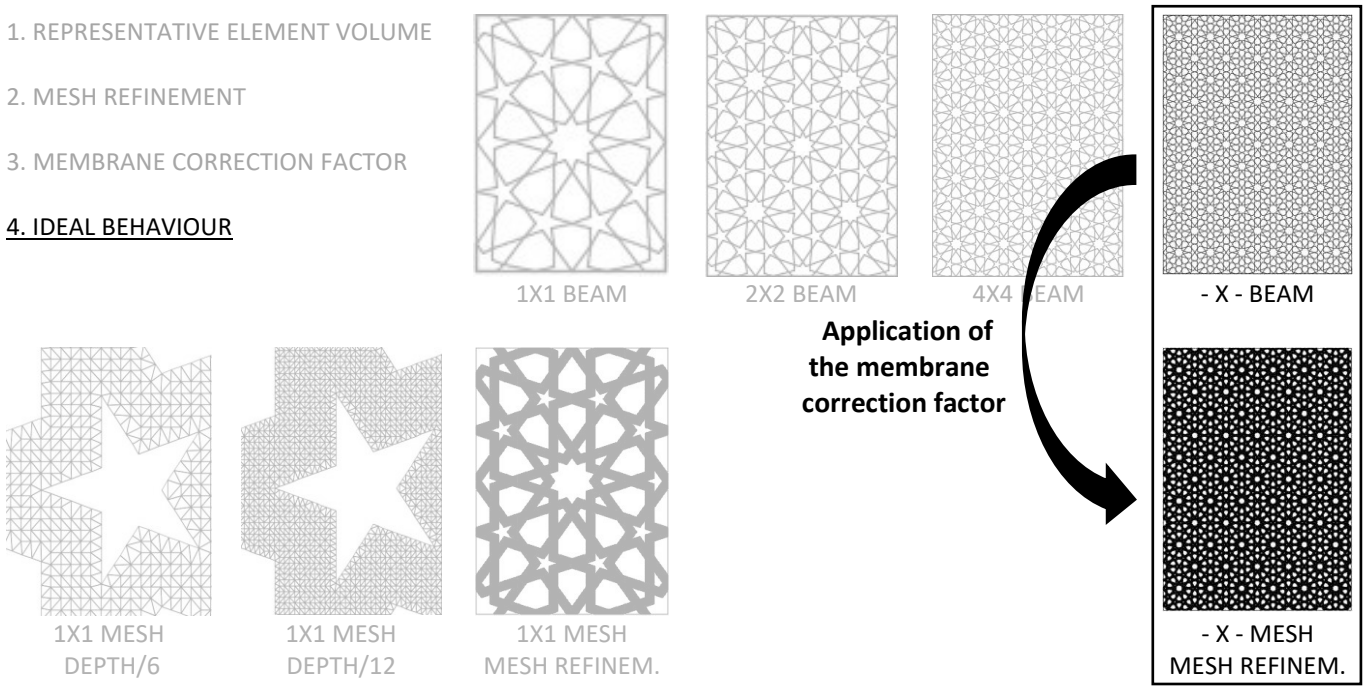

FIG 4.21. Homogenization methodology. Step 4

4.3. REPRESENTATIVE ELEMENT VOLUME (REV)

For the analysis, the tessellation ROS-I-6.10.10. θ =72º, type Star, with a relative beam depth of 4%, has been chosen. To observe the effect due to the variation of modules in the x--, y-direction and a combination of both, the following models have been tested:

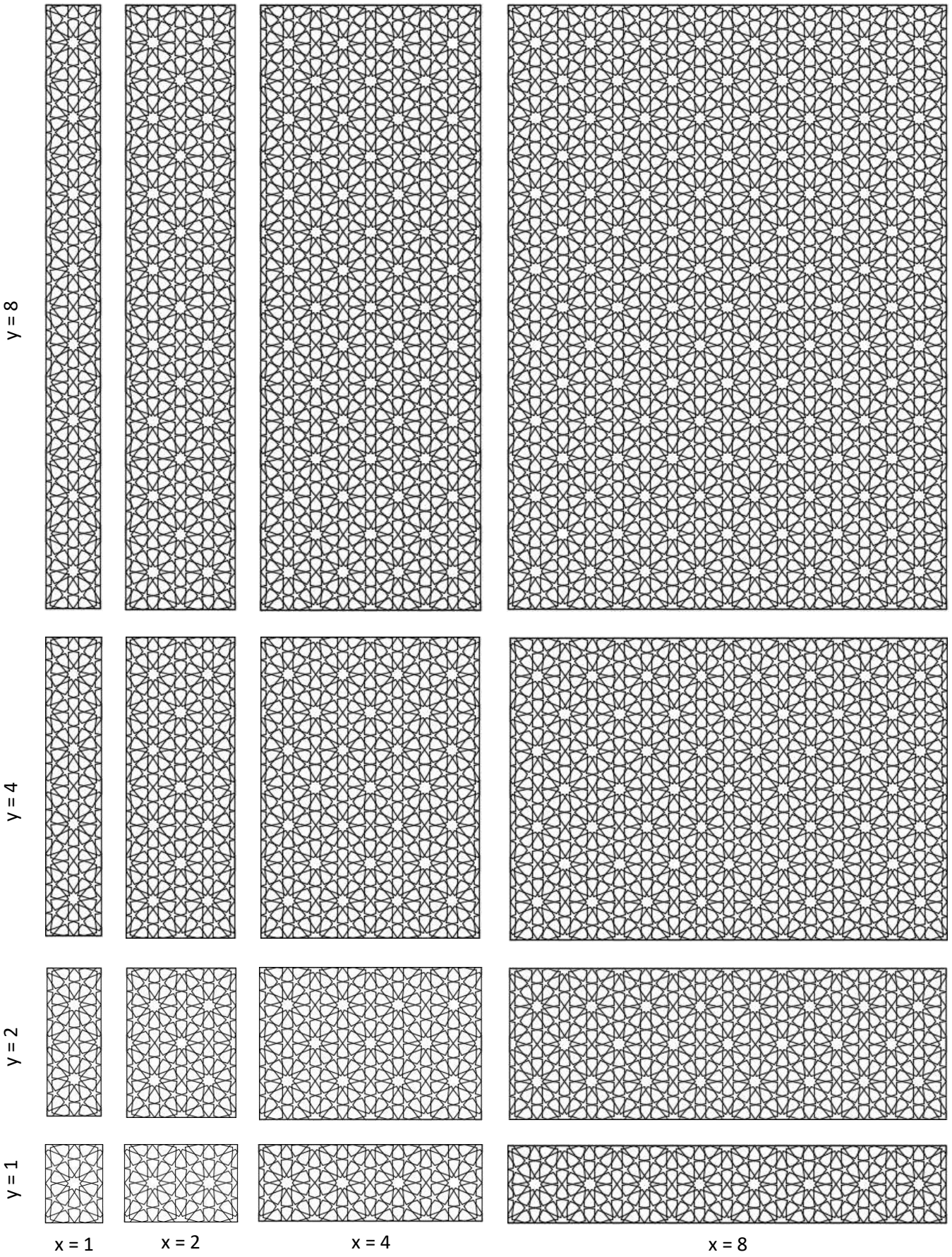

FIG 4.22. Panels under study for the Representative Element Volume assessment.

Homogenized mechanical properties for rotation dof not constrained at the supports:

Modules	Lx	Ly	Ex	Ey	vxy	vyx	G
1x1	5,0	6,9	2,691%	3,335%	0,42582	0,5277	1,441%
1x2	5,0	13,8	2,709%	3,425%	0,42080	0,5320	1,441%
1x4	5,0	27,5	2,718%	3,471%	0,41820	0,5342	1,441%
1x8	5,0	55,1	2,722%	3,495%	0,41695	0,5353	1,441%

Modules	Lx	Ly	Ex	Ey	vxy	vyx	G
4x1	20,0	6,9	2,698%	3,347%	0,4264	0,5289	1,441%
4x2	20,0	13,8	2,716%	3,436%	0,4214	0,5331	1,441%
4x4	20,0	27,5	2,725%	3,482%	0,4189	0,5353	1,441%
4x8	20,0	55,1	2,729%	3,505%	0,4176	0,5364	1,441%

Modules	Lx	Ly	Ex	Ey	vxy	vyx	G
2x1	10,0	6,9	2,696%	3,343%	0,4262	0,5285	1,441%
2x2	10,0	13,8	2,714%	3,432%	0,4212	0,5327	1,441%
2x4	10,0	27,5	2,723%	3,478%	0,4187	0,5349	1,441%
2x8	10,0	55,1	2,727%	3,502%	0,4174	0,5360	1,441%

Modules	Lx	Ly	Ex	Ey	vxy	vyx	G
8x1	40,0	6,9	2,700%	3,349%	0,4265	0,5291	1,441%
8x2	40,0	13,8	2,717%	3,438%	0,4215	0,5333	1,441%
8x4	40,0	27,5	2,726%	3,484%	0,419	0,5355	1,441%
8x8	40,0	55,1	2,731%	3,507%	0,4178	0,5366	1,441%

TABLE 4.1. Homogenized mechanical properties for rotation dof not constrained at the supports.

There is convergence, an increment of the number of modules leads to more accurate results in all cases. A deviation from the square shape does not affect negatively the results obtained as long as that deviation is obtained by means of an increment of modules in the panel. Panels 1x8 and 2x8 are good examples of how a façade of a tall building could look like with this system. However, the application is not direct. These tests are aimed to characterize the homogenized material, they are not aimed to search a direct application since the boundary conditions of the tests (restrained edges) differ to those of the built tower (cantilever beam).

The chosen number of modules in x- and y-direction for the tests follow the rule that each one is twice as big as the precedent one (namely 1. 2. 4. 8). This, allows to estimate the convergence ratio and have a better insight.

Rotation dof not constrained at the supports:

PINNED	Lx (m)	Ly (m)	E_x	Diff %	E_y	Diff %	ν_{xy}	Diff %	ν_{yx}	Diff %	G	Diff %
1x1	5.0	6.9	0.02691	-	0.03335	-	0.42582	-	0.5277	-	0.01441	-
2x2	10.0	13.8	0.02714	0.829	0.03432	2.900	0.421187	-1.087	0.53268	0.945	0.01441	0.000
4x4	20.0	27.5	0.02725	0.416	0.03482	1.455	0.418897	-0.544	0.53527	0.486	0.01441	0.000
8x8	40.0	55.1	0.02731	0.208	0.03507	0.728	0.41776	-0.272	0.53659	0.246	0.01441	0.000

TABLE 4.2. REV assessment with free rotation at the supports

Rotation dof constrained at the supports

FIXED	Lx (m)	Ly (m)	E_x	Diff %	E_y	Diff %	ν_{xy}	Diff %	ν_{yx}	Diff %	G	Diff %
1x1	5.0	6.9	0.02736	-	0.03533	-	0.41663	-	0.5379	-	0.01509	-
2x2	10.0	13.8	0.02736	0.000	0.03533	0.000	0.416628	0.000	0.53792	0.000	0.01476	-2.205
4x4	20.0	27.5	0.02736	0.000	0.03533	0.000	0.416628	0.000	0.53792	0.000	0.01458	-1.164
8x8	40.0	55.1	0.02736	0.000	0.03533	0.000	0.416628	0.000	0.53792	0.000	0.01450	-0.598

TABLE 4.3. REV assessment with constrained rotation at the supports

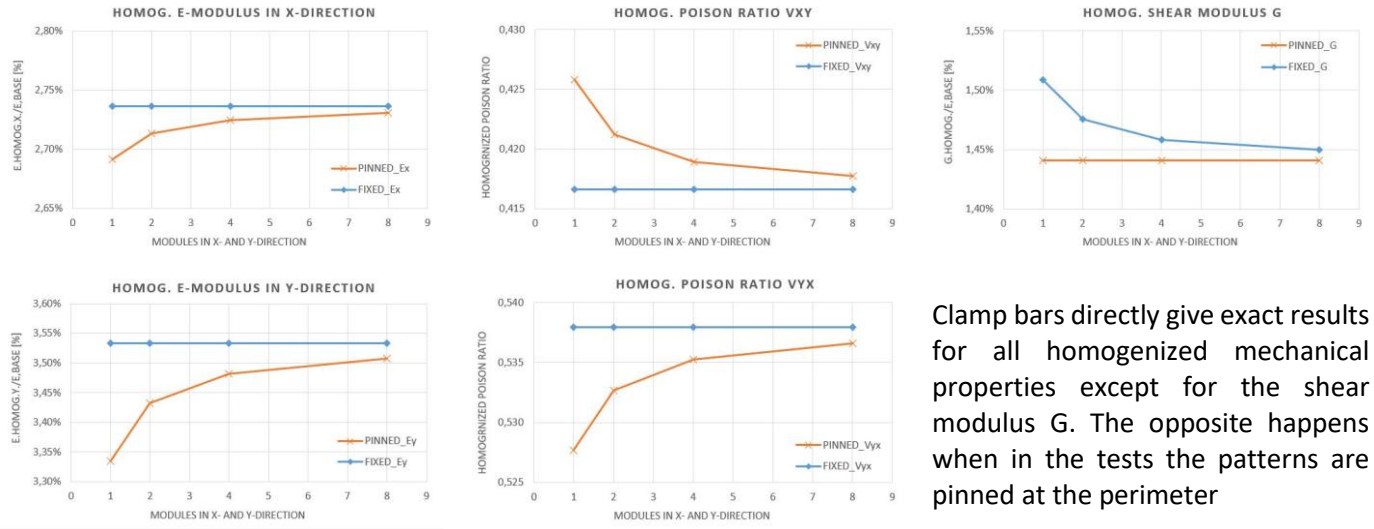

Clamp bars directly give exact results for all homogenized mechanical properties except for the shear modulus G. The opposite happens when in the tests the patterns are pinned at the perimeter

FIG 4.23. Homogenized mechanical properties obtained with symmetric (blue) and antisymmetric (orange) boundary conditions for different panel sizes

As explained in *Chapter 4.1.6. Boundary constrains regarding rotation*, symmetric boundary conditions provide the ideal values for the symmetric mechanical properties, while antisymmetric boundary conditions provide the ideal values for the antisymmetric mechanical properties. Symmetric boundary conditions are used in combination with Representative Element Volume refinement to allow direct relationship between the 1x1 panels with beam and membrane elements for the membrane correction factors determination. The patterns present an **order of convergence of two O(h²),** meaning that twice the number of modules leads to half the error. In each case, the difference between the 4x4 and 2x2 panel results are added to the result of the 4x4 panel to calculate the ideal behaviour. It is verified that the same convergence ratio is valid for all historic patterns studied, but is shown for 3 representative patterns:

D) LAHORE FORT COMPLEX

(Tessellation 4.8.8. θ =67.5º) Square symmetry. Relative beam depth = 5%

D	$E_{h,x}$	Diff %	$E_{h,y}$	Diff %	$\nu_{h,xy}$	Diff %	$\nu_{h,yx}$	Diff %	G_h	Diff %
1x1	7.05%	-	7.05%	-	0.221	-	0.221	-	1.19%	-
2x2	7.05%	0.00	7.05%	0.00	0.221	0.00	0.221	0.00	1.08%	-8.65
4x4	7.05%	0.00	7.05%	0.00	0.221	0.00	0.221	0.00	1.02%	-5.52

TABLE 4.4. REV. Convergence for pattern D

F) MUSTANSIRIYA MADRASA

(Tessellation 3.6.3.6. θ =30º). Hexagonal symmetry. Relative beam depth = 6%

F	$E_{h,x}$	Diff %	$E_{h,y}$	Diff %	$\nu_{h,xy}$	Diff %	$\nu_{h,yx}$	Diff %	G_h	Diff %
1x1	0.84%	-	0.84%	-	0.914	-	0.914	-	0.30%	-
2x2	0.84%	0.00	0.84%	0.00	0.914	0.00	0.914	0.00	0.25%	-16.41
4x4	0.84%	-0.01	0.84%	-0.01	0.914	0.00	0.914	0.00	0.24%	-7.57

TABLE 4.5. REV. Convergence for pattern F

R) FATEHPUR SIKRI

(Tessellation ROS-I-6.10.10. θ =72º type Star) Hexagonal symmetry. Relative beam depth = 3%

R	$E_{h,x}$	Diff %	$E_{h,y}$	Diff %	$\nu_{h,xy}$	Diff %	$\nu_{h,yx}$	Diff %	G_h	Diff %
1x1	1.49%	-	2.00%	-	0.458	-	0.615	-	0.91%	-
2x2	1.49%	0.00	2.00%	0.00	0.458	0.00	0.615	0.00	0.88%	-2.61
4x4	1.49%	0.00	2.00%	0.00	0.458	0.00	0.615	0.00	0.87%	-1.38

TABLE 4.6. REV. Convergence for pattern R

VARIATION IN SIZE

This point is aimed to verify that changing the panel's size won't have any effect in the obtained equivalent mechanical properties. The chosen pattern is *Alhambra* (tessellation ROS-I-6.9.12.9. θ =70º, L =35%) due to its high complexity and hexagonal symmetry. The sizes under study will be 5m, 10m and 20m in the x-direction. The beam depth chosen is 4%, corresponding to 20cm, 40cm and 80cm. The panel thickness is 1m.

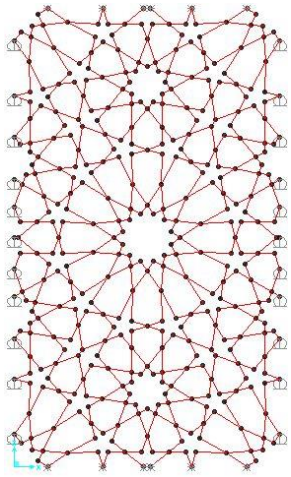

FIG 4.24. ROS-I-6.9.12.9. θ =70º, L =35%

Alhambra, $L_x = 5m$, rel. beam depth = 4% (20cm)

rel beam depth	HOMOGENIZED MECHANICAL PROPERTIES				
[%]	Ex	Ey	vxy	vyx	G
4	9,33%	9,40%	0,301	0,303	3,62%

Alhambra, $L_x = 10m$, rel. beam depth = 4% (40cm)

rel beam depth	HOMOGENIZED MECHANICAL PROPERTIES				
[%]	Ex	Ey	vxy	vyx	G
4	9,33%	9,40%	0,301	0,303	3,62%

Alhambra, $L_x = 20m$, rel. beam depth = 4% (80cm)

rel beam depth	HOMOGENIZED MECHANICAL PROPERTIES				
[%]	Ex	Ey	vxy	vyx	G
4	9,33%	9,40%	0,301	0,303	3,62%

TABLE 4.7. Homogenized mechanical properties for same pattern with different sizes.

The results are exactly identical independently of the module size or the imposed strain (linear elastic analysis)

4.4. FEM BEAM ELEMENTS

These homogenized equivalent properties are obtained using beam elements and refining the results to take into account the Representative Element Volume for an order of converge of 2 as per *Chapter 4.3. Representative Element Volume (REV).* It corresponds to the first stage in the scheme described in Chapter 4.2. *Homogenization methodology,* named "- X - BEAM":

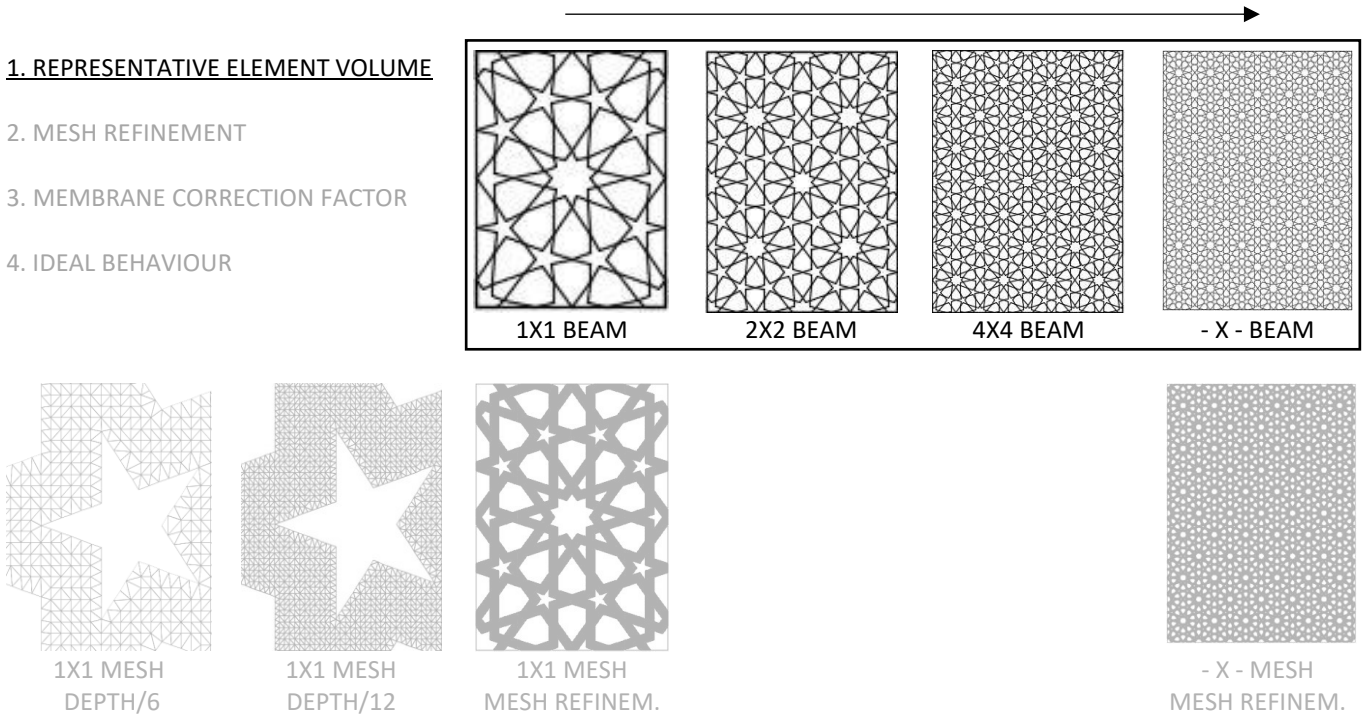

FIG 4.25. Homogenization methodology. Step 1

The information included in each case from left to right is:

- Given name to the pattern and the tessellation and parameters to draw it with the Hankin method.
- Picture of the pattern displaying what is considered as its module. The module length in the x-direction (horizontally in the picture) is needed for the relative beam depth (rbd %) definition.
- Table of homogenized mechanical properties taking into account the Representative Element Volume
- Graphs with the evolution of the homogenized mechanical properties as the rbd increases.

In this chapter, only three representative results are included (Square, pentagonal and hexagonal symmetries). For the complete set of tables for historic and parametric variations, see *Appendix I. Design guide.*

The numerical results for 2x2 and 4x4 panels, leading to the obtained homogenized mechanical properties are collected in *Appendix II. Numerical results.*

D) LAHORE FORT COMPLEX. Tessellation 4.8.8. θ =67.5º. Square symmetry.

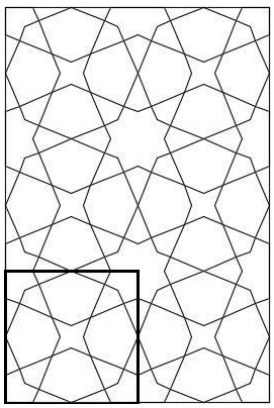

D67.5		HOMOGENIZED MECHANICAL PROPERTIES				
rbd [%]	Sat [%]	$E_{h,x}$	$E_{h,y}$	$\nu_{h,xy}$	$\nu_{h,yx}$	G_h
1	7.23	0.18%	0.18%	0.191	0.191	0.01%
2	14.12	1.10%	1.10%	0.197	0.197	0.08%
3	20.69	2.76%	2.76%	0.207	0.207	0.25%
4	26.93	4.82%	4.82%	0.215	0.215	0.55%
5	32.83	7.05%	7.05%	0.221	0.221	0.96%
6	38.41	9.36%	9.36%	0.224	0.224	1.49%
7	43.66	11.69%	11.69%	0.225	0.225	2.12%
8	48.58	14.04%	14.04%	0.225	0.225	2.82%
9	53.17	16.41%	16.41%	0.223	0.223	3.58%

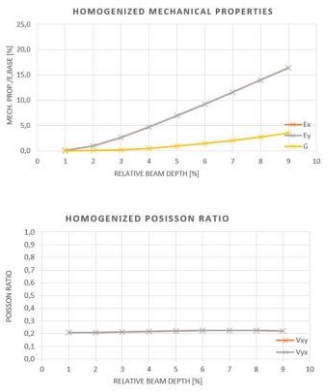

FIG 4.26. Pattern D. Homogenized mechanical properties with beams FE.

F) MUSTANSIRIYA MADRASA. Tessellation 3.6.3.6. θ =30º. Hexagonal symmetry.

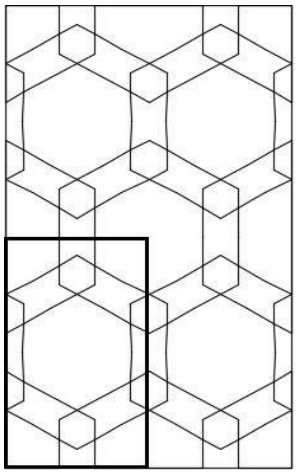

F30		HOMOGENIZED MECHANICAL PROPERTIES				
rbd [%]	Sat [%]	$E_{h,x}$	$E_{h,y}$	$\nu_{h,xy}$	$\nu_{h,yx}$	G_h
2	9.68	0.03%	0.03%	0.973	0.973	0.01%
3	14.28	0.11%	0.11%	0.963	0.963	0.03%
4	18.72	0.26%	0.26%	0.949	0.949	0.07%
5	23.00	0.50%	0.50%	0.933	0.933	0.13%
6	27.12	0.84%	0.84%	0.914	0.914	0.22%
7	31.08	1.28%	1.28%	0.893	0.893	0.33%
8	34.88	1.84%	1.84%	0.870	0.870	0.49%
9	38.52	2.51%	2.51%	0.846	0.846	0.67%
10	42.00	3.29%	3.29%	0.822	0.822	0.89%
11	45.32	4.17%	4.17%	0.798	0.798	1.15%
12	48.48	5.14%	5.14%	0.774	0.774	1.44%

FIG 4.27. Pattern F. Homogenized mechanical properties with beams FE.

R) FATEHPUR SIKRI. Tessellation ROS-I-6.10.10. type Star. Pentagonal symmetry.

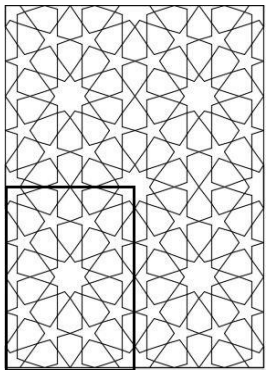

R72		HOMOGENIZED MECHANICAL PROPERTIES				
rbd [%]	Sat [%]	$E_{h,x}$	$E_{h,y}$	$\nu_{h,xy}$	$\nu_{h,yx}$	G_h
1	13.86	0.07%	0.10%	0.517	0.730	0.04%
2	26.49	0.50%	0.69%	0.493	0.680	0.30%
3	37.90	1.49%	2.00%	0.458	0.615	0.86%
4	48.08	3.06%	3.99%	0.420	0.548	1.68%
5	57.03	5.11%	6.50%	0.382	0.486	2.72%
6	64.76	7.52%	9.37%	0.348	0.433	3.94%
7	x	x	x	x	x	x
8	x	x	x	x	x	x

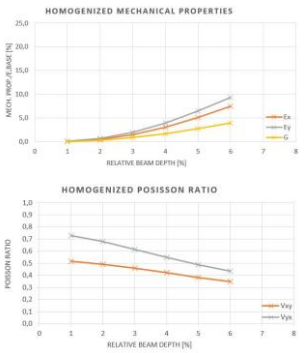

FIG 4.28. Pattern R. Homogenized mechanical properties with beams FE.

The homogenized mechanical properties are normalized dividing the results by the base material modulus of elasticity (E_{base}). A fully continuous opaque panel has a homogenized modulus of elasticity of 1 (100%), so a value of 5.69% for the homogenized modulus of elasticity (E) means that it will have a modulus of elasticity that is 5.69% of a fully filled panel with the same thickness. The results ae obtained with beam elements in a linear elastic analysis. Therefore, it does not have into account effects such as overlaps as the pattern grows opaquer or non-linear effects derived from the different stress levels inside the pattern.

The patterns are generated with Grasshopper and then exported to Autocad files (dxf). Then, they are imported in SAP2000 and analysed for a series of rectangular cross-sections. In all cases, the panel thickness is kept in 1m as the beam depth varies not to affect the results. All the panels are generated with a module size in the x-direction of 5m. It is to say, 1x1 panels measure 5m in the x-direction, 2x2 panels 10m and 4x4 panels 20m. This way, 5cm always corresponds to a relative beam depth (rbd) of 1% and the varying relative beam depth input can be automated.

4.5. FEM MEMBRANE ELEMENTS.

So far, the patterns' behaviour and their homogenized mechanical properties have been obtained in static linear analyses using beam elements. Those frame elements provide an approximate response with a small computational effort. Thus, their use is justified to assess the applicability of the homogenization method for the bearing system of tall building as the number of elements required in façade surpass greatly the computational capacity of the laptop used for the analysis in this research. In the case of characterizing the patterns, it also becomes handy to broaden the range of patterns under study by the inclusion of alternatives. And finally, it facilitates the refinement study of the Representative Volume Element for the shear modulus, so the analysis with membrane elements are required just for 1x1 panels.

Nevertheless, this simple analysis with beam elements leaves aside some rather important aspects. As the relative beam depth increases the beam's theory becomes less and less applicable becoming D-regions. In the nodes, the actual node stiffness and the effects introduced by the bars overlapping are neglected. Confinement effects do not appear with beam elements as the base material Poisson ratio plays no role in 1D elements.

For those reasons, it becomes clear the convenience to carry an in-plane analysis with membrane elements to get more realistic values for the homogenized mechanical properties.

This chapter is aimed to highlight in a simple model the differences in the results from using beam elements (1D) and membrane elements (2D). This will help to better understand the differences in the results when applied to a complex pattern. The material used for the tests is a 30MPa concrete with mechanical properties in accordance with EC2 ($E = 28.576 * 791 \frac{kN}{m^2}$, $v = 0.2$. $G = 11 * 906 * 996\ kN/m^2$)

FULL PANEL

The tested panel has a length of 10m in the x-direction and 5m in the y-direction. In the case of bar elements, it is model just by 5 horizontal bars of 1m depth.

Lx [m]	10.00	LONGITUDINAL ANALYSIS				TRANSVERSAL ANALYSIS			
Ly [m]	5.00	dx=1	Nx≠0	dx=0	Nx≠0	dx,up=1	Nxy≠0	dx=0	Nxy≠0
Bars [m]	100.00	dy=0	Ny≠0	dy=1	Ny≠0	dy=0	Nyx≠0	dy,right=1	Nyx≠0
GEOMETRY		HORIZONTAL		VERTICAL		HORIZ. DISTORTION		VERTICAL DISTORTION	
depth	Sat.	$N_{xh} = Q_{11}$	$N_{yh} = Q_{21}$	$N_{xv} = Q_{12}$	$N_{yv} = Q_{22}$	$N_{xy,h}$	$N_{yx,h}$	$N_{xy,v}$	$N_{yx,v}$
[m]	[%]	[kN]	[kN]	[kN]	[kN]	[kN]	[kN]	[kN]	[kN]
1.00	100	14,288,396	0	0	57,153,582	8,929,107	3,227,987	3,227,987	2,074,626

TABLE 4.8. Reactions from full panel modelled with beam FE

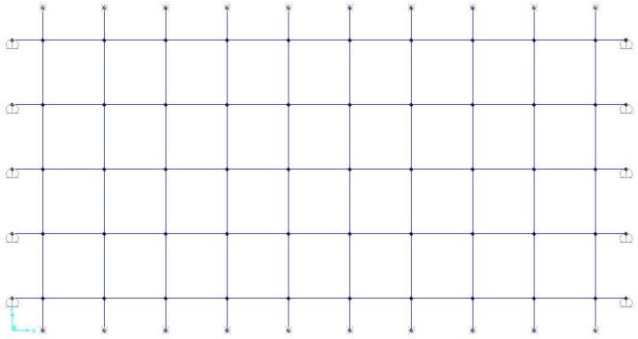

FIG 4.29.Full panel with beam FE

10x5m	HOMOGENIZED MECHANICAL PROPERTIES				
Sat. [%]	$E_{h,x}$	$E_{h,y}$	$\nu_{h,xy}$	$\nu_{h,yx}$	G_h
100	100.00%	100.00%	0.000	0.000	13.18%

TABLE 4.9. Homogenized mechanical properties model full panel with beam FE

The grid opening and the beam depth are both 1m, resulting in a full panel in the x- and y-direction. This leads to a real modelled saturation of 200%, but not considering the overlaps the saturation is 100%.

In the analysis the Poisson ratio of the base material plays no role. The bars in the imposed deformation direction do not change their cross-section and the transversal bars move as rigid bodies. As result, the confinement effect is not included in the results and the obtained Poisson ratio is zero. On the other hand, the Young's modulus in the x- and y-direction are accurately obtained, but the shear modulus is greatly underestimated as it should be in the order of 40% of the base modulus of elasticity.

The same panel modelled with membrane elements:

Lx [m]	10.00	LONGITUDINAL ANALYSIS				TRANSVERSAL ANALYSIS			
Ly [m]	5.00	dx=1	Nx≠0	dx=0	Nx≠0	dx,up=1	Nxy≠0	dx=0	Nxy≠0
Bars [m]	0.00	dy=0	Ny≠0	dy=1	Ny≠0	dy=0	Nyx≠0	dy,right=1	Nyx≠0
GEOMETRY		HORIZONTAL		VERTICAL		HORIZ. DISTORTION		VERTICAL DISTORTION	
Thick.	Sat.	$N_{xh}=Q_{11}$	$N_{yh}=Q_{21}$	$N_{xv}=Q_{12}$	$N_{yv}=Q_{22}$	$N_{xy,h}$	$N_{yx,h}$	$N_{xy,v}$	$N_{yx,v}$
[m]	[%]	[kN]	[kN]	[kN]	[kN]	[kN]	[kN]	[kN]	[kN]
1.00	100	14,883,745	5,953,498	5,953,498	59,534,981	23,813,993	11,906,996	11,906,996	5,953,498

TABLE 4.10. Reactions from full panel modelled with membrane FE

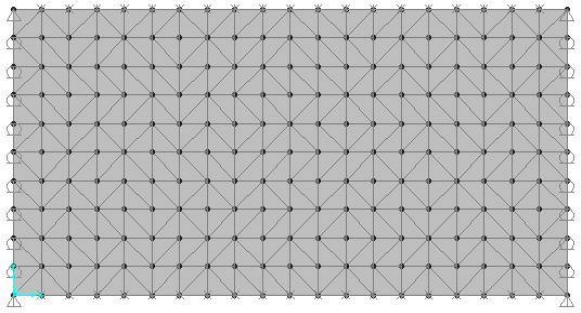

10x5m	HOMOGENIZED MECHANICAL PROPERTIES				
Sat. [%]	$E_{h,x}$	$E_{h,y}$	$\nu_{h,xy}$	$\nu_{h,yx}$	G_h
100	100.00%	100.00%	0.200	0.200	41.67%

The same results are obtained regardless of the mesh size. The amount of material modelled corresponds exactly with the saturation as no overlapping occurs.

TABLE 4.11. Homogenized mechanical properties model full panel with membrane FE
FIG 4.30. Full panel with membrane FE

In this case, the Poisson ratio of the base material plays a role. There is a confinement effect that can be observed in the measured reactions ($Q_{11} = 14 * 883.745kN$ instead of $Q_{11} = 14 * 288.396kN$) but that does not deviate the homogenized mechanical properties from their actual values. All the obtained properties (Young's modulus in x- and y-direction, Poisson ratios and shear modulus) are accurately obtained and have the same values as the base material.

GRID

The same analysis is repeated with a varying relative beam depth:

Lx [m]	10.00	LONGITUDINAL ANALYSIS				TRANSVERSAL ANALYSIS			
Ly [m]	5.00	dx=1	Nx≠0	dx=0	Nx≠0	dx,up=1	Nxy≠0	dx=0	Nxy≠0
Bars [m]	100.00	dy=0	Ny≠0	dy=1	Ny≠0	dy=0	Nyx≠0	dy,right=1	Nyx≠0
GEOMETRY		HORIZONTAL		VERTICAL		HORIZ. DISTORTION		VERTICAL DISTORTION	
depth	Sat.	$N_{xh}=Q_{11}$	$N_{yh}=Q_{21}$	$N_{xv}=Q_{12}$	$N_{yv}=Q_{22}$	$N_{xy,h}$	$N_{yx,h}$	$N_{xy,v}$	$N_{yx,v}$
[m]	[%]	[kN]	[kN]	[kN]	[kN]	[kN]	[kN]	[kN]	[kN]
0.1	19.00	1,428,840	0	0	5,715,358	33,940	14,719	14,719	7,684
0.3	51.00	4,286,519	0	0	17,146,075	737,972	314,335	314,335	167,591
0.5	75.00	7,144,198	0	0	28,576,791	2,473,828	1,018,767	1,018,767	564,883
0.7	91.00	10,001,877	0	0	40,007,507	4,843,386	1,905,166	1,905,166	1,113,456
0.9	99.00	12,859,556	0	0	51,438,224	7,521,469	2,801,273	2,801,273	1,741,472

TABLE 4.12. Reactions from grid modelled with membrane FE

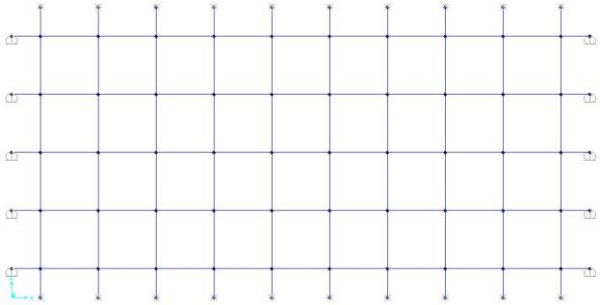

Beam depth	HOMOGENIZED MECHANICAL PROPERTIES				
[m]	$E_{h,x}$	$E_{h,y}$	$\nu_{h,xy}$	$\nu_{h,yx}$	G_h
0.1	10.00%	10.00%	0.000	0.000	0.05%
0.3	30.00%	30.00%	0.000	0.000	1.17%
0.5	50.00%	50.00%	0.000	0.000	3.85%
0.7	70.00%	70.00%	0.000	0.000	7.40%
0.9	90.00%	90.00%	0.000	0.000	11.24%

TABLE 4.13. Homogenized mechanical properties modelling grid with beam FE
FIG 4.31. Grid with beam FE

Young's modulus directly proportional to beam depth. Contrary to observations for the full panel experiment, in this case there is a small difference on the results depending on the mesh size. The following results are obtained with a mesh size of 10cm, producing an error smaller than 1%

Lx [m]	10.00	LONGITUDINAL ANALYSIS				TRANSVERSAL ANALYSIS			
Ly [m]	5.00	dx=1	Nx≠0	dx=0	Nx≠0	dx,up=1	Nxy≠0	dx=0	Nxy≠0
Bars [m]	0.00	dy=0	Ny≠0	dy=1	Ny≠0	dy=0	Nyx≠0	dy,right=1	Nyx≠0
GEOMETRY		HORIZONTAL		VERTICAL		HORIZ. DISTORTION		VERTICAL DISTORTION	
depth	Sat.	$N_{xh} = Q_{11}$	$N_{yh} = Q_{21}$	$N_{xv} = Q_{12}$	$N_{yv} = Q_{22}$	$N_{xy,h}$	$N_{yx,h}$	$N_{xy,v}$	$N_{yx,v}$
[m]	[%]	[kN]	[kN]	[kN]	[kN]	[kN]	[kN]	[kN]	[kN]
0.1	19.00	1,510,726	82,016	82,016	6,044,273	113,401	56,700	56,700	28,350
0.3	51.00	4,731,860	797,348	797,348	18,816,140	1,617,977	808,989	808,989	404,494
0.5	75.00	8,251,526	2,429,771	2,429,771	32,881,589	7,470,909	3,735,454	3,735,454	1,867,727
0.7	91.00	12,034,572	4,560,757	4,560,757	48,018,369	17,328,413	8,664,207	8,664,207	4,332,103
0.9	99.00	14,628,367	5,827,369	5,827,369	58,597,359	23,357,899	11,678,950	11,678,950	5,839,475

TABLE 4.14. Reactions from full panel modelled with membrane FE

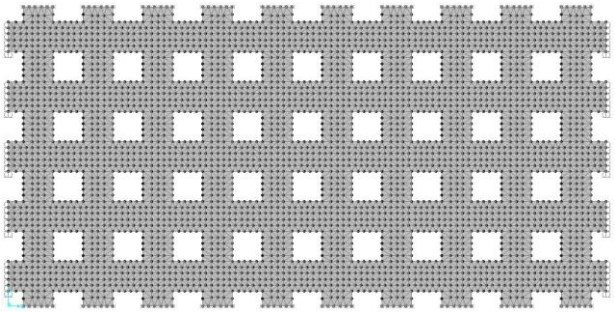

Mesh 10cm	HOMOGENIZED MECHANICAL PROPERTIES				
Depth [m]	$E_{h,x}$	$E_{h,y}$	$\nu_{h,xy}$	$\nu_{h,yx}$	G_h
0.1	10.57%	10.57%	0.027	0.027	0.20%
0.3	32.88%	32.69%	0.085	0.084	2.83%
0.5	56.49%	56.28%	0.148	0.147	13.07%
0.7	81.19%	80.99%	0.190	0.189	30.32%
0.9	98.32%	98.46%	0.199	0.199	40.87%

TABLE 4.15. Homogenized mechanical properties model grid with membrane FE

FIG 4.32. Grid with membrane FE. Beam depth 50cm, Sat. 75%

The small difference in the homogenized mechanical properties in the x- and y-direction shows that the result obtained depends on the Representative Volume Element.

The ***Membrane Correction Factors*** **(C_{2D}) are defined as the relation between the homogenized mechanical properties obtained from using membrane elements and 1D beam elements in the analysis**. This way it is possible to simulate more accurately the pattern performance. Correction Factors with 10cm mesh

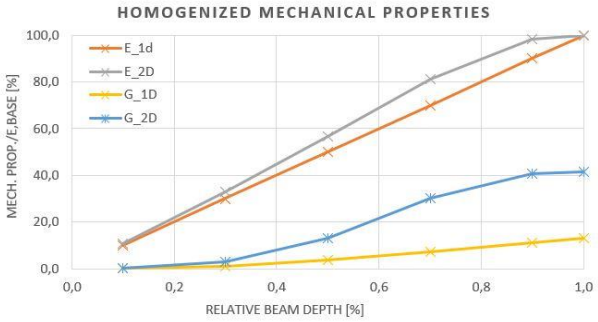

FIG 4.33. Mechanical properties grid with beam and membrane FE.

Beam depth	Saturation	C2D CORRECTION FACTORS			
[m]	[%]	C_{2D_EX}	C_{2D_EY}	C_{2D_V}	C_{2D_G}
0.1	19	1.056	1.057	-	3.65
0.3	51	1.095	1.089	-	2.41
0.5	75	1.129	1.125	-	3.38
0.7	91	1.159	1.156	-	4.09
0.9	99	1.092	1.094	-	3.64
1.0	100	1.000	1.000	-	3.16

TABLE 4.16. Membrane correction factors for the grid

As could be expected, the **membrane correction factors (C_{2D}) for the modulus of elasticity are slightly bigger than 1. increasing as the relative beam depth increases**. The same phenomenon is to be expected for the other properties, however, in this particular case the shear modulus was underestimated by a factor around 3 and the Poisson ratio was zero as the beams were aligned with the imposed deformations. As a result, it can be stated that these results satisfactorily verify the analysis procedure.

GEOMETRIC ISLAMIC PATTERN

The patterns included in this research are much complex than the above models and deserve a closer look themselves. For that purpose, the F Mustansiriya Madrasa pattern (Tessellation 3.6.3.6. θ =30º) is chosen. The analysis done with beam elements had an order of convergence of 2 or $O(h^2)$ regarding the effect introduced by the Representative Element Volume. It is expected that the same behaviour will occur when the beam elements are substituted by membrane elements. The following reactions are obtained for the study pattern for 1x1. 2x2 and 4x4 panels with a relative mesh size of beam depth divided by 6.

Lx [m]	5.00	LONGITUDINAL ANALYSIS				TRANSVERSAL ANALYSIS			
Ly [m]	8.66	dx=1	Nx≠0	dx=0	Nx≠0	dx,up=1	Nxy≠0	dx=0	Nxy≠0
Panel	1x1	dy=0	Ny≠0	dy=1	Ny≠0	dy=0	Nyx≠0	dy,right=1	Nyx≠0
GEOMETRY		HORIZONTAL		VERTICAL		HORIZ. DISTORTION		VERT. DISTORTION	
depth	rbd	$N_{xh}=Q_{11}$	$N_{yh}=Q_{21}$	$N_{xv}=Q_{12}$	$N_{yv}=Q_{22}$	$N_{xy,h}$	$N_{yx,h}$	$N_{xy,v}$	$N_{yx,v}$
[m]	[%]	[kN]	[kN]	[kN]	[kN]	[kN]	[kN]	[kN]	[kN]
0.2	4.00	1,656,823	901,454	901,454	551,594	15,972	27,665	27,665	47,917
0.4	8.00	4,943,060	2,311,587	2,311,587	1,651,324	156,942	271,832	271,832	470,827
0.6	12.00	9,449,799	3,278,438	3,278,438	3,142,868	628,962	1,089,395	1,089,395	1,886,887
0.8	16.00	15,247,388	3,692,923	3,692,923	5,061,042	1,505,628	2,560,822	2,560,822	4,469,074

TABLE 4.17. Analysis numerical results for pattern F, 1x1 panel, membrane elements

Lx [m]	10.00	LONGITUDINAL ANALYSIS				TRANSVERSAL ANALYSIS			
Ly [m]	17.32	dx=1	Nx≠0	dx=0	Nx≠0	dx,up=1	Nxy≠0	dx=0	Nxy≠0
Panel	2x2	dy=0	Ny≠0	dy=1	Ny≠0	dy=0	Nyx≠0	dy,right=1	Nyx≠0
GEOMETRY		HORIZONTAL		VERTICAL		HORIZ. DISTORTION		VERT. DISTORTION	
depth	rbd	$N_{xh}=Q_{11}$	$N_{yh}=Q_{21}$	$N_{xv}=Q_{12}$	$N_{yv}=Q_{22}$	$N_{xy,h}$	$N_{yx,h}$	$N_{xy,v}$	$N_{yx,v}$
[m]	[%]	[kN]	[kN]	[kN]	[kN]	[kN]	[kN]	[kN]	[kN]
0.2	4.00	1,655,331	900,415	900,415	550,832	17,081	28,647	28,647	50,340
0.4	8.00	4,955,297	2,317,188	2,317,188	1,653,658	165,430	281,199	281,199	490,371
0.6	12.00	9,412,864	3,282,074	3,282,074	3,135,943	643,005	1,101,285	1,101,285	1,912,296
0.8	16.00	15,164,148	3,701,167	3,701,167	5,056,671	1,491,389	2,558,384	2,558,384	4,441,271

TABLE 4.18.Analysis numerical results for pattern F, 2x2 panel, membrane elements

Lx [m]	20.00	LONGITUDINAL ANALYSIS				TRANSVERSAL ANALYSIS			
Ly [m]	34.64	dx=1	Nx≠0	dx=0	Nx≠0	dx,up=1	Nxy≠0	dx=0	Nxy≠0
Panel	4x4	dy=0	Ny≠0	dy=1	Ny≠0	dy=0	Nyx≠0	dy,right=1	Nyx≠0
GEOMETRY		HORIZONTAL		VERTICAL		HORIZ. DISTORTION		VERT. DISTORTION	
depth	rbd	$N_{xh}=Q_{11}$	$N_{yh}=Q_{21}$	$N_{xv}=Q_{12}$	$N_{yv}=Q_{22}$	$N_{xy,h}$	$N_{yx,h}$	$N_{xy,v}$	$N_{yx,v}$
[m]	[%]	[kN]	[kN]	[kN]	[kN]	[kN]	[kN]	[kN]	[kN]
0.2	4.00	1,654,665	900,272	900,272	550,899	16,604	28,240	28,240	49,218
0.4	8.00	4,958,530	2,319,273	2,319,273	1,653,587	161,799	278,059	278,059	483,093
0.6	12.00	9,413,039	3,281,698	3,281,698	3,138,598	638,079	1,098,647	1,098,647	1,904,869
0.8	16.00	15,182,705	3,694,873	3,694,873	5,054,831	1,471,087	2,536,375	2,536,375	4,400,342

TABLE 4.19. Analysis numerical results for pattern F, 4x4 panel, membrane elements

The comparison of their respective homogenized mechanical properties is as follows:

rbd 4%	$E_{h,x}$	Diff %	$E_{h,y}$	Diff %	$\nu_{h,xy}$	Diff %	$\nu_{h,yx}$	Diff %	G_h	Diff %
1x1	0.37%	-	0.37%	-	0.944	-	0.942	-	0.10%	-
2x2	0.37%	-0.07	0.37%	-0.12	0.944	0.02	0.942	-0.03	0.10%	4.77
4x4	0.37%	-0.01	0.37%	0.04	0.943	-0.03	0.942	0.02	0.10%	1.97

TABLE 4.20. Comparison homogenized mechanical properties with different panel sizes for pattern F, rbd 4%

rbd 8%	$E_{h,x}$	Diff %	$E_{h,y}$	Diff %	$\nu_{h,xy}$	Diff %	$\nu_{h,yx}$	Diff %	G_h	Diff %
1x1	3.45%	-	3.46%	-	0.808	-	0.810	-	0.67%	-
2x2	3.45%	0.07	3.46%	-0.04	0.810	0.22	0.810	-0.01	0.57%	-15.41
4x4	3.45%	-0.16	3.45%	-0.23	0.810	-0.02	0.810	0.02	0.53%	-7.11

TABLE 4.21. Comparison homogenized mechanical properties with different panel sizes for pattern F, rbd 8%

rbd 12%	$E_{h,x}$	Diff %	$E_{h,y}$	Diff %	$\nu_{h,xy}$	Diff %	$\nu_{h,yx}$	Diff %	G_h	Diff %
1x1	12.18%	-	12.16%	-	0.602	-	0.601	-	3.81%	-
2x2	12.08%	-0.86	12.07%	-0.69	0.604	0.33	0.604	0.50	3.87%	1.44
4x4	12.09%	0.06	12.09%	0.15	0.604	-0.10	0.604	-0.01	3.85%	-0.41

TABLE 4.22. Comparison homogenized mechanical properties with different panel sizes for pattern F, rbd 12%

Despite modelling the edge nodes as pinned, the displacement is constrained at different heights of the beam, leading to an indirect **rotation constrain at the supports.** As seen for the 1D beam elements, the shear modulus has an order of convergence of 2 while the other mechanical properties are accurate enough with 1x1 panels.

4.6. MESH REFINEMENT

This chapter corresponds to the second stage in the scheme described in Chapter 4.2. *Homogenization methodology.* By *mesh refinement* it is referred to study of the effect that the mesh size employed in the analysis will have in the final results. The objective is to find the ideal homogenized mechanical properties of the geometric Islamic patterns with membrane stress FE for 1x1 panels. In this chapter the order of convergence and sensitivity of the results on the mesh size is studied.

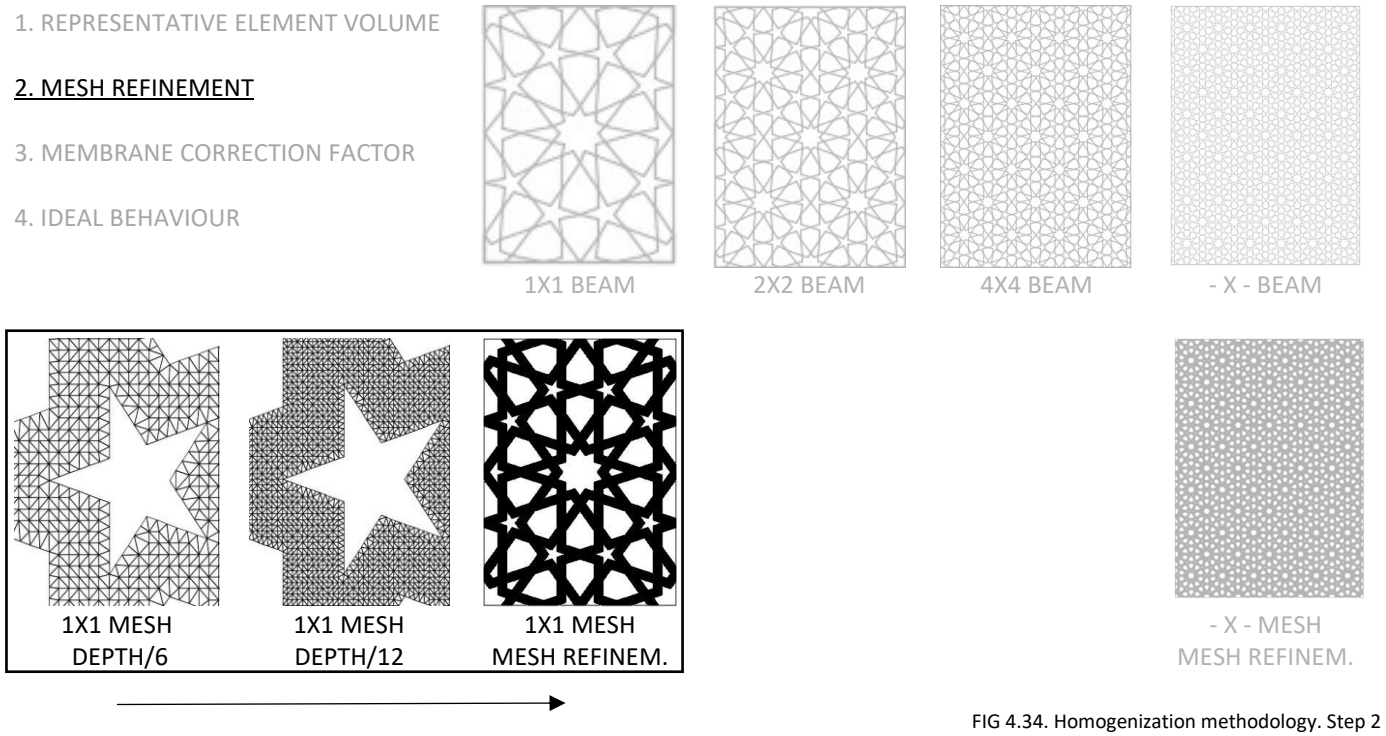

FIG 4.34. Homogenization methodology. Step 2

Normally, the mesh size has importance when dealing with peak values as singularities may develop locally, but this influence is limited when dealing with the global behaviour. In the case of the full panel, the mesh size played no role and in the case of the grid the effect of the mesh refinement was below 1%. The displacements are imposed in some nodes and the force reactions measured in other nodes. The behaviour to study is global and linear elastic and the previous experiments shows a negligible influence of the mesh size. For those reasons, it could seem that the mesh size effect should be very limited. Nevertheless, that is not the case. **The mesh size has a big influence in the results, making it necessary to perform a mesh refinement.** Here, the mesh size effect on the results will be studied for the F Mustansiriya Madrasa pattern (Tessellation 3.6.3.6. θ =30º) for a 1x1 panel. Homogenized mechanical properties are obtained from the reactions included in *Appendix II. Numerical results.*

As the patterns are very sensitive to the mesh size, it is necessary to test the pattern for different mesh sizes to identify the ideal behaviour to which it converges. In addition, different beam depths can be assigned to each pattern, increasing the complexity of the analysis. There are two main practical approaches to define the mesh size:

- Absolute mesh size: The mesh size has a determined value for all cases to run. All the models are tested for a given mesh size of for instance of 5cm, 2.5cm and 1.25cm. It is convenient when all the models have similar geometry and size. Its application to this research would lead to an exponential increment of computational requirements as the beam depth increases. It would lead to inaccurate results for small beam depths and big computational efforts for big beam depths.
- Relative mesh size: The mesh size increases with the beam depth. What it is defined is the needed number of elements in the beam depth to have a good discretization. For instance, a mesh size of d/5 means that the mesh size is the beam depth divided by 5. The level of accuracy is kept constant as the beam size increases and the required computational effort decreases.

The analysis is linear elastic with an imposed displacement of 1m and triangular membrane elements:

d/1	HOMOGENIZED MECHANICAL PROPERTIES				
rbd [%]	$E_{h,x}$	$E_{h,y}$	$\nu_{h,xy}$	$\nu_{h,yx}$	G_h
2	0.12%	0.12%	0.956	0.956	0.04%
4	0.96%	0.96%	0.883	0.883	0.30%
6	3.26%	3.26%	0.769	0.769	1.03%
8	7.42%	7.43%	0.646	0.647	2.47%
10	12.91%	12.91%	0.529	0.528	4.55%
12	19.67%	19.65%	0.424	0.424	7.21%
14	27.09%	27.15%	0.340	0.341	10.48%
16	34.04%	34.03%	0.292	0.292	13.48%
18	40.18%	40.19%	0.260	0.260	16.25%

TABLE 4.23. Homog. mech. properties pattern F, mesh size beam depth/1

d/2	HOMOGENIZED MECHANICAL PROPERTIES				
rbd [%]	$E_{h,x}$	$E_{h,y}$	$\nu_{h,xy}$	$\nu_{h,yx}$	G_h
2	0.08%	0.08%	0.969	0.962	0.03%
4	0.70%	0.70%	0.912	0.908	0.23%
6	2.30%	2.30%	0.830	0.829	0.75%
8	5.99%	6.04%	0.693	0.699	1.92%
10	10.74%	10.73%	0.591	0.590	3.75%
12	17.79%	17.73%	0.469	0.467	6.43%
14	24.11%	24.21%	0.393	0.395	8.91%
16	30.73%	31.77%	0.327	0.338	12.30%
18	37.82%	38.03%	0.286	0.287	15.01%

TABLE 4.24. Homog. mech. properties pattern F, mesh size beam depth/2

d/3	HOMOGENIZED MECHANICAL PROPERTIES				
rbd [%]	$E_{h,x}$	$E_{h,y}$	$\nu_{h,xy}$	$\nu_{h,yx}$	G_h
2	0.05%	0.05%	0.973	0.969	0.02%
4	0.48%	0.48%	0.933	0.933	0.15%
6	1.73%	1.73%	0.867	0.866	0.54%
8	4.31%	4.30%	0.772	0.770	1.33%
10	8.47%	8.55%	0.658	0.664	2.78%
12	14.40%	14.46%	0.542	0.545	4.90%
14	21.19%	21.23%	0.450	0.451	7.66%
16	28.68%	28.42%	0.370	0.367	10.55%
18	35.21%	35.23%	0.321	0.321	13.62%

TABLE 4.25. Homog. mech. properties pattern F, mesh size beam depth/3

d/4	HOMOGENIZED MECHANICAL PROPERTIES				
rbd [%]	$E_{h,x}$	$E_{h,y}$	$\nu_{h,xy}$	$\nu_{h,yx}$	G_h
2	0.05%	0.05%	0.972	0.972	0.01%
4	0.41%	0.41%	0.939	0.938	0.13%
6	1.52%	1.52%	0.878	0.880	0.45%
8	3.84%	3.84%	0.793	0.793	1.17%
10	7.80%	7.84%	0.682	0.685	2.48%
12	13.05%	13.03%	0.579	0.579	4.32%
14	19.81%	19.65%	0.477	0.473	6.76%
16	27.11%	27.02%	0.393	0.392	9.84%
18	33.52%	33.68%	0.340	0.341	12.79%

TABLE 4.26. Homog. mech. properties pattern F, mesh size beam depth/4

d/5	HOMOGENIZED MECHANICAL PROPERTIES				
rbd [%]	$E_{h,x}$	$E_{h,y}$	$\nu_{h,xy}$	$\nu_{h,yx}$	G_h
2	0.04%	0.04%	0.973	0.972	0.01%
4	0.39%	0.38%	0.942	0.941	0.11%
6	1.42%	1.42%	0.885	0.885	0.42%
8	3.60%	3.60%	0.803	0.804	1.07%
10	7.28%	7.28%	0.702	0.702	2.29%
12	12.53%	12.54%	0.592	0.592	4.06%
14	18.84%	18.86%	0.493	0.494	6.52%
16	25.85%	25.77%	0.413	0.412	9.36%
18	32.70%	32.82%	0.351	0.352	12.35%

TABLE 4.27. Homog. mech. properties pattern F, mesh size beam depth/5

d/6	HOMOGENIZED MECHANICAL PROPERTIES				
rbd [%]	$E_{h,x}$	$E_{h,y}$	$\nu_{h,xy}$	$\nu_{h,yx}$	G_h
2	0.04%	0.04%	0.973	0.973	0.01%
4	0.37%	0.37%	0.944	0.942	0.11%
6	1.36%	1.36%	0.888	0.889	0.40%
8	3.45%	3.46%	0.808	0.810	1.01%
10	7.03%	7.04%	0.708	0.710	2.13%
12	12.19%	12.16%	0.602	0.601	3.93%
14	18.19%	18.22%	0.507	0.508	6.22%
16	25.36%	25.25%	0.421	0.420	9.02%
18	32.09%	32.09%	0.361	0.361	11.95%

TABLE 4.28. Homog. mech. properties pattern F, mesh size beam depth/6

d/8	HOMOGENIZED MECHANICAL PROPERTIES				
rbd [%]	$E_{h,x}$	$E_{h,y}$	$\nu_{h,xy}$	$\nu_{h,yx}$	G_h
2	0.04%	0.04%	0.973	0.973	0.01%
4	0.35%	0.35%	0.944	0.944	0.10%
6	1.30%	1.30%	0.892	0.892	0.37%
8	3.30%	3.31%	0.815	0.817	0.96%
10	6.68%	6.69%	0.720	0.721	2.02%
12	11.57%	11.62%	0.615	0.618	3.68%
14	17.68%	17.66%	0.518	0.517	5.91%
16	24.44%	24.43%	0.435	0.435	8.65%
18	31.20%	31.18%	0.371	0.371	11.47%

TABLE 4.29. Homog. mech. properties pattern F, mesh size beam depth/8

d/12	HOMOGENIZED MECHANICAL PROPERTIES				
rbd [%]	$E_{h,x}$	$E_{h,y}$	$\nu_{h,xy}$	$\nu_{h,yx}$	G_h
2	0.04%	0.04%	0.973	0.973	0.01%
4	0.34%	0.34%	0.945	0.945	0.09%
6	1.26%	1.25%	0.895	0.895	0.35%
8	3.18%	3.18%	0.821	0.821	0.91%
10	6.46%	6.45%	0.729	0.728	1.91%
12	11.19%	11.19%	0.627	0.627	3.51%
14	17.05%	17.05%	0.531	0.530	5.65%
16	23.71%	23.71%	0.446	0.446	8.27%
18	30.51%	30.50%	0.380	0.380	11.12%

TABLE 4.30. Homog. mech. properties pattern F, mesh size beam depth/12

d/16	HOMOGENIZED MECHANICAL PROPERTIES				
rbd [%]	$E_{h,x}$	$E_{h,y}$	$\nu_{h,xy}$	$\nu_{h,yx}$	G_h
2	0.04%	0.04%	0.973	0.973	0.01%
4	0.34%	0.34%	0.945	0.946	0.09%
6	1.24%	1.24%	0.896	0.895	0.34%
8	3.12%	3.12%	0.823	0.823	0.88%
10	6.37%	6.38%	0.731	0.731	1.88%
12	11.00%	11.00%	0.631	0.631	3.43%
14	16.78%	16.80%	0.536	0.536	5.53%
16	23.32%	23.33%	0.453	0.453	8.11%
18	30.07%	30.09%	0.386	0.387	10.93%

TABLE 4.31. Homog. mech. properties pattern F, mesh size beam depth/16.

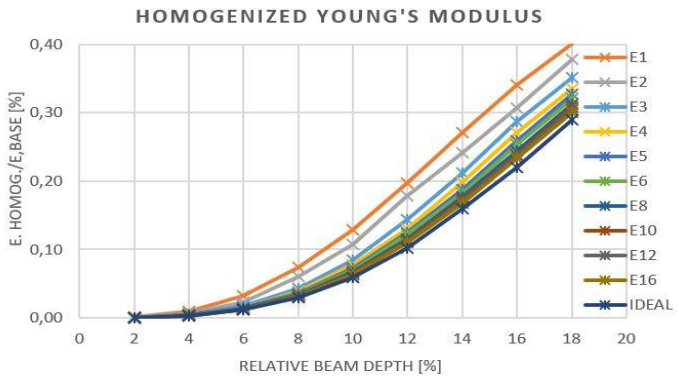

FIG 4.35.Comparison homog modulus elasticity pattern F for different mesh sizes

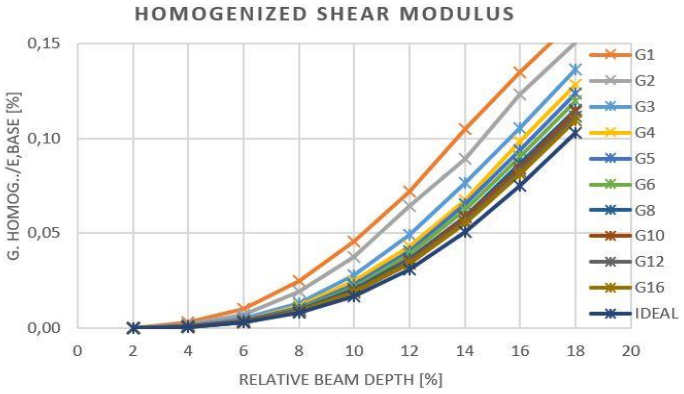

FIG 4.36.. Comparison homog. Shear modulus pattern F for different mesh sizes

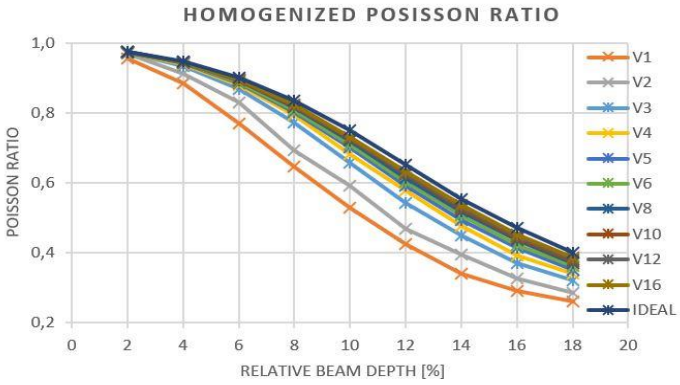

FIG 4.37. Comparison homog. Poisson ratio pattern F for different mesh sizes

The mesh refinement presents an **order of convergence of two O(h²),** meaning that half the mesh size leads to half the error. It is clearly shown in the next tables for the relative beam depths of 10% and 16%, but that is not the case for the relative beam depth of 4%:

rbd 4%	$E_{h,x}$	Diff %	$E_{h,y}$	Diff %	$\nu_{h,xy}$	Diff %	$\nu_{h,yx}$	Diff %	G_h	Diff %
d/3	0.48%	-	0.48%	-	0.933	-	0.933	-	0.15%	-
d/6	0.37%	-21.96	0.37%	-22.06	0.944	1.18	0.942	1.04	0.11%	-28.72
d/12	0.34%	-7.52	0.34%	-7.41	0.945	0.18	0.945	0.29	0.09%	-13.43

TABLE 4.32. Comparison homogenized mechanical properties with different mesh sizes for pattern F, rbd 4%

rbd 10%	$E_{h,x}$	Diff %	$E_{h,y}$	Diff %	$\nu_{h,xy}$	Diff %	$\nu_{h,yx}$	Diff %	G_h	Diff %
d/3	8.47%	-	8.55%	-	0.658	-	0.664	-	2.78%	-
d/6	7.03%	-17.08	7.04%	-17.67	0.708	7.62	0.710	6.86	2.13%	-23.31
d/12	6.46%	-8.07	6.45%	-8.34	0.729	2.89	0.728	2.59	1.91%	-10.43

TABLE 4.33. Comparison homogenized mechanical properties with different mesh sizes for pattern F, rbd 10%

rbd 16%	$E_{h,x}$	Diff %	$E_{h,y}$	Diff %	$\nu_{h,xy}$	Diff %	$\nu_{h,yx}$	Diff %	G_h	Diff %
d/3	28.68%	-	28.42%	-	0.370	-	0.367	-	10.55%	-
d/6	25.36%	-11.57	25.25%	-11.15	0.421	13.86	0.420	14.40	9.02%	-14.48
d/12	23.71%	-6.50	23.71%	-6.10	0.446	5.90	0.446	6.35	8.27%	-8.33

TABLE 4.34. Comparison homogenized mechanical properties with different mesh sizes for pattern F, rbd 16%

If the mesh refinement is done such that each step has a mesh size that is half the size the previous step, O(h²) has the property that the difference with the previous step is the error with respect to the exact solution. This property can be used to get the ideal solution by adding the difference between two consecutives steps to the most accurate one. Despite being an ideal behaviour in the sense that the mesh size effect has been taken into account, it is still not completely accurate as there will be a small error derived from the mesh sizes used in the process. The last step is to define the biggest relative mesh size to get an accurate enough ideal behaviour.

For that purpose, the ideal behaviour obtained from different mesh sizes are compared:

d/4 to d/8	IDEAL HOMOG. MECH. PROPERTIES				
rbd [%]	$E_{h,x}$	$E_{h,y}$	$\nu_{h,xy}$	$\nu_{h,yx}$	G_h
2	0.03%	0.03%	0.974	0.974	0.01%
4	0.29%	0.29%	0.950	0.950	0.07%
6	1.09%	1.08%	0.906	0.904	0.30%
8	2.77%	2.78%	0.838	0.841	0.75%
10	5.56%	5.54%	0.759	0.758	1.56%
12	10.09%	10.21%	0.650	0.657	3.04%
14	15.54%	15.67%	0.558	0.561	5.05%
16	21.77%	21.84%	0.476	0.477	7.47%
18	28.88%	28.68%	0.403	0.401	10.15%

TABLE 4.35. Ideal homog. mech. prop. pattern F, mesh refinement d/4 and d/8

d/5 to d/10	IDEAL HOMOG. MECH. PROPERTIES				
rbd [%]	$E_{h,x}$	$E_{h,y}$	$\nu_{h,xy}$	$\nu_{h,yx}$	G_h
2	0.04%	0.04%	0.973	0.974	0.01%
4	0.31%	0.31%	0.948	0.948	0.08%
6	1.12%	1.13%	0.902	0.903	0.29%
8	2.89%	2.88%	0.835	0.833	0.77%
10	5.86%	5.86%	0.748	0.748	1.64%
12	10.12%	10.10%	0.655	0.654	3.10%
14	15.81%	15.80%	0.556	0.556	5.11%
16	22.04%	22.10%	0.472	0.473	7.41%
18	29.05%	29.12%	0.399	0.400	10.39%

TABLE 4.36. Ideal homog. mech. prop. pattern F, mesh refinement d/5 and d/10

d/6 to d/12	IDEAL HOMOG. MECH. PROPERTIES				
rbd [%]	$E_{h,x}$	$E_{h,y}$	$\nu_{h,xy}$	$\nu_{h,yx}$	G_h
2	0.04%	0.04%	0.973	0.973	0.01%
4	0.32%	0.32%	0.947	0.948	0.08%
6	1.15%	1.15%	0.902	0.900	0.30%
8	2.91%	2.91%	0.834	0.833	0.81%
10	5.89%	5.87%	0.749	0.746	1.69%
12	10.20%	10.22%	0.651	0.652	3.09%
14	15.91%	15.87%	0.554	0.553	5.07%
16	22.06%	22.17%	0.471	0.473	7.52%
18	28.93%	28.92%	0.399	0.399	10.30%

TABLE 4.37. Ideal homog. mech. prop. pattern F, mesh refinement d/6 and d/12

d/8 to d/16	IDEAL HOMOG. MECH. PROPERTIES				
rbd [%]	$E_{h,x}$	$E_{h,y}$	$\nu_{h,xy}$	$\nu_{h,yx}$	G_h
2	0.04%	0.04%	0.973	0.973	0.01%
4	0.32%	0.32%	0.946	0.947	0.08%
6	1.18%	1.18%	0.899	0.899	0.31%
8	2.95%	2.94%	0.832	0.830	0.80%
10	6.07%	6.06%	0.741	0.741	1.73%
12	10.44%	10.38%	0.648	0.645	3.18%
14	15.89%	15.93%	0.554	0.555	5.15%
16	22.20%	22.24%	0.471	0.472	7.56%
18	28.94%	29.00%	0.401	0.402	10.40%

TABLE 4.38.Ideal homog. mech. prop. pattern F, mesh refinement d/8 and d/16

Considering the ideal homogenized mechanical properties obtained from the extrapolation of the results with a relative mesh size of 1/8 and 1/16 beam depth (d/8 to d/16) as the reference value, the accuracy of the other idealization can be measured comparing their results:

rbd 4%	$E_{h,x}$	Diff %	$E_{h,y}$	Diff %	$\nu_{h,xy}$	Diff %	$\nu_{h,yx}$	Diff %	G_h	Diff %
d/8 to d/16	0.32%	-	0.32%	-	0.946	-	0.947	-	0.08%	-
d/4 to d/8	0.29%	-9.80	0.29%	-9.74	0.950	0.33	0.950	0.36	0.07%	-10.00
d/5 to d/10	0.31%	-4.09	0.31%	-4.06	0.948	0.15	0.948	0.16	0.08%	0.93
d/6 to d/12	0.32%	-2.64	0.32%	-2.56	0.947	0.05	0.948	0.12	0.08%	-4.49

TABLE 4.39. Comparison of ideal homog. mech. prop. pattern F, depending on how the mesh refinement is done, for rbd 4%

rbd 10%	$E_{h,x}$	Diff %	$E_{h,y}$	Diff %	$\nu_{h,xy}$	Diff %	$\nu_{h,yx}$	Diff %	G_h	Diff %
d/8 to d/16	6.07%	-	6.06%	-	0.741	-	0.741	-	1.73%	-
d/4 to d/8	5.56%	-8.32	5.54%	-8.57	0.759	2.36	0.758	2.25	1.56%	-9.57
d/5 to d/10	5.86%	-3.40	5.86%	-3.30	0.749	1.07	0.748	0.97	1.64%	-4.94
d/6 to d/12	5.89%	-2.87	5.87%	-3.23	0.749	1.07	0.746	0.75	1.69%	-2.57

TABLE 4.40. Comparison of ideal homog. mech. prop. pattern F, depending on how the mesh refinement is done, for rbd 10%

rbd 16%	$E_{h,x}$	Diff %	$E_{h,y}$	Diff %	$\nu_{h,xy}$	Diff %	$\nu_{h,yx}$	Diff %	G_h	Diff %
d/8 to d/16	22.20%	-	22.24%	-	0.471	-	0.472	-	7.56%	-
d/4 to d/8	21.77%	-1.94	21.84%	-1.77	0.476	1.19	0.477	1.25	7.47%	-1.30
d/5 to d/10	22.04%	-0.71	22.10%	-0.62	0.472	0.23	0.473	0.26	7.41%	-2.00
d/6 to d/12	22.06%	-0.60	22.17%	-0.27	0.471	0.03	0.473	0.26	7.52%	-0.62

TABLE 4.41. Comparison of ideal homog. mech. prop. pattern F, depending on how the mesh refinement is done, for rbd 16%

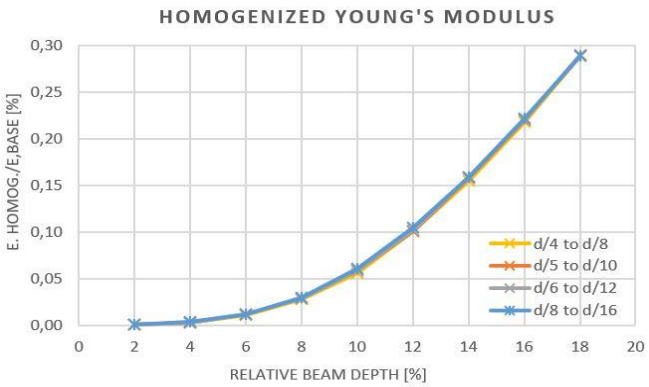

FIG 4.38. Comparison of ideal homog. modulus of elasticity pattern F, depending on how the mesh refinement is done, for increasing rbd

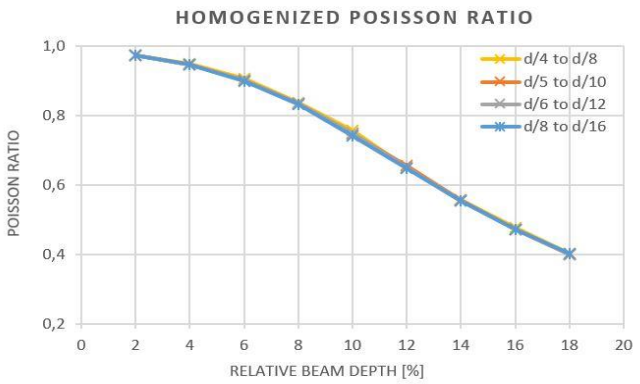

FIG 4.39.Comparison of ideal homog. Poisson ratio pattern F, depending on how the mesh refinement is done, for increasing rbd

Choosing a relative mesh size of 1/6 and 1/12 beam depth for the obtention of the ideal behaviour, the error is limited approximately to the range from 0% to 3%.

4.7. MEMBRANE CORRECTION FACTOR (C_{2D}).

The membrane correction factor (C_{2D}) is defined as the relation between the homogenized mechanical properties obtained with membrane elements (2D) and those obtained with beam elements (1D). It takes into account the effect that bars overlaps have on the nodes' stiffness and on the reduction of the effective bars' length. These effects stiffen the structure, so their values are expected to be bigger than 1. increasing with the relative beam depth for shear and Young's modulus and decreasing for the Poisson ratio. It corresponds to the third stage in the scheme described in Chapter 4.2. *Homogenization methodology.*

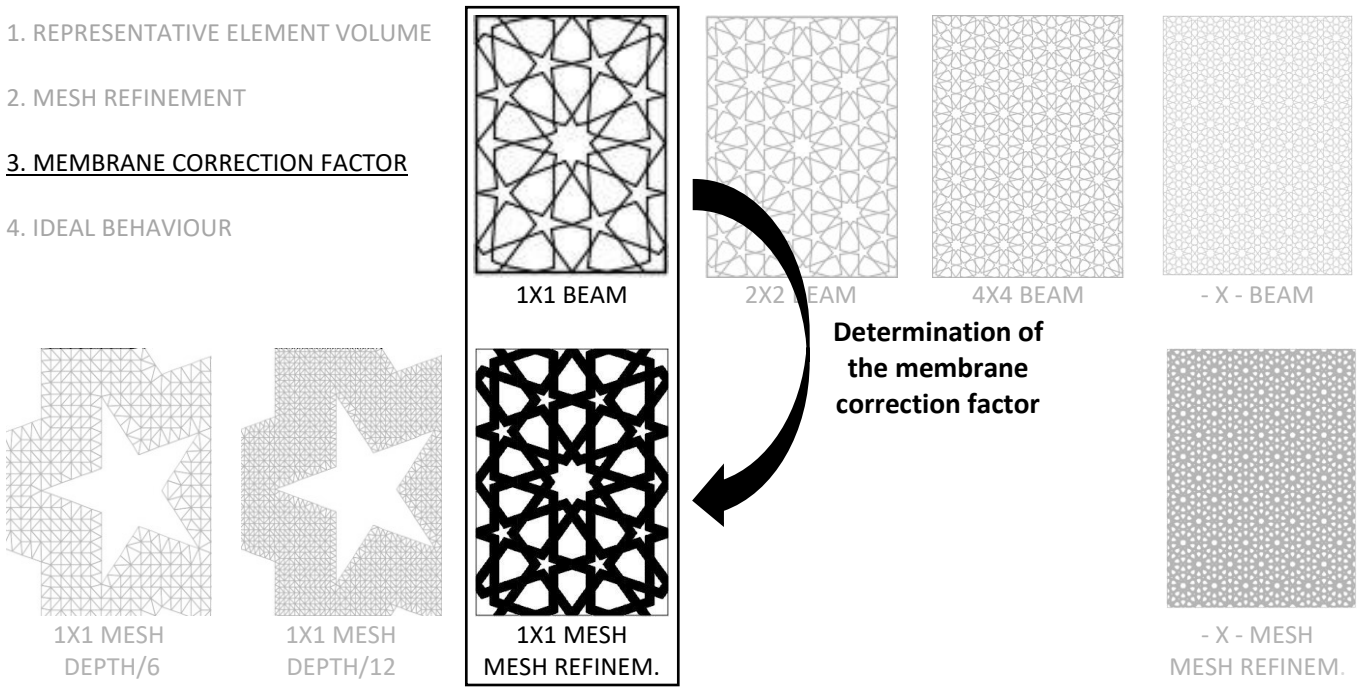

FIG 4.40. Homogenization methodology. Step 3

In the analysis with membrane elements, the rotation of the bars at the supports is indirectly constrained as the differential displacement is impeded at different heights of the beam. As aforementioned, the homogenized mechanical properties obtained are exact regardless of the number of modules composing the panel, except for the shear modulus that has an order of convergence of two. To calculate the membrane correction factors (C_{2D}), the

results of the 1x1 membrane elements panel is divided by the results of the 1x1 1D beam elements panel with the rotation constrained. That way, the Representative Volume Element effect in the shear modulus is indirectly solved with 1D beam element analysis.

If the designer prefers to model the tower without making use of the predesign method developed in this research, the designer is warned to **use an appropriate mesh size due to the patterns' sensitivity to the mesh refinement.** In this document, it is only included the Membrane correction factors (C_{2D}) for the same 3 historic patterns chosen in *Chapter 4.4. FEM beam elements*. For the rest of the historic geometric Islamic patterns, see *Appendix I. Design guide.*

D) LAHORE FORT COMPLEX. Tessellation 4.8.8. θ =67.5º. Square symmetry.

D67.5	C2D CORRECTION FACTORS				
rbd [%]	C_{2D_EX}	C_{2D_EY}	C_{2D_VXY}	C_{2D_VYX}	C_{2D_G}
1	1.02	1.02	1.07	1.07	0.71
2	1.08	1.08	1.18	1.18	0.94
3	1.15	1.15	1.28	1.29	0.98
4	1.19	1.19	1.34	1.34	1.16
5	1.23	1.23	1.38	1.38	1.34
6	1.25	1.25	1.40	1.40	1.53
7	1.27	1.27	1.40	1.40	1.66
8	1.30	1.30	1.41	1.41	1.78
9	1.32	1.32	1.41	1.41	1.86

TABLE 4.42. Membrane correction factors pattern D

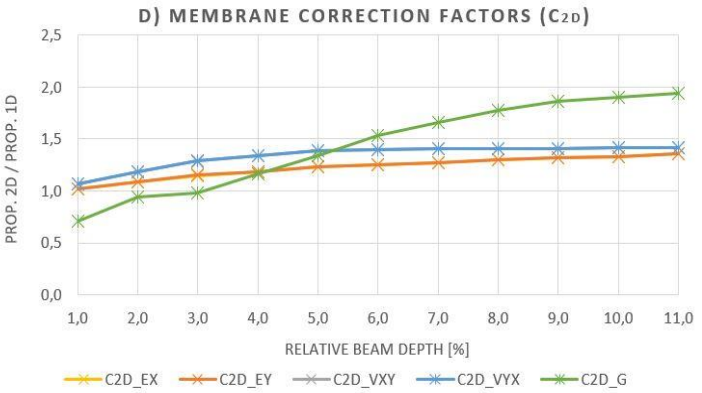

FIG 4.41. Membrane correction factors pattern D

F) MUSTANSIRIYA MADRASA. Tessellation 3.6.3.6. θ =30º. Hexagonal symmetry.

F30	C2D CORRECTION FACTORS				
rbd [%]	C_{2D_EX}	C_{2D_EY}	C_{2D_VXY}	C_{2D_VYX}	C_{2D_G}
2	1.01	1.01	1.00	1.00	0.70
3	1.06	1.06	1.00	1.00	0.73
4	1.14	1.14	1.00	1.00	0.80
5	1.20	1.20	1.00	1.00	0.84
6	1.30	1.30	0.99	0.99	0.93
7	1.37	1.37	0.99	0.99	0.97
8	1.47	1.48	0.97	0.97	1.08
9	1.58	1.58	0.96	0.96	1.20
10	1.69	1.69	0.94	0.93	1.28
11	1.79	1.78	0.91	0.91	1.40
12	1.90	1.91	0.87	0.88	1.53

TABLE 4.43. Membrane correction factors pattern F

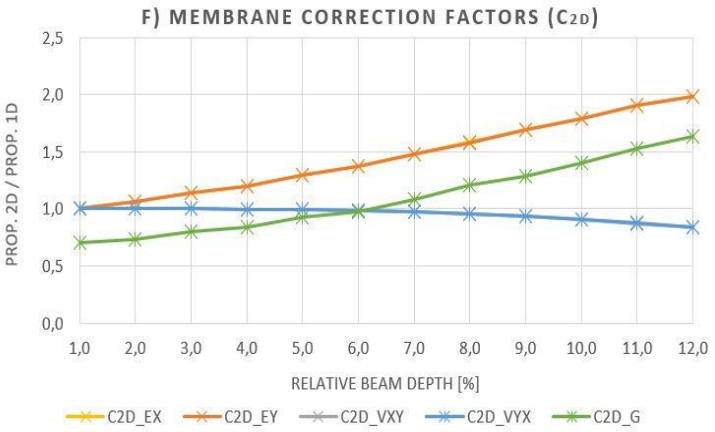

FIG 4.42. Membrane correction factors pattern F

R) FATEHPUR SIKRI. Tessellation ROS-I-6.10.10. θ =72º type Star. Pentagonal symmetry.

R72	C2D CORRECTION FACTORS				
rbd [%]	C_{2D_EX}	C_{2D_EY}	C_{2D_VXY}	C_{2D_VYX}	C_{2D_G}
0.5	1.08	1.08	1.01	1.01	1.00
1.0	1.24	1.24	1.02	1.03	1.16
2.0	1.68	1.68	1.05	1.05	1.50
3.0	2.31	2.25	1.05	1.02	1.93
4.0	3.07	2.85	0.99	0.92	2.41
5.0	3.67	3.26	0.87	0.78	2.76
6.0	3.90	3.34	0.82	0.71	2.85

TABLE 4.44. Membrane correction factors pattern R

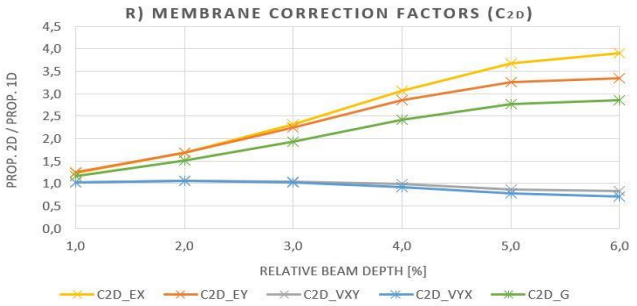

FIG 4.43. Membrane correction factors pattern R

4.8. IDEAL HOMOGENIZED MECHANICAL PROPERTIES.

This is last step in the homogenization process described in *Chapter 4.2. Homogenization methodology*. The application of the Membrane correction factors (C_{2D}) to the homogenized mechanical properties introduce effects such as overlaps, reduction of effective beam length or transversal shortening of the beams in the homogenized mechanical properties obtained with beam elements with Representative Element Volume refinement.

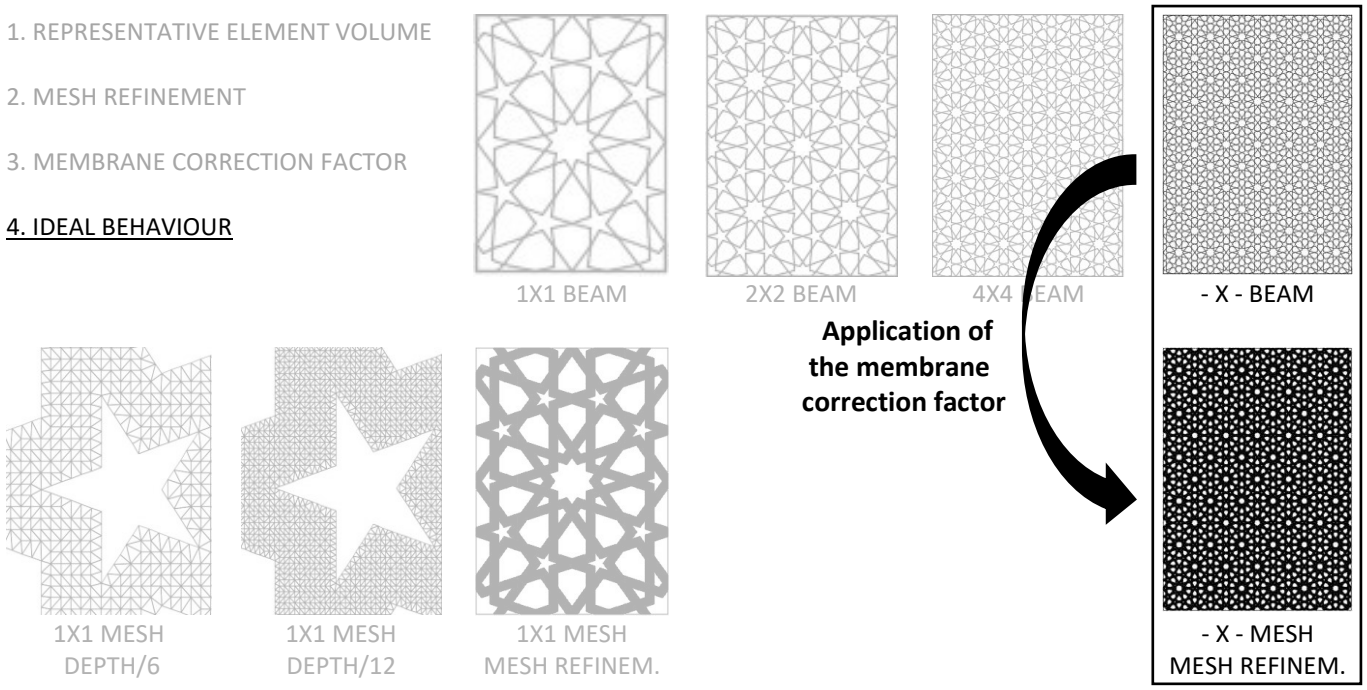

FIG 4.44. Homogenization methodology. Step 4

This ideal behaviour is what will allow a fair comparison of the chosen historic patterns' performance. The saturation is a comparable parameter as it indicates the amount of material used, so the following tables are linearly interpolated to present the ideal homogenized mechanical properties with regards a varying saturation.

The information included in each case is (from left to right):

- Given name to the pattern and the tessellation and parameters to draw it with the Hankin method.
- Picture of the pattern displaying what is considered as its module. The module length in the x-direction (horizontally in the picture) is needed for the relative beam depth (rbd %) definition.
- Table of homogenized mechanical properties taking into account the Representative Element Volume
- Graphs with the evolution of the homogenized mechanical properties as the rbd increases.

In this chapter, only three representative results are included (square, pentagonal and hexagonal symmetries). For the complete set of tables for historic patterns, see *Appendix I. Design guide.*

D) LAHORE FORT COMPLEX. Tessellation 4.8.8. θ =67.5º. Square symmetry.

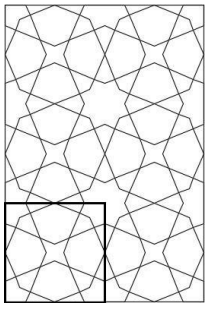

D67.5		HOMOGENIZED MECHANICAL PROPERTIES				
Sat [%]	rbd [%]	$E_{h,x}$	$E_{h,y}$	$\nu_{h,xy}$	$\nu_{h,yx}$	G_h
10	1.40	0.59%	0.59%	0.216	0.216	0.03%
20	2.90	2.96%	2.96%	0.262	0.263	0.23%
30	4.52	7.25%	7.25%	0.297	0.297	0.98%
40	6.30	12.68%	12.67%	0.314	0.314	2.65%
50	8.31	19.31%	19.31%	0.315	0.315	5.52%
60	10.66	27.47%	27.47%	0.309	0.309	9.56%

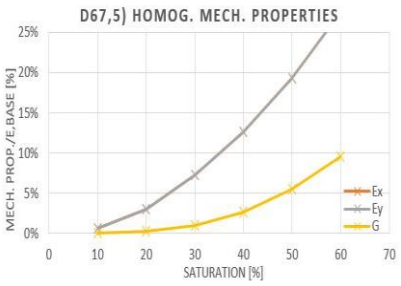

FIG 4.45. Pattern D. Ideal homogenized mechanical properties.

F) MUSTANSIRIYA MADRASA. Tessellation 3.6.3.6. θ =30º. Hexagonal symmetry.

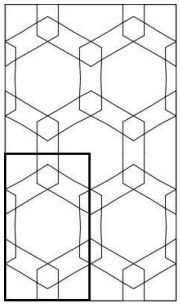

F30		HOMOGENIZED MECHANICAL PROPERTIES				
Sat [%]	rbd [%]	$E_{h,x}$	$E_{h,y}$	$\nu_{h,xy}$	$\nu_{h,yx}$	G_h
10	2.07	0.04%	0.04%	0.973	0.973	0.01%
20	4.30	0.41%	0.42%	0.941	0.941	0.07%
30	6.73	1.69%	1.69%	0.877	0.878	0.32%
40	9.43	4.95%	4.93%	0.774	0.772	1.03%
50	12.52	11.61%	11.62%	0.626	0.626	2.74%
60	16.21	22.76%	22.87%	0.464	0.465	6.23%

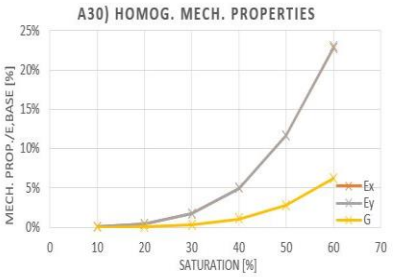

FIG 4.46. Pattern F. Ideal homogenized mechanical properties.

R) FATEHPUR SIKRI. Tessellation ROS-I-6.10.10. type Star. Pentagonal symmetry.

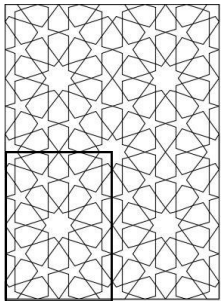

R72		HOMOGENIZED MECHANICAL PROPERTIES				
Sat [%]	rbd [%]	$E_{h,x}$	$E_{h,y}$	$\nu_{h,xy}$	$\nu_{h,yx}$	G_h
10	0.69	0.04%	0.05%	0.529	0.752	0.02%
20	1.49	0.45%	0.62%	0.524	0.733	0.25%
30	2.31	1.64%	2.18%	0.506	0.689	0.83%
40	3.21	4.67%	5.91%	0.467	0.602	2.15%
50	4.21	11.39%	13.46%	0.399	0.476	4.80%
60	5.38	22.80%	25.07%	0.316	0.349	8.94%

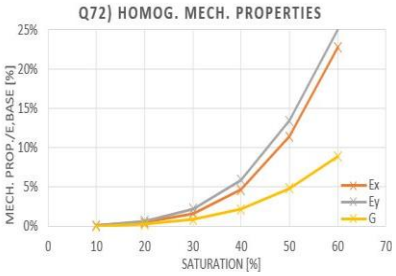

FIG 4.47. Pattern R. Ideal homogenized mechanical properties.

5. RESEARCH QUESTION 2. PATTERN LEVEL

The main objective of this thesis is to provide insight into the structural behaviour and design of geometric Islamic patterns as alternative to conventional diagrid systems for tall buildings. This research objective is articulated at three levels: method level, pattern level and building level. Each of the three research questions addresses one of those levels and they are further developed in a series of sub-questions described in the following document structure:

METHOD LEVEL:
Can a simple tool be developed for the design of geometric Islamic patterns as a non-conventional diagrid system?

- Method chosen and methodology for its adoption
- Development of a pre-design tool.
- Assessment of the developed tool

PATTERN LEVEL:
How do geometric Islamic patterns behave and compare when loaded in their plane?

- **Selection of historic Islamic patterns and their parametric variations**
- **Characterization of the patterns' structural behaviour**
- **Performance comparison of the different patterns**
- **Proposals for their improvement**

BUILDING LEVEL:
Can Islamic inspired patterns become a feasible alternative to traditional diagrid systems for tall buildings?

- Performance comparison of the different patterns and the conventional diagrids
- Overview practical applications of best performing patterns
- Special cases in tall buildings

The objective "Selection of historic Islamic patterns and their parametric variations" is already fulfilled in *Chapter 3. Geometric Islamic patterns.*

5.1. DIRECTIONAL MECHANICAL PROPERTIES

Up to this point, all the patterns have been tested in two perpendicular directions for a given orientation. However, a deep understanding of the pattern's behaviour requires to assess their performance for other orientations. This way it will be possible to know if any given pattern is isotropic, orthotropic, anisotropic or anisotropic with certain symmetries at 60 or 90 degrees as a simple glimpse into the patterns suggest. This rotation will also allow to better compare the pattern's performance as the orientation can be chosen for their maximum stiffness in all cases. Finally, it will also provide of more freedom to the designer applying this Design Guide as he will be able to apply the proposed patterns rotated for mechanical, constructive or aesthetic reasons.

5.1.1. FORMULATION

The formulation has been already explained in *Chapter 2.7. Rotation of the constitutive matrix*. Based on the use of direction cosines to a second order tensor, the resulting equations to be applied are as follows:

$$\bar{Q}_{11} = Q_{11}m^4 + 2(Q_{12} + 2Q_{33})m^2n^2 + Q_{22}n^4 \quad (1.33)$$

$$\bar{Q}_{12} = (Q_{11} + Q_{22} - 4Q_{33})m^2n^2 + Q_{12}(n^4 + m^4) = \bar{Q}_{21} \quad (1.34)$$

$$\bar{Q}_{13} = (Q_{11} - Q_{12} - 2Q_{33})m^3n + (Q_{12} - Q_{22} + 2Q_{33})n^3m = \bar{Q}_{31} \to 0 \quad (1.35)$$

$$\bar{Q}_{22} = Q_{11}n^4 + 2(Q_{12} + 2Q_{33})m^2n^2 + Q_{22}m^4 \quad (1.36)$$

$$\bar{Q}_{23} = (Q_{11} - Q_{12} - 2Q_{33})mn^3n + (Q_{12} - Q_{22} + 2Q_{33})nm^3 = \bar{Q}_{32} \to 0 \quad (1.37)$$

$$\bar{Q}_{33} = (Q_{11} + Q_{22} - 2Q_{12} - 2Q_{33})m^2n^2 + Q_{33}(n^4 + m^4) \quad (1.38)$$

5.1.2. ASSESSMENT OF THE FORMULATION APPLICABILITY

SQUARE SYMMETRY

Pattern D Lahore Fort Complex (Tessellation 4.8.8. θ =67.5º) has apparently an isotropic behaviour since the homogenized mechanical properties are the same in the x- and y-direction. However, a visual inspection suggests that those mechanical properties will change when the pattern is rotated to other orientation.

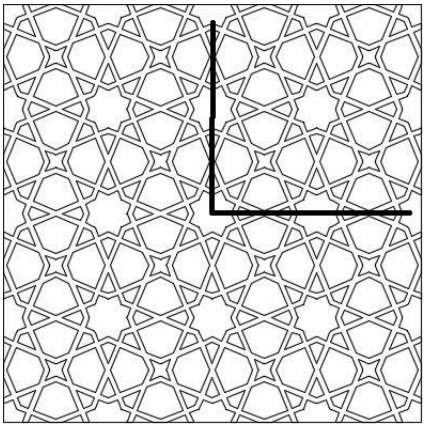

FIG 5.1. Pattern D. Directions of symmetry at 0º and 90º.

Another issue of interest is the accuracy of the approximation, especially for the planes that deviate from the principal directions. And how that accuracy relates to the relative beam depth as the relation axial strain energy / bending strain energy is not constant for a varying saturation.

It is to be expected that once the pattern is rotated 90º, the homogenized mechanical properties in the x- and y-direction will swap. The pattern is analysed, then it is rotated 90º with the formulation, and finally the results are compared to see the differences for that specific rotation:

Lx [m]	10.00	LONGITUDINAL ANALYSIS				TRANSVERSAL ANALYSIS			
Ly [m]	10.00	dx=1	Nx≠0	dx=0	Nx≠0	dx,up=1	Nxy≠0	dx=0	Nxy≠0
Panel	2x2	dy=0	Ny≠0	dy=1	Ny≠0	dy=0	Nyx≠0	dy,right=1	Nyx≠0
GEOMETRY		HORIZONTAL		VERTICAL		HORIZ. DISTORTION		VERTICAL DISTORTION	
depth	rbd	$N_{xh}=Q_{11}$	$N_{yh}=Q_{21}$	$N_{xv}=Q_{12}$	$N_{yv}=Q_{22}$	$N_{xy,h}$	$N_{yx,h}$	$N_{xy,v}$	$N_{yx,v}$
[m]	[%]	[kN]	[kN]	[kN]	[kN]	[kN]	[kN]	[kN]	[kN]
0.05	1.0	52,028	9,914	9,914	52,028	3,868	3,698	3,698	3,868
0.15	3.0	823,482	170,257	170,257	823,482	87,831	83,608	83,608	87,831
0.25	5.0	2,117,984	467,753	467,753	2,117,984	318,424	300,999	300,999	318,424
0.35	7.0	3,519,686	792,422	792,422	3,519,686	679,134	636,393	636,393	679,134
0.45	9.0	4,934,525	1,100,091	1,100,091	4,934,525	1,135,475	1,053,332	1,053,332	1,135,475

TABLE 5.1. Numerical results for pattern D, 2x2 panel, beam FE

Lx [m]	20.00	LONGITUDINAL ANALYSIS				TRANSVERSAL ANALYSIS			
Ly [m]	20.00	dx=1	Nx≠0	dx=0	Nx≠0	dx,up=1	Nxy≠0	dx=0	Nxy≠0
Panel	4x4	dy=0	Ny≠0	dy=1	Ny≠0	dy=0	Nyx≠0	dy,right=1	Nyx≠0
GEOMETRY		HORIZONTAL		VERTICAL		HORIZ. DISTORTION		VERTICAL DISTORTION	
depth	rbd	$N_{xh}=Q_{11}$	$N_{yh}=Q_{21}$	$N_{xv}=Q_{12}$	$N_{yv}=Q_{22}$	$N_{xy,h}$	$N_{yx,h}$	$N_{xy,v}$	$N_{yx,v}$
[m]	[%]	[kN]	[kN]	[kN]	[kN]	[kN]	[kN]	[kN]	[kN]
0.05	1.0	52,028	9,914	9,914	52,028	3,422	3,336	3,336	3,422
0.15	3.0	823,482	170,257	170,257	823,482	79,850	77,752	77,752	79,850
0.25	5.0	2,117,984	467,753	467,753	2,117,984	296,899	288,360	288,360	296,899
0.35	7.0	3,519,686	792,422	792,422	3,519,686	641,870	621,117	621,117	641,870
0.45	9.0	4,934,525	1,100,091	1,100,091	4,934,525	1,079,254	1,039,616	1,039,616	1,079,254

TABLE 5.2. Numerical results for pattern D, 4x4 panel, beam FE

Ideal coefficients derived for a continuous panel:

GEOMETRY		HORIZONTAL		VERTICAL		HORIZ. DISTORTION		VERTICAL DISTORTION	
depth	rbd	$N_{xh}=Q_{11}$	$N_{yh}=Q_{21}$	$N_{xv}=Q_{12}$	$N_{yv}=Q_{22}$	$N_{xy,h}$	$N_{yx,h}$	$N_{xy,v}$	$N_{yx,v}$
[m]	[%]	[kN]	[kN]	[kN]	[kN]	[kN]	[kN]	[kN]	[kN]
0.05	1.0	52,028	9,914	9,914	52,028	2,976	2,974	2,974	2,976
0.15	3.0	823,482	170,257	170,257	823,482	71,869	71,896	71,896	71,869
0.25	5.0	2,117,984	467,753	467,753	2,117,984	275,375	275,722	275,722	275,375
0.35	7.0	3,519,686	792,422	792,422	3,519,686	604,606	605,842	605,842	604,606
0.45	9.0	4,934,525	1,100,091	1,100,091	4,934,525	1,023,032	1,025,901	1,025,901	1,023,032

TABLE 5.3. Representative Element Volume refinement for pattern D at constitutive coefficients level

To normalize the results, they are divided by the base material modulus of elasticity ($E_b = 28.576 * 791\ kN/m^2$), the panel side and the imposed strain as explained in *Chapter 4.1.5. Homogenization process.*

67.5º (-x-)	CONSTITUTIVE COEFFICIENTS				
rbd [%]	Q_{11}	Q_{12}	Q_{21}	Q_{22}	Q_{33}
1	0.0018	0.0003	0.0003	0.0018	0.0001
3	0.0288	0.0060	0.0060	0.0288	0.0025
5	0.0741	0.0164	0.0164	0.0741	0.0096
7	0.1232	0.0277	0.0277	0.1232	0.0212
9	0.1727	0.0385	0.0385	0.1727	0.0358

TABLE 5.4. Normalized constitutive coefficients pattern D

67.5º (-x-)	HOMOGENIZED MECHANICAL PROPERTIES				
rbd [%]	$E_{h,x}$	$E_{h,y}$	$\nu_{h,xy}$	$\nu_{h,yx}$	G_h
1	0.18%	0.18%	0.191	0.191	0.01%
3	2.76%	2.76%	0.207	0.207	0.25%
5	7.05%	7.05%	0.221	0.221	0.96%
7	11.69%	11.69%	0.225	0.225	2.12%
9	16.41%	16.41%	0.223	0.223	3.58%

TABLE 5.5. Homogenized mechanical properties pattern D

Results from rotating the constitutive matrix 90º with the transform matrix:

Rot. 90º	CONSTITUTIVE COEFFICIENTS				
rbd [%]	Q_{11}	Q_{12}	Q_{21}	Q_{22}	Q_{33}
1	0.0018	0.0003	0.0003	0.0018	0.0001
3	0.0288	0.0060	0.0060	0.0288	0.0025
5	0.0741	0.0164	0.0164	0.0741	0.0096
7	0.1232	0.0277	0.0277	0.1232	0.0212
9	0.1727	0.0385	0.0385	0.1727	0.0358

TABLE 5.6. Rotated constitutive coefficients pattern D

Rot. 90º	HOMOGENIZED MECHANICAL PROPERTIES				
rbd [%]	$E_{h,x}$	$E_{h,y}$	$\nu_{h,xy}$	$\nu_{h,yx}$	G_h
1	0.18%	0.18%	0.191	0.191	0.01%
3	2.76%	2.76%	0.207	0.207	0.25%
5	7.05%	7.05%	0.221	0.221	0.96%
7	11.69%	11.69%	0.225	0.225	2.12%
9	16.41%	16.41%	0.223	0.223	3.58%

TABLE 5.7. Rotated homogenized mechanical properties pattern D

Error:

Rot. 90º	DIFFERENCE IN CONSTITUTIVE COEFFICIENTS				
rbd [%]	Q_{11}	Q_{12}	Q_{21}	Q_{22}	Q_{33}
1	0.00%	0.00%	0.00%	0.00%	0.00%
3	0.00%	0.00%	0.00%	0.00%	0.00%
5	0.00%	0.00%	0.00%	0.00%	0.00%
7	0.00%	0.00%	0.00%	0.00%	0.00%
9	0.00%	0.00%	0.00%	0.00%	0.00%

TABLE 5.8. Difference in constitutive coeff pattern D rotated 0º and 90ª

Rot. 90º	DIFFERENCE IN MECHANICAL PROPERTIES				
rbd [%]	$E_{h,x}$	$E_{h,y}$	$\nu_{h,xy}$	$\nu_{h,yx}$	G_h
1	0.00%	0.00%	0.00%	0.00%	0.00%
3	0.00%	0.00%	0.00%	0.00%	0.00%
5	0.00%	0.00%	0.00%	0.00%	0.00%
7	0.00%	0.00%	0.00%	0.00%	0.00%
9	0.00%	0.00%	0.00%	0.00%	0.00%

TABLE 5.9. Difference in mech. properties pattern D rotated 0º and 90ª

The pattern presents the same homogenized mechanical properties in the x- and y-direction. The applicability of this transform matrix for the principal directions is verified and no influence of the relative beam depth has been observed.

So far, the verification has consisted in retrieving Q_{ij} coefficients from the tests, in applying the transformation matrix and finally verifying that the rotated Q_{ij} coefficients and their respective homogenized mechanical properties are as expected. However, for a rotation of 45º we only have a qualitative idea of the expected results (same properties in the rotated x- and y-direction), but no quantitative values. For this reason and in other to quantify the errors introduced by the approximation, the pattern has been tested with a rotation of 0º and 45º

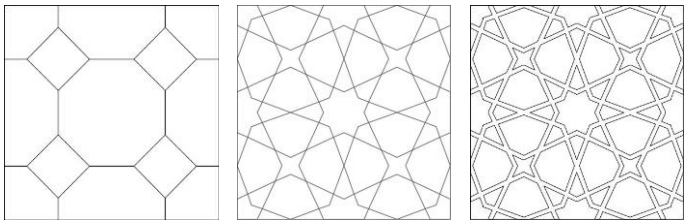

FIG 5.2. Pattern D, rotation 0º. rbd 5%, Sat. 32.83%

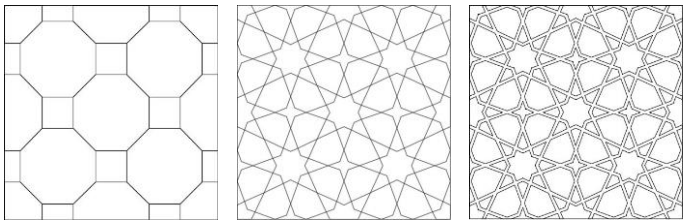

FIG 5.3. Pattern D, rotation 45º. Rbd 3.54%, Sat. 32.83%

The first picture displays 4.8.8. tessellation in a 2x2 panel. The second picture corresponds to D Lahore Fort Complex pattern and it is the result of applying the Hankin method with a contact angle θ =67.5º and a number of crossings for each polygon as specified in *Chapter 3.2. Drawing of geometric Islamic patterns* to that tessellation. The third picture corresponds to a relative beam depth of 5% of that pattern. In this research, a modulus size of 5m in the x-direction has been used in all tests. As the panel is composed of 2 modules in the x-direction (2x2), the total length of the panel in the x-direction is 10m. However, the relative beam depth is defined with regard the module size in the x-direction (5m), so a relative beam depth of 5% will be modelled with a beam whose depth is 25cm (5cm = 1%).

The three pictures in the right are the same with the 4.8.8. tessellation being rotated 45º. The rotation has influence in the definition of the module. Before the rotation, each module comprised 1 octagon (four fourths) and 1 square. However, after the rotation of 45º, the new module is comprised of 2 octagons (one complete plus four fourths) and 2 squares (four halves). As the relative beam depth is defined as a relation with the module size in the x-direction, using the same relative beam depth would lead to a coarser drawing.

It is expected that once the pattern is rotated 45ª, the homogenized mechanical properties in the new x- and y-direction are the same, but different to the values obtained before the rotation. For this verification, 2x2 and 4x4 panels with a relative beam depth of 5% (25cm for a module size of 5m in the x-direction) are tested

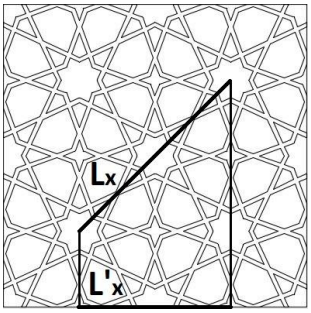

The new module length in the x-direction (L'_x) can be seen as a projection of the old module length (L_x) into the new x-direction.

As the relative beam depth is directly proportional to the module length in x-direction, to get the same saturation the new relative beam depth will be old one times the cosine of the rotated angle. For an angle of 90º, this approach is not applicable and the relation between Ly and Lx has to be used instead.

$$L'_x = L_x \cos(\alpha) \qquad (5.1)$$

FIG 5.4. Difference in the module length in the x-direction before and after the rotation.

In this particular case where the rotated angle is 45ª and the relative beam depth 5%, the new relative beam depth to get the same saturation (32.83%) is $5 * cos(45) = 3.54\%$

The process to assess the results for a rotation of 45º is as follows:

1. Test a 2x2 and a 4x4 panel of the pattern without rotation (0º).
2. Get the ideal Q_{ij} coefficients of the pattern without rotation (0º) as the result from the 4x4 panel plus the difference with the 2x2 panel and the homogenized mechanical properties derived from it.
3. Test the 2x2 and a 4x4 panel of the pattern rotated 45º.
4. Get the ideal Q_{ij} coefficients of the pattern rotated (45º) as the result from the 4x4 panel plus the difference with the 2x2 panel and the homogenized mechanical properties derived from it.
5. Apply the transform formulation to rotate analytically 45º the ideal Q_{ij} coefficients.
6. Compare the results obtained from testing the rotated pattern and from rotating analytically to assess the error introduced by the approximation in the formulation.

1. <u>Test of the 2x2 and 4x4 panel of the original pattern (rotated 0º)</u>

Lx [m]	10.00	**LONGITUDINAL ANALYSIS**				**TRANSVERSAL ANALYSIS**			
Ly [m]	10.00	dx=1	Nx≠0	dx=0	Nx≠0	dx,up=1	Nxy≠0	dx=0	Nxy≠0
Panel	2x2	dy=0	Ny≠0	dy=1	Ny≠0	dy=0	Nyx≠0	dy,right=1	Nyx≠0
GEOMETRY		HORIZONTAL		VERTICAL		HORIZ. DISTORTION		VERTICAL DISTORTION	
depth	rbd	$N_{xh} = Q_{11}$	$N_{yh} = Q_{21}$	$N_{xv} = Q_{12}$	$N_{yv} = Q_{22}$	$N_{xy,h}$	$N_{yx,h}$	$N_{xy,v}$	$N_{yx,v}$
[m]	[%]	[kN]	[kN]	[kN]	[kN]	[kN]	[kN]	[kN]	[kN]
0.05	1.0	52,028	9,914	9,914	52,028	3,868	3,698	3,698	3,868
0.15	3.0	823,482	170,257	170,257	823,482	87,831	83,608	83,608	87,831
0.25	5.0	2,117,984	467,753	467,753	2,117,984	318,424	300,999	300,999	318,424
0.35	7.0	3,519,686	792,422	792,422	3,519,686	679,134	636,393	636,393	679,134
0.45	9.0	4,934,525	1,100,091	1,100,091	4,934,525	1,135,475	1,053,332	1,053,332	1,135,475

TABLE 5.10. Numerical results for pattern D, 2x2 panel rotated 0º, beam FE

Lx [m]	20.00	**LONGITUDINAL ANALYSIS**				**TRANSVERSAL ANALYSIS**			
Ly [m]	20.00	dx=1	Nx≠0	dx=0	Nx≠0	dx,up=1	Nxy≠0	dx=0	Nxy≠0
Panel	4x4	dy=0	Ny≠0	dy=1	Ny≠0	dy=0	Nyx≠0	dy,right=1	Nyx≠0
GEOMETRY		HORIZONTAL		VERTICAL		HORIZ. DISTORTION		VERTICAL DISTORTION	
depth	rbd	$N_{xh} = Q_{11}$	$N_{yh} = Q_{21}$	$N_{xv} = Q_{12}$	$N_{yv} = Q_{22}$	$N_{xy,h}$	$N_{yx,h}$	$N_{xy,v}$	$N_{yx,v}$
[m]	[%]	[kN]	[kN]	[kN]	[kN]	[kN]	[kN]	[kN]	[kN]
0.05	1.0	52,028	9,914	9,914	52,028	3,422	3,336	3,336	3,422
0.15	3.0	823,482	170,257	170,257	823,482	79,850	77,752	77,752	79,850
0.25	5.0	2,117,984	467,753	467,753	2,117,984	296,899	288,360	288,360	296,899
0.35	7.0	3,519,686	792,422	792,422	3,519,686	641,870	621,117	621,117	641,870
0.45	9.0	4,934,525	1,100,091	1,100,091	4,934,525	1,079,254	1,039,616	1,039,616	1,079,254

TABLE 5.11. Numerical results for pattern D, 4x4 panel rotated 0º, beam FE

2. Ideal homogenized mechanical properties of the original pattern (rotated 0º)

Ideal coefficients derived for a continuous panel:

GEOMETRY		HORIZONTAL		VERTICAL		HORIZ. DISTORTION		VERTICAL DISTORTION	
depth	rbd	$N_{xh}=Q_{11}$	$N_{yh}=Q_{21}$	$N_{xv}=Q_{12}$	$N_{yv}=Q_{22}$	$N_{xy,h}$	$N_{yx,h}$	$N_{xy,v}$	$N_{yx,v}$
[m]	[%]	[kN]	[kN]	[kN]	[kN]	[kN]	[kN]	[kN]	[kN]
0.05	1.0	52,028	9,914	9,914	52,028	2,976	2,974	2,974	2,976
0.15	3.0	823,482	170,257	170,257	823,482	71,869	71,896	71,896	71,869
0.25	5.0	2,117,984	467,753	467,753	2,117,984	275,375	275,722	275,722	275,375
0.35	7.0	3,519,686	792,422	792,422	3,519,686	604,606	605,842	605,842	604,606
0.45	9.0	4,934,525	1,100,091	1,100,091	4,934,525	1,023,032	1,025,901	1,025,901	1,023,032

TABLE 5.12. Representative Element Volume refinement for pattern D, rotated 0º, at constitutive coefficients level

To normalize the results, they are divided by the base material modulus of elasticity ($E_b = 28.576 * 791\ kN/m^2$), the panel side and the imposed strain as explained in *Chapter 4.1.5. Homogenization process.*

67.5º (-x-)	CONSTITUTIVE COEFFICIENTS				
rbd[%]	Q_{11}	Q_{12}	Q_{21}	Q_{22}	Q_{33}
1	0.0018	0.0003	0.0003	0.0018	0.0001
3	0.0288	0.0060	0.0060	0.0288	0.0025
5	0.0741	0.0164	0.0164	0.0741	0.0096
7	0.1232	0.0277	0.0277	0.1232	0.0212
9	0.1727	0.0385	0.0385	0.1727	0.0358

TABLE 5.13. Normalized constitutive coefficients pattern D, rotated 0º

67.5º (-x-)	HOMOGENIZED MECHANICAL PROPERTIES				
rbd [%]	$E_{h,x}$	$E_{h,y}$	$\nu_{h,xy}$	$\nu_{h,yx}$	G_h
1	0.18%	0.18%	0.191	0.191	0.01%
3	2.76%	2.76%	0.207	0.207	0.25%
5	7.05%	7.05%	0.221	0.221	0.96%
7	11.69%	11.69%	0.225	0.225	2.12%
9	16.41%	16.41%	0.223	0.223	3.58%

TABLE 5.14. Homogenized mechanical properties pattern D, rotated 0º

3. Test of the 2x2 and 4x4 panel of the pattern rotated 45º

Lx [m]	10.00	**LONGITUDINAL ANALYSIS**				**TRANSVERSAL ANALYSIS**			
Ly [m]	10.00	dx=1	Nx≠0	dx=0	Nx≠0	dx,up=1	Nxy≠0	dx=0	Nxy≠0
Panel	2x2	dy=0	Ny≠0	dy=1	Ny≠0	dy=0	Nyx≠0	dy,right=1	Nyx≠0
GEOMETRY		HORIZONTAL		VERTICAL		HORIZ. DISTORTION		VERTICAL DISTORTION	
depth	rbd	$N_{xh}=Q_{11}$	$N_{yh}=Q_{21}$	$N_{xv}=Q_{12}$	$N_{yv}=Q_{22}$	$N_{xy,h}$	$N_{yx,h}$	$N_{xy,v}$	$N_{yx,v}$
[m]	[%]	[kN]	[kN]	[kN]	[kN]	[kN]	[kN]	[kN]	[kN]
0.0354	0.71	33,946	27,995	27,995	33,946	21,952	21,829	21,829	21,952
0.1061	2.12	568,600	425,139	425,139	568,600	338,819	335,727	335,727	338,819
0.1768	3.54	1,567,772	1,017,965	1,017,965	1,567,772	855,990	842,977	842,977	855,990
0.2475	4.95	2,760,339	1,551,768	1,551,768	2,760,339	1,418,794	1,386,346	1,386,346	1,418,794
0.3182	6.36	4,040,902	1,993,713	1,993,713	4,040,902	2,001,970	1,938,991	1,938,991	2,001,970

TABLE 5.15. Numerical results for pattern D, 2x2 panel rotated 45º, beam FE

Lx [m]	20.00	**LONGITUDINAL ANALYSIS**				**TRANSVERSAL ANALYSIS**			
Ly [m]	20.00	dx=1	Nx≠0	dx=0	Nx≠0	dx,up=1	Nxy≠0	dx=0	Nxy≠0
Panel	4x4	dy=0	Ny≠0	dy=1	Ny≠0	dy=0	Nyx≠0	dy,right=1	Nyx≠0
GEOMETRY		HORIZONTAL		VERTICAL		HORIZ. DISTORTION		VERTICAL DISTORTION	
depth	rbd	$N_{xh}=Q_{11}$	$N_{yh}=Q_{21}$	$N_{xv}=Q_{12}$	$N_{yv}=Q_{22}$	$N_{xy,h}$	$N_{yx,h}$	$N_{xy,v}$	$N_{yx,v}$
[m]	[%]	[kN]	[kN]	[kN]	[kN]	[kN]	[kN]	[kN]	[kN]
0.0354	0.71	33,946	27,995	27,995	33,946	21,496	21,433	21,433	21,496
0.1061	2.12	568,600	425,139	425,139	568,600	332,624	331,058	331,058	332,624
0.1768	3.54	1,567,772	1,017,965	1,017,965	1,567,772	840,341	833,830	833,830	840,341
0.2475	4.95	2,760,339	1,551,768	1,551,768	2,760,339	1,390,808	1,374,708	1,374,708	1,390,808
0.3182	6.36	4,040,902	1,993,713	1,993,713	4,040,902	1,958,894	1,927,850	1,927,850	1,958,894

TABLE 5.16. Numerical results for pattern D, 4x4 panel rotated 45º, beam FE

4. Ideal homogenized mechanical properties for pattern rotated 45º from tests

Ideal coefficients derived for a continuous panel:

GEOMETRY		HORIZONTAL		VERTICAL		HORIZ. DISTORTION		VERTICAL DISTORTION	
depth	rbd	$N_{xh} = Q_{11}$	$N_{yh} = Q_{21}$	$N_{xv} = Q_{12}$	$N_{yv} = Q_{22}$	$N_{xy,h}$	$N_{yx,h}$	$N_{xy,v}$	$N_{yx,v}$
[m]	[%]	[kN]	[kN]	[kN]	[kN]	[kN]	[kN]	[kN]	[kN]
0.0354	0.71	33,946	27,995	27,995	33,946	21,040	21,036	21,036	21,040
0.1061	2.12	568,600	425,139	425,139	568,600	326,429	326,390	326,390	326,429
0.1768	3.54	1,567,772	1,017,965	1,017,965	1,567,772	824,692	824,683	824,683	824,692
0.2475	4.95	2,760,339	1,551,768	1,551,768	2,760,339	1,362,821	1,363,070	1,363,070	1,362,821
0.3182	6.36	4,040,902	1,993,713	1,993,713	4,040,902	1,915,819	1,916,709	1,916,709	1,915,819

TABLE 5.17. Representative Element Volume refinement for pattern D, rotated 45º, at constitutive coefficients level

To normalize the results, they are divided by the base material modulus of elasticity ($E_b = 28 * 576 * 791\ kN/m^2$), the panel side and the imposed strain as explained in *Chapter 4.1.5. Homogenization process.*

	CONSTITUTIVE COEFFICIENTS				
rbd [%]	Q_{11}	Q_{12}	Q_{21}	Q_{22}	Q_{33}
0.71	0.0012	0.0010	0.0010	0.0012	0.0007
2.12	0.0199	0.0149	0.0149	0.0199	0.0114
3.54	0.0549	0.0356	0.0356	0.0549	0.0289
4.95	0.0966	0.0543	0.0543	0.0966	0.0477
6.36	0.1414	0.0698	0.0698	0.1414	0.0671

TABLE 5.18. Normalized constitutive coefficients pattern D, rotated 45º

67.5º (- x -)	HOMOGENIZED MECHANICAL PROPERTIES				
rbd [%]	$E_{h,x}$	$E_{h,y}$	$\nu_{h,xy}$	$\nu_{h,yx}$	G_h
0.71	0.04%	0.04%	0.825	0.825	0.07%
2.12	0.88%	0.88%	0.748	0.748	1.14%
3.54	3.17%	3.17%	0.649	0.649	2.89%
4.95	6.61%	6.61%	0.562	0.562	4.77%
6.36	10.70%	10.70%	0.493	0.493	6.71%

TABLE 5.19. Homogenized mechanical properties pattern D, rotated 45º

5. Analytical rotation of 45º with matrix transform

Rot. 45º	CONSTITUTIVE COEFFICIENTS				
rbd [%]	Q_{11}	Q_{12}	Q_{21}	Q_{22}	Q_{33}
0.71	0.0012	0.0010	0.0010	0.0012	0.0007
2.12	0.0199	0.0149	0.0149	0.0199	0.0114
3.54	0.0549	0.0356	0.0356	0.0549	0.0289
4.95	0.0966	0.0543	0.0543	0.0966	0.0477
6.36	0.1414	0.0697	0.0697	0.1414	0.0671

TABLE 5.20. Constitutive coefficients pattern D analytically rotated 45º

Rot. 45º	HOMOGENIZED MECHANICAL PROPERTIES				
rbd [%]	$E_{h,x}$	$E_{h,y}$	$\nu_{h,xy}$	$\nu_{h,yx}$	G_h
0.71	0.04%	0.04%	0.825	0.825	0.07%
2.12	0.88%	0.88%	0.747	0.747	1.14%
3.54	3.18%	3.18%	0.649	0.649	2.89%
4.95	6.61%	6.61%	0.562	0.562	4.77%
6.36	10.71%	10.71%	0.493	0.493	6.71%

TABLE 5.21.Mechanical properties pattern D, analytically rotated 45º

Note that the relative beam depth also changes as the pattern rotates, to maintain the reference to the same saturation (amount of material used). The new value is obtained multiplying the reference relative beam depth times the cosine of the rotated angle.

6. Comparison of results from essayed tests and rotation transformation.

TESTS	CONSTITUTIVE COEFFICIENTS				
rbd [%]	Q_{11}	Q_{12}	Q_{21}	Q_{22}	Q_{33}
0.71	0.0012	0.0012	0.0012	0.0012	0.0012
2.12	0.0199	0.0199	0.0199	0.0199	0.0199
3.54	0.0549	0.0549	0.0549	0.0549	0.0549
4.95	0.0966	0.0966	0.0966	0.0966	0.0966
6.36	0.1414	0.1414	0.1414	0.1414	0.1414

TABLE 5.22. Constitutive coefficients, pattern D rotated 45º in tests

FORMUL.	CONSTITUTIVE COEFFICIENTS				
rbd [%]	Q_{11}	Q_{12}	Q_{21}	Q_{22}	Q_{33}
0.71	0.0012	0.0012	0.0012	0.0012	0.0012
2.12	0.0199	0.0199	0.0199	0.0199	0.0199
3.54	0.0549	0.0549	0.0549	0.0549	0.0549
4.95	0.0966	0.0966	0.0966	0.0966	0.0966
6.36	0.1414	0.1414	0.1414	0.1414	0.1414

TABLE 5.23. Constitutive coefficients pattern D rotated 45º with formulation

TESTS	HOMOGENIZED MECHANICAL PROPERTIES				
rbd [%]	$E_{h,x}$	$E_{h,y}$	$\nu_{h,xy}$	$\nu_{h,yx}$	G_h
0.71	0.04%	0.04%	0.825	0.825	0.07%
2.12	0.88%	0.88%	0.748	0.748	1.14%
3.54	3.17%	3.17%	0.649	0.649	2.89%
4.95	6.61%	6.61%	0.562	0.562	4.77%
6.36	10.70%	10.70%	0.493	0.493	6.71%

TABLE 5.24. Mechanical properties, pattern D rotated 45º in tests

FORMUL.	HOMOGENIZED MECHANICAL PROPERTIES				
rbd [%]	$E_{h,x}$	$E_{h,y}$	$\nu_{h,xy}$	$\nu_{h,yx}$	G_h
0.71	0.04%	0.04%	0.825	0.825	0.07%
2.12	0.88%	0.88%	0.747	0.747	1.14%
3.54	3.18%	3.18%	0.649	0.649	2.89%
4.95	6.61%	6.61%	0.562	0.562	4.77%
6.36	10.71%	10.71%	0.493	0.493	6.71%

TABLE 5.25. Mechanical properties, pattern D rotated 45º with formulation

ERROR	CONSTITUTIVE COEFFICIENTS				
rbd [%]	Q_{11}	Q_{12}	Q_{21}	Q_{22}	Q_{33}
0.71	0.0%	0.0%	0.0%	0.0%	0.1%
2.12	0.0%	0.0%	0.0%	0.0%	0.1%
3.54	0.0%	-0.1%	-0.1%	0.0%	0.1%
4.95	0.0%	-0.1%	-0.1%	0.0%	0.1%
6.36	0.0%	0.0%	0.0%	0.0%	0.0%

TABLE 5.26. Difference in constitutive coefficients, pattern D rotated 45º

ERROR	HOMOGENIZED MECHANICAL PROPERTIES				
rbd [%]	$E_{h,x}$	$E_{h,y}$	$\nu_{h,xy}$	$\nu_{h,yx}$	G_h
0.71	0.0%	0.0%	0.0%	0.0%	0.1%
2.12	0.2%	0.2%	-0.1%	-0.1%	0.1%
3.54	0.2%	0.2%	-0.1%	-0.1%	0.1%
4.95	0.1%	0.1%	-0.1%	-0.1%	0.1%
6.36	0.1%	0.1%	-0.1%	-0.1%	0.0%

TABLE 5.27. Difference in mechanical properties, pattern D rotated 45º

In conclusion, the error is negligible, so this simplified formulation can be applied as described with complete guarantee of the accuracy obtained.

Now that it has been verified the applicability of this analytical rotation, the pattern is rotated 90º in steps of 10º to have a better insight into its behaviour. The relative beam depth considered for this purpose is 5%.

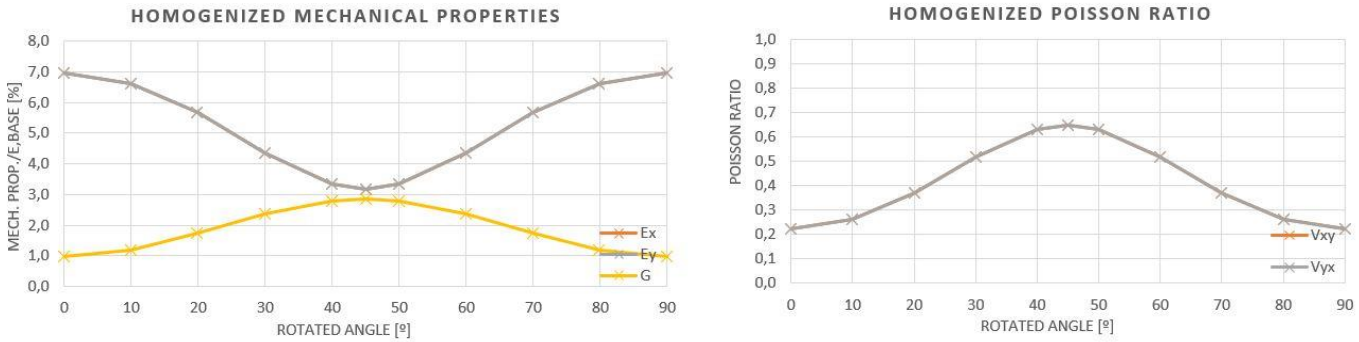

FIG 5.28. Pattern D. Rotation of the homogenized mechanical properties obtained with beam FE

The graphs demonstrate that this pattern has a type of **anisotropy** (different mechanical properties in different directions) **with isotropy for axes under 90º** ($E_x = E_y$ and $v_{xy} = v_{yx}$ in all cases). It also shows that the chosen orientation is the stiffest.

PENTAGONAL SYMMETRY

Pattern R *Fatehpur Sikri* (Tessellation ROS-I-6.10.10. type star, θ =72º) has a marked orthotropic behaviour with planes of symmetry at 54º, 126º, 234º and 306º, making it a good candidate to assess the applicability of the formulation obtained. For that purpose, a 2x2 panel with a relative beam depth of 4% (20cm for a module size of 5m in the x-direction) is tested and its Q_{ij} coefficients retrieved. A rotation of 90º in steps of 6º is included. It is to be expected that Ex rotated 54ª equals Ey rotated 36ª.

Note that if derived, the homogenized mechanical properties would differ slightly from the properties included in the *homogenized properties tables* as they are the direct result from testing a 2x2 panel, affected by the Representative Elementary Volume and not the ideal behaviour.

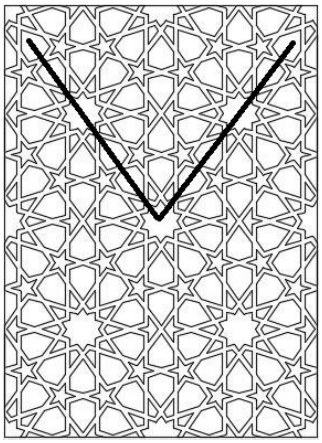

FIG 5.29. Pattern R. Directions of symmetry at 54º and 126º.

It has been explained theoretically in *Chapter 4.1.6. Boundary constrains regarding rotation* and it has been proved numerically in *Chapter 4.3. Representative Element Volume,* that constraining the rotation dof at the supports provide exact results for the Poisson ratio and modulus of elasticity, but the shear modulus presents an order of converge 2.

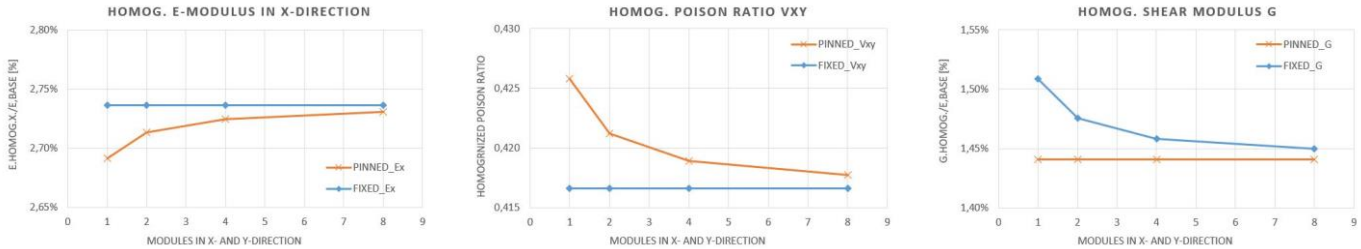

FIG 5.30. Homogenized mechanical properties obtained with symmetric (blue) and antisymmetric (orange) boundary conditions for different panel sizes

The shear modulus (G) is the only mechanical property whose constitutive coefficients (Q_{ij}) are not coupled which the other mechanical properties. In other words, the Representative Volume Element effect can be refined at the level of the constitutive coefficients (Q_{ij}) or at the level of the mechanical property (G).

2x2 panel, 4% relative beam depth:

Lx [m]	10.00	**LONGITUDINAL ANALYSIS**				**TRANSVERSAL ANALYSIS**			
Ly [m]	13.76	dx=1	Nx≠0	dx=0	Nx≠0	dx,up=1	Nxy≠0	dx=0	Nxy≠0
Panel	398.38	dy=0	Ny≠0	dy=1	Ny≠0	dy=0	Nyx≠0	dy,right=1	Nyx≠0
GEOMETRY		HORIZONTAL		VERTICAL		HORIZ. DISTORTION		VERTICAL DISTORTION	
depth	rbd	$N_{xh}=Q_{11}$	$N_{yh}=Q_{21}$	$N_{xv}=Q_{12}$	$N_{yv}=Q_{22}$	$N_{xy,h}$	$N_{yx,h}$	$N_{xy,v}$	$N_{yx,v}$
[m]	[%]	[kN]	[kN]	[kN]	[kN]	[kN]	[kN]	[kN]	[kN]
0.20	4.0	1,562,203	621,542	621,542	1,075,003	359,310	481,027	481,027	699,601

TABLE 5.28. Numerical results for pattern R, 2x2 panel, rbd 4%, beam FE

4x4 panel, 4% relative beam depth:

Lx [m]	20.00	**LONGITUDINAL ANALYSIS**				**TRANSVERSAL ANALYSIS**			
Ly [m]	27.53	dx=1	Nx≠0	dx=0	Nx≠0	dx,up=1	Nxy≠0	dx=0	Nxy≠0
Bars [m]	398.38	dy=0	Ny≠0	dy=1	Ny≠0	dy=0	Nyx≠0	dy,right=1	Nyx≠0
GEOMETRY		HORIZONTAL		VERTICAL		HORIZ. DISTORTION		VERTICAL DISTORTION	
depth	rbd	$N_{xh}=Q_{11}$	$N_{yh}=Q_{21}$	$N_{xv}=Q_{12}$	$N_{yv}=Q_{22}$	$N_{xy,h}$	$N_{yx,h}$	$N_{xy,v}$	$N_{yx,v}$
[m]	[%]	[kN]	[kN]	[kN]	[kN]	[kN]	[kN]	[kN]	[kN]
0.20	4.0	1,562,203	621,542	621,542	1,075,003	354,080	480,769	480,769	680,166

TABLE 5.29. Numerical results for pattern R, 4x4 panel, rbd 4%, beam FE

Ideal coefficients derived for a continuous panel:

GEOMETRY		HORIZONTAL		VERTICAL		HORIZ. DISTORTION		VERTICAL DISTORTION	
depth	rbd	$N_{xh}=Q_{11}$	$N_{yh}=Q_{21}$	$N_{xv}=Q_{12}$	$N_{yv}=Q_{22}$	$N_{xy,h}$	$N_{yx,h}$	$N_{xy,v}$	$N_{yx,v}$
[m]	[%]	[kN]	[kN]	[kN]	[kN]	[kN]	[kN]	[kN]	[kN]
0.20	4.0	1,562,203	621,542	621,542	1,075,003	348,849	480,511	480,511	660,731

TABLE 5.30. Representative Element Volume refinement for pattern R, rbd 4%, at constitutive coefficients level

To normalize the results, they are divided by the base material modulus of elasticity ($E_b = 28 * 576 * 791\ kN/m^2$), the panel side and the imposed strain as explained in *Chapter 4.1.5. Homogenization process.*

72º (-x-)	CONSTITUTIVE COEFFICIENTS				
rbd [%]	Q_{11}	Q_{12}	Q_{21}	Q_{22}	Q_{33}
4	0.03972	0.02175	0.02175	0.05178	0.01681

TABLE 5.31. Normalized constitutive coefficients pattern R, rbd 4%

72º (-x-)	HOMOGENIZED MECHANICAL PROPERTIES				
rbd [%]	$E_{h,x}$	$E_{h,y}$	$\nu_{h,xy}$	$\nu_{h,yx}$	G_h
4	3.06%	3.99%	0.420	0.548	1.68%

TABLE 5.32. Homogenized mechanical properties pattern R, rbd 4%

The results of applying the formulation for the rotation to the pattern R constitutive coefficients in steps of 6º is:

Rotation	CONSTITUTIVE COEFFICIENTS				
[º]	Q_{11}	Q_{12}	Q_{21}	Q_{22}	Q_{33}
0	0.0397	0.0217	0.0217	0.0518	0.0168
6	0.0401	0.0215	0.0215	0.0519	0.0166
12	0.0410	0.0210	0.0210	0.0521	0.0160
18	0.0425	0.0201	0.0201	0.0523	0.0151
24	0.0444	0.0191	0.0191	0.0524	0.0142
30	0.0463	0.0181	0.0181	0.0524	0.0132
36	0.0482	0.0174	0.0174	0.0520	0.0125
42	0.0499	0.0170	0.0170	0.0511	0.0121
48	0.0511	0.0170	0.0170	0.0499	0.0121
54	0.0520	0.0174	0.0174	0.0482	0.0125
60	0.0524	0.0181	0.0181	0.0463	0.0132
66	0.0524	0.0191	0.0191	0.0444	0.0142
72	0.0523	0.0201	0.0201	0.0425	0.0151
78	0.0521	0.0210	0.0210	0.0410	0.0160
84	0.0519	0.0215	0.0215	0.0401	0.0166
90	0.0518	0.0217	0.0217	0.0397	0.0168

TABLE 5.33. Rotated constitutive coefficients pattern R, rbd 4%,

Rotation	HOMOGENIZED MECHANICAL PROPERTIES				
[º]	$E_{h,x}$	$E_{h,y}$	$\nu_{h,xy}$	$\nu_{h,yx}$	G_h
0	3.06%	3.99%	0.420	0.548	1.68%
6	3.11%	4.03%	0.415	0.538	1.66%
12	3.26%	4.14%	0.403	0.511	1.60%
18	3.48%	4.28%	0.384	0.472	1.51%
24	3.74%	4.42%	0.364	0.430	1.42%
30	4.01%	4.53%	0.346	0.392	1.32%
36	4.24%	4.57%	0.335	0.361	1.25%
42	4.42%	4.53%	0.332	0.341	1.21%
48	4.53%	4.42%	0.341	0.332	1.21%
54	4.57%	4.24%	0.361	0.335	1.25%
60	4.53%	4.01%	0.392	0.346	1.32%
66	4.42%	3.74%	0.430	0.364	1.42%
72	4.28%	3.48%	0.472	0.384	1.51%
78	4.14%	3.26%	0.511	0.403	1.60%
84	4.03%	3.11%	0.538	0.415	1.66%
90	3.99%	3.06%	0.548	0.420	1.68%

TABLE 5.34. Rotated homogenized mechanical properties pattern R, rbd 4%

Observation of the results:

Rotation of 90º. The homogenized mechanical properties in x- and y-direction swap as the pattern is rotated 90º

Rotation of 54º and 36ª. It was expected that the modulus of elasticity in the x-direction (E_x) rotating 54º and in the y-direction (E_Y) rotating 36ª would be the same. This verification is satisfied, but it is also shown that for the rest of mechanical properties x- and y-direction swap, which was not foreseen.

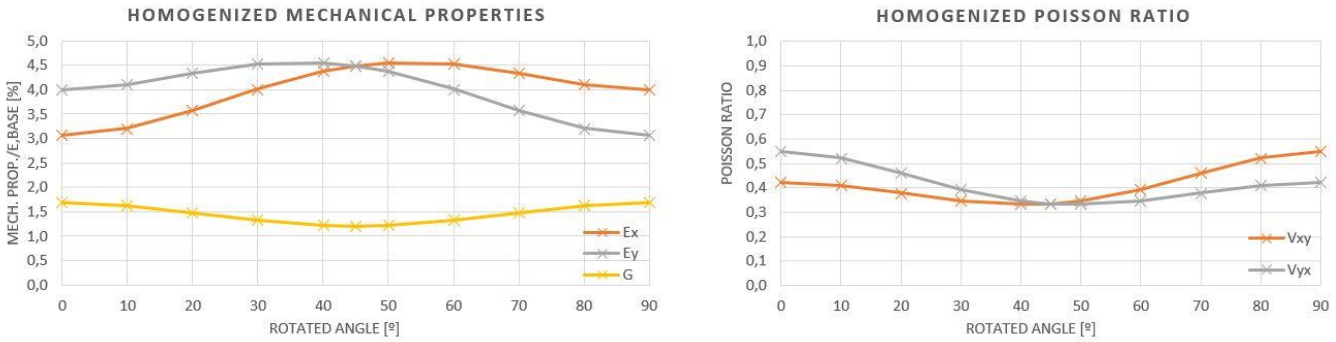

FIG 5.31. Pattern R. Rotation of the homogenized mechanical properties obtained with beam FE

HEXAGONAL SYMMETRY

Finally, pattern F Mustansiriya madrasa (tessellation 3.6.36. θ =30º) is studied as representative of the patterns with hexagonal symmetry. The steps followed are the same as explained for the "square symmetry" and just used for the "pentagonal symmetry" in this chapter.

The directions of symmetry in hexagonally symmetric patterns are at steps of 60º (0º, 60º, 120º, 180º, 240º, 300º and 360º). A priori it is expected that the homogenized mechanical properties will be the same for the symmetry directions. However, in this exercise it is also proved numerically that the homogenized mechanical properties will be the same for any direction, behaving as pure isotropic.

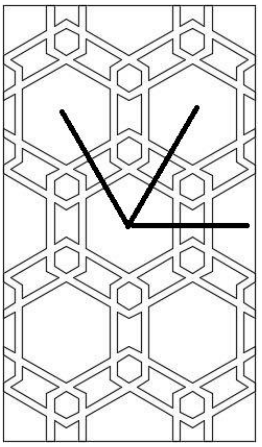

FIG 5.32. Pattern F. Directions of symmetry at 0º, 60º and 120º.

Ideal coefficients derived for a continuous panel:

GEOMETRY		HORIZONTAL		VERTICAL		HORIZ. DISTORTION		VERTICAL DISTORTION	
depth	rbd	$N_{xh} = Q_{11}$	$N_{yh} = Q_{21}$	$N_{xv} = Q_{12}$	$N_{yv} = Q_{22}$	$N_{xy,h}$	$N_{yx,h}$	$N_{xy,v}$	$N_{yx,v}$
[m]	[%]	[kN]	[kN]	[kN]	[kN]	[kN]	[kN]	[kN]	[kN]
0.30	6.0	2,510,263	1,324,209	1,324,209	836,754	35,347	62,023	62,023	106,528

TABLE 5.35. Representative Element Volume refinement for pattern F, rbd 6%, at constitutive coefficients level

To normalize the results, they are divided by the base material modulus of elasticity ($E_b = 28 * 576 * 791\ kN/m^2$), the panel side and the imposed strain as explained in *Chapter 4.1.5. Homogenization process.*

30º (-x-)	CONSTITUTIVE COEFFICIENTS				
rbd [%]	Q_{11}	Q_{12}	Q_{21}	Q_{22}	Q_{33}
6	0.05072	0.04634	0.04634	0.05072	0.00216

TABLE 5.36. Normalized constitutive coefficients pattern F, rbd 6%

30º (-x-)	HOMOGENIZED MECHANICAL PROPERTIES				
rbd [%]	$E_{h,x}$	$E_{h,y}$	$\nu_{h,xy}$	$\nu_{h,yx}$	G_h
6	0.84%	0.84%	0.914	0.914	0.22%

TABLE 5.37.Homogenized mechanical properties pattern F, rbd 6%

The results of applying the formulation for the rotation to the pattern R constitutive coefficients in steps of 6º is:

Rotation	CONSTITUTIVE COEFFICIENTS				
[º]	Q_{11}	Q_{12}	Q_{21}	Q_{22}	Q_{33}
0	0.0507	0.0463	0.0463	0.0507	0.0022
10	0.0507	0.0463	0.0463	0.0507	0.0022
20	0.0507	0.0464	0.0464	0.0507	0.0022
30	0.0507	0.0464	0.0464	0.0507	0.0022
40	0.0507	0.0464	0.0464	0.0507	0.0022
45	0.0507	0.0464	0.0464	0.0507	0.0022
50	0.0507	0.0464	0.0464	0.0507	0.0022
60	0.0507	0.0464	0.0464	0.0507	0.0022
70	0.0507	0.0464	0.0464	0.0507	0.0022
80	0.0507	0.0463	0.0463	0.0507	0.0022
90	0.0507	0.0463	0.0463	0.0507	0.0022

TABLE 5.38. Rotated constitutive coefficients pattern F, rbd 6%,

Rotation	HOMOGENIZED MECHANICAL PROPERTIES				
[º]	$E_{h,x}$	$E_{h,y}$	$\nu_{h,xy}$	$\nu_{h,yx}$	G_h
0	0.84%	0.84%	0.914	0.914	0.22%
10	0.84%	0.84%	0.914	0.914	0.22%
20	0.83%	0.83%	0.914	0.914	0.22%
30	0.83%	0.83%	0.915	0.915	0.22%
40	0.83%	0.83%	0.915	0.915	0.22%
45	0.83%	0.83%	0.915	0.915	0.22%
50	0.83%	0.83%	0.915	0.915	0.22%
60	0.83%	0.83%	0.915	0.915	0.22%
70	0.83%	0.83%	0.914	0.914	0.22%
80	0.84%	0.84%	0.914	0.914	0.22%
90	0.84%	0.84%	0.914	0.914	0.22%

TABLE 5.39. Rotated homogenized mechanical properties pattern F, rbd 6%

The pattern is pure isotropic as the mechanical properties are the same regardless of the orientation under study. The small differences in the results cannot be attributed to the simplification in the formulation as the constitutive coefficients made zero in the approximation are actually zero in isotropic materials. It is, therefore, produced by the errors in the Representative Element Volume refinement.

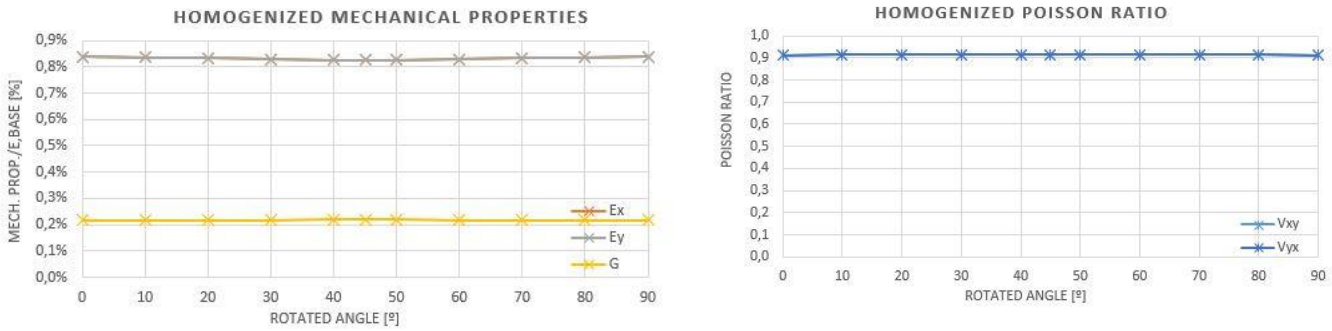

FIG 5.33. Pattern f. Rotation of the homogenized mechanical properties obtained with beam FE

The analytical rotation makes use of all the constitutive coefficients in its formulation. That is the reason why it is so important to take into account the Representative Element Volume in order to work with ideal values. The refinement is done at the level of the constitutive coefficients instead of the level of the mechanical properties, so the results from beam FE are used. In order to rotate the results with membrane elements, the designer must take into account the Representative Element Volume, for instance by getting a correction factor between the ideal behaviour results with beam FE and the results for 1x1 panel with beam FE.

5.1.3. ROTATION FACTOR

It has been proved that the derived formulation for rotating analytically any pattern, is suitable and very accurate when working with ideal behaviours (when the Representative Element Volume has been taken into account). In this point, the previous steps are repeated for all patterns to have a better insight into their behaviour, to choose the appropriate orientation for the comparison tables and to provide an extra tool for the designer to freely choose the orientation that best meets his needs.

The first thing is to realize that **the rotation factors are defined as the relationship between the rotated and the original pattern** and vary for with the relative beam depth. Using as an example the values obtained previously for the D Lahore Fort Complex pattern for a rotation of 45º:

(-x-)	HOMOGENIZED MECHANICAL PROPERTIES				
rbd [%]	$E_{h,x}$	$E_{h,y}$	$\nu_{h,xy}$	$\nu_{h,yx}$	G_h
1.00	0.18%	0.18%	0.191	0.191	0.01%
3.00	2.76%	2.76%	0.207	0.207	0.25%
5.00	7.05%	7.05%	0.221	0.221	0.96%
7.00	11.69%	11.69%	0.225	0.225	2.12%
9.00	16.41%	16.41%	0.223	0.223	3.58%

TABLE 5.40. Pattern D, ideal behaviour original pattern, rotation 0º

(-x-)	HOMOGENIZED MECHANICAL PROPERTIES				
rbd [%]	$E_{h,x}$	$E_{h,y}$	$\nu_{h,xy}$	$\nu_{h,yx}$	G_h
0.71	0.04%	0.04%	0.825	0.825	0.07%
2.12	0.88%	0.88%	0.747	0.747	1.14%
3.54	3.18%	3.18%	0.649	0.649	2.89%
4.95	6.61%	6.61%	0.562	0.562	4.77%
6.36	10.71%	10.71%	0.493	0.493	6.71%

TABLE 5.41. Pattern D, ideal behaviour pattern rotated 45º

Relationship between the homogenized mechanical properties of the pattern rotated 45º and those of the original pattern before the rotation, for varying relative beam depth:

(-x-)	C_{R45}. RELATIONSHIP MECH. PROP. 45º / 0º				
rbd [%]	C_{R45_EX}	C_{R45_EY}	C_{R45_VXY}	C_{R45_VYX}	C_{R45_G}
1.00	0.22	0.22	4.33	4.33	7.08
3.00	0.32	0.32	3.61	3.61	4.54
5.00	0.45	0.45	2.94	2.94	2.99
7.00	0.57	0.57	2.49	2.49	2.25
9.00	0.65	0.65	2.21	2.21	1.87

TABLE 5.42. Rotation factors for a rotation of 45º of pattern D

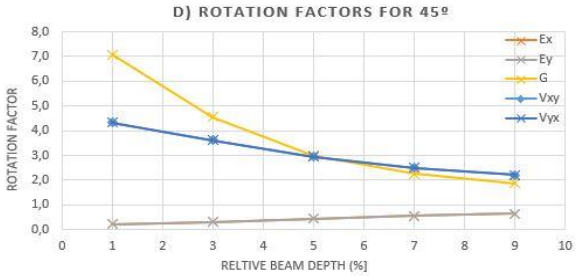

FIG 5.34. Rotation factors for a rotation of 45º of pattern D

The rotation coefficients vary with the relative beam depth, meaning that if a pattern is rotated a certain angle, the relation between the mechanical properties of the rotated pattern and the original pattern depends on the relative beam depth. For the homogenized modulus of elasticity and Poisson ratios, the variation is linear and can be defined by linear interpolation from two points. However, the variation of the shear modulus is curved and requires of three points if considered parabolic. For this reason, the rotation coefficients are provided for three different relative beam depths, so the designer can derive the approximate value for other relative beam depths. However, to get more accurate results and to rotate the variation patterns which are not included in this chapter, it is strongly recommended to **retrieve the Q_{ij} coefficients and repeat the rotation process that has been shown step by step**. The test results for 2x2 and 4x4 panels to enable the calculation of the ideal behaviour are included in *Appendix II. Numerical results*.

The information included in each case from top to bottom is:

- Given name to the pattern and the tessellation and parameters to draw it with the Hankin method.
- Picture of the pattern displaying what is considered as its module. The module length in the x-direction (horizontally in the picture) is needed for the relative beam depth (rbd %) definition.
- Graph of the variation of the mechanical properties with a varying rotation, for a given relative beam depth
- Tables of the rotation factors of each mechanical property for a varying rotation, for a given saturation.

Only three representative results are included (square, pentagonal and hexagonal symmetries). For the complete set of historic geometric Islamic patterns, see *Appendix I. Design guide*.

D) LAHORE FORT COMPLEX. Tessellation 4.8.8. θ =67.5º. Square symmetry.

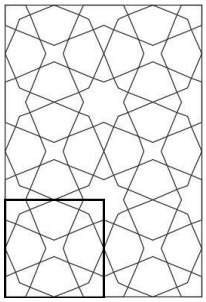

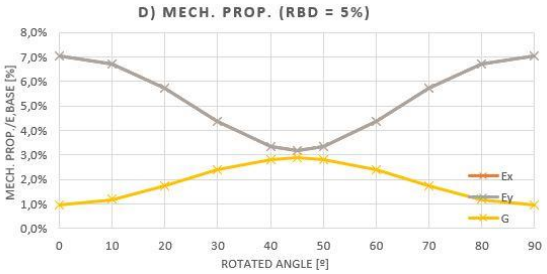

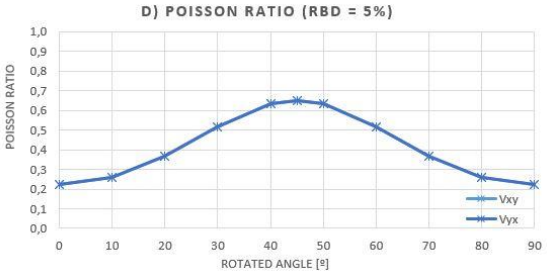

FIG 5.35. Homogenized mechanical properties pattern D, for different pattern orientations.

2%	ROTATION FACTORS				
Rot [º]	C_{R_EX}	C_{R_EY}	C_{R_VX}	C_{R_VY}	C_{R_G}
0	1.00	1.00	1.00	1.00	1.00
10	0.94	0.94	1.24	1.24	1.56
20	0.76	0.76	1.96	1.96	2.97
30	0.51	0.51	3.01	3.01	4.58
40	0.29	0.29	3.88	3.88	5.63
45	0.26	0.26	4.01	4.01	5.78
50	0.29	0.29	3.88	3.88	5.63
60	0.51	0.51	3.01	3.01	4.58
70	0.76	0.76	1.96	1.96	2.97
80	0.94	0.94	1.24	1.24	1.56
90	1.00	1.00	1.00	1.00	1.00

5%	ROTATION FACTORS				
Rot [º]	C_{R_EX}	C_{R_EY}	C_{R_VX}	C_{R_VY}	C_{R_G}
0	1.00	1.00	1.00	1.00	1.00
10	0.95	0.95	1.17	1.17	1.23
20	0.81	0.81	1.66	1.66	1.82
30	0.62	0.62	2.34	2.34	2.50
40	0.47	0.47	2.86	2.86	2.93
45	0.45	0.45	2.94	2.94	2.99
50	0.47	0.47	2.86	2.86	2.93
60	0.62	0.62	2.34	2.34	2.50
70	0.81	0.81	1.66	1.66	1.82
80	0.95	0.95	1.17	1.17	1.23
90	1.00	1.00	1.00	1.00	1.00

8%	ROTATION FACTORS				
Rot [º]	C_{R_EX}	C_{R_EY}	C_{R_VX}	C_{R_VY}	C_{R_G}
0	1.00	1.00	1.00	1.00	1.00
10	0.96	0.96	1.13	1.13	1.12
20	0.86	0.86	1.48	1.48	1.43
30	0.73	0.73	1.95	1.95	1.78
40	0.63	0.63	2.29	2.29	2.00
45	0.61	0.61	2.34	2.34	2.03
50	0.63	0.63	2.29	2.29	2.00
60	0.73	0.73	1.95	1.95	1.78
70	0.86	0.86	1.48	1.48	1.43
80	0.96	0.96	1.13	1.13	1.12
90	1.00	1.00	1.00	1.00	1.00

TABLE 5.43. Rotation factors pattern D, for different pattern orientations and saturations of 2%, 5% and 8%.

F) MUSTANSIRIYA MADRASA. Tessellation 3.6.3.6. θ =30º. Hexagonal symmetry

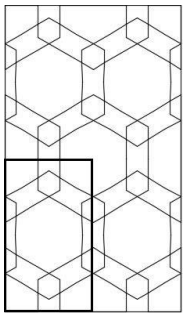

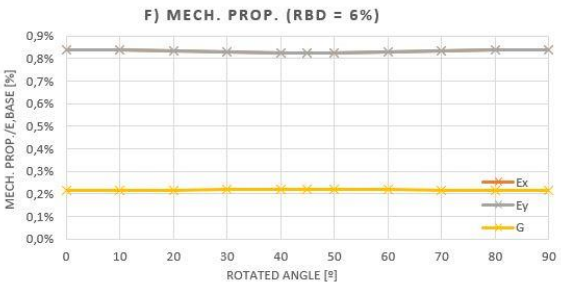

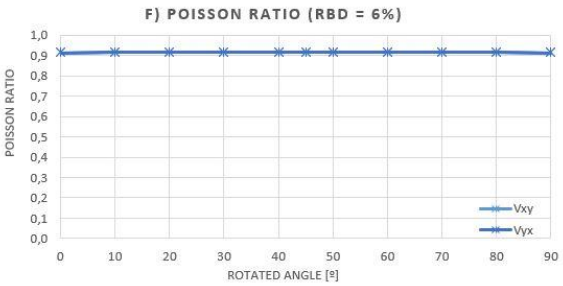

FIG 5.36. Homogenized mechanical properties pattern F, for different pattern orientations.

2%	ROTATION FACTORS				
Rot [º]	C_{R_EX}	C_{R_EY}	C_{R_VX}	C_{R_VY}	C_{R_G}
0	1.00	1.00	1.00	1.00	1.00
10	1.00	1.00	1.00	1.00	1.00
20	1.00	1.00	1.00	1.00	1.00
30	1.00	1.00	1.00	1.00	1.00
40	1.00	1.00	1.00	1.00	1.00
45	1.00	1.00	1.00	1.00	1.00
50	1.00	1.00	1.00	1.00	1.00
60	1.00	1.00	1.00	1.00	1.00
70	1.00	1.00	1.00	1.00	1.00
80	1.00	1.00	1.00	1.00	1.00
90	1.00	1.00	1.00	1.00	1.00

6%	ROTATION FACTORS				
Rot [º]	C_{R_EX}	C_{R_EY}	C_{R_VX}	C_{R_VY}	C_{R_G}
0	1.00	1.00	1.00	1.00	1.00
10	1.00	1.00	1.00	1.00	1.00
20	1.00	1.00	1.00	1.00	1.00
30	1.00	1.00	1.00	1.00	1.00
40	1.00	1.00	1.00	1.00	1.00
45	1.00	1.00	1.00	1.00	1.00
50	1.00	1.00	1.00	1.00	1.00
60	1.00	1.00	1.00	1.00	1.00
70	1.00	1.00	1.00	1.00	1.00
80	1.00	1.00	1.00	1.00	1.00
90	1.00	1.00	1.00	1.00	1.00

10%	ROTATION FACTORS				
Rot [º]	C_{R_EX}	C_{R_EY}	C_{R_VX}	C_{R_VY}	C_{R_G}
0	1.00	1.00	1.00	1.00	1.00
10	1.00	1.00	1.00	1.00	1.00
20	1.00	1.00	1.00	1.00	1.00
30	1.00	1.00	1.00	1.00	1.00
40	1.00	1.00	1.00	1.00	1.00
45	1.00	1.00	1.00	1.00	1.00
50	1.00	1.00	1.00	1.00	1.00
60	1.00	1.00	1.00	1.00	1.00
70	1.00	1.00	1.00	1.00	1.00
80	1.00	1.00	1.00	1.00	1.00
90	1.00	1.00	1.00	1.00	1.00

TABLE 5.44. Rotation factors pattern F, for different pattern orientations and saturations of 2%, 6% and 10%

R) FATEHPUR SIKRI. Tessellation ROS-I-6.10.10. θ =72º type Star. Pentagonal symmetry

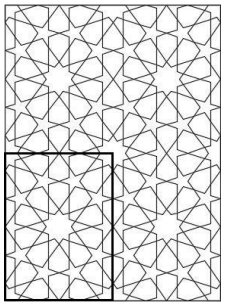

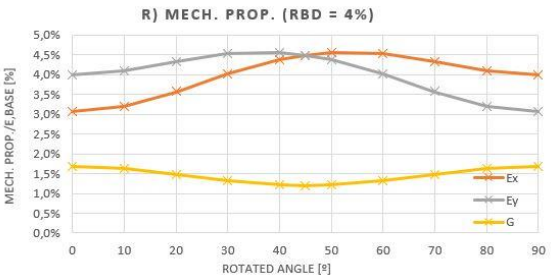

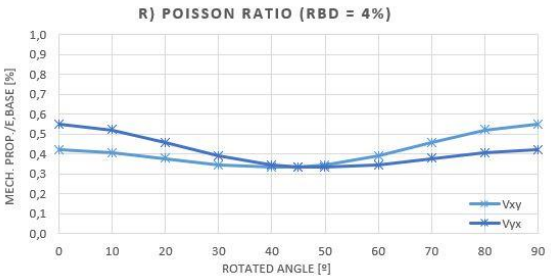

FIG 5.37. Homogenized mechanical properties pattern R, for different pattern orientations.

2%	ROTATION FACTORS				
Rot [º]	C_{R_EX}	C_{R_EY}	C_{R_VX}	C_{R_VY}	C_{R_G}
0	1.00	1.00	1.00	1.00	1.00
10	1.07	1.05	0.97	0.95	0.96
20	1.25	1.15	0.90	0.82	0.85
30	1.47	1.23	0.82	0.69	0.72
40	1.65	1.25	0.79	0.60	0.64
45	1.70	1.23	0.80	0.58	0.63
50	1.73	1.19	0.83	0.57	0.64
60	1.70	1.07	0.95	0.60	0.72
70	1.58	0.91	1.13	0.65	0.85
80	1.44	0.78	1.31	0.70	0.96
90	1.38	0.72	1.38	0.72	1.00

4%	ROTATION FACTORS				
Rot [º]	C_{R_EX}	C_{R_EY}	C_{R_VX}	C_{R_VY}	C_{R_G}
0	1.00	1.00	1.00	1.00	1.00
10	1.05	1.03	0.97	0.95	0.97
20	1.17	1.09	0.90	0.84	0.88
30	1.31	1.14	0.82	0.71	0.79
40	1.43	1.14	0.79	0.63	0.72
45	1.47	1.13	0.80	0.61	0.71
50	1.49	1.10	0.82	0.61	0.72
60	1.48	1.00	0.93	0.63	0.79
70	1.42	0.89	1.09	0.69	0.88
80	1.34	0.80	1.24	0.74	0.97
90	1.30	0.77	1.30	0.77	1.00

6%	ROTATION FACTORS				
Rot [º]	C_{R_EX}	C_{R_EY}	C_{R_VX}	C_{R_VY}	C_{R_G}
0	1.00	1.00	1.00	1.00	1.00
10	1.03	1.02	0.97	0.95	0.97
20	1.12	1.05	0.90	0.85	0.91
30	1.22	1.08	0.82	0.73	0.83
40	1.30	1.08	0.78	0.65	0.78
45	1.33	1.07	0.78	0.63	0.78
50	1.35	1.05	0.81	0.63	0.78
60	1.35	0.98	0.91	0.66	0.83
70	1.31	0.90	1.05	0.72	0.91
80	1.27	0.83	1.19	0.78	0.97
90	1.25	0.80	1.25	0.80	1.00

TABLE 5.45. Rotation factors pattern R, for different pattern orientations and saturations of 2%, 4% and 6%

5.2. WIRE PATTERNS PERFORMANCE

The saturation is the best parameter to use as reference as it is an indirect way of expressing the amount of material. A 45% saturation is used as it is a representative saturation for the filled patterns as well. Results are obtained for this document orientation. Patterns E, J and P have strong orientation at 45 degrees and patterns I and R at 54 degrees.

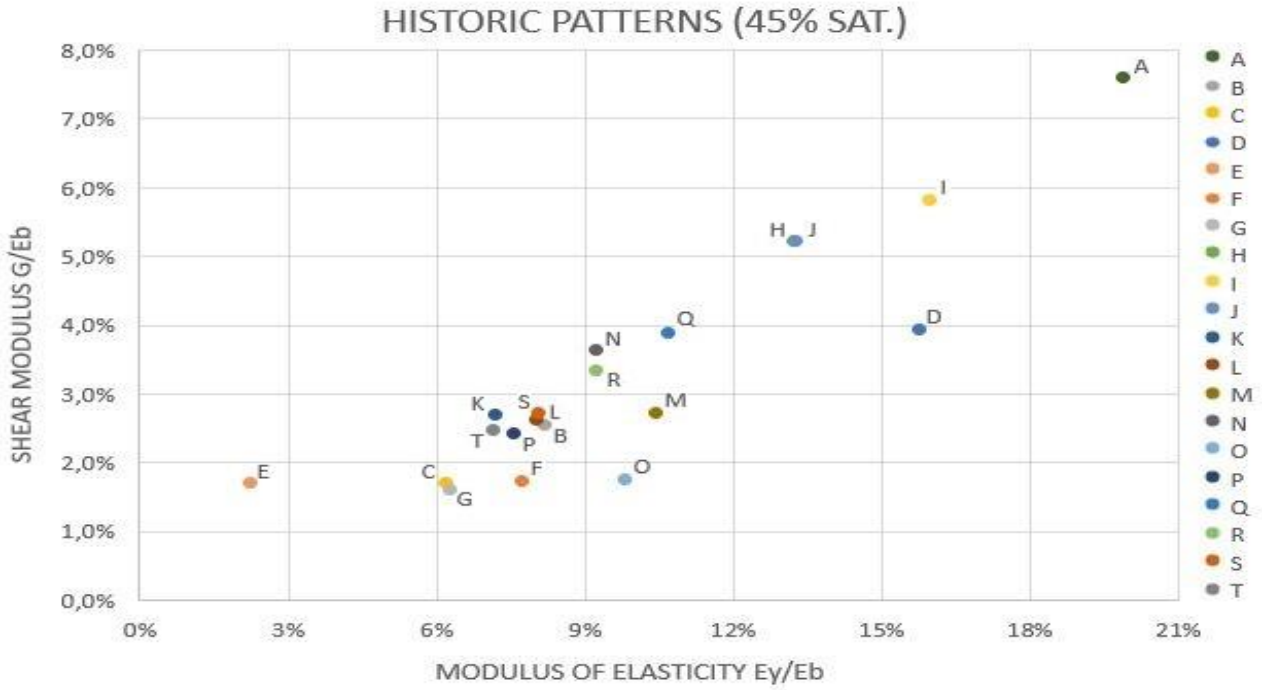

FIG 5.38.Performance comparison of historic patterns. Wire variation, saturation 45%

BEST PERFORMING PATTERNS

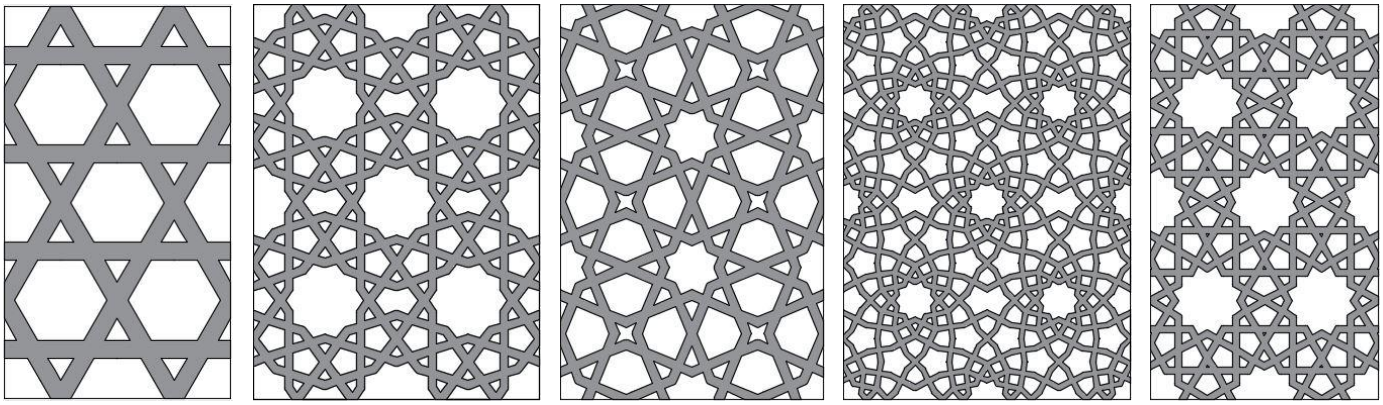

A) YESLI MOSQUE | I) HASHT BEHESHT | D) LAHORE FORT COMPLEX | J) MODARI-KHAN MADRASH | H) GENERALIFE

FIG 5.39.Best performing historic patterns. Wire variation, saturation 45%

WORST PERFORMING PATTERNS

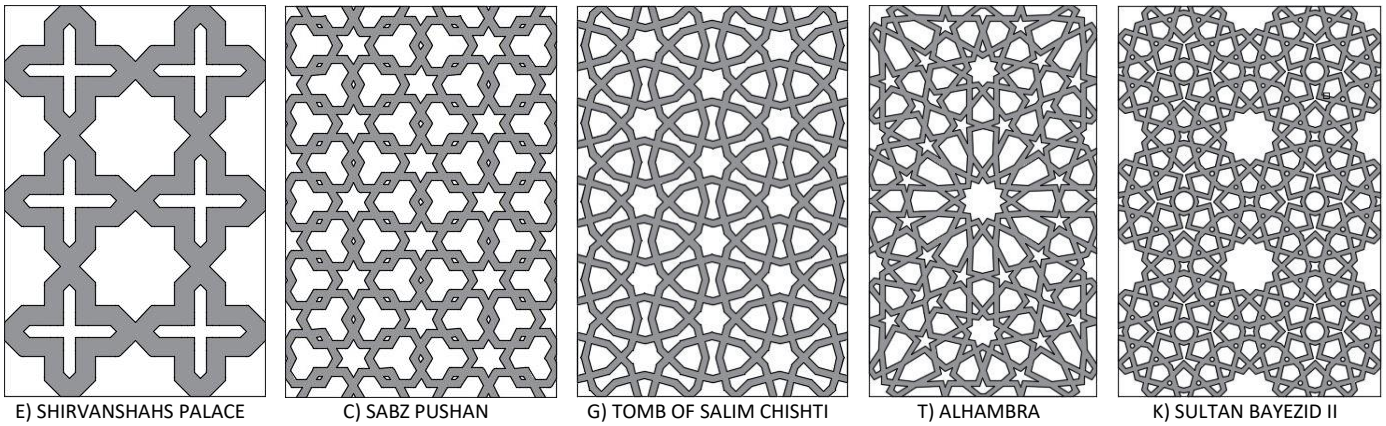

E) SHIRVANSHAHS PALACE | C) SABZ PUSHAN | G) TOMB OF SALIM CHISHTI | T) ALHAMBRA | K) SULTAN BAYEZID II

FIG 5.40. Worst performing historic patterns. Wire variation, saturation 45%

5.3. STAR FILLING

When there is a sharp turn in the force path, bending moments develop in the internal bars to get equilibrium. As axial stiffness is much bigger than bending stiffness, the most efficient and best performing patterns are those that maximize the ratio between their axial and bending strain energy. From this conclusion, a new set of solutions is proposed. Filling the stars will lead to much more efficient solutions since continuity in the force path is reestablished, minimizing the bending strain energy. The picture below shows the tessellation 6.6.6. θ =75º, Sat. = 40%, for the wired and filled variations. The continuity in the force path of the fill solution will increase extraordinary the stiffness and performance of the pattern.

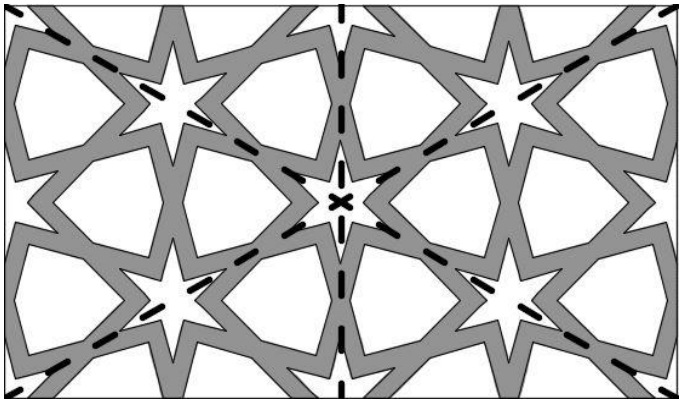

FIG 5.41. Tessellation 6.6.6. θ =75º Sat. = 40%, wire variation

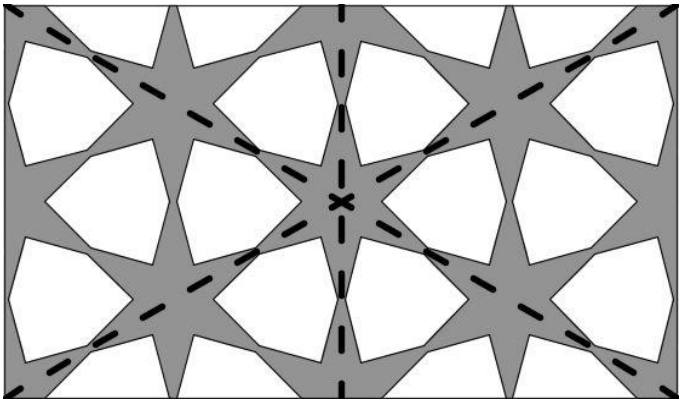

FIG 5.42. Tessellation 6.6.6. θ =75º Sat. = 40%, filled variation

The stars of the historic Islamic patterns studied in this document are filled to increase their continuity and stiffness. They cannot be modelled with bar elements so they are directly analysed with membrane elements. The star-filled patterns are **named after the original patterns with an asterisk to indicate that their stars are filled**.

It is possible to reach much higher saturation grades filling the stars, however, the pattern blurs very fast as the relative beam depth increases, **limiting the range to very small relative beam depths so the pattern can still be recognized**. For comparison purposes, it is more useful to have the mechanical properties expressed in terms of the saturation. The saturation and the mechanical properties have an exponential evolution. So far, the intermediate values have been obtained by the means of linear interpolation, considering that the results would be accurate enough because the control points were very close to each other. In this chapter however, a more precise and short approach is followed. Instead of providing a large amount of control points, just 3 points are given, so any intermediate value can be accurately calculated by quadratic interpolation.

In this case, linking the mesh size with the beam depth does not have that much sense so the absolute mesh size is adopted instead of a relative mesh size, in the terms that they have been defined in *Chapter 4.6. Mesh refinement*. **The mesh refinement** is done in the same manner as described for the membrane elements assuming an order of converge $O(h^2)$, **with a mesh size of 1cm and 2cm with a modulus size in the x-direction of 5m**. On the other hand, the Representative Element Volume is not taken into account as the bars behave as clamped in the perimeter, providing exact solutions for all the mechanical properties with exception of the shear modulus with a 1x1 panel. Reactions from tests used for the homogenization process are included in *Appendix II. Numerical results.* For the complete set of pictures and tables for historic patterns, see *Appendix I. Design guide.*

D*) LAHORE FORT COMPLEX

D67.5,		HOMOG. MECHANICAL PROPERTIES				
Sat [%]	rbd [%]	$E_{h,x}$	$E_{h,y}$	$\nu_{h,xy}$	$\nu_{h,yx}$	G_h
35	1.58	5.90%	5.89%	0.589	0.589	2.86%
40	3.02	9.32%	9.32%	0.521	0.521	4.31%
45	4.52	13.08%	13.08%	0.465	0.465	5.92%

TABLE 5.46. Homogenized mechanical properties, pattern D*

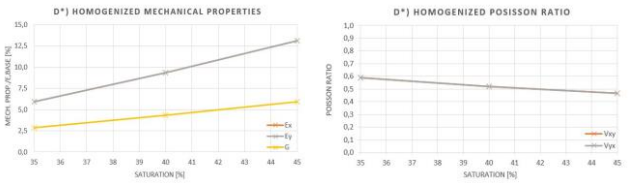

FIG 5.43. Homogenized mechanical properties, pattern D*

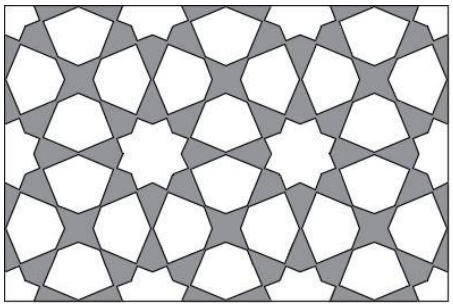

FIG 5.44. Pattern D*. Saturation 35%

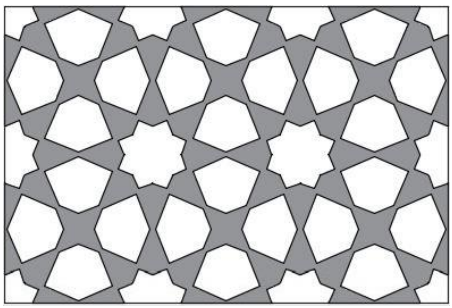

FIG 5.45. Pattern D*. Saturation 40%

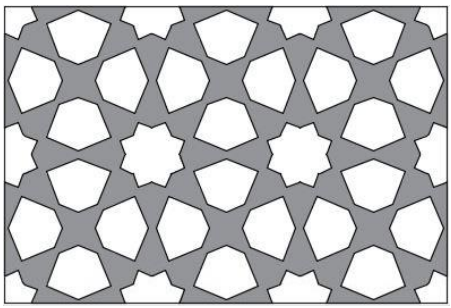

FIG 5.46. Pattern D*. Saturation 45%

F*) MUSTANSIRIYA MADRASA

F30,		HOMOG. MECHANICAL PROPERTIES				
Sat [%]	rbd [%]	$E_{h,x}$	$E_{h,y}$	$\nu_{h,xy}$	$\nu_{h,yx}$	G_h
35	1.53	9.80%	9.82%	0.349	0.349	3.68%
40	3.66	13.79%	13.79%	0.349	0.349	5.15%
45	5.92	17.45%	17.45%	0.348	0.348	6.50%

TABLE 5.47. Homogenized mechanical properties, pattern F*

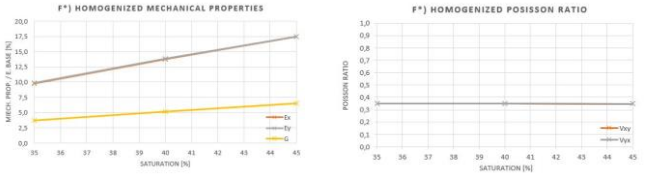

FIG 5.47. Homogenized mechanical properties, pattern F*

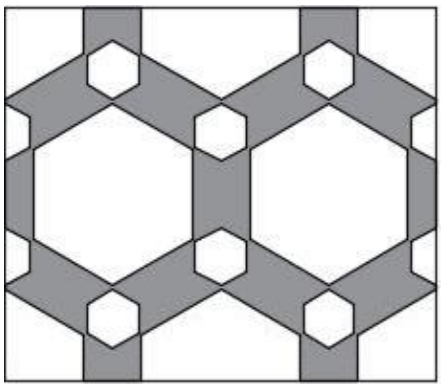

FIG 5.48. Pattern F*. Saturation 35%

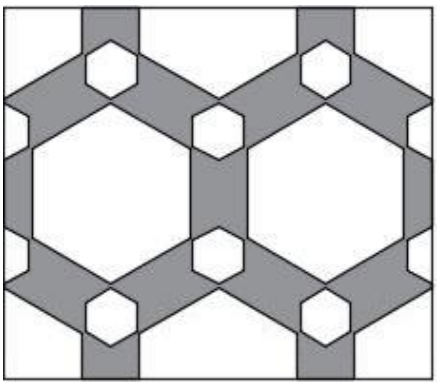

FIG 5.49. Pattern F*. Saturation 40%

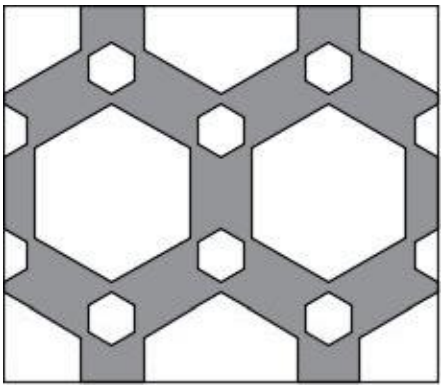

FIG 5.50. Pattern F*. Saturation 45%

R*) FATEHPUR SIKRI

R72,		HOMOG. MECHANICAL PROPERTIES				
Sat [%]	rbd [%]	$E_{h,x}$	$E_{h,y}$	$\nu_{h,xy}$	$\nu_{h,yx}$	G_h
40	1.31	8.94%	9.01%	0.531	0.535	2.59%
45	2.06	12.98%	13.09%	0.465	0.469	3.90%
50	2.86	17.39%	17.64%	0.411	0.417	5.49%

TABLE 5.48. Homogenized mechanical properties, pattern R*

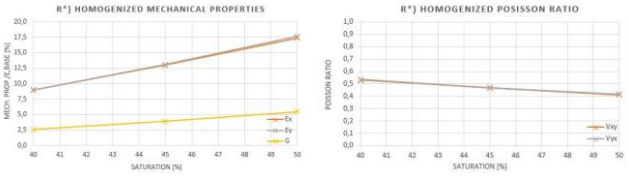

FIG 5.51. Homogenized mechanical properties, pattern R*

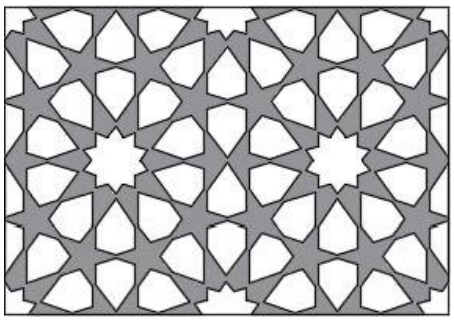

FIG 5.52. Pattern R*. Saturation 40%

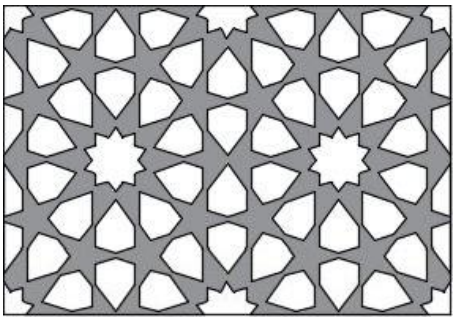

FIG 5.53. Pattern R*. Saturation 45%

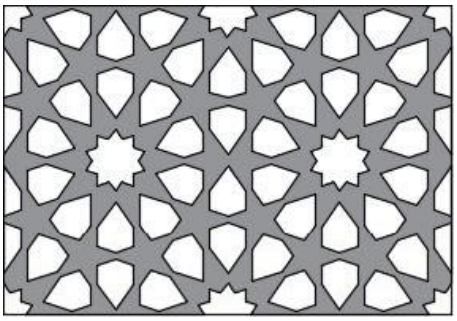

FIG 5.54. Pattern R*. Saturation 50%

5.4. FILLED PATTERNS PERFORMANCE

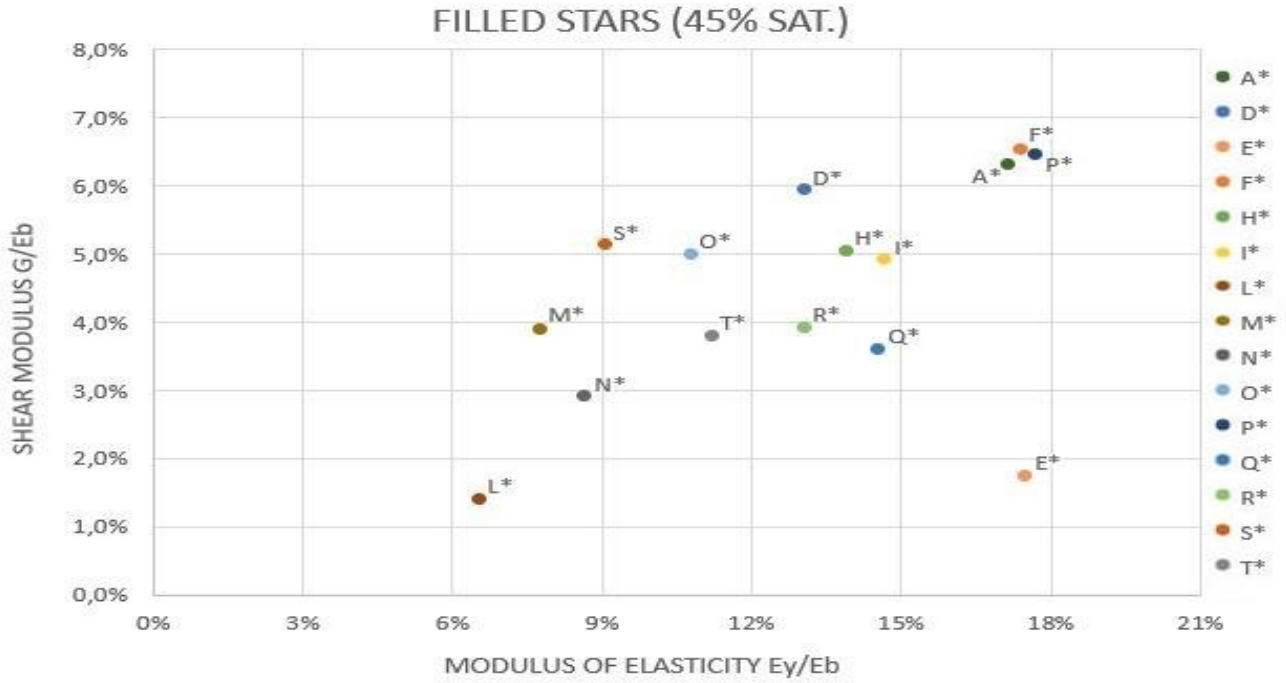

FIG 5.55. Performance comparison of historic patterns. Filled variation, saturation 45%

BEST PERFORMING PATTERNS (SAT. 45%)

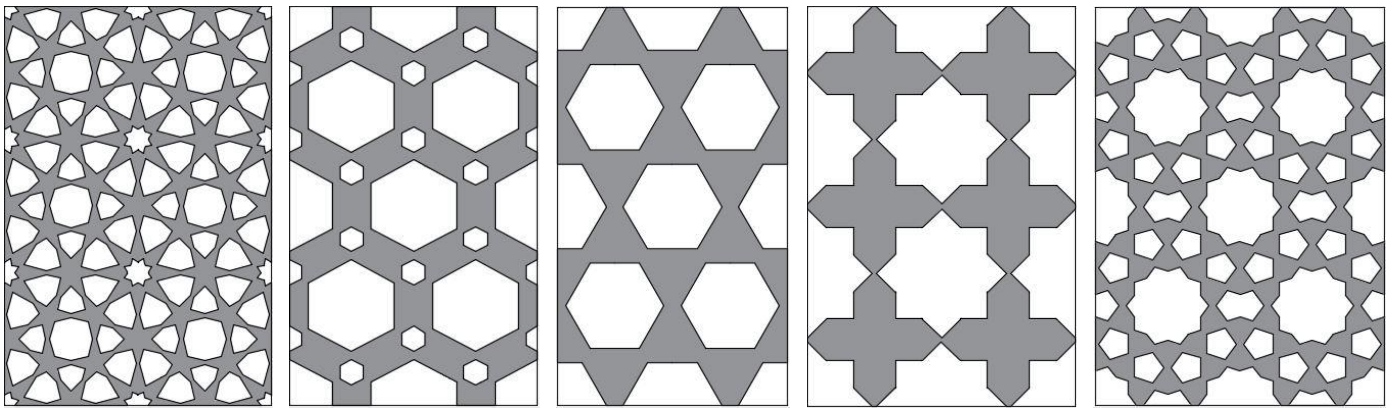

P*) MOSQUE OF AL-SALIH TALA'I | F*) MUSTANSIRIYA MADRASA | A*) YESLI MOSQUE | E*) SHIRVANSHAHS PALACE | I*) HASHT BEHESHT

FIG 5.56. Best performing historic patterns. Filled variation, saturation 45%

WORST PERFORMING PATTERNS (SAT. 45%)

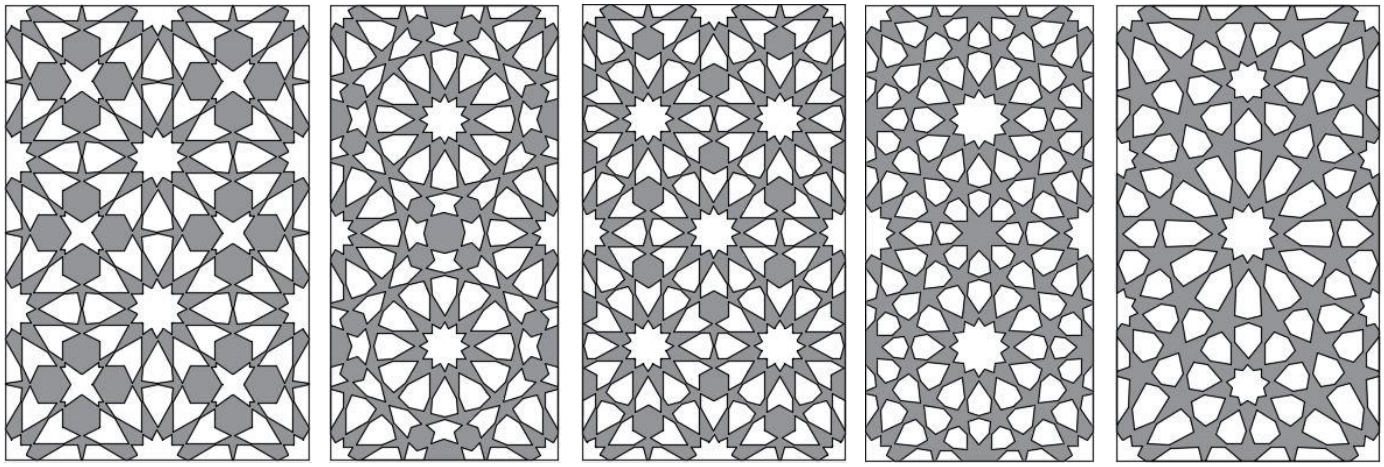

L*) BEN YUSUF MADRASA | M*) AL-NASIR MUHAMMAD MINBAR | N*) AL-NASIR MUHAMMAD | S*) JAMEH MOSQUE | T*) ALHAMBRA

FIG 5.57. Best performing historic patterns. Filled variation, saturation 45%

5.5. FROM WIRE TO FILLED PATTERNS

Providing continuity leads to an increment in the stiffness and resistance, but also of material use. The effect that filling the patterns has on the pattern performance can be grouped in three categories:

- Great improvement. There is a considerable gain in the continuity of the load path so the axial strain energy increases to the detriment of the bending strain energy. Patterns A, B, E, P, Q and R.
- Moderate effect. Under this category can be found either starred patterns with a high degree of continuity such as o patterns or classic geometric patterns such as patterns H and I.
- Worsening of the pattern performance in the case of patterns with arrows. Filling the arrows goes at the expense of making slenderer the already very weak arrows points. It is the case of patterns L, N and M.

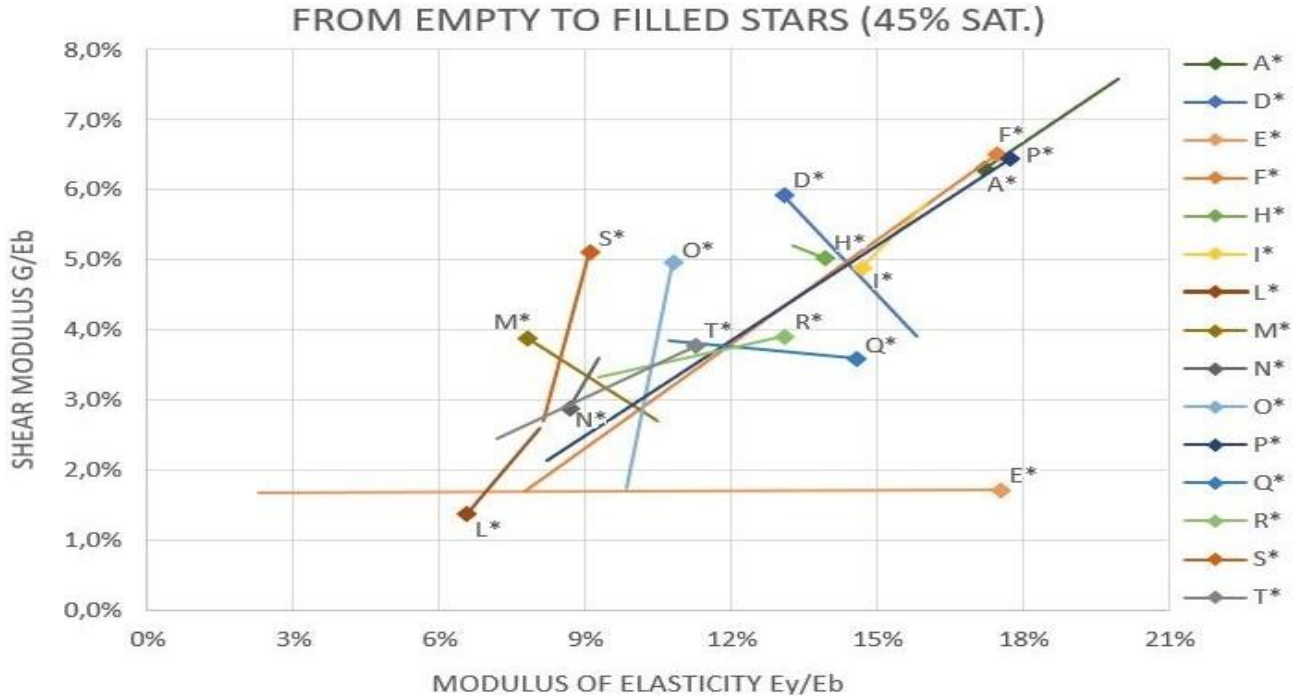

FIG 5.58. Change of mechanical properties for historic patterns, Sat. 45%, from wire to filled patterns

Sat. 45%	$E_{h,y}$	$\nu_{h,yx}$	G_h
A	19.93%	0.303	7.59%
A*	17.18%	0.406	6.30%
A*/A	0.86	1.34	0.83

Sat. 45%	$E_{h,y}$	$\nu_{h,yx}$	G_h
D	15.80%	0.316	3.92%
D*	13.08%	0.465	5.92%
D*/D	0.83	1.47	1.51

Sat. 45%	$E_{h,y}$	$\nu_{h,yx}$	G_h
E	2.28%	0.782	1.69%
E*	17.52%	0.050	1.71%
E*/E	7.70	0.06	1.02

Sat. 45%	$E_{h,y}$	$\nu_{h,yx}$	G_h
F	7.76%	0.703	1.71%
F*	17.45%	0.348	6.50%
F*/F	2.25	0.49	3.80

Sat. 45%	$E_{h,y}$	$\nu_{h,yx}$	G_h
H	13.24%	0.240	5.21%
H*	13.93%	0.385	5.02%
H*/H	1.05	1.60	0.96

Sat. 45%	$E_{h,y}$	$\nu_{h,yx}$	G_h
I	15.99%	0.323	5.80%
I*	14.67%	0.395	4.89%
I*/I	0.92	1.22	0.84

Sat. 45%	$E_{h,y}$	$\nu_{h,yx}$	G_h
L	8.07%	0.304	2.61%
L*	6.57%	0.536	1.38%
L*/L	0.81	1.77	0.53

Sat. 45%	$E_{h,y}$	$\nu_{h,yx}$	G_h
M	10.48%	0.389	2.69%
M*	7.81%	0.626	3.88%
M*/M	0.74	1.61	1.44

Sat. 45%	$E_{h,y}$	$\nu_{h,yx}$	G_h
N	9.27%	0.259	3.61%
N*	8.67%	0.534	2.89%
N*/N	0.94	2.06	0.80

Sat. 45%	$E_{h,y}$	$\nu_{h,yx}$	G_h
O	9.86%	0.415	1.74%
O*	10.81%	0.560	4.97%
O*/O	1.10	1.35	2.85

Sat. 45%	$E_{h,y}$	$\nu_{h,yx}$	G_h
P	8.21%	0.430	2.14%
P*	17.71%	0.345	6.44%
P*/P	2.16	0.80	3.01

Sat. 45%	$E_{h,y}$	$\nu_{h,yx}$	G_h
Q	10.70%	0.333	3.86%
Q*	14.57%	0.410	3.59%
Q*/Q	1.36	1.23	0.93

Sat. 45%	$E_{h,y}$	$\nu_{h,yx}$	G_h
R	9.28%	0.541	3.33%
R*	13.09%	0.469	3.90%
R*/R	1.41	0.87	1.17

Sat. 45%	$E_{h,y}$	$\nu_{h,yx}$	G_h
S	8.12%	0.321	2.70%
S*	9.09%	0.606	5.11%
S*/S	1.12	1.89	1.90

Sat. 45%	$E_{h,y}$	$\nu_{h,yx}$	G_h
T	7.17%	0.458	2.46%
T*	11.25%	0.533	3.77%
T*/T	1.57	1.17	1.54

TABLE 5.49. Change of mechanical properties for historic patterns, Sat. 45%, from wire to filled pattern

6. RESEARCH QUESTION 3. BUILDING LEVEL

The main objective of this thesis is to provide insight into the structural behaviour and design of geometric Islamic patterns as alternative to conventional diagrid systems for tall buildings. This research objective is articulated at three levels: method level, pattern level and building level. Each of the three research questions addresses one of those levels and they are further developed in a series of sub-questions described in the following document structure:

METHOD LEVEL:

Can a simple tool be developed for the design of geometric Islamic patterns as a non-conventional diagrid system?

- Method chosen and methodology for its adoption
- Development of a pre-design tool.
- Assessment of the developed tool

PATTERN LEVEL:

How do geometric Islamic patterns behave and compare when loaded in their plane?

- Selection of historic Islamic patterns and their parametric variations
- Characterization of the patterns' structural behaviour
- Performance comparison of the different patterns
- Proposals for their improvement

BUILDING LEVEL:

Can Islamic inspired patterns become a feasible alternative to traditional diagrid systems for tall buildings?

- **Performance comparison of the different patterns and the conventional diagrids**
- **Overview practical applications of best performing patterns**
- **Special cases in tall buildings**

6.1. CONVENTIONAL DIAGRIDS

In this research, it is considered that the conventional diagrid system is made of equilateral triangles as it is the most widespread use as introduced in *Chapter 2.2. Diagrid systems*. This corresponds directly with the tessellation 3.3.3.3.3.3.

In complex volumes the triangles can be distorted to adapt to the building surface, as in the Museum of the future[8] in Dubai. In tall buildings, the equilateral triangle has also been used in several buildings such as 30st Mary Axe[9] in London. However, the current tendency in tall buildings is to go to more acute triangles that develop higher mechanical properties in y-direction making them more optimal for that building typology as the Hearst Tower[10] in New York. In this chapter, the homogenization method will be applied to the conventional diagrid system in the same manner as it was applied to the historic geometric Islamic patterns in the previous chapters so their relative performance can be qualitatively and quantitatively compared with the same reference framework.

FIG 6.1. Museum of the future

FIG 6.2. 30st Mary Axe

FIG 6.3. Hearst Tower

SATURATION TABLES (Ch. 3.5.2.)

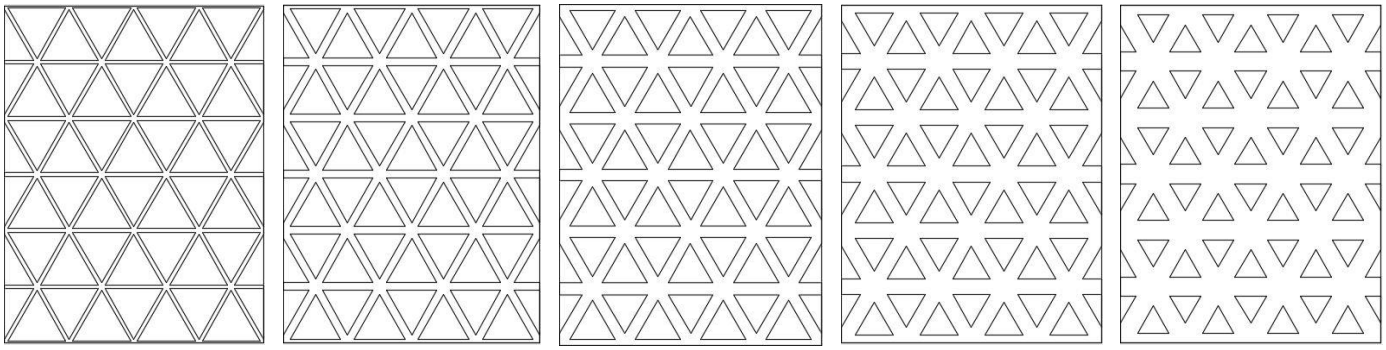

rbd 6% - Sat.19.70% | rbd 12% - Sat. 37.25% | rbd 18% - Sat. 52.63% | rbd 24% - Sat. 65.86% | rbd 30% - Sat. 76.92%

FIG 6.4. Z) Conventional diagrid pattern with 15%, 25%, 35% and 45% saturations

FE BEAM HOMOGENIZED MECHANICAL PROPERTIES (Ch 4.4.)

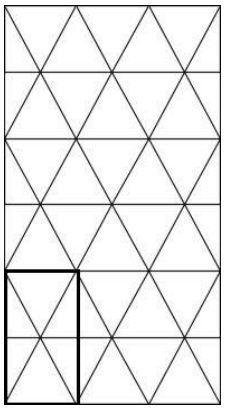

Z60		HOMOGENIZED MECHANICAL PROPERTIES				
rbd [%]	Sat [%]	$E_{h,x}$	$E_{h,y}$	$\nu_{h,xy}$	$\nu_{h,yx}$	G_h
3	10.12	3.47%	3.47%	0.333	0.330	1.30%
6	19.70	6.94%	6.95%	0.332	0.329	2.61%
9	28.75	10.45%	10.46%	0.330	0.327	3.93%
12	37.25	13.99%	14.00%	0.327	0.325	5.27%
15	45.21	17.57%	17.58%	0.324	0.322	6.63%
18	52.63	21.20%	21.21%	0.320	0.318	8.03%
21	59.52	24.88%	24.90%	0.316	0.314	9.45%
24	65.86	28.62%	28.64%	0.311	0.309	10.91%
27	71.66	32.42%	32.44%	0.307	0.305	12.40%
30	76.92	36.27%	36.30%	0.302	0.300	13.92%

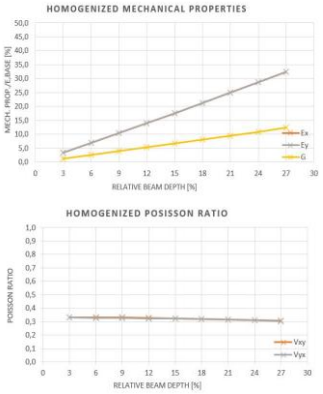

FIG 6.5. Pattern Z. Homogenized mechanical properties with beams FE.

MEMBRANE CORRECTION FACTOR (Ch 4.7.)

Z60	C2D CORRECTION FACTORS				
rbd [%]	C_{2D_EX}	C_{2D_EY}	C_{2D_VXY}	C_{2D_VYX}	C_{2D_G}
3	1.013	1.01	1.01	1.01	1.01
6	1.03	1.03	1.01	1.01	1.03
9	1.05	1.05	1.01	1.01	1.05
12	1.07	1.07	1.00	1.00	1.07
15	1.10	1.10	0.99	0.99	1.10
18	1.13	1.13	0.97	0.97	1.14
21	1.16	1.16	0.94	0.94	1.18
24	1.20	1.19	0.92	0.92	1.22
27	1.24	1.24	0.88	0.88	1.26
30	1.28	1.28	0.85	0.84	1.32

TABLE 6.1. Membrane correction factors pattern Z

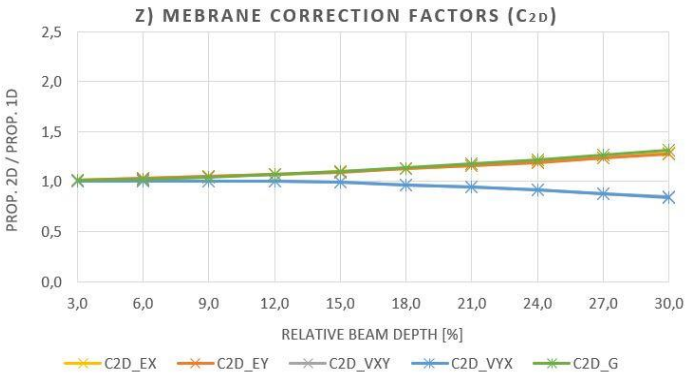

FIG 6.6. Membrane correction factors pattern Z

IDEAL HOMOGENIZED MECHANICAL PROPERTIES (Ch 4.8.)

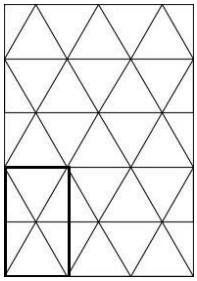

Z60		HOMOGENIZED MECHANICAL PROPERTIES				
Sat [%]	rel [%]	Ex	Ey	Vxy	Vyx	G
10	2.96	3.47%	3.47%	0.335	0.335	1.30%
20	6.10	7.27%	7.27%	0.335	0.335	2.72%
30	9.44	11.56%	11.56%	0.331	0.331	4.34%
40	13.04	16.48%	16.47%	0.325	0.325	6.22%
50	16.94	22.24%	22.24%	0.314	0.314	8.47%
60	21.23	29.33%	29.29%	0.298	0.297	11.28%

FIG 6.7. Pattern Z. Ideal homogenized mechanical properties.

6.2. DIAGRID VS HISTORIC PATTERNS PERFORMANCE

All the studied patterns can be either built up with bars (empty stars, named wired patterns) or carved in a continuous wall (filled stars, named filled patterns). Some patterns perform better when their stars are filled while others perform better keeping the stars empty. For this chart, the best performing solution for each pattern is chosen and compared against the conventional diagrid systems. One more time the orientation is not taken into account so the patterns´ mechanical properties might be slightly improved finding a better orientation that the one used or worsened when applied with another orientation to meet construction requirements.

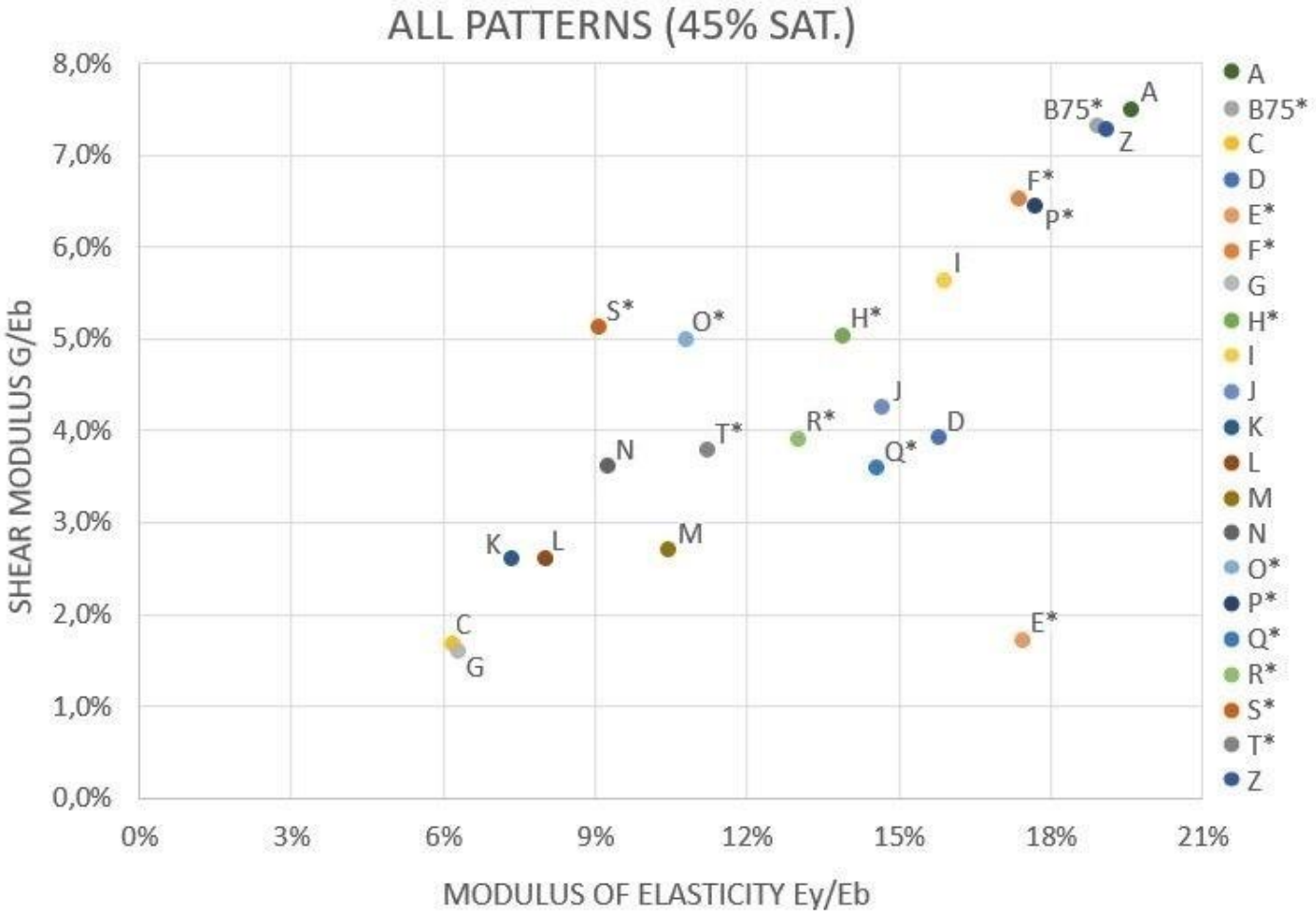

FIG 6.8.. Performance comparison of historic patterns against conventional diagrid system, saturation 45%

In general terms, diagrid systems perform better than the historic Islamic geometric patterns. The triangulation minimizes the bending strain to axial strain energy ratio making them more efficient. However, the following patterns have a great performance so their feasibility will be assessed alternatives in *Chapter 6.3. Overview of best performing patterns*

FEASIBLE ALTERNATIVES TO CONVENTIONAL DISAGRIDS (SAT. 45%)

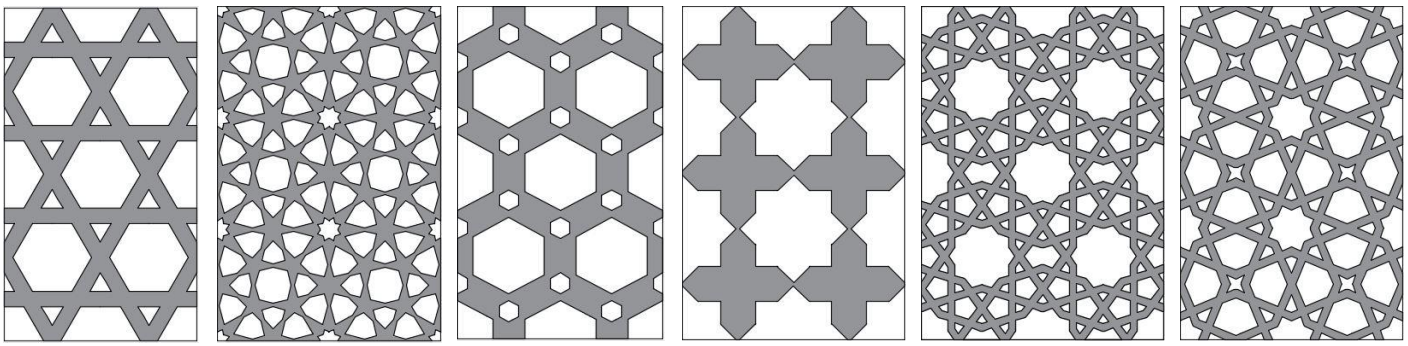

A) YESLI MOSQUE | P*) MOSQUE OF AL-SALIH TALA'I | F*) MUSTANSIRIYA MADRASA | E*) SHIRVANSHAHS PALACE | I) HASHT BEHESHT | D) LAHORE FORT COMPLEX

FIG 6.9. Best performing historic patterns, saturation 45%

6.3. OVERVIEW OF BEST PERFORMING PATTERNS

Specific issues related to the best performing patterns are succinctly addressed in this chapter to assess their applicability and feasibility as alternatives to conventional diagrid systems:

A) YESLI MOSQUE

From the structural point of view, it is the best performing pattern and therefore the best candidate to become a feasible alternative to conventional diagrids. It can be seen as a variation of the conventional diagrid as it can be obtained by erasing diagonals from the conventional diagrid layout.

From the constructive point of view, it has a horizontal continuous line that can be used as part of the floor slab. This line is equidistant, allowing to connect the façade regularly. All the nodes connect just 4 beams and the angles in all nodes are the same, leading to an easy and economic prefabrication.

This is an excellent solution from the economic, construction and structural point of view. Nevertheless, developers in Arabic countries may be reluctant to adopt this pattern for their buildings as it can be seen as composed of David stars. In fact, traditionally Yesli Mosque pattern always appear with its "filled pattern" variation. The structural performance of the filled pattern version is a bit lower, but it is similar to patterns P, Mosque of Al-Salih Tala'i and F, Mustansiriya madrasa, see *Chapter 5.5. From wired to filled patterns*.

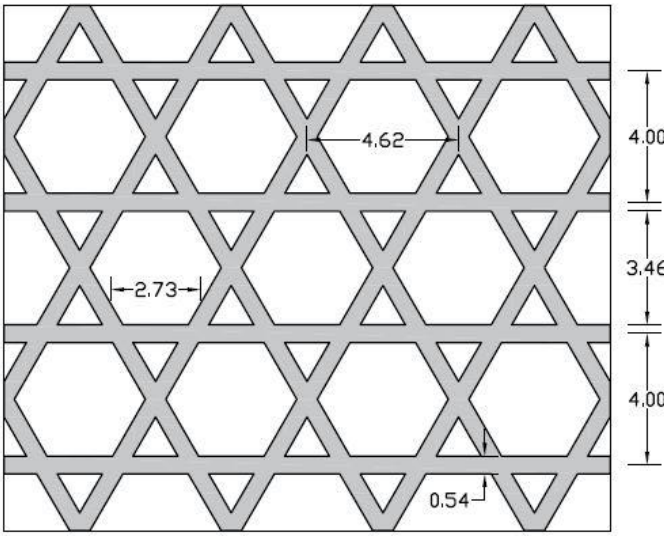

FIG 6.10. Application of pattern A to 4m inter-story building. Sat. 35%

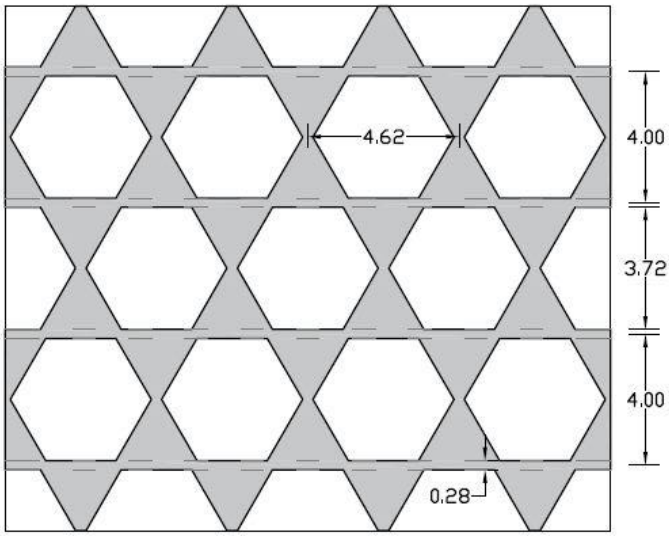

FIG 6.11. Application of pattern A, to 4m inter-story building. Sat. 35%

In conclusion, this is an excellent solution from the economic, construction and structural point of view. The wired variation could become a feasible alternative to conventional diagrids in non-Muslim countries whereas the filled variation would be more suitable in Muslim countries.

P*) MOSQUE OF AL-SALIH TALA'I

This is a much more complex pattern that conveys what is commonly understood when speaking about geometric Islamic star patterns. Due to its complexity there are several possibilities when applying it to a building.

One possibility is to connect the horizontal strand to every floor as done in the previous patterns. The left solution corresponds to making coincide the horizontal brand every two floors. With a 45% saturation and a floor height of 4m, the floor slab depth can be up to 24cm. In this solution the floor height is same at each level. On the other hand, the right solution corresponds to making coincide the horizontal brand every three floors. With a 45% saturation and a floor height of 4m, the floor slab depth can be up to 35cm. This option simplifies the construction as it reduces the number of modules and connections but at the same time there are two different floor heights (4.24m and 3.88m). Finally, all possibilities are considered unsatisfactory.

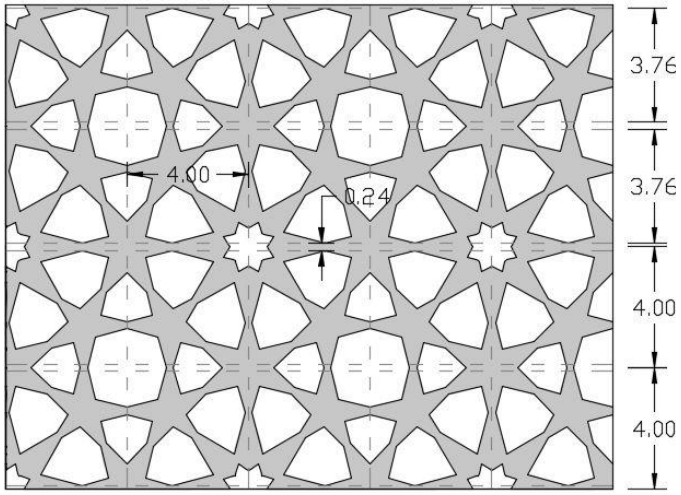

FIG6.12. Application of pattern P* to 4m inter-story building. Sat. 45%

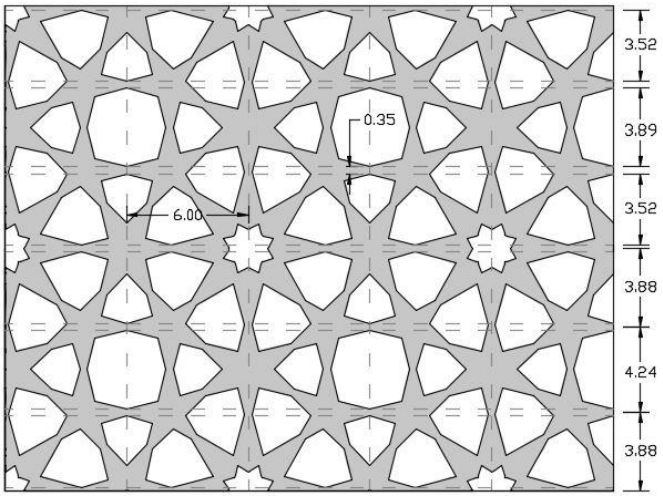

FIG 6.13. Application of pattern P* to 4m inter-story building. Sat. 45%

From the structural point of view, this pattern homogenized mechanical properties can compete with the homogenized mechanical properties of the conventional diagrid, insofar the resistance and non-linear effects due to the concentration of stresses are verified. It presents a square symmetry leading to a perpendicular isotropic behaviour, so the orientation and principal stress directions have to be taken into consideration when designing with this pattern.

However, from the constructive point of view its complexity is a big obstacle to overcome. Several modules can be found consisting of various stars but it will inevitably to complex unions and cladding systems.

In conclusion, this pattern meets all theoretical structural requirements to become a feasible alternative to conventional diagrids, but lacks the practical constructive applicability. Therefore, it can become a feasible alternative to conventional diagrids when that constructive limitation is overcome, for instance being applied to 3D printed shell structures.

F*) MUSTANSIRIA MADRASA

From the structural point of view, this pattern is as well suited as the previous patterns. It presents a hexagonal symmetry leading to an isotropic behaviour, so it can be directly rotated to find the best fitting orientation.

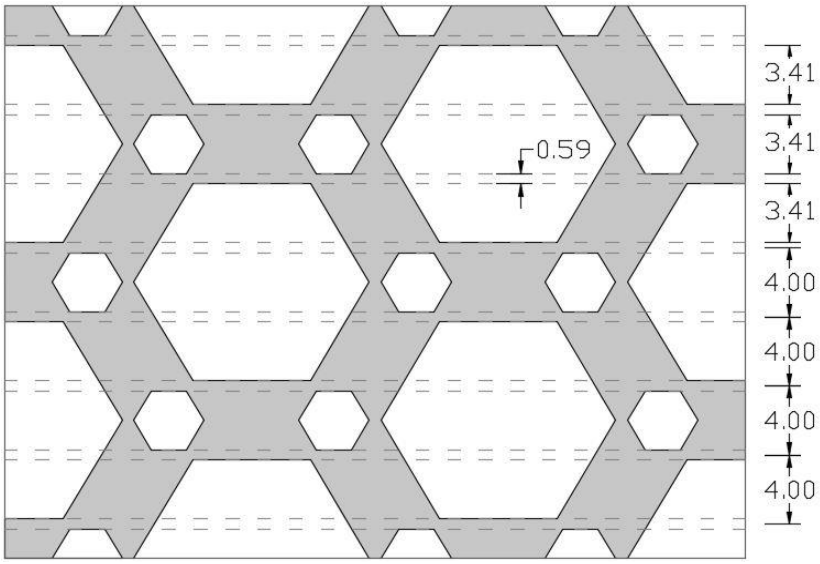

FIG 6.14. Application of pattern F* rotated 30º, to 4m inter-story building. Sat. 40%

The picture displays how the elevation of the building would look like with the pattern rotated 30º and each module spanning four floors.

The values correspond to a saturation of 40% so the original pattern is not blurred and a floor height of 4m that can be considered standard for tall buildings. In this case, a slab depth of 59cm can be embedded in the façade, which is enough for deep floor systems.

The mega-structure can be easily built with traditional construction means, pouring one-story tall concrete walls.

In conclusion, this pattern has a structural performance similar to conventional diagrid systems. It works functionally, it gives a strong aesthetic image and it is easy to build.

E*) PALACE OF THE SHIRVANSHAHS

Palace of the Shirvanshahs pattern (E*) can be seen as a variation of the frames constituting the external tube of the traditional tube-in-tube system. When acting as lateral load bearing system, the frames resist by bending and have a considerable shear deformation. The beams in the tube-in-tube system must be very deep to provide of enough rotation stiffness to the nodes. This pattern excels precisely in this, it takes the material from the less stressed sections (centre of the van) to concentrated in the sections where shear and bending are maximum (near the nodes).

From the structural point of view, this pattern can be considered an improvement of the frame solution for the tube-in-tube system. Its performance is similar to the conventional diagrid with a higher shear deformation that is secondary. The cross-section variation introduces a weak point at the narrowest section that must checked for Ultimate Limit State. These stress concentrations might cause local yielding and second order effects that reduce the overall stiffness and that are not included in this linear elastic analysis. Also, a strut-and-tie model would show that transverse stresses will appear inside the beams as the stress path opens. Finally, the pattern presents a square symmetry leading to a perpendicular isotropic behaviour.

From the constructive point of view, it has horizontal and vertical continuity. Those lines are equidistant, allowing to connect the façade regularly with the front of the floor slabs at each level. The floor height can be the same for the whole building and the vertical equidistant lines can become very handy when designing the lay out in plan to define the rooms. If prefabricated, only one cross module is needed. If the window panes are located in the wall openings, just a star module is needed too.

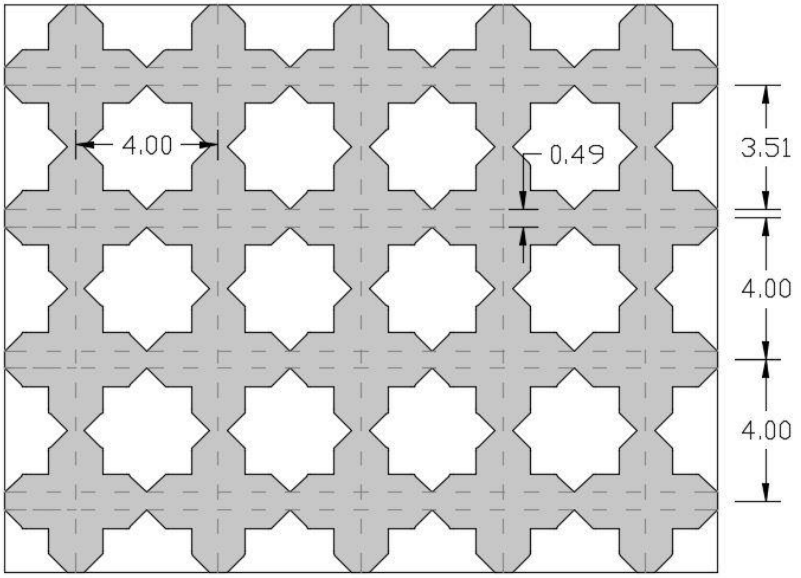

FIG 6.15. Application of pattern E* to 4m inter-story building. Sat. 55%

The picture displays how the elevation of the building would look like, with a horizontal brand that travels around the front of the floor slabs. The floor height is the same at each level.

The values correspond to a saturation of 55% which is representative for this solution and a floor height of 4m that can be considered standard for tall buildings. In this case a slab depth of 49cm can be embedded in the pattern, which is enough for deep floor systems.

It is possible to visually reconstruct a conventional frame inside the pattern.

In conclusion, this pattern meets all the requirements to become a feasible alternative to conventional diagrids in emblematic towers in Muslim countries and it could be considered an improvement of the frame solution for the tube-in-tube system.

I) HASHT BEHESHT

From the structural point of view, this pattern presents a pentagonal symmetry, leading to an orthotropic behaviour. The steps and tables provided in *Chapter 5.1 Directional mechanical properties,* can be directly applied. The orthotropy is very small in this case and the effect is negligible for the modulus of elasticity in the y-direction for relative beam depths over 5%. With a homogenized modulus of elasticity in the y-direction of 16% of the equivalent full wall, this pattern performs 20% worse than the conventional diagrid regarding that mechanical property. Nevertheless, it is still a suitable value to be considered a feasible alternative in justified cases.

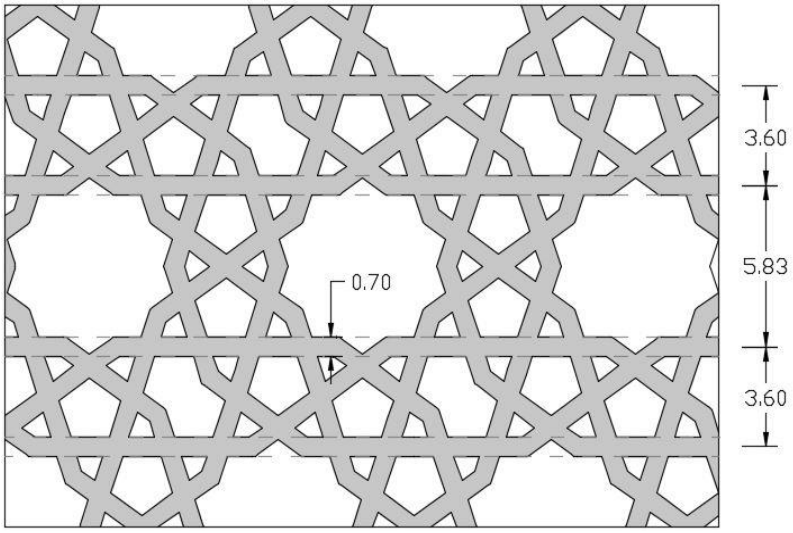

FIG 6.16. Application of pattern I rotated 54º, to 4m inter-story building. Sat. 45%

From the constructive point of view, rotating the pattern 54º provides a continuous horizontal brand that can collect the front of the slab floors. Despite the possibility of constructing it with bars, due to its complexity the structure is likely to be built of prefabricated panels.

The values correspond to a saturation of 45% and a floor height of 3.6m and 5.8m. This alternation in the floor height is precisely the main problem of this pattern. In this case, a slab depth up to 70cm can be embedded in the façade.

In conclusion, this pattern performs well from the structural point of view but its application in tall buildings comes at the expense of having two considerable different floor heights. For this reason, it can only be considered a feasible alternative to conventional diagrids in other applications such as iconic shell structures.

D) LAHORE FORT COMPLEX (EMPTY)

From the structural point of view, it has a square symmetry, entailing an orthogonal isotropic behaviour. For this form, the tables from *Chapter 5.1 Directional mechanical properties* can be directly applied. In order to get horizontal strips that are not even continuous in all the panel length, the pattern has to be rotated 22.5º. That leads to a rotated homogenized modulus of elasticity in the y-direction of 13% due to the corresponding rotation factor of around 0.8. Therefore, it is not worth it to rotate the pattern.

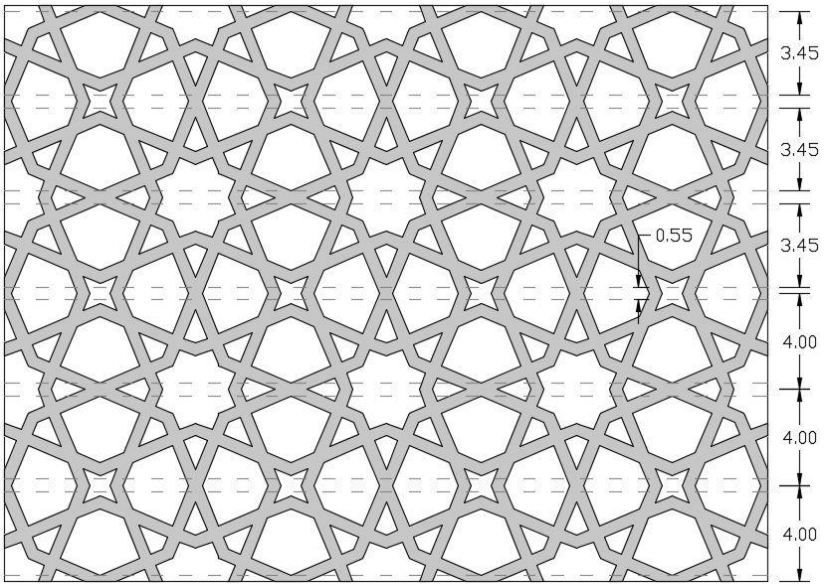

FIG 6.17. Application of pattern D, to 4m inter-story building. Sat. 40%

From the constructive point of view, the pattern is very complex and hard to build. There are no continuous horizontal strands to receive the front of the floor slabs, but on the other hand it is not indispensable.

The attached values correspond to a saturation of 40% and a floor height of 4m, which can be considered a standard height for tall buildings.

The load path is not straight, introducing bending moments in the internal bars. An Ultimate Limit State analysis will be required to check the resistance and non-linear effect of stress concentrations.

In conclusion, this pattern has a good structural performance but on the other hand it is quite complex and involves some construction deficiencies. It can become a suitable alternative for conventional diagrids for other shell structures where the constructive issues can be addressed such as steel shells.

B75*) GREAT MOSQUE OF DAMASCUS (θ =75º VARIATION)

In this research, the Great Mosque of Damascus (B) pattern has been defined as the Hankin method applied to the tessellation 6.6.6 with a contact angle of 60 degrees (θ =60º). This choice is made based on the graphic evidence of the ceramic tilling on its walls as shown in *Chapter 3.3. Selection of historic geometric Islamic patterns*. However, Eric Broug, in his book *Islamic Geometric Pattern*[19.] assigns the Great Mosque of Damascus label to the Hankin method applied to the same tessellation with a contact angle of 75 degrees (θ =75º). That indicates that both patterns are present inside the same building. Both alternatives (θ =60º and θ =75º) perform structurally rather poorly but their mechanical properties improve greatly when their stars are filled. The comparison graph in *Chapter 6.2. Diagrid vs historic patterns performance* is assembled with all the patterns with a 45% saturation. As the smallest possible saturation for pattern B60, is 55% (see *Appendix I. Design Guide*), it is left outside the comparison. Nevertheless, pattern B75, can have a 45% saturation and therefore it is included instead of pattern B60 or B60*.

From the structural point of view, it performs similarly to the conventional diagrid system. It can be seen as a variation of the conventional diagrid system as it can be obtained by applying a varying cross-section to its beams. Despite having the same mechanical properties, the variation of the cross-section entails some structural complications. The cross-section variation introduces a weak point at the narrowest section that must checked for Ultimate Limit State. These stress concentrations might cause local yielding and second order effects that reduce the overall stiffness and that are not included in this linear elastic analysis. Also, a strut-and-tie model would show that transverse stresses will appear inside the beams as the stress path opens. Finally, the pattern presents a hexagonal symmetry leading to an isotropic behaviour so it can be directly rotated at wish.

From the constructive point of view, it is possible to obtain a horizontal continuous line by rotating the pattern 30º. This line is equidistant, allowing to connect the façade regularly with the front of the floor slabs. If prefabricated, only one a six-star module is needed. If the window panes are located in the wall openings, just a module is needed too.

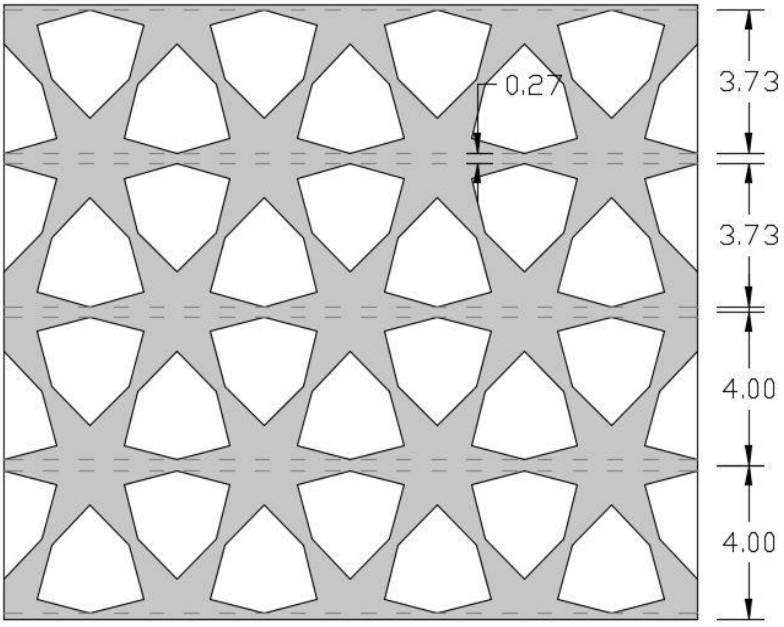

FIG 6.18. Application of pattern B75* rotated 30º, to 4m inter-story building. Sat. 45%

The picture displays how the elevation of the building would look like when the pattern is rotated 30º in order to create a horizontal brand that travels around the front of the floor slabs. The floor height is the same at each level.

The values correspond to a saturation of 45% which is quite low for this solution and a floor height of 4m that can be considered standard for tall buildings. In this case a slab depth of 27cm can be embedded in the pattern.

It is possible to visually reconstruct a conventional diagrid inside the pattern. The engineer might be tempted to go all the way around and build a conventional diagrid and then cover it to simulate this pattern.

In conclusion, this pattern meets all the requirements to become a feasible alternative to conventional diagrids in emblematic towers in Muslim countries.

Due to its good performance and applicability, and bearing in mind that other authors consider pattern B75 as a historic Islamic pattern, it has been included in all steps in *Appendix I. Design guide*.

6.4. ACCURACY ASSESSMENT.

The predesign tool consists in the predesign process described in *Chapter 7.1.1. RQ1 Summary,* and the graphs, pictures and tables gathered in the *Appendix I. Design Guide*. The application of both resources together leads to results in a fast and simple way, useful for the study of alternatives in early stages of the project. The purpose of this chapter is to assess how accurate those results would actually be in the case of tall building,

The homogenized beam mechanical properties were obtained by testing the panels modelled with beam elements in from *Chapter 4.4. FEM Beam elements*. **Ideally, testing a building modelled with beam elements or walls with beam homogenized mechanical properties should provide the same results. That difference in the results is a measure of the error introduced by the method and the assumptions adopted**.

The drift at top floor under wind load will be the parameter of comparison as it is the variable that is latter employed in the stiffness-based design. The variation between the three experiments is the pattern employed. It is specified in each case the relative beam depth, saturation and corresponding homogenized mechanical properties used. The façade and the floor slabs are the only elements modelled so there will be no distortion in the compassion introduced by third elements such as columns or core walls.

The model analysed consist in all cases in a prismatic 50-storeys tower with 30m base length. The patterns chosen are the three best performing patterns from *Chapter 5.2. Wire patterns performance* as they are the ones most likely to be used by the designer and they have square, pentagonal and hexagonal symmetries.

FIG 6.19. Pattern D ETABS models.

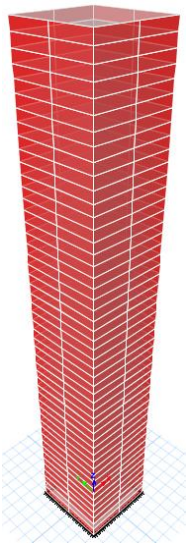

FIG 6.20. Pattern I ETABS models

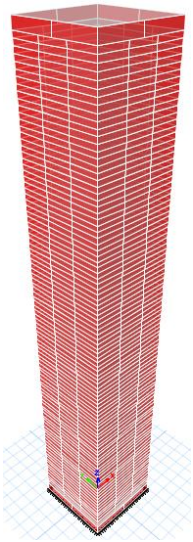

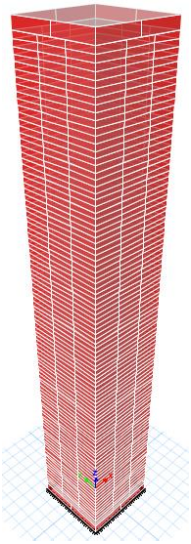

FIG 6.21. Pattern A ETABS models

6.4.1. SQUARE SYMMETRY

D) LAHORE FORT COMPLEX**.** Tessellation 4.8.8. θ =67.5º. Square symmetry.

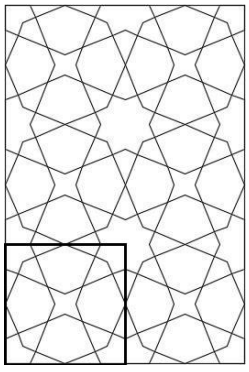

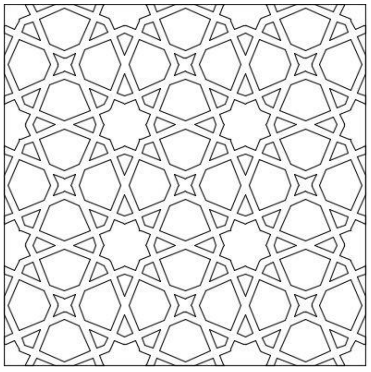

FIG 6.22. Pattern D. Module definition and rbd 6% appearance.

D67.5		HOMOGENIZED MECHANICAL PROPERTIES				
rbd [%]	Sat [%]	$E_{h,x}$	$E_{h,y}$	$\nu_{h,xy}$	$\nu_{h,yx}$	G_h
1	7.23	0.18%	0.18%	0.191	0.191	0.01%
2	14.12	1.10%	1.10%	0.197	0.197	0.08%
3	20.69	2.76%	2.76%	0.207	0.207	0.25%
4	26.93	4.82%	4.82%	0.215	0.215	0.55%
5	32.83	7.05%	7.05%	0.221	0.221	0.96%
6	38.41	9.36%	9.36%	0.224	0.224	1.49%
7	43.66	11.69%	11.69%	0.225	0.225	2.12%
8	48.58	14.04%	14.04%	0.225	0.225	2.82%

TABLE 6.2. Pattern D. Homogenized mechanical properties with beam FE.

D67.5 DIV6	HOMOGENIZED MECHANICAL PROPERTIES				
rbd [%]	$E_{h,x}$	$E_{h,y}$	$\nu_{h,xy}$	$\nu_{h,yx}$	G_h
4	6.24%	6.24%	0.296	0.296	0.94%
5	9.25%	9.26%	0.308	0.308	1.82%
6	12.49%	12.48%	0.315	0.315	3.03%
7	15.89%	15.90%	0.317	0.317	4.59%
8	19.24%	19.24%	0.315	0.315	6.36%

TABLE 6.3. Pattern D. Homog. mech. properties with mesh size depth/6

D67.5 DIV12	HOMOGENIZED MECHANICAL PROPERTIES				
rbd [%]	$E_{h,x}$	$E_{h,y}$	$\nu_{h,xy}$	$\nu_{h,yx}$	G_h
4	5.71%	5.71%	0.287	0.287	0.82%
5	8.68%	8.68%	0.305	0.305	1.59%
6	11.72%	11.72%	0.314	0.314	2.72%
7	14.88%	14.88%	0.316	0.316	4.08%
8	18.26%	18.26%	0.316	0.316	5.73%

TABLE 6.4. Pattern D. Homog. mech. properties with mesh size depth/12

D67.5		HOMOGENIZED MECHANICAL PROPERTIES FROM BEAM ELEMENTS				
rbd [%]	Sat [%]	$E_{h,x}$	$E_{h,y}$	$\nu_{h,xy}$	$\nu_{h,yx}$	G_h
6	38.41	9.36%	9.36%	0.224	0.224	1.49%

TABLE 6.5. Pattern D. Homogenized mechanical properties with beam FE

D67.5		IDEAL HOMOGENIZED MECHANICAL PROPERTIES AFTER MESH REFINEMENT				
rbd [%]	Sat [%]	$E_{h,x}$	$E_{h,y}$	$\nu_{h,xy}$	$\nu_{h,yx}$	G_h
6	38.41	11.72%	11.72%	0.314	0.314	2.72%

TABLE 6.6. Pattern D. Ideal homogenized mechanical properties

BEAM MODEL
Floor height: 3.75m
Number of floors:50
Total height: 187.5m
Base length: 30m
Modules in the base: 8
Module size x-direction: 3.75m
Relative beam depth: 6%
Beam depth: 22.5cm
Beam geometry: 225x250 mm
Base beam material: C70/85
Base density: 25.00 kN/m^3
E_b: 41 000 MPa
ν_b: 0.2
G_b: 17 080 MPa
Drift top Ux: 836mm

MEMBRANE WITH BEAM PROP.
Floor height: 3.75m
Number of floors:50
Total height: 187.5m
Base length: 30m
Relative beam depth: 6%
Saturation: 38.41%
Homog. density: 9.60 kN/m^3
Pattern rotation: 0º
$E_{h,y}$: 9.36% (3 838 MPa)
$E_{h,x}$: 9.36% (3 838 MPa)
$\nu_{h,yx}$: 0.224
$\nu_{h,xy}$: 0.224
G_h: 611 MPa
Thickness: 250mm
Drift top Ux: 897mm

MEMBRANE WITH IDEAL PROP.
Floor height: 3.75m
Number of floors:50
Total height: 187.5m
Base length: 30m
Relative beam depth: 6%
Saturation: 38.41%
Homog. density: 9.60 kN/m^3
Pattern rotation: 0º
$E_{h,y}$: 11.72% (4 805 MPa)
$E_{h,x}$: 11.72% (4 805 MPa)
$\nu_{h,yx}$: 0.314
$\nu_{h,xy}$: 0.314
G_h: 1 115 MPa
Thickness: 250mm
Drift top Ux: 647mm

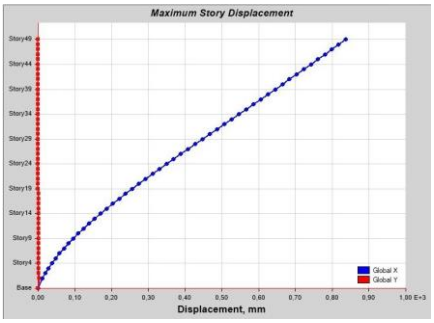

FIG 6.23. Displacement, beam model

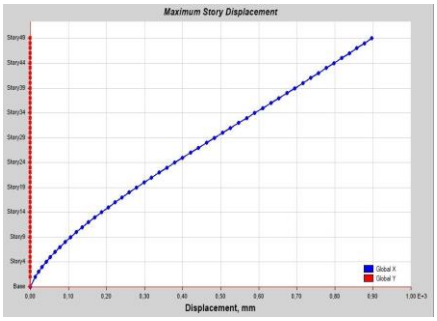

FIG 6.24. Drift, walls with beam mech prop

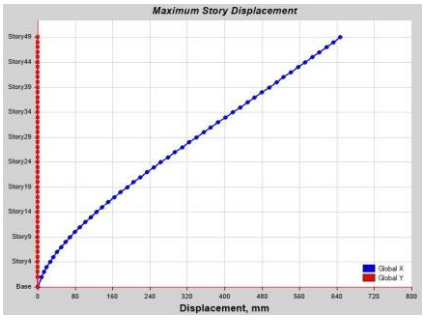

FIG 6.25 Drift, walls with ideal mech prop

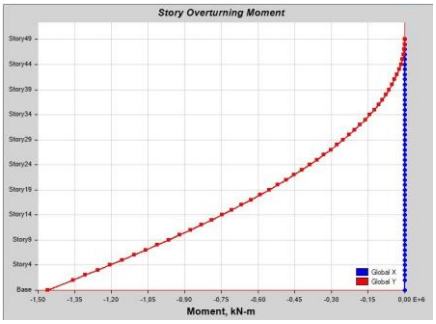

FIG 6.26. Overturning moment, beam model

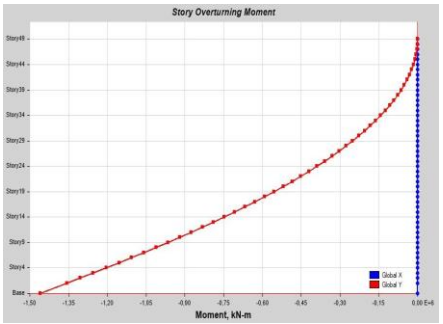

FIG 6.27. Moment, walls with beam mech prop

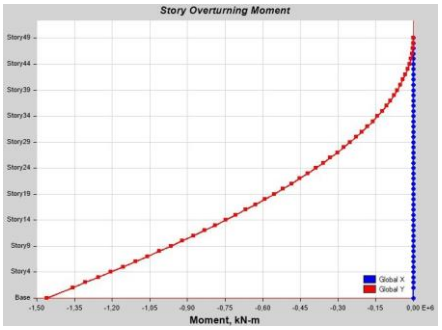

FIG 6.28. Moment, walls with ideal mech prop

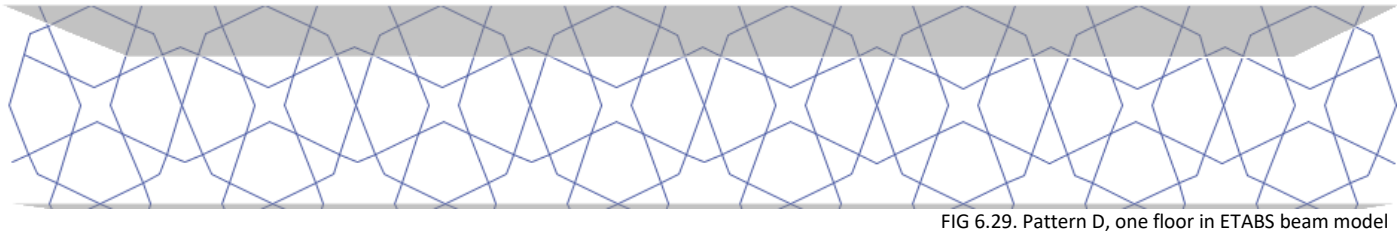

FIG 6.29. Pattern D, one floor in ETABS beam model

6.4.2. PENTAGONAL SYMMETRY

I) HASHT BEHESHT. Tessellation I-6.10.10., θ =54º. Pentagonal symmetry.

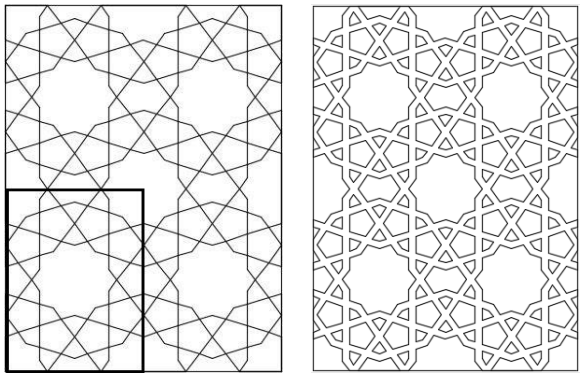

FIG 6.30. Pattern I. Module definition and rbd 5% appearance.

I54		HOMOGENIZED MECHANICAL PROPERTIES				
rbd [%]	Sat [%]	$E_{h,x}$	$E_{h,y}$	$\nu_{h,xy}$	$\nu_{h,yx}$	G_h
1	8.89	0.34%	0.40%	0.263	0.312	0.14%
2	17.23	1.89%	2.14%	0.279	0.317	0.78%
3	25.03	4.27%	4.68%	0.290	0.317	1.75%
4	32.27	6.98%	7.46%	0.295	0.315	2.85%
5	38.96	9.80%	10.29%	0.296	0.311	3.98%
6	45.10	12.66%	13.13%	0.295	0.306	5.13%
7	50.69	15.55%	15.97%	0.293	0.301	6.29%
8	55.74	18.45%	18.82%	0.290	0.296	7.48%

TABLE 6.7. Pattern I. Homogenized mechanical properties with beam FE.

I54 DIV6	HOMOGENIZED MECHANICAL PROPERTIES				
rbd [%]	$E_{h,x}$	$E_{h,y}$	$\nu_{h,xy}$	$\nu_{h,yx}$	G_h
3	5.41%	5.84%	0.303	0.327	2.14%
4	9.00%	9.42%	0.310	0.325	3.50%
5	12.80%	13.12%	0.315	0.323	4.93%
6	16.71%	16.92%	0.316	0.320	6.40%
7	20.74%	20.81%	0.316	0.317	7.94%

TABLE 6.8. Pattern I. Homog. mech. properties with mesh size depth/6

I54 DIV12	HOMOGENIZED MECHANICAL PROPERTIES				
rbd [%]	$E_{h,x}$	$E_{h,y}$	$\nu_{h,xy}$	$\nu_{h,yx}$	G_h
3	5.20%	5.63%	0.302	0.326	2.06%
4	8.70%	9.13%	0.311	0.326	3.39%
5	12.40%	12.78%	0.315	0.325	4.79%
6	16.22%	16.48%	0.317	0.322	6.22%
7	20.14%	20.30%	0.317	0.319	7.72%

TABLE 6.9. Pattern I. Homog. mech. properties with mesh size depth/12

I54		HOMOGENIZED MECHANICAL PROPERTIES FROM BEAM ELEMENTS				
rbd [%]	Sat [%]	$E_{h,x}$	$E_{h,y}$	$\nu_{h,xy}$	$\nu_{h,yx}$	G_h
5	38.96	9.80%	10.29%	0.296	0.311	3.98%

TABLE 6.10. Pattern I. Homogenized mechanical properties with beam FE

I54		IDEAL HOMOGENIZED MECHANICAL PROPERTIES AFTER MESH REFINEMENT				
rbd [%]	Sat [%]	$E_{h,x}$	$E_{h,y}$	$\nu_{h,xy}$	$\nu_{h,yx}$	G_h
5	38.96	11.99%	12.45%	0.314	0.326	4.65%

TABLE 6.11. Pattern I. Ideal homogenized mechanical properties

BEAM MODEL
Floor height: 3.63m
Number of floors:50
Total height: 181.6m
Base length: 30m
Modules in the base: 6
Module size x-direction: 5.00m
Relative beam depth: 5%
Beam depth: 18.16cm (90º)
Beam geometry: 182x250 mm
Base beam material: C70/85
Base density: 25.00 kN/m^3
E_b: 41 000 MPa
ν_b: 0.2
G_b: 17 080 MPa
Drift top Ux: 600mm

MEMBRANE WITH BEAM PROP.
Floor height: 3.63m
Number of floors:50
Total height: 181.6m
Base length: 30m
Relative beam depth: 5%
Saturation: 38.96%
Homog. density: 9.74 kN/m^3
Pattern rotation: 90º
$E_{h,y}'$: 9.80% (4 018 MPa)
$E_{h,x}'$: 10.29% (4 219 MPa)
$\nu_{h,yx}'$: 0.311
$\nu_{h,xy}'$: 0.296
G_h: 1 631 MPa
Thickness: 250mm
Drift top Ux: 703mm

MEMBRANE WITH IDEAL PROP.
Floor height: 3.63m
Number of floors:50
Total height: 181.6m
Base length: 30m
Relative beam depth: 5%
Saturation: 38.96%
Homog. density: 9.74 kN/m^3
Pattern rotation: 90º
$E_{h,y}'$: 11.99% (4 915 MPa)
$E_{h,x}'$: 12.45% (5 104 MPa)
$\nu_{h,yx}'$: 0.314
$\nu_{h,xy}'$: 0.326
G_h: 1 907 MPa
Thickness: 250mm
Drift top Ux: 575mm

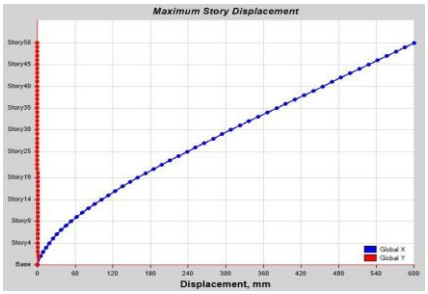

FIG 6.31. Displacement, beam model

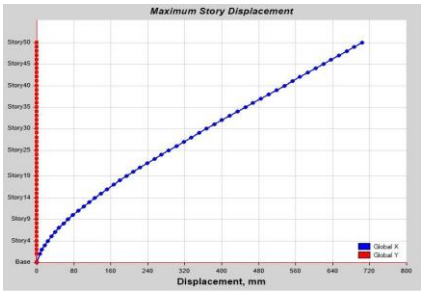

FIG 6.32. Drift, walls with beam mech prop

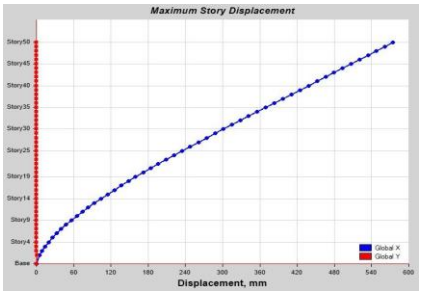

FIG 6.33. Drift, walls with ideal mech prop

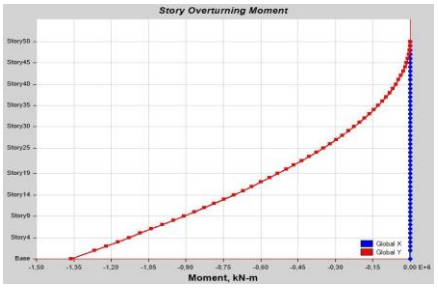

FIG 6.34. Overturning moment, beam model

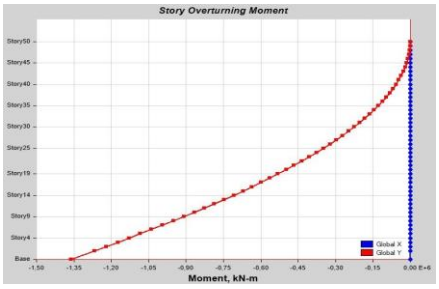

FIG 6.35. Moment, walls with beam mech prop

FIG 6.36. Moment, walls with ideal mech prop

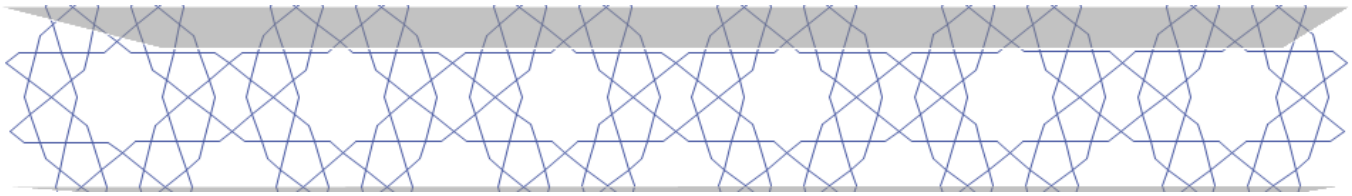
FIG 6.37. Pattern I, one floor in ETABS beam model

6.4.3. HEXAGONAL SYMMETRY

A) YESLI MOSQUE**.** Tessellation 3.6.3.6. Hexagonal symmetry.

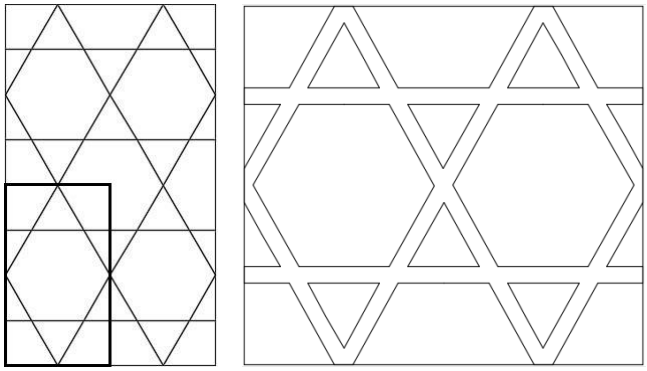
FIG 6.38. Pattern A. Module definition and rbd 8% appearance.

A0		HOMOGENIZED MECHANICAL PROPERTIES				
rbd [%]	Sat [%]	$E_{h,x}$	$E_{h,y}$	$\nu_{h,xy}$	$\nu_{h,yx}$	G_h
2	6.77	2.31%	2.31%	0.333	0.333	0.87%
4	13.24	4.63%	4.63%	0.332	0.332	1.74%
6	19.34	6.96%	6.96%	0.330	0.330	2.62%
8	25.15	9.31%	9.31%	0.328	0.328	3.51%
10	30.66	11.69%	11.69%	0.325	0.325	4.41%
12	35.82	14.10%	14.10%	0.322	0.322	5.33%
14	40.67	16.54%	16.54%	0.318	0.318	6.28%
16	45.20	19.02%	19.02%	0.314	0.314	7.24%

TABLE 6.12. Pattern A. Homogenized mechanical properties with beam FE.

A DIV6	HOMOGENIZED MECHANICAL PROPERTIES				
rbd [%]	$E_{h,x}$	$E_{h,y}$	$\nu_{h,xy}$	$\nu_{h,yx}$	G_h
4	4.73%	4.72%	0.329	0.329	1.78%
6	7.16%	7.16%	0.326	0.326	2.71%
8	9.67%	9.66%	0.322	0.322	3.67%
10	12.24%	12.24%	0.318	0.318	4.67%
12	14.94%	14.91%	0.313	0.313	5.72%

TABLE 6.13. Pattern A. Homog. mech. properties with mesh size depth/6

A DIV12	HOMOGENIZED MECHANICAL PROPERTIES				
rbd [%]	$E_{h,x}$	$E_{h,y}$	$\nu_{h,xy}$	$\nu_{h,yx}$	G_h
4	4.71%	4.71%	0.329	0.329	1.77%
6	7.13%	7.13%	0.326	0.326	2.69%
8	9.62%	9.61%	0.322	0.322	3.65%
10	12.15%	12.16%	0.318	0.318	4.62%
12	14.76%	14.76%	0.314	0.314	5.63%

TABLE 6.14. Pattern A. Homog. mech. properties with mesh size depth/12

A0		HOMOGENIZED MECHANICAL PROPERTIES FROM BEAM ELEMENTS				
rbd [%]	Sat [%]	$E_{h,x}$	$E_{h,y}$	$\nu_{h,xy}$	$\nu_{h,yx}$	G_h
8	25.15	9.31%	9.31%	0.328	0.328	3.51%

TABLE 6.15. Pattern A. Homogenized mechanical properties with beam FE

A0		IDEAL HOMOGENIZED MECHANICAL PROPERTIES AFTER MESH REFINEMENT				
rbd [%]	Sat [%]	$E_{h,x}$	$E_{h,y}$	$\nu_{h,xy}$	$\nu_{h,yx}$	G_h
8	25.15	9.56%	9.56%	0.323	0.323	3.62%

TABLE 6.16. Pattern A. Ideal homogenized mechanical properties

BEAM MODEL
Floor height: 3.71m
Number of floors:50
Total height: 185.6m
Base length: 30m
Modules in the base: 14
Module size x-direction: 2.14m
Relative beam depth: 8%
Beam depth: 17.1cm
Beam geometry: 171x250 mm
Base beam material: C70/85
Base density: 25.00 kN/m^3
E_b: 41 000 MPa
ν_b: 0.2
G_b: 17 080 MPa
Drift top Ux: 804mm

MEMBRANE WITH BEAM PROP
Floor height: 3.71m
Number of floors:50
Total height: 185.6m
Base length: 30m
Relative beam depth: 8%
Saturation: 25.15%
Homog. density: 6.29 kN/m^3
Pattern rotation: 0º
$E_{h,y}$: 9.31% (3 817 MPa)
$E_{h,x}$: 9.31% (3 817 MPa)
$\nu_{h,yx}$: 0.328
$\nu_{h,xy}$: 0.328
G_h: 1 439 MPa
Thickness: 250mm
Drift top Ux: 800mm

MEMBRANE WITH IDEAL PROP
Floor height: 3.71m
Number of floors:50
Total height: 185.6m
Base length: 30m
Relative beam depth: 8%
Saturation: 25.15%
Homog. density: 6.29 kN/m^3
Pattern rotation: 0º
$E_{h,y}$: 9.56% (3 919 MPa)
$E_{h,x}$: 9.56% (3 919 MPa)
$\nu_{h,yx}$: 0.323
$\nu_{h,xy}$: 0.323
G_h: 1 484MPa
Thickness: 250mm
Drift top Ux: 782mm

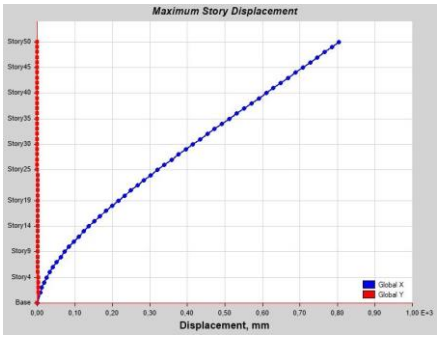

FIG 6.39. Displacement, beam model

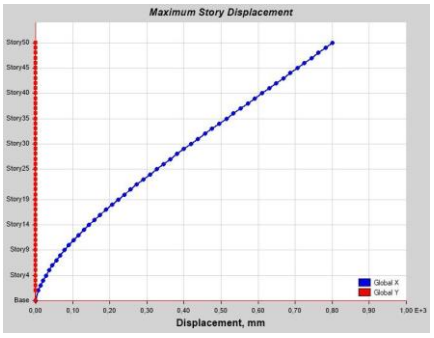

FIG 6.40. Drift, walls with beam mech prop

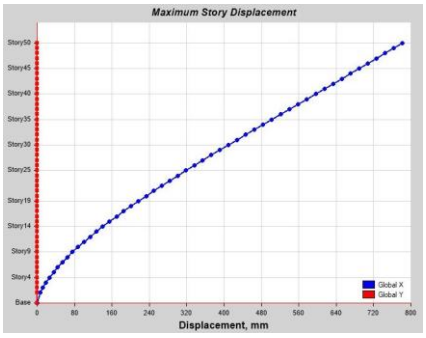

FIG 6.41. Drift, walls with ideal mech prop

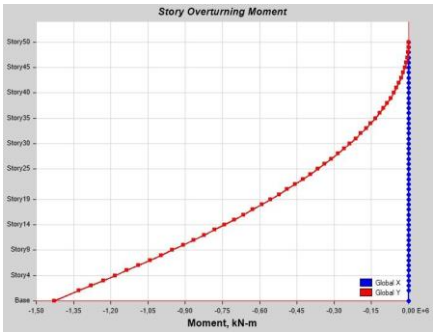

FIG 6.42. Overturning moment, beam model

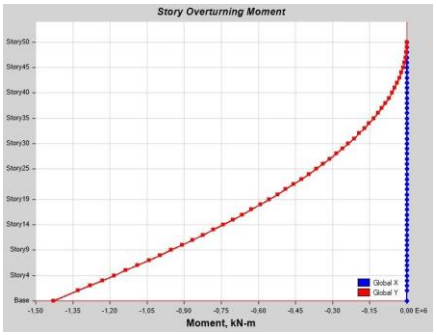

FIG 6.43. Moment, walls with beam mech prop

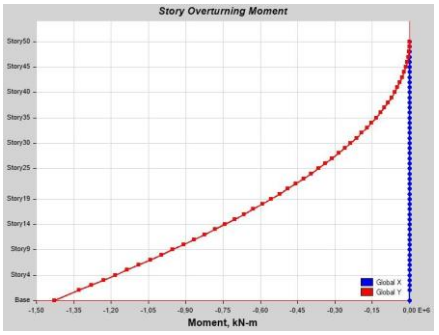

FIG 6.44. Moment, walls with ideal mech prop

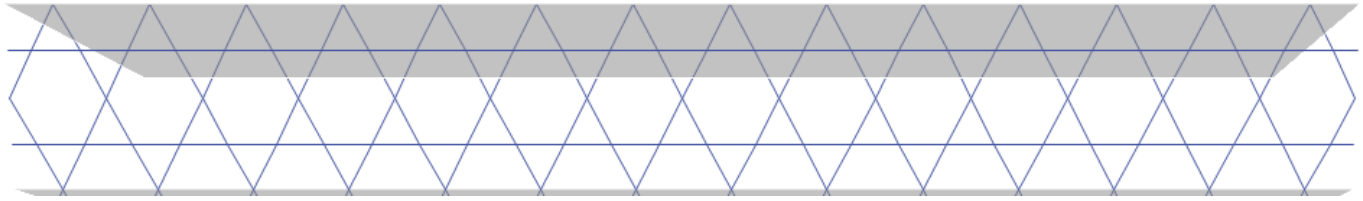
FIG 6.45. Pattern A, ETABS beam model

6.5. SPECIAL CASES IN TALL BUILDINGS

In practice, the application of the developed predesign tool to real life projects leads to more complex situations than the studied prismatic case. **The accuracy of the method has already been assessed in the previous chapter, the aim of this chapter is just to identify possible sources of deviations in the results that the engineer will face when applying the method to tall buildings**. Some of the most important effects are addressed in this chapter in increasing complexity, for the same patterns and saturations as in *Chapter 6.4. Accuracy assessment:*

- Squeezing: The number of modules in each floor are kept constant to provide continuity regardless of any variation of the floor size. A smaller perimeter with the same number of modules would lead to smaller panels. However, as the floor height is kept constant, it finally leads to a "squeezing" of the pattern. This has an important effect on the saturation and its relationship with module size in the x-direction.
- Distortion: Patterns get distorted if a rotation is introduced into the building geometry. The panels in their undeformed shape are no longer square but rhomboid.
- Intermediate supports: As the pattern grows bigger, each module will occupy more than floor at the same time. It changes the boundary conditions for which the pattern was tested, introducing intermediate support that constrain the pattern horizontal deformation at intermediate points.

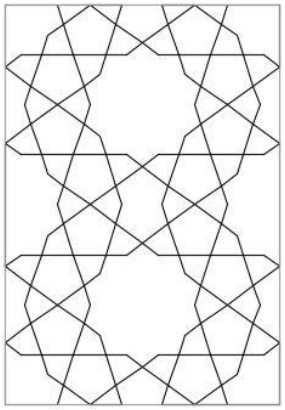
FIG 6.46. Homogenized pattern

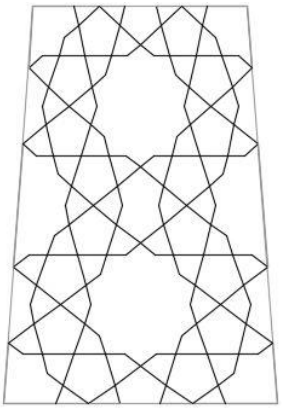
FIG 6.47. Squeezing effect

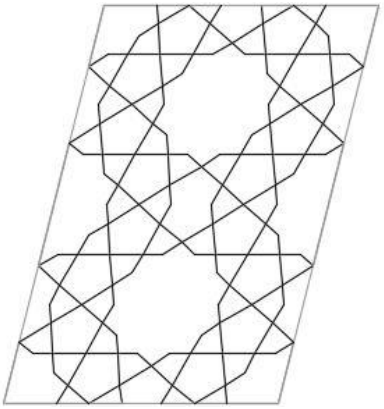
FIG 6.48. Distortion effect

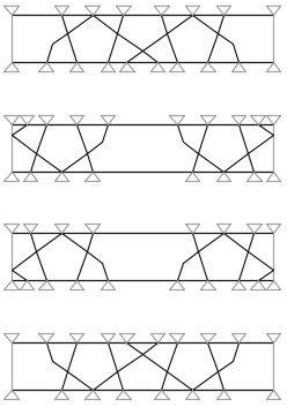
FIG 6.49. Intermediate supports

The aim of this chapter is not to provide a quantitative estimation of the deviation of the results introduced by the above mentioned effects. In fact, in some cases not even a qualitative estimation would apply. The deviation of the performance depends ultimately on the magnitude of the squeezing and distortion applied and its location on the building, the number of intermediate supports modelled, and ultimately the pattern under consideration itself. **A qualitative estimation would require to test all patterns for those effects, and a quantitative estimation to test each one of them for different levels of squeezing, distortion and number of intermediate supports**. Therefore, the aim of this chapter is just to highlight the existence of these effects to make the designer aware of the limitations of the developed method to tall buildings.

Each of the following examples will have an increasing geometry complexity and a different pattern applied. Those patterns are the same as in the previous chapter and will have the same saturation to serve as comparison. All the beams are square so the wall thickness will be adapted to correspond to it.

6.5.1. SQUEEZING

PATTERN A) YESLI MOSQUE:

Number of floors:	50	Floor height:	4.00 m	Total height:	195.9 m
Rel. beam depth:	8.00 %	Saturation:	25.15 %	Homog. Density:	6.29 kN/m^3
Pattern rotation:	0º	Floor rotation:	0º	Rotated rbd:	-
Base material:	C70/85	E_b:	41 000 MPa	G_b:	17 080 MPa

Floor	01	03	05	07	09	11	13	15	17	19	21	23	25
Perimeter (m)	110.8	110.8	110.8	110.8	110.8	110.7	110.6	110.4	110.1	109.8	109.3	108.7	108.0
Module x-dir (m)	2.31	2.31	2.31	2.31	2.31	2.31	2.30	2.30	2.29	2.29	2.28	2.26	2.25
Depth (mm)	185	185	185	185	185	185	184	184	184	183	182	181	180

TABLE 6.17. Wall width, beam width and depth definition for the ETABS beam model. Levels 00 to

Floor	27	29	31	33	35	37	39	41	43	45	47	48	49
Perimeter (m)	107.2	106.2	104.9	103.4	101.5	99.2	96.3	92.6	87.6	80.5	69.0	59.4	44.8
Module x-dir (m)	2.23	2.21	2.19	2.15	2.11	2.07	2.01	1.93	1.83	1.68	1.44	1.24	0.93
Depth (mm)	179	177	175	172	169	165	161	154	146	134	115	99	75

TABLE 6.18. Wall width, beam width and depth definition for the ETABS beam model. Levels 20 to 38

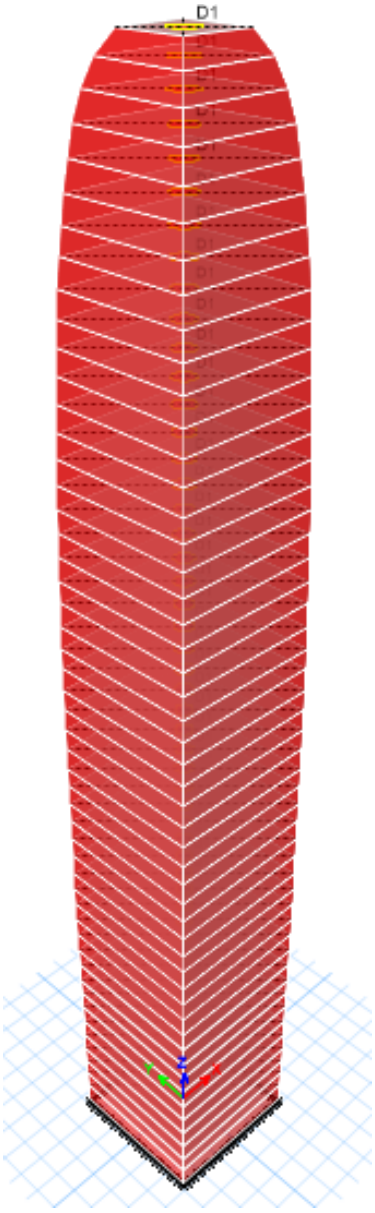

BEAM MODEL

Patter rotation: 0º
Rotated rbd: 8.00 %
Number of modules: 12
Module x-direction: 2.31 m to 0.93 m
Relative beam depth: 8.00%
Beam depth: 75 mm to 185 mm
Beam geometry: depth x 300 mm
Drift top Ux: 826 mm

MEMBRANE WITH BEAM PROPERTIES

Pattern rotation: 0º
Relative beam depth: 8.00 %
$E_{h,y}$: 9.31 % (3 817 MPa)
$E_{h,x}$: 9.31 % (3 817 MPa)
$\nu_{h,yx}$: 0.328
$\nu_{h,xy}$: 0.328
G_h: 3.51 % (1 439 MPa)
Thickness: 300 mm
Drift top Ux: 746 mm

MEMBRANE WITH IDEAL MECH. PROPERTIES

Pattern rotation: 0º
Relative beam depth: 8.00 %
$E_{h,y}$: 9.56 % (3 920 MPa)
$E_{h,x}$: 9.56 % (3 920 MPa)
$\nu_{h,yx}$: 0.323
$\nu_{h,xy}$: 0.323
G_h: 3.62 % (1 484 MPa)
Thickness: 300 mm
Drift top Ux: 728 mm

FIG 6.50. ETABS model with beam elements
FIG 6.51. ETABS model with membrane elements

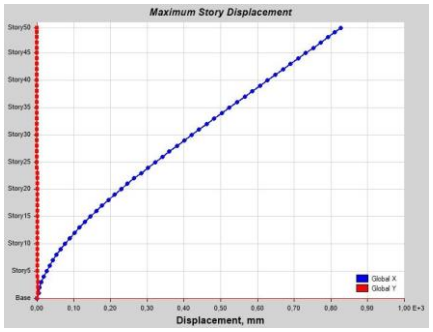

FIG 6.52. Displacement, beam model

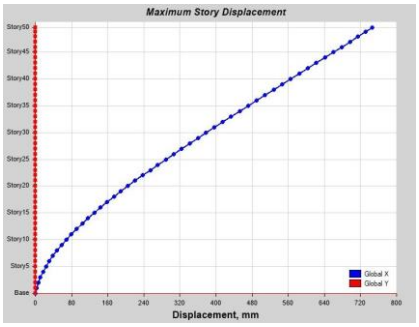

FIG 6.53. Drift, walls with beam mech prop

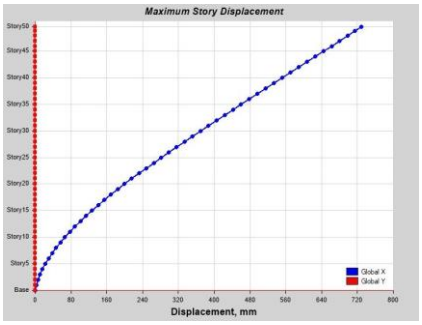

FIG 6.54. Drift, walls with ideal mech prop

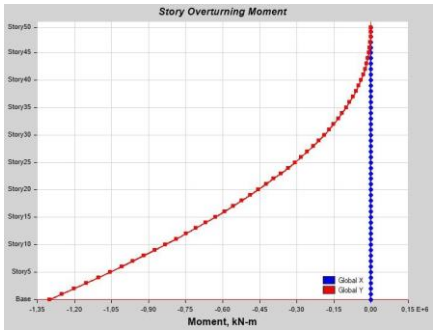

FIG 6.55. Overturning moment, beam model

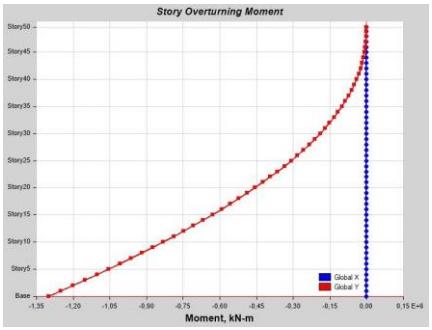

FIG 6.56. Moment, walls with beam mech prop

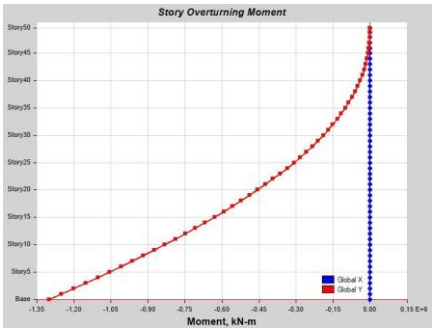

FIG 6.57. Moment, walls with ideal mech prop

6.5.2. SQUEEZING + DISTORSION

PATTERN D) LAHORE FORT COMPLEX.

Number of floors:	50	Floor height:	4.00 m	Total height:	200.0 m
Rel. beam depth:	6.00 %	Saturation:	38.41 %	Homog. Density:	19.36 kN/m^3
Pattern rotation:	0º	Floor rotation:	2.0º per floor	Rotated rbd:	6.00 %
Base material:	S355	E_b:	210 000 MPa	G_b:	80 769 MPa

BEAM MODEL

Patter rotation: 0º
Rotated rbd: 6.00 %
Number of modules: 31
Module x-direction: 3.17m to 4.73m
Relative beam depth: 6.00%
Beam depth: 190 mm to 284 mm
Beam geometry: Square
Drift top Ux: 985 mm

MEMBRANE WITH BEAM PROPERTIES

Pattern rotation: 0º
Relative beam depth: 6.00 %
$E_{h,y}$: 9.36 % (3 838 MPa)
$E_{h,x}$: 9.36 % (3 838 MPa)
$\nu_{h,yx}$: 0.224
$\nu_{h,xy}$: 0.224
G_h: 1.49 % (611 MPa)
Thickness: 190 mm to 284 mm
Drift top Ux: 836 mm

MEMBRANE WITH IDEAL MECH. PROPERTIES

Pattern rotation: 0º
Relative beam depth: 6.00 %
$E_{h,y}$: 11.72 % (4 805 MPa)
$E_{h,x}$: 11.72 % (4 805 MPa)
$\nu_{h,yx}$: 0.314
$\nu_{h,xy}$: 0.314
G_h: 2.72 % (1 115 MPa)
Thickness: 190 mm to 284 mm
Drift top Ux: 601 mm

FIG 6.58. ETABS model with beam elements
FIG 6.59. ETABS model with membrane elements

Floor	00	02	04	06	08	10	12	14	16	18	20	22	24
Perimeter (m)	146.7	144.9	143.0	141.1	139.2	137.3	135.3	133.3	131.3	129.3	127.3	125.3	123.3
Module x-dir (m)	4.73	4.67	4.61	4.55	4.49	4.43	4.36	4.30	4.24	4.17	4.11	4.04	3.98
Width (mm)	284	280	277	273	269	266	262	258	254	250	246	243	239

TABLE 6.19. Wall width, beam width and depth definition for the ETABS beam model. Levels 00 to 18

Floor	26	28	30	32	34	36	38	40	42	44	46	48	50
Perimeter (m)	121.3	119.3	117.3	115.3	113.3	111.4	109.4	107.5	105.6	103.8	102.0	100.2	98.4
Module x-dir (m)	3.91	3.85	3.78	3.72	3.65	3.59	3.53	3.47	3.41	3.35	3.29	3.23	3.17
Width (mm)	235	231	227	223	219	216	212	208	204	201	197	194	190

TABLE 6.20. Wall width, beam width and depth definition for the ETABS beam model. Levels 20 to 38

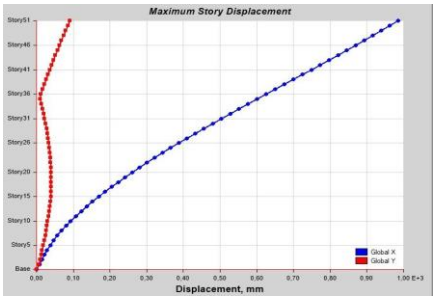

FIG 6.60. Displacement, beam model

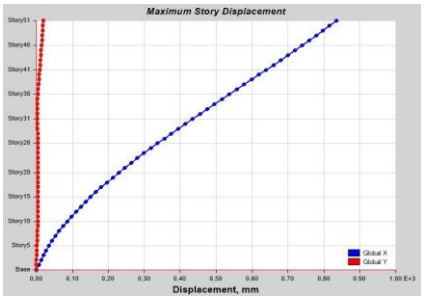

FIG 6.61. Drift, walls with beam mech prop

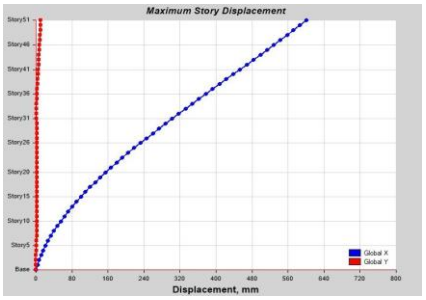

FIG 6.62. Drift, walls with ideal mech prop

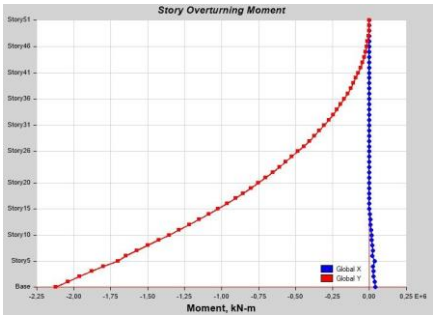

FIG 6.63. Overturning moment, beam model

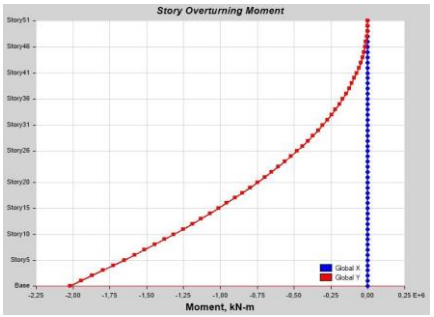

FIG 6.64. Moment, walls with beam mech prop

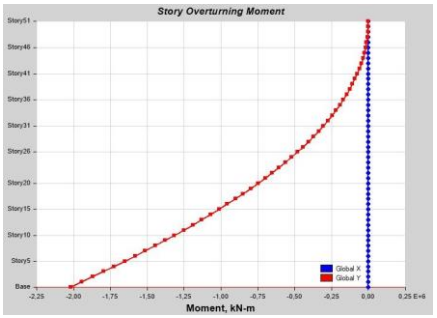

FIG 6.65. Moment, walls with ideal mech prop

6.5.3. SQUEEZING + DISTORTION + INTERMEDIATE SUPPORTS

PATTERN I) HASHT BEHESHT

Number of floors:	60	Floor height:	3.91 m	Total height:	236.0 m
Rel. beam depth	5 %	Saturation:	38.96 %	Homog. Density:	9.74 kN/m^3
Pattern rotation:	18º	Floor rotation:	0.5º per floor	Rotated rbd:	4.76 %
Base material:	C70/85	E_b:	41 000 MPa	G_b:	17 080 MPa

Floor	00	02	04	06	08	10	12	14	16	18
Perimeter (m)	146.5	141.4	136.3	131.1	126.5	122.1	120.0	114.3	111.0	108.6
Module x-dir (m)	13.32	12.85	12.39	11.94	11.50	11.10	10.91	10.39	10.09	9.87
Width (mm)	633	611	589	568	547	528	519	494	480	469

TABLE 6.21. Wall width, beam width and depth definition for the ETABS beam model. Levels 00 to 18

Floor	20	22	24	26	28	30	32	34	36	38
Perimeter (m)	106.2	104.7	103.9	103.6	104.1	105.2	106.9	109.2	112.0	115.4
Module x-dir (m)	9.66	9.52	9.44	9.42	9.46	9.56	9.71	9.92	10.19	10.49
Width (mm)	459	453	449	448	450	455	462	472	484	499

TABLE 6.22. Wall width, beam width and depth definition for the ETABS beam model. Levels 20 to 38

Floor	40	42	44	46	48	50	52	54	56	58
Perimeter (m)	119.3	123.5	128.1	132.9	137.9	143.0	148.2	153.3	158.0	163.1
Module x-dir (m)	10.84	11.23	11.64	12.08	12.54	13.00	13.47	13.94	14.37	14.83
Width (mm)	516	534	554	575	596	618	641	663	683	705

TABLE 6.23. Wall width, beam width and depth definition for the ETABS beam model. Levels 40 to 58

The beam sizes are modified every two floors. There are 11 modules in each floor. The 5% relative beam depth is substituted by 4.76% because of the 18ª rotation according to formula (5.1) $\boldsymbol{L'_x = L_x\, cos(\alpha)}$

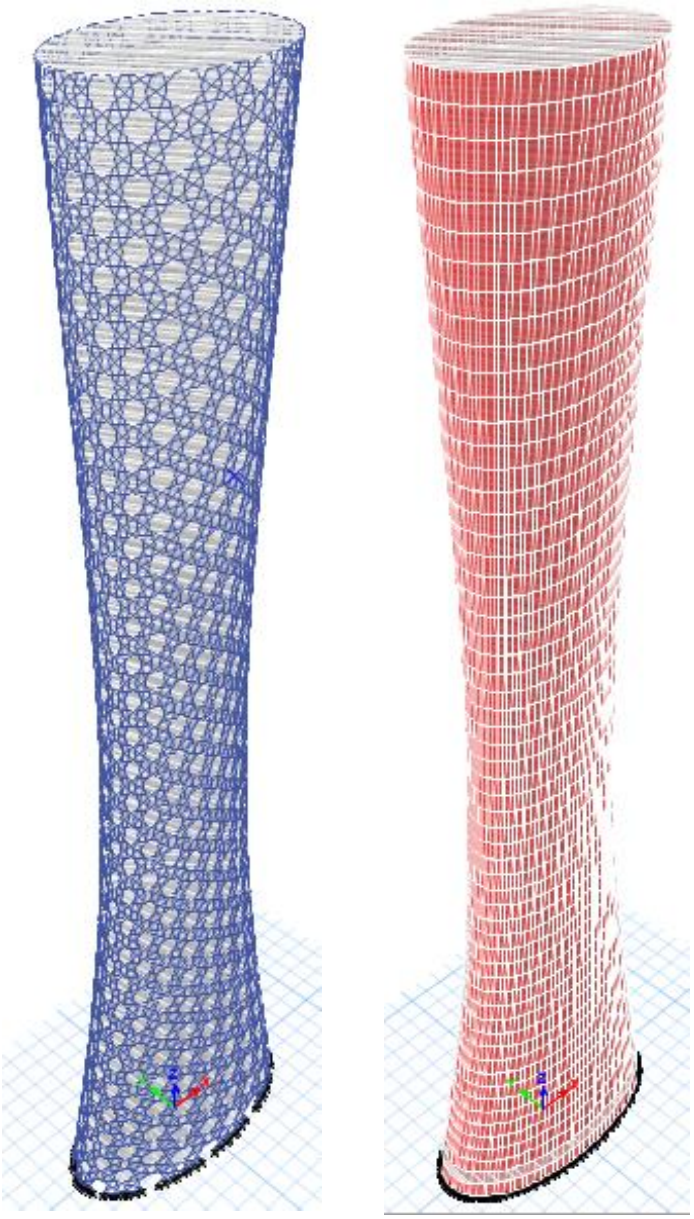

BEAM MODEL

Patter rotation: 18º
Rotated rbd: 4.76 %
Number of modules: 11
Module x-direction: 9.42m to 15.04m
Relative beam depth: 4.76% (5% for rotation 18º)
Beam depth: 448 mm to 715 mm
Beam geometry: Square
Drift top Ux: 307 mm

MEMBRANE WITH BEAM PROPERTIES

Pattern rotation: 18º
Relative beam depth: 5.00 %
$E_{h,y}{}'$: 10.29 % (4 219 MPa)
$E_{h,x}{}'$: 9.80 % (4 018 MPa)
$\nu_{h,yx}{}'$: 0.302
$\nu_{h,xy}{}'$: 0.293
$G_h{}'$: 3.98 % (1 615 MPa)
Thickness: 448 mm to 715 mm
Drift top Ux: 586 mm

MEMBRANE WITH IDEAL MECH. PROPERTIES

Pattern rotation: 18º
Relative beam depth: 5.00 %
$E_{h,y}{}'$: 12.45 % (5 105 MPa)
$E_{h,x}{}'$: 11.99 % (4 916 MPa)
$\nu_{h,yx}{}'$: 0.316
$\nu_{h,xy}{}'$: 0.291
$G_h{}'$: 4.65 % (9 765 MPa)
Thickness: 448 mm to 715 mm
Drift top Ux: 485 mm

FIG 6.66. ETABS model with beam elements
FIG 6.67. ETABS model with membrane elements

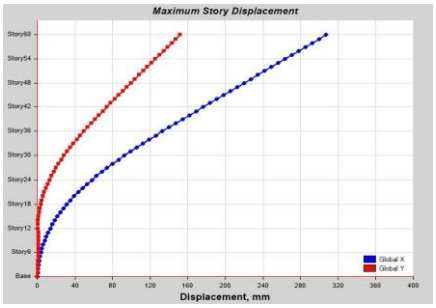

FIG 6.68. Displacement, beam model

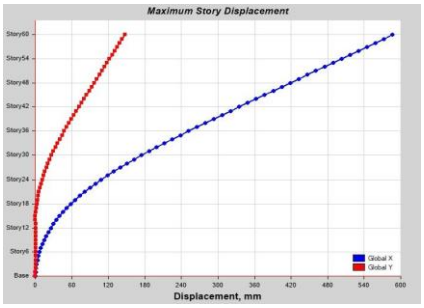

FIG 6.69. Drift, walls with beam mech prop

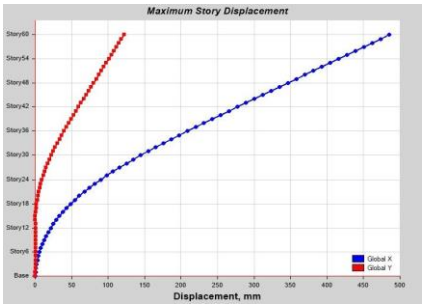

FIG6.70. Drift, walls with ideal mech prop

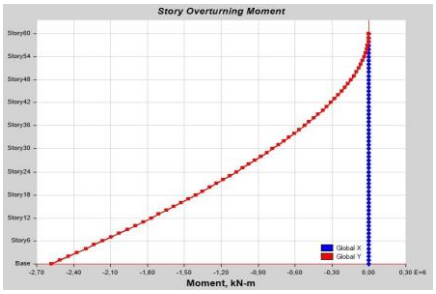

FIG 6.71. Overturning moment, beam model

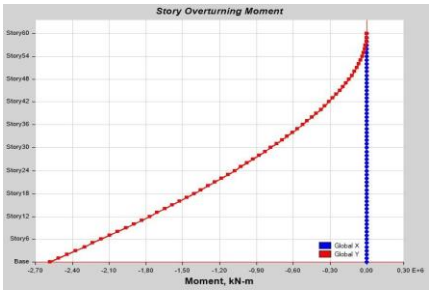

FIG 6.72. Moment, walls with beam mech prop

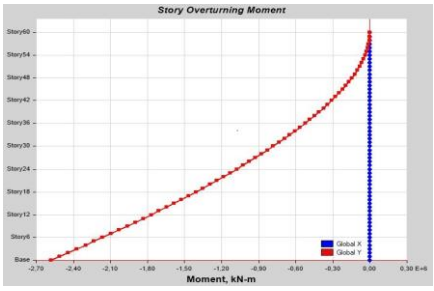

FIG 6.73. Moment, walls with ideal mech prop

7. CONCLUSIONS

7.1. RESEARCH QUESTION 1. METHOD LEVEL

Can a simple tool be developed for the predesign of geometric Islamic patterns as a non-conventional diagrid system?

- Method chosen and methodology for its adoption
- Development of a pre-design tool.
- Assessment of the developed tool

7.1.1. RQ1. SUMMARY

The proposed predesign tool is **based on the homogenization method** at the pattern scale and the **stiffness-based design** at the building scale. In other words, the tall building is considered as a long cantilever whose SLS drift limitations govern over the ULS resistance limitations. The tube-in-tube distribution is adopted with the geometric Islamic pattern applied to the outer tube that works as a thin-wall hollow section braced against out-of-plane loading at each level by the floor slabs. The main objective is to obtain a continuous heterogeneous orthotropic material that simulates the behaviour that the geometric Islamic pattern would have when loaded in its plane. This method enables the performance assessment of different patterns by creating a common ground of comparison with their homogenized mechanical properties.

METHODOLOGY

Through the homogenization process the geometric Islamic patterns are transformed into an equivalent meta-material whose mechanical properties will vary depending on the pattern under study, the base material and its relative beam depth. The methodology is organized in four steps:

1. Representative Element Volume. It takes into account the number of modules that make the panel
2. Mesh refinement. It takes into account the mesh size employed with the membrane elements.
3. Membrane correction factor. It links the results with beam FE and membrane FE.
4. Ideal behaviour. The ideal homogenized mechanical properties are obtained after the whole process.

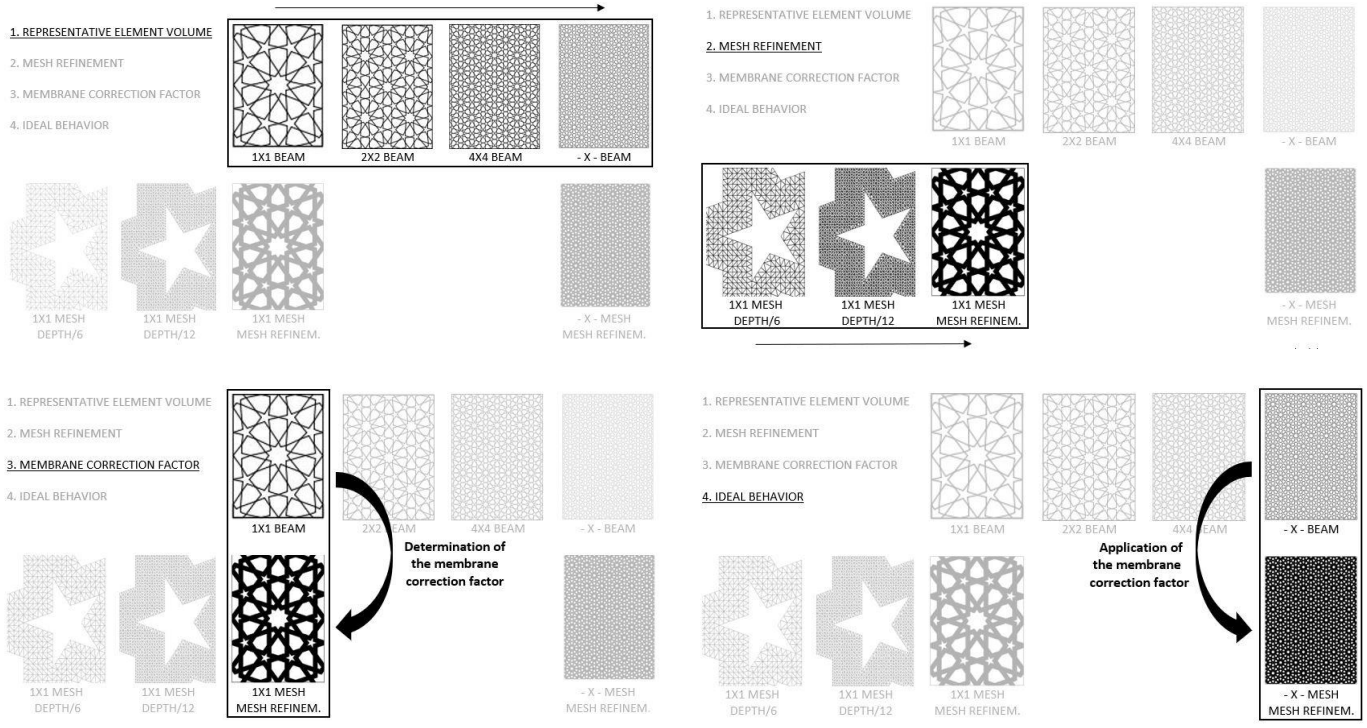

FIG 7.1. Homogenization methodology.as per *Chapter 4.2. Homogenization methodology*

The resulting design tables and pictures for all steps are collected in *Appendix I. Design Guide*. The numerical results from the tests are gathered in *Appendix II. Numerical results*.

THE PREDESIGN TOOL STEP BY STEP

This method can be applied indistinctively of the building shape, size and base material. Furthermore, this tool is very simple to implement in the sense that the pattern itself does not need to be drawn nor its bars to be modelled in order to have a rough idea of its performance, aesthetic view and amount of used material. At the same time, it gives enough freedom to the designer to change a variety of parameters to meet the drift limitations. The most straight-forward approach to apply the method is:

1. In *Chapter 3.3 Selection of historic geometric Islamic patterns*, there are displayed a series of historic geometric Islamic patterns and some parametric variations of them. The first step would be to **choose the desired pattern**. In order to make an informed choice, the designer should verify the suitability of the pattern in terms of structural performance with the help of the patterns performance comparison graphs included in *Chapter 5.2. Wire patterns performance* and Chapter *5.4.Filled patterns performance*. The resulting information of this step is the definition of the generating tessellation, number of crossings, contact angle and filled or wire variation.
2. The number and size of modules is chosen for architectonic and structural purposes. For instance, if the pattern has regularly spaced horizontal lines it is convenient to make them coincide with the floor slabs. This step will **define the module size in the x-direction**. For instance, if the perimeter of the building façade measures 120m and 20 modules are chosen to cover horizontally that distance, each module will have a length in the x-direction of 120/20 = 6m.
3. From the saturation tables introduced in *Chapter 3.5.Saturation and relative beam depth* and fully collected in *Appendix I. Design guide*, the designer will be able to visually **choose a desired saturation and its corresponding relative beam depth** that fits his needs such a determined opacity for solar gain, material minimization or overall aesthetic appearance. If the chosen relative beam depth is 5%, for the previous example the beam depth will be 6,5/100 = 0.3m. It is suggested to choose a range of acceptable solutions instead of just one value to have a better insight on the possible solutions
4. **Obtain the homogenized mechanical properties** of an equivalent metamaterial, there are two alternatives:
   a) For wire patterns (as they have appeared in this document so far, built up with assembled beams), use the ideal homogenized mechanical properties introduced in *Chapter 4.8. Ideal homogenized mechanical properties* and fully collected in *Appendix I. Design guide.*
   b) For filled-stars patterns use the homogenized mechanical properties introduced in *Chapter 5.3. Stars filling.*
5. **Rotate the pattern to its desired orientation**. For historic Islamic geometric patterns with empty stars, it is done multiplying directly the mechanical properties times the rotation factors from *Chapter 5.1. Directional mechanical properties*. In case of the proposed variations and filled stars patterns, the designer has to calculate the rotation factor himself following the steps explained in that same chapter with the constitutive coefficients obtained from the tests and included in the *Appendix II. Numerical results.*
6. **Chose the structural base material**, being it high strength concrete, steel, a composite or any other material. The homogenized mechanical properties times the modulus of elasticity of the base are the mechanical properties of the equivalent continuous material (except for the Poisson ratio that is taken directly) that will be inputted in the orthotropic material crated in a FEM software.
7. **Model the building with a FEM software**, using continuous shear wall elements covering the whole façade. Apply the design loads and run the wind combination with a displacement limitation in the top floor.
8. Run the model iteratively so the program can get the **required wall thickness to meet the drift limitation**.
9. Saturation times the façade surface times the mean thickness, is an **estimation of the required use of material**

APPLICATION OF THE METHOD ASSESSMENT

The homogenization method is assessed in *Chapter 6.4. Accuracy assessment*. For that purpose, a 50-storeys tall prismatic tower with a base length of 30m is analysed.

FIG 7.2. Pattern D ETABS models.

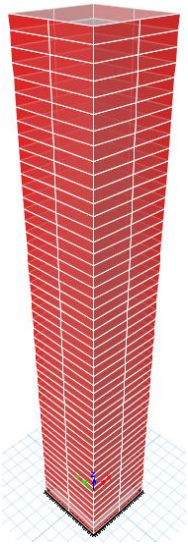

FIG 7.3. Pattern I ETABS models

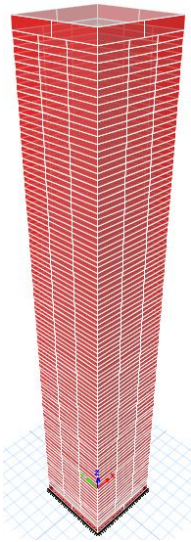

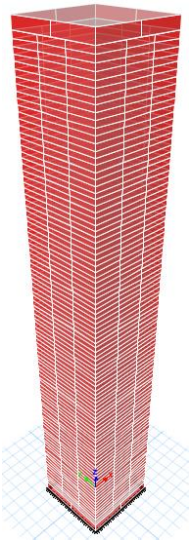

FIG 7.4. Pattern A ETABS models

	Pattern	D	I	A
1	Beam model. Top displacement	836 mm	600 mm	804 mm
2	Membrane model with beam mech. properties. Top displacement	897 mm	703 mm	800 mm
3	Error introduced with the use of membrane elements (2/1 -100%)	+ 7.3 %	+ 17.1 %	- 0.1 %
4	Membrane model with ideal mech. properties. Top displacement	647 mm	575 mm	782 mm
5	Effect of overlaps in final displacement (4/2 – 100%)	-27.9 %	-18.2 %	-2.3 %
6	Corrected top displacement ((1/2)*4)	603 mm	491 mm	786 mm
7	Difference beam model with corrected top displ. (1/6 – 100%)	+ 38.6 %	+ 22.2 %	+ 2.3 %
8	Difference predesign tool with corrected top displ. (4/6 – 100%)	+ 7.3%	+ 17.1 %	- 0.1 %

TABLE 7.1. Comparative beam model against predesign tool results

Line 1 shows the top displacement when the diagrid is modelled with beam elements for a given pattern and saturation. Line 2 shows that top displacement when that same diagrid is modelled as a continuous wall with the corresponding homogenized mechanical properties obtained with beam elements. **The error introduced with the substitution of the beam elements for a continuous wall is the difference between lines 1 and 2 and it stands below 20% for the three patterns analysed and a relative beam depth in the middle of the design tables range**. Line 4 shows the top displacement when the ideal homogenized mechanical properties are used and in all cases it is smaller as it takes into account overlaps that reduce the beams effective length. The effect of the overlaps is shown quantitatively in line 5 and it grows in importance with the relative bending strain energy present in each pattern.

Assuming that the error introduced by the homogenization process is negligible in comparison with the error introduced by the stiffness-based design approach assumptions (accounted for with the substitution of the beam elements for a continuous wall), **it is possible to estimate the expected top displacement of the structure**. It has been done in line 6 by adding to the top displacement for the continuous wall with the ideal homogenized mechanical properties, the error introduced with the substitution of the beam elements for a continuous wall.

Once the expected top displacement is obtained, it is possible to compare that value against the top displacement from modelling all the beams (line 1) and against the top displacement obtained by applying the predesign tool (line 4). **The estimation error incurred by modelling the building with beam elements is displayed in line 7 and the estimation for the error incurred by using the developed pre-design tool is displayed in line 8**. As the error introduced in the homogenization process has been neglected, the predesign tool error (line 8) is the same as the error introduced with the substitution of the beam elements for a continuous wall (line 3)

7.1.2. RQ1. DISCUSSION

It is possible to develop a methodology that automates and normalizes the study and comparison of any geometric Islamic patterns The result is a pre-design tool based on figures and tables with a satisfactory accuracy for pre-design and comparison of alternatives purposes. In fact, this fast and easy to apply pre-design tool is in some cases more accurate than modelling all the beam elements as it takes into account phenomena such as overlaps and mesh refinement.

METHODOLOGY

Each step of the methodology addresses a source of imperfection in the homogenized mechanical properties. The final result is an equivalent meta-material with an **ideal behaviour corresponding to a panel of infinite by infinite modules restrained at its perimeter**. The ideal homogenized mechanical properties obtained are a good benchmark for comparison of the different patterns and it is the best way to define that equivalent meta-material. Deviations in the results inherent to the Finite Element Method such as singularities at the openings corners, the mesh size or the use of linear triangular elements (TRI3) instead of parabolic rectangular elements (QUAD8), are addressed in the mesh refinement.

Conceptually, the homogenization errors are derived from the fact that in **realty the structure will never be infinite**, so the Representative Element Volume effect that has been accounted for in the refinement will appear again. However, the **homogenization errors are smaller than the errors introduced by other assumptions derived from the stiffness-based design approach such as considering the façade as a thin-wall hollow section loaded in-plane**.
In some cases, the designer might be interested in applying this methodology for different patterns of his own creation, for variations from *Chapter 3.3 Selection of historic geometric Islamic patterns* or for the patterns already studied but with some distortions or modifications such as intermediate supports to assess their effects on the pattern performance. T**he designer willing to repeat this homogenization process, in a faster and more simple manner for practical purposes, is encouraged to test 1x1 panels with an appropriate module definition and a mesh size of approximately beam depth divided by 12.**

In *Chapter 4.3. Representative Element Volume (REV)* it has been proved that symmetric boundary conditions provide an exact homogenization for symmetric mechanical properties (modulus of elasticity and Poisson ratio) whereas antisymmetric boundary conditions provide exact results for the antisymmetric mechanical properties (shear modulus). Thus, the symmetric mechanical properties are directly obtained when using membrane finite elements in the tests as the boundary conditions are in practice symmetric as the beams are restrained at different points of their depth. The antisymmetric mechanical properties can be addressed without the need of a refinement by choosing a module definition that goes from node to node without cutting any beam. Finally, in Chapter 4.6. Mesh refinement it has been observed that a mesh size of beam depth divided by 12 is small enough to give an error or 2% in the results for a representative pattern.

THE PREDESIGN TOOL STEP BY STEP

The algorithm for the predesign tool is fast and easy to apply in early stages of the project to compare the feasibility and relative performance of different building shapes and geometric Islamic patterns. The homogenization method was based on continuous linear elastic material shaping solid rectangular beam cross-sections, whose modulus of elasticity (E_b) is multiplied by some factors to retrieve the equivalent homogenized mechanical properties. **This approach is well suited for concrete structures and it allows the use of different concrete grades. Nevertheless, this is approach is poorly suited for steel structures that is the material most likely to be used, as it will not have a rectangular solid cross-sections.** Still, this method can be used for steel and composite structures identifying which cross-sections (with their corresponding saturations) have an equivalent area and in-plane inertia. The saturation will no longer provide a measure f the material employed, but the first chapter of the *Appendix II. Numerical results,* provides the bar lengths involved in a 1x1 panel for a given pattern.

In the case of concrete structures, other effects such as creep for long-term deformations and cracking, can be estimated and applied indirectly via the base material modulus of elasticity. At any rate**, the tool is labelled as "pre-design" because the stress levels in the beams are unknown, making it impossible to perform strength checks or more exact deflection estimations based on stress levels and cracks such as time history analyses.**

APPLICATION OF THE METHOD ASSESSMENT

In the table 7.1 three different geometric Islamic patterns corresponding to square, pentagonal and hexagonal symmetries are applied to a prismatic 50-storeys tall building. When the diagrid is modelled with beam elements, the error introduced stands below 30**%** for the studied cases. In the model with beam elements, the reduced effective beam length from the overlaps is not taken into account, leading to increasing errors for patterns with increasing bending strain. In other words, the less efficient is the pattern, the less suitable is the modelling of the beam elements. In the case of the pre-design tool, the error is smaller as the overlaps are taken into account and it stands below 20% for the studied cases. **As a conclusion, according to the three cases studied, the pre-design tool is actually more accurate than modelling all the elements of the diagrid with beam elements.**

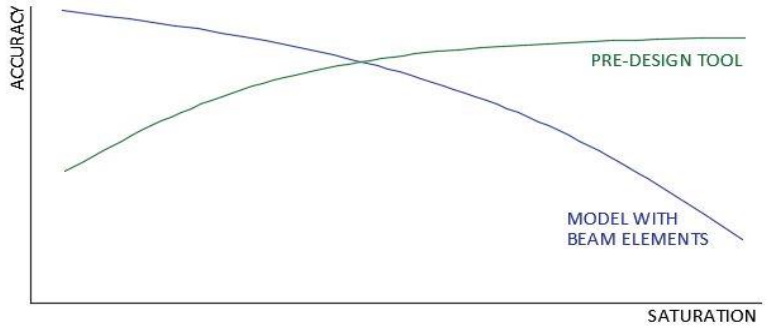

FIG 7.5. Saturation effect on accuracy of pre-design tool against beam elements

But that level of accuracy is not homogeneous (it depends on each pattern) or continuous (it varies with the saturation). As the figure shows, **as the saturation increases, the real behaviour is more susceptible to the overlaps effects**, reducing the accuracy of the beam models. On the other hand **as the saturation decreases, the beam theory applies better** and the errors introduced by the predesign tool become more relevant.

At the same time, the relative position of those curves will change for each pattern. The coarse patterns with a lot of short beams, with higher bending train energy ratio and more overlaps, will be prone to be more accurately designed with the pre-design tool whereas the patterns with triangular-shaped geometries and a few but slender elements will be more accurately designed with the beam model.

As it does not depend just on the pattern but also the saturation and materiality of the structure, the engineer has to be able to judge whether the grid behaves as a wall or as a frame. **The higher the relative beam depth in the provided tables, the more suitable will the pre-design tool be.**

The conclusion is that the developed pre-design tool is a success as it provides a level of accuracy higher than modelling all the beams. It is also faster and easier to implement to compare alternatives in early stages as the complexity of modelling the patterns is postponed to later stages. As the saturation decreases and the effective beam length influence in the beam model diminishes, the beam model will become more reliable than the pre-design tool and vice versa.

7.1.3. RQ1. FURTHER RESEARCH

Further research can be carried out on the method level of the performance of structural grids inspired in historical geometric Islamic ornamental art:

- Out-of-plane behaviour of the patterns for their application in domes and other shell structures with combined in- and out-of-plane behaviour. Interest: High
- Assessment of the application to other materials such as steel and composite. Those materials are likely to be used in the design of tall buildings, but the accuracy of the pre-design tool is low for slender beams and the complexity of the nodes makes them economically inefficient. Interest: Moderate
- Study of the effect of local high stresses on the strength, stability and long-term behaviour of the diagrid. In this research it is left to the engineers at later stages. Interest: Moderate

7.2. RESEARCH QUESTION 2. PATTERN LEVEL

How do geometric Islamic patterns behave and compare when loaded in their plane?

- Selection of historic Islamic patterns and their parametric variations
- Characterization of the patterns' structural behaviour
- Performance comparison of the different patterns
- Proposals for their improvement

7.2.1. RQ2. SUMMARY

SELECTION OF HISTORIC ISLAMIC PATTERNS

The selection of the historic Islamic patterns and their parametric variation is done in *Chapter 3.3.Selection of historic geometric Islamic Patterns*. The patterns are generated from more basic geometric tessellation with an algorithm called Hankin method.

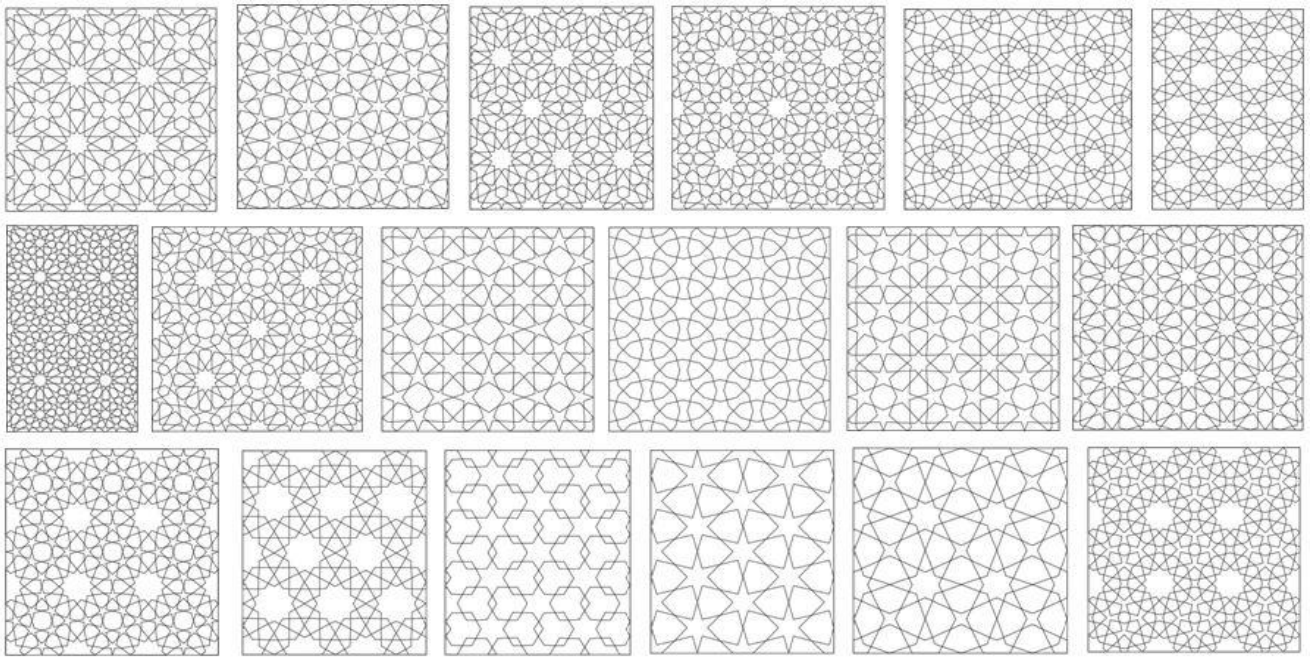

FIG 7.6. Overview of some selected patterns

CHARACTERIZATION OF THE PATTERNS´STRUCTURAL BEHAVIOUR

The patterns are clustered in three main categories depending on their geometric symmetries:

1. **SQUARE SYMMETRY (Perpendicular isotropy)**

Patterns in this group are not isotropic as their homogenized mechanical properties vary depending on the direction under study. However, those mechanical properties are always identical for two perpendicular axes. $E_x = E_y$ and $E_x{}' = E_y{}'$, but $E_x \neq E_x{}'$. Patterns in this category have contact angles for dividers of 90º (45º 60º, 67.5º, 75º…) as those are the cases in which continuous straight lines can be formed.

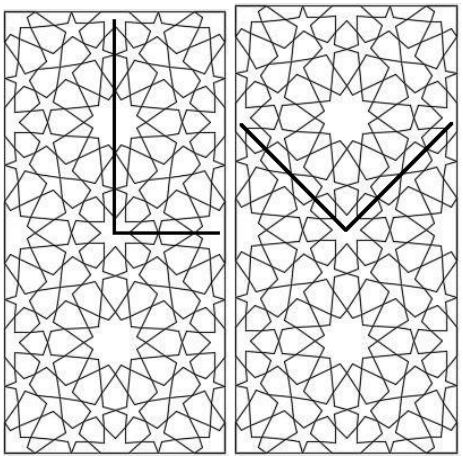

2%	S) HOMOG.MECH. PROPERTIES				
Rot [º]	$E_{h,x}$	$E_{h,y}$	$\nu_{h,xy}$	$\nu_{h,yx}$	G_h
0	2.12%	2.12%	0.271	0.271	0.70%
10	2.09%	2.09%	0.280	0.280	0.72%
20	2.03%	2.03%	0.302	0.302	0.76%
30	1.95%	1.95%	0.328	0.328	0.80%
40	1.90%	1.90%	0.346	0.346	0.83%
45	1.89%	1.89%	0.348	0.348	0.83%
50	1.90%	1.90%	0.346	0.346	0.83%
60	1.95%	1.95%	0.328	0.328	0.80%
70	2.03%	2.03%	0.302	0.302	0.76%
80	2.09%	2.09%	0.280	0.280	0.72%
90	2.12%	2.12%	0.271	0.271	0.70%

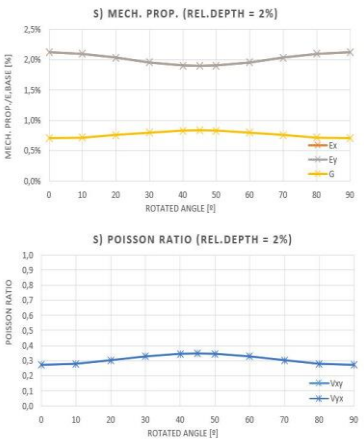

FIG 7.7. Mechanical properties rotated analytically for pattern S (square symmetry)

2. PENTAGONAL SYMMETRY (Orthotropy)

Patterns in this group are orthotropic as their homogenized mechanical properties are different in the x- and y-direction. Those mechanical properties remain different for two perpendicular axes $E_x' \neq E_y'$, except for the particular case of 45º at which the pattern behaves as isotropic. It is called pentagonal symmetry because the two directions of symmetry are located under 72º, which is one fifth of the circle. Patterns in this category have contact angles for dividers of 72º (36º, 54º and 72º) as those are the cases in which continuous straight lines can be formed.

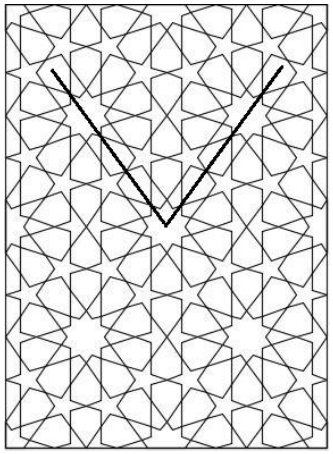

4%	R) HOMOG.MECH. PROPERTIES				
Rot [º]	$E_{h,x}$	$E_{h,y}$	$\nu_{h,xy}$	$\nu_{h,yx}$	G_h
0	3.06%	3.99%	0.420	0.548	1.68%
10	3.20%	4.09%	0.408	0.521	1.62%
20	3.57%	4.33%	0.377	0.458	1.48%
30	4.01%	4.53%	0.346	0.392	1.32%
40	4.37%	4.55%	0.332	0.346	1.21%
45	4.49%	4.49%	0.335	0.335	1.20%
50	4.55%	4.37%	0.346	0.332	1.21%
60	4.53%	4.01%	0.392	0.346	1.32%
70	4.33%	3.57%	0.458	0.377	1.48%
80	4.09%	3.20%	0.521	0.408	1.62%
90	3.99%	3.06%	0.548	0.420	1.68%

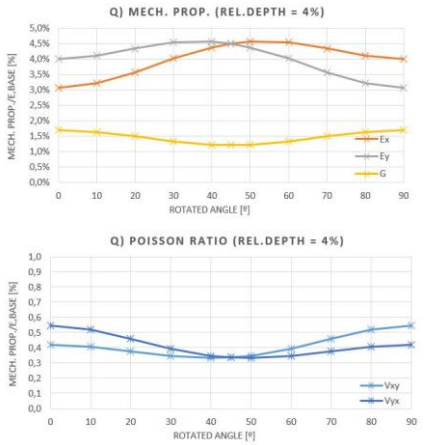

FIG 7.8. Mechanical properties rotated analytically for pattern R (pentagonal symmetry)

3. HEXAGONAL SYMMETRY (Pure isotropy)

Patterns in this group are pure isotropic as their homogenized mechanical properties are the same regardless on the direction under study. Those mechanical properties are always identical for two axes. $E_x = E_y = E_x' = E_y'$ in all cases. Patterns in this category have contact angles for dividers of 60º (30º, 45º 60º, 75º…) as those are the cases in which continuous straight lines can be formed.

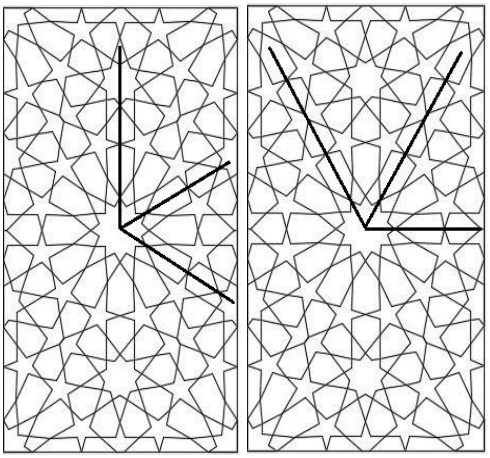

2.5%	T) HOMOG.MECH. PROPERTIES				
Rot [º]	$E_{h,x}$	$E_{h,y}$	$\nu_{h,xy}$	$\nu_{h,yx}$	G_h
0	3.19%	3.19%	0.397	0.397	1.14%
10	3.19%	3.19%	0.397	0.397	1.14%
20	3.19%	3.19%	0.397	0.397	1.14%
30	3.19%	3.19%	0.397	0.397	1.14%
40	3.19%	3.19%	0.397	0.397	1.14%
45	3.19%	3.19%	0.397	0.397	1.14%
50	3.19%	3.19%	0.397	0.397	1.14%
60	3.19%	3.19%	0.397	0.397	1.14%
70	3.19%	3.19%	0.397	0.397	1.14%
80	3.19%	3.19%	0.397	0.397	1.14%
90	3.19%	3.19%	0.397	0.397	1.14%

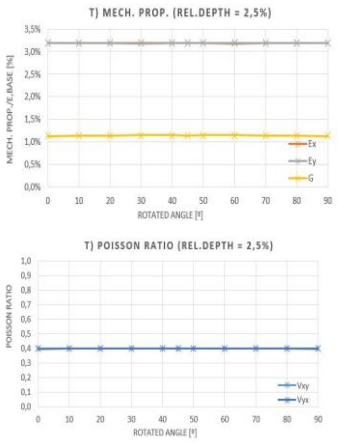

FIG 7.9. Mechanical properties rotated analytically for pattern S (square symmetry)

Symmetry	Square	Pentagonal	Hexagonal
Pattern	D, E, K, L, M, O, P, Q, S	I, J, R	A, B, C, F, G, H, N, T

TABLE 7.2. Type of symmetry of all patterns

PERFORMANCE COMPARISON OF THE DIFFERENT PATTERNS

As it is to be expected, the best performing patterns are those that present a higher continuity for the load path. Discontinuities and changes in the load path lead to higher bending strain energy that are less efficient. For “higher performance”, here it is understood that a great stiffness is achieved with the same amount of material, not taking into account other aspects as complexity or number of nodes and elements. The comparison graph is available in Chapter 5.2. Wire patterns performance. The following pictures show in order the best and worst performing patterns with 45% saturation.

BEST PERFORMING PATTERNS

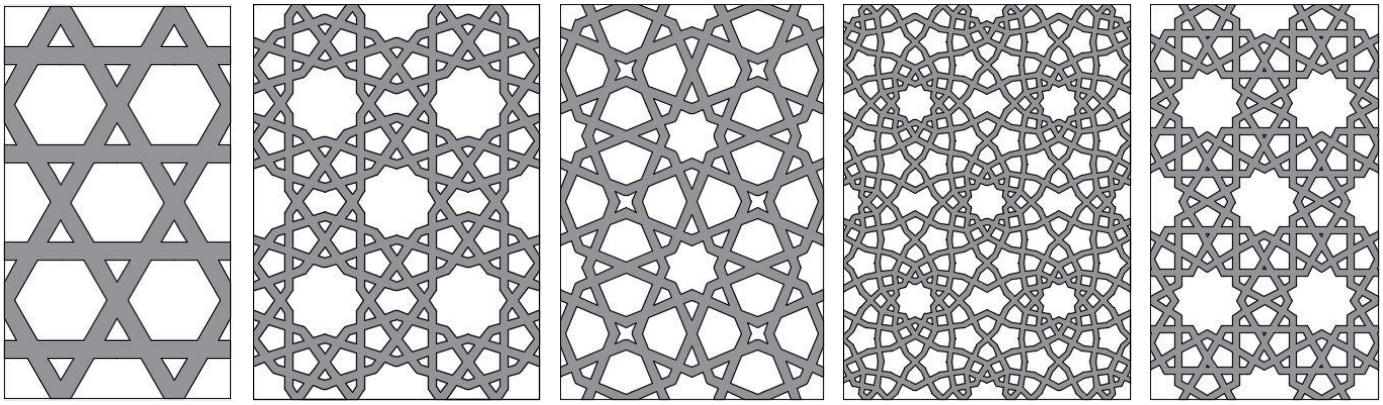

A) YESLI MOSQUE I) HASHT BEHESHT D) LAHORE FORT COMPLEX J) MODARI-KHAN MADRASH H) GENERALIFE

FIG 7.10. Best performing historic patterns. Wire variation, saturation 45%

WORST PERFORMING PATTERNS

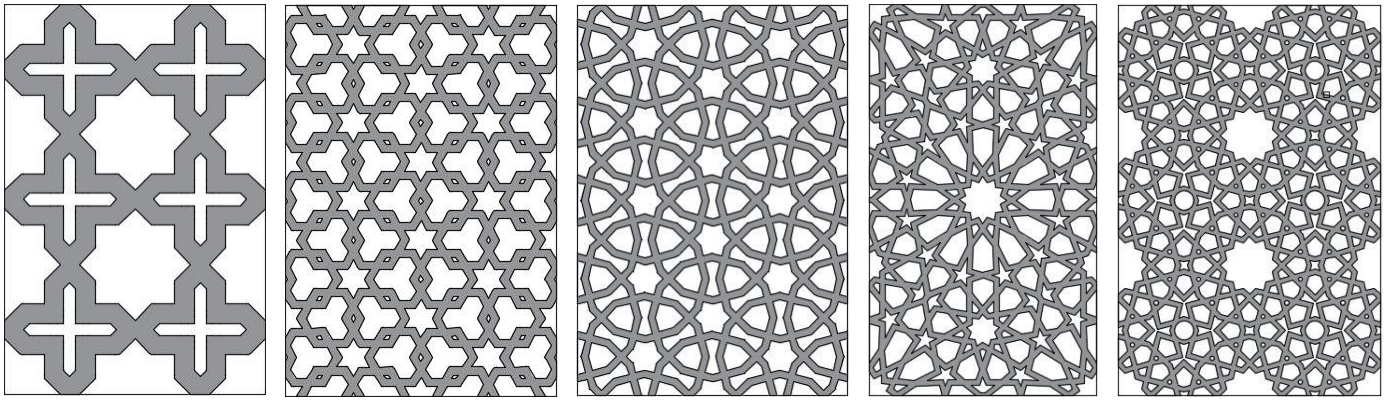

E) SHIRVANSHAHS PALACE C) SABZ PUSHAN G) TOMB OF SALIM CHISHTI T) ALHAMBRA K) SULTAN BAYEZID II

FIG 7.11. Worst performing historic patterns. Wire variation, saturation 45%

PROPOSALS FOR IMPROVEMENT

The best performing patterns are those that present a shorter load path. The improvement proposed at pattern level to enhance the grid performance is to fill the stars to provide continuity to the load path.

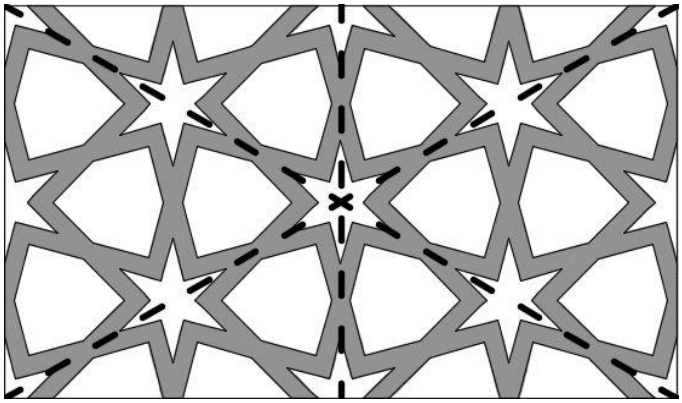

FIG 7.12. Tessellation 6.6.6. θ =75º Sat. = 40%, wire variation

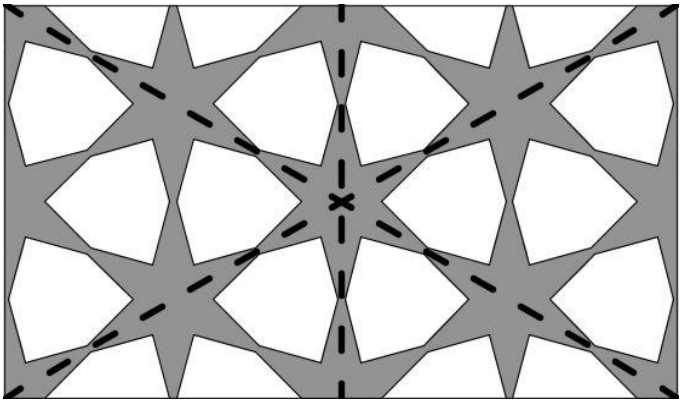

FIG 7.13. Tessellation 6.6.6. θ =75º Sat. = 40%, filled variation

Contrary to intuition, filling the gaps does not always lead to stiffer solutions for the same amount of material. Despite providing a higher degree of continuity in the path load and reducing the bending to axial strain energy ratio, filling the stars also involves an increment of the material use. Comparing for the same amount of material, filling the gaps leads to more slender cross-sections at their weakest points, which are more heavily affected by the bending deformations and increase the risk of collapse.

7.2.2. RQ2. DISCUSSION

SELECTION OF HISTORIC ISLAMIC PATTERNS

A first selection was originally carried out with the help of the book *Islamic Geometric Patterns*[19], but a closer look on showed that many of the most spread patterns were not included in that book and pictures of some of the patterns from the book were not easily available on the internet (as pattern L. Ben Yusuf madrasa). The final selection comes from browsing thousands of pictures on the internet and choosing those that seemed the most representative. The names are given after the location where the attached picture was taken, not meaning that that is the only or first place where that pattern was used. It is worth noting that some of the patterns in this document have different names than the ones from the book *Islamic Geometric Patterns*[19] due to the pictures' availability (as E. Palace of the Shirvanshahs or H. Generalife). The variations are the result of changing one of the parameters involved in the implementation of the Hankin method.

Besides the identification from pictures of many of the patterns included here, **the deduction of the generating tessellation and the implementation of the Hankin method to automate its drawing has been done in most of the cases by the first time by the author of this master thesis**.

In conclusion, **it does not exist a defined directory that compiles all the existing geometric Islamic patterns, names them and provides rules for their generation**. Some researchers as Y. Abdullahi and M. R. Bin Embi in their article Evolution of geometric Islamic patterns17 have been able to track their evolution in time and space and other authors as Eric Borough in his book Islamic Geometric Patterns[19] provide a recipe for the drawing of many of them step by step. But still, the final selection, naming and drawing methodology has been arbitrary and will differ in many cases with other authors.

CHARACTERIZATION OF THE PATTERNS´STRUCTURAL BEHAVIOUR

At early stages of the research it was not possible to know if the grids based on historic Islamic patterns were going to have an isotropic, orthotropic or anisotropic behaviour when loaded in their plane. The result of this research shows that the patterns can show a isotropic, orthotropic or perpendicular isotropic behaviour depending on the angles between their directions of symmetry. Just by testing the patterns in two different directions would have been not enough to appropriately define their behaviour as the perpendicular isotropy would have gotten mixed up with pure isotropy. Is it precisely the use of the direction cosines that allowed this identification.

The directional structural behaviour definition of the patterns provides a tool to the designer to rotate the panels as best suited, but it also allows to identify the strong and weak directions for the patterns performance comparison.

The structural grids inspired in historic Islamic patterns are treated here as continuous meta-materials but they are actually structural grids. **This artificial assimilation done in the homogenization leads in some cases to uncommon situation such as negative Poisson ratios, Poisson ratios over 0.5, or in this cases to perpendicular isotropies. The perpendicular isotropy being defined as having the same mechanical properties for any two in-plane perpendicular directions, but different for other angles.**

The most important outcome from this point is that the patterns with square symmetry (symmetry directions at 90º) display a perpendicular isotropic behaviour, the patterns with pentagonal symmetry (symmetry directions at 72ª) display an orthotropic behaviour, and the patterns with hexagonal symmetry (symmetry directions at 60ª) display an isotropic behaviour

PERFORMANCE COMPARISON OF THE DIFFERENT PATTERNS

One of the first lessons in structural engineering is that triangles are the simplest self-stable structures. When a truss is loaded in its plane, the load distribution methods based on graphic statics will decompose the load into vectors in the elements directions, assigning to each one just an axial force. **The geometric Islamic patterns are not trusses, in fact, most of them develop bending stresses that would lead to the collapse of the structure if the nodes were pinned**. This has been an issue throughout the document as the patterns performance was not linear with the relative beam depth, due to the cubic increment of the cross-section inertia with its depth. **This, has required the reiterative use of tables and the performance quantification of each pattern for different beam depths**

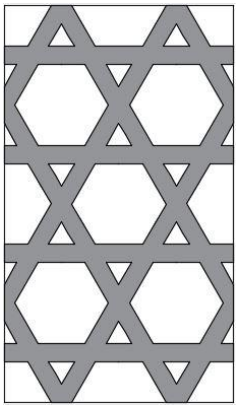

FIG 7.14. A. Yesli mosque

However, when it comes to assessing the patterns performance the principles are the same and they meet the basic engineering judgement: The patterns will perform better as the level of continuity and the level of triangularization increases. Or in other words: The patterns will perform better as the bending vs axial strain energy ratio decreases.

It does not come as a surprise that the best performing pattern (A. Yesli mosque) is almost a truss composed of triangles and completely continuous, while the worse performing pattern (E. Shirvanshahs palace) with sharp turn in the load path leading to big bending moments.

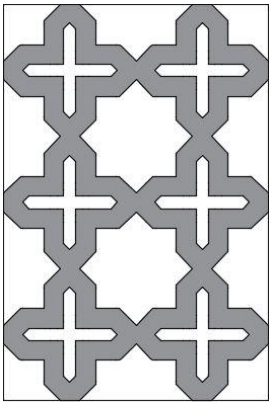

FIG 7.15. Shirvanshahs palace

PROPOSALS FOR IMPROVEMENT

Throughout history, the geometric Islamic patterns have been used ornamentally in a wide range of materials and artistic ways. In many cases, their contour has been carved in walls, painted or built up in sun blockers. However, in other cases the are the result of the wire idealization of the contact lines between different color tiles. In the case of the figure 7.16**, it can be argued that the assembly of the full white stars is a more faithful representation of the composition than the mere outline of its silhouette with lines**.

The proposal for improvement at the pattern retakes this composition concept at the time that it addresses the key feature of a pattern performance: its load path. By filling the stars (or the gaps in those patterns that are not actually starred), the continuity in the load path is improved and reducing the bending to axial strain energy ratio. **Filling the stars increases the gird stiffness in all cases, but it incurs on more material use. When the performance of the grid filled and unfilled is compared for the same use of material (or saturation) it might occur that the simplification of the load path does not compensate the extra material needed resulting in a worse performing solution**. This phenomenon varies for each pattern. While some patterns´ performance increases significantly, in other cases they can be barely affected or they can even see their performance reduced as displayed in figure 7.17.

FIG 7.16. Alhambra tiles[30]

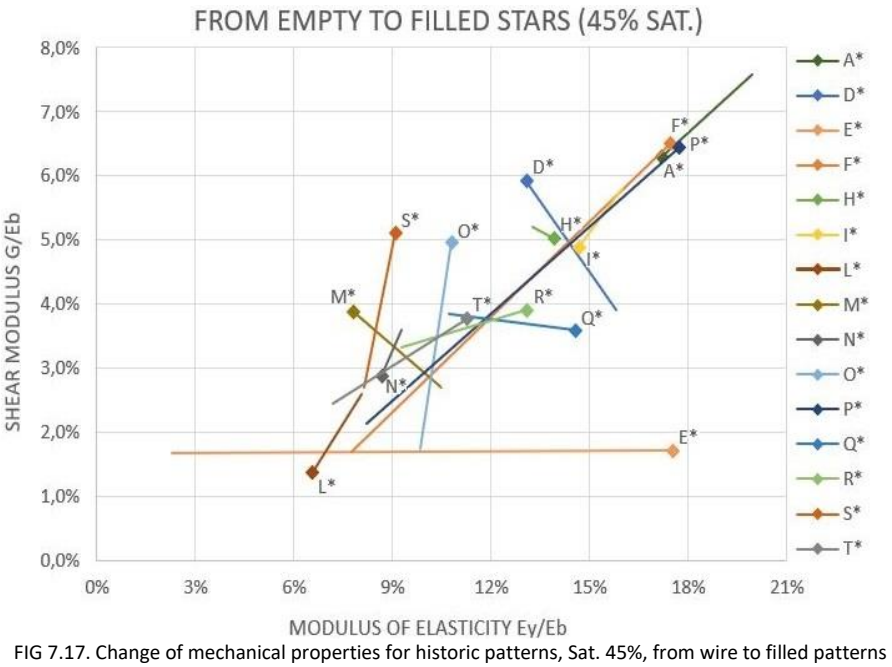

FIG 7.17. Change of mechanical properties for historic patterns, Sat. 45%, from wire to filled patterns

A simplification of their behaviour would be to consider the filled stars as rigid bodies connected between them by pinned nodes. The result is that the worse performing patterns are those with thin points of contact such as the arrows and star patterns whereas the best performing patterns are those with a balanced cross-section in all locations

The designer must bear in mind that the results provided in this document and the graphs derived from them are obtained from a linear elastic analysis. The contact points between the star will experience a concentration of stresses level that in many cases can lead to plastic hinges and other non-linear effects.

Finally, the degree of opacity required for other design purposes such as solar gain in their application on domes in public spaces will affect the solution adopted. Whereas it is recommended to use the wire solutions with light and strong materials such as timber, steel or composite beams to accomplish low saturations, for a high saturation the filled patterns made of concrete or 3D printed cementious materials will be probably better suited.

7.2.3. RQ2. FURTHER RESEARCH

Further research can be carried out on the pattern level of the performance of structural grids inspired in historical geometric Islamic ornamental art:

- Broadening of the scope to other historic patterns not included in this research, to the variations proposed or to new creations. The most important patterns have already been included and with 20 patterns the range is very large, however it might provide a very efficient pattern not considered so far. Interest: Low
- Further studies on the stress levels reached and their effects on strength and stability of the grid. Special importance in the case of filled patterns with low saturations due to small cross-section at the contact points. Interest: Low

7.3. RESEARCH QUESTION 3. BUILDING LEVEL

Can Islamic inspired patterns become a feasible alternative to traditional diagrid systems for tall buildings?

- Performance comparison of the different patterns and the conventional diagrids
- Overview of practical applicability best performing patterns
- Special cases on tall buildings

7.3.1. RQ3. SUMMARY

PERFORMANCE COMPARISON AGAINST CONVENTIONAL DIAGRIDS

In *Chapter 6.2. Diagrids vs historic patterns performance*, the wire and filled variations of the historic patterns are compared against the conventional diagrid (Z). The following graph is the result of that comparison and it shows that patterns F*, P*, I, D and E, could become a feasible alternative to conventional diagrids in punctual cases, whereas patter A (Yesli Mosque) actually overcomes the conventional diagrid performance. Pattern B75* is a variation of the filled pattern B (Great Mosque of Damascus), with similar homogenized mechanical properties to the conventional diagrid for a 45% saturation in both cases. That pattern is considered historic for other authors as E. Broug[19.] but it has not been included as such due to the difficulties to find a picture that justifies its spread use.

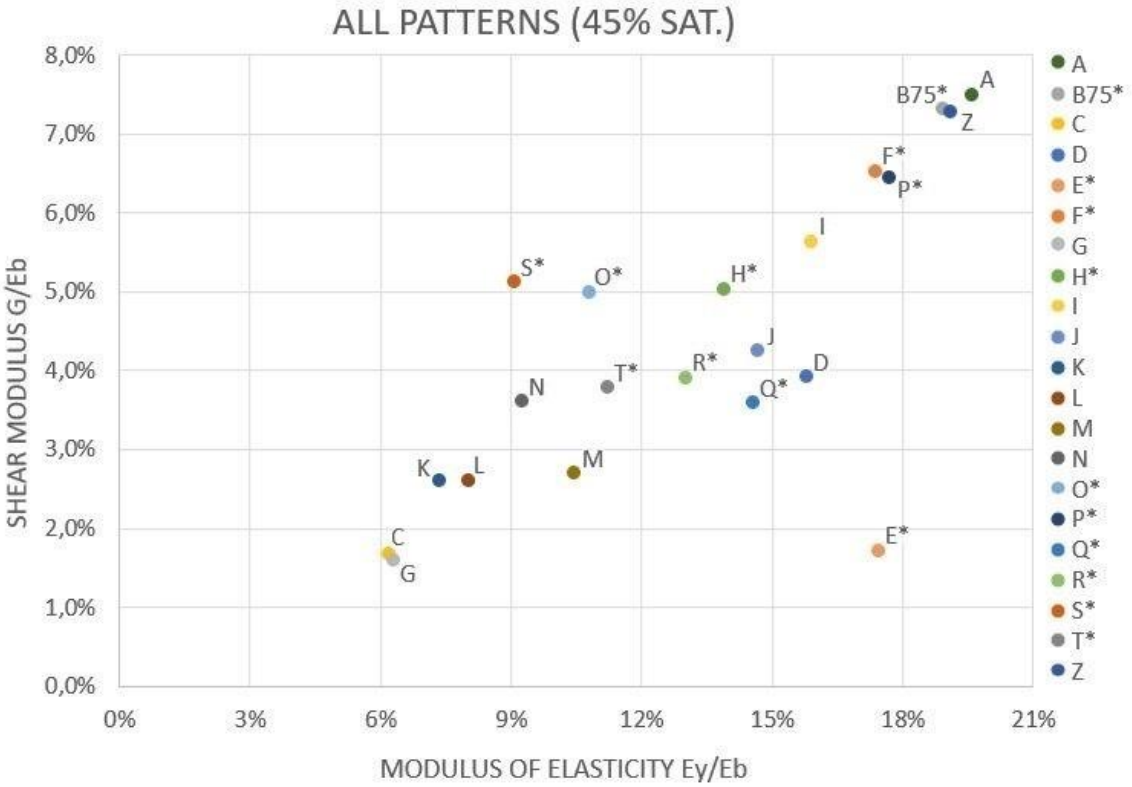

FIG 7.18. Performance comparison of historic patterns against conventional diagrid system, saturation 45

GRIDS WITH SIMILART PERFORMANCE TO CONVENTIONAL DISAGRIDS (SAT. 45%)

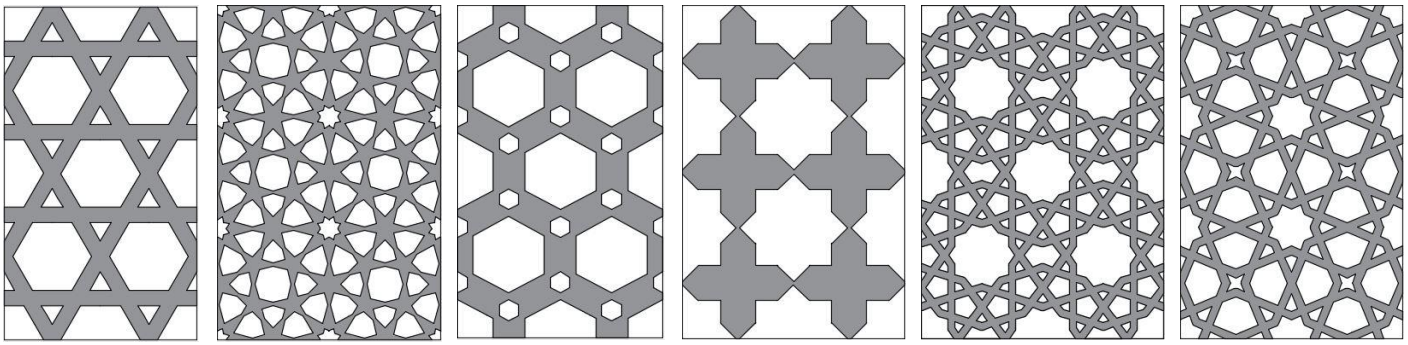

A) YESLI MOSQUE | P*) MOSQUE OF AL-SALIH TALA'I | F*) MUSTANSIRIYA MADRASA | E*) SHIRVANSHAHS PALACE | I) HASHT BEHESHT | D) LAHORE FORT COMPLEX

FIG 7.19. Best performing historic patterns

OVERVIEW APPLICABILITY

Their suitability and applicability in practice is extensively discussed in Chapter 6.3. Overview of best performing patterns. The most suitable for tall building due to their simplicity, performance and possibility to integrate the floor slabs, are in order:

1. A) Yesli Mosque wire and filled variations
2. B75*) Great Mosque of Damascus filled variation
3. E*) Palace of the Shirvanshahs filled variation
4. F*) Mustansiriya Madrasa
5. I) Hast Behesht wire variation

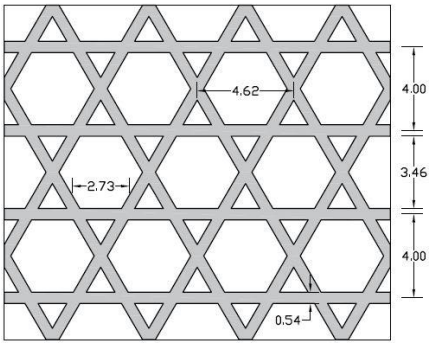

FIG 7.20. Application of pattern A to 4m inter-story building. Sat. 35%

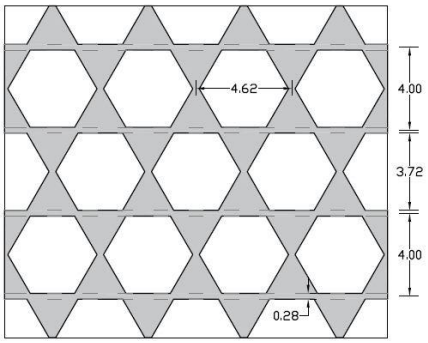

FIG 7.21. Application of pattern A, to 4m inter-story building. Sat. 35%

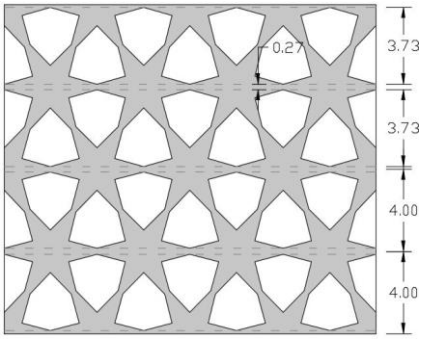

FIG 7.22. Application of pattern B75* rotated 30º, to 4m inter-story building. Sat. 45

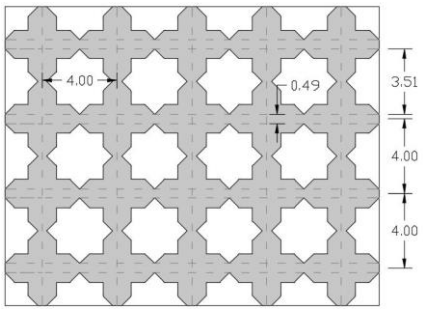

FIG 7.23. Application of pattern E* to 4m inter-story building. Sat. 55%

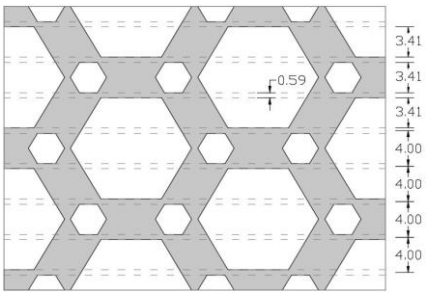

FIG 7.24. Application of pattern F* rotated 30º, to 4m inter-story building. Sat. 40%

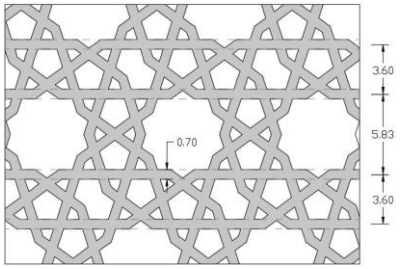

FIG 7.23. Application of pattern I rotated 54º, to 4m inter-story building. Sat. 45%

SPECIAL CASES IN TALL BUILDINGS

the three best performing wire patterns (A, I and D) have previously been used to assess the accuracy of the homogenization method and the pre- design tool providing satisfactory results in *Research Question 1 Method level*. The pre-design tool was estimated to have an approximate error of 10% for a middle of the range beam size. That error level is similar to the error estimated for beam model but less scattered for all patterns.

The implementation of the pre-design tool in real projects can lead to geometries much more complex than the studied prismatic case, introducing distortions in the grid that have not been accounted for in the homogenization process. The quantification of those deviations will depend on the kind of effect, its location and extension in the building, the degree of misshape incurred and even on the pattern chosen**. In order to have a quantitative estimation on the error introduced by the following effects, it would be necessary to test each pattern for each effect at different degrees individually and in combination, which is beyond the scope of this research.** This chapter has been included to make the designer aware of the existence of those effects and what kind of influence in the results would be reasonable to be expected. The exercise has been designed to introduce and combine the following effects one by one in increasing complexity:

- Squeezing: Patterns get squeezed as the floor extension reduces keeping the same storey height.
- Distortion: Patterns get distorted if a rotation is introduced between consecutive storeys.
- Intermediate supports: As the panel size increases, each module will span more than one floor at the time.

The following pictures display the abovementioned three effects for pattern I. Hasht Behesht rotated 90º:

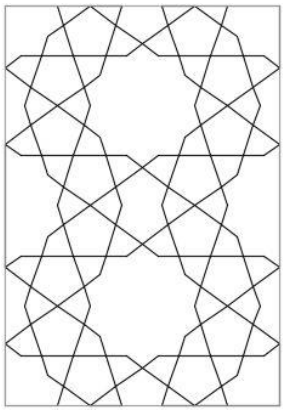

FIG 7.30. Homogenized pattern

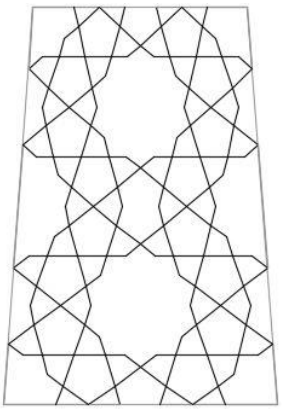

FIG 7.31. Squeezing effect

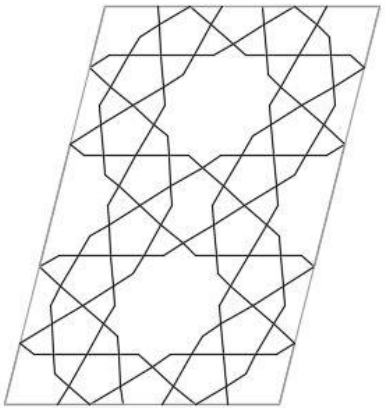

FIG 7.32. Distortion effect

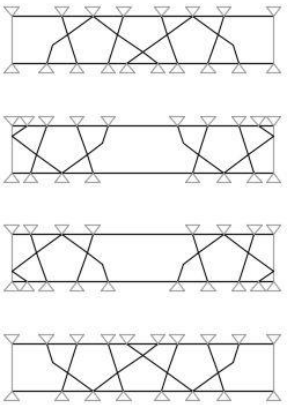

FIG 7.33. Intermediate supports

Those effects have been introduced gradually in 3 following examples, combining them in increasing complexity. It does not provide a quantitative estimation of the error introduced by each effect, it simply shows when and where those effects appear to make the designer aware of their existence and point out the need of further research.

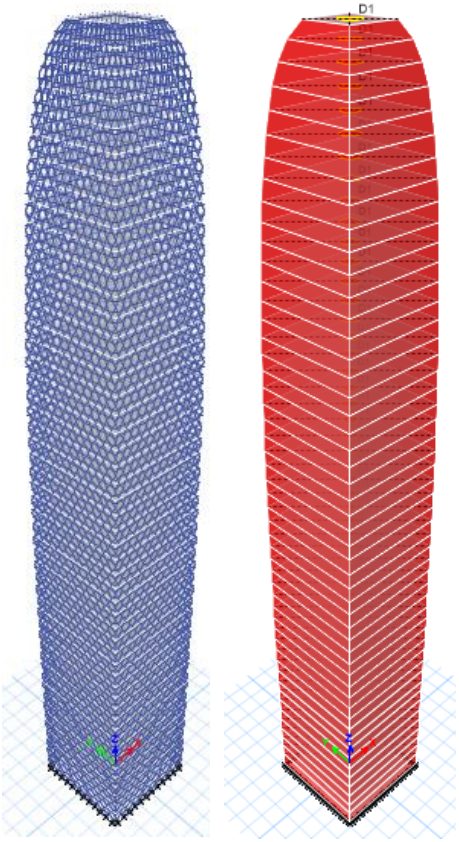

FIG 7.24. ETABS models tower A

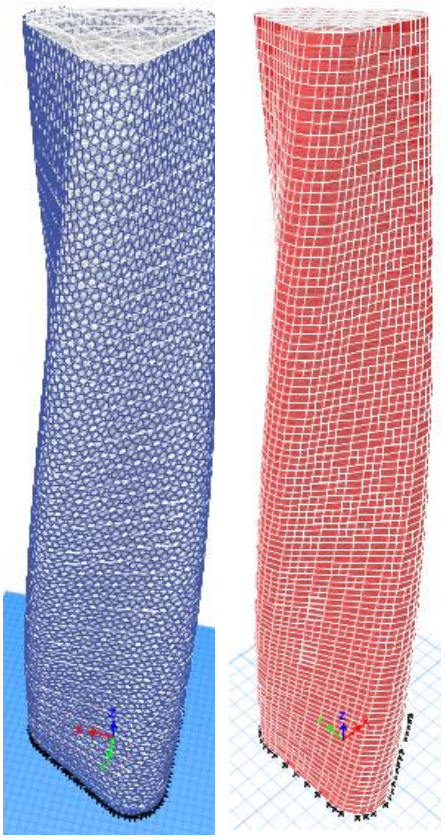

FIG 7.25. ETABS models tower D

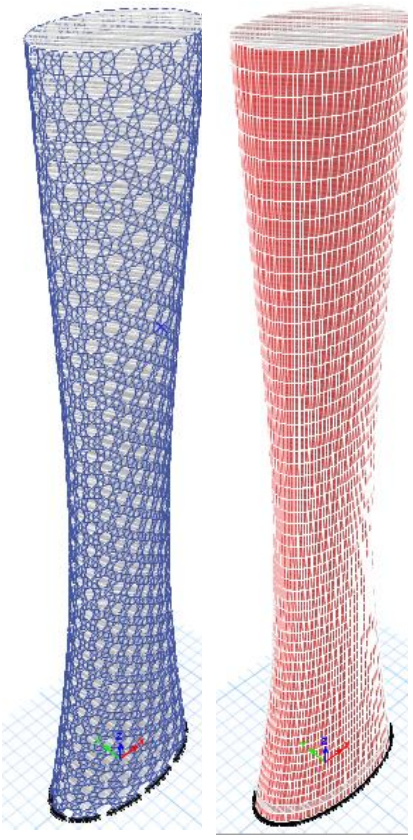

FIG 7.26. ETABS models tower I

	Pattern	A	D	I
1	Beam model. Top displacement	826 mm	985 mm	307 mm
2	Membrane model with beam mech. properties. Top displacement	746 mm	836 mm	586 mm
3	Error introduced with the use of membrane elements (2/1 -100%)	- 9.6 %	- 15.1 %	+ 90.9 %
4	Membrane model with ideal mech. properties. Top displacement	728 mm	601 mm	485 mm
5	Effect of overlaps in final displacement (4/2 – 100%)	- 2.4 %	-28.1 %	-17.2 %
6	Corrected top displacement ((1/2)*4)	806 mm	708 mm	254 mm
7	Difference beam model with corrected top displ. (1/6 – 100%)	+ 2.5 %	+ 39.1 %	+ 20.8 %
8	Difference predesign tool with corrected top displ. (4/6 – 100%)	- 9.6 %	- 15.1%	+ 90.1 %

TABLE 7.3. Comparative beam model against predesign tool results

Line 1 shows the top displacement when the diagrid is modelled with beam elements for a given pattern and saturation, whereas line 2 shows that top displacement when that same diagrid is modelled as a continuous wall with the corresponding homogenized mechanical properties obtained with beam elements. **The error introduced with the substitution of the beam elements for a continuous wall is the difference between lines 1 and 2 and it is 10- 20% for towers A and D, and 90% for tower I.** Line 4 shows the top displacement when the ideal homogenized mechanical properties are used and in all cases it is smaller as it takes into account overlaps that reduce the beams effective length. The effect of the overlaps is shown quantitatively in line 5 and it grows in importance with the relative bending strain energy present in each pattern. Assuming that the error introduced by the homogenization process is negligible in comparison with the error introduced by the stiffness-based design approach assumptions (accounted for with the substitution of the beam elements for a continuous wall), it is possible to estimate the expected top displacement of the structure. It has been done in line 6 by adding to the top displacement for the continuous wall with the ideal homogenized mechanical properties, the error introduced with the substitution of the beam elements for a continuous wall. Once the expected top displacement is obtained, it is possible to compare that value against the top displacement from modelling all the beams (line 1) and against the top displacement obtained by applying the predesign tool (line 4). The estimation error incurred by modelling the building with beam elements is displayed in line 7 and the estimation for the error incurred by using the developed pre-design tool is displayed in line 8. As the error introduced in the homogenization process has been neglected, the predesign tool error (line 8) is the same as the error introduced with the substitution of the beam elements for a continuous wall (line 3)

7.3.2. RQ3. DISCUSSION

PERFORMANCE COMPARISON AGAINST CONVENTIONAL DIAGRIDS

Triangulated structural systems such as trusses and diagrid systems are commonly used in structural engineering as the stiffest structural systems. That is why it comes as a surprise that a structural grid based on geometric Islamic patterns has been found with a higher performance than the conventional diagrids (A. Yesli Mosque), another one with the same level performance (B75*. Great Mosque of Damascus) and a few more with smaller but close level of performance.

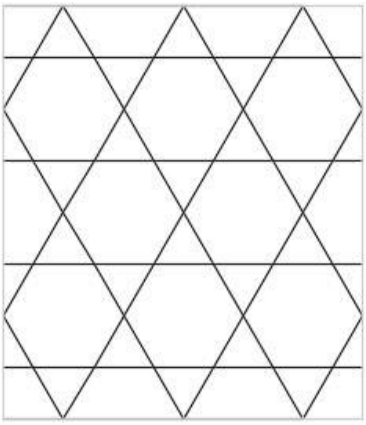

FIG 7.27. Pattern A (Yesli Mosque)

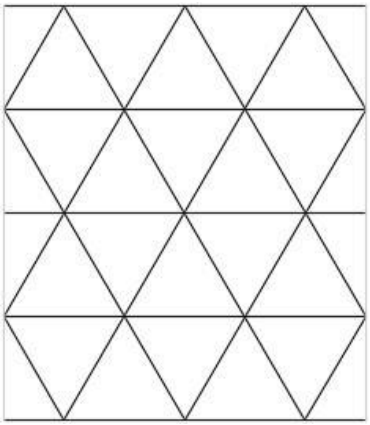

FIG 7.28. Pattern Z (Conventional diagrid)

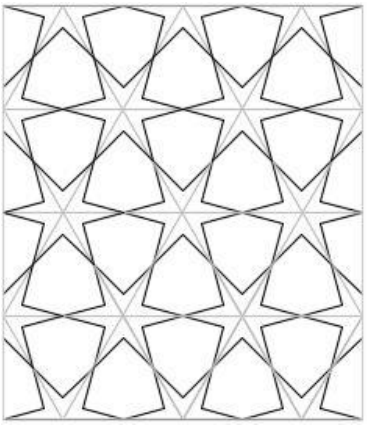

FIG 7.29. Pattern B75* (Great Mosque of Damascus)

Pattern A) Yesli Mosque. A closer look to Figure 7.27 and Figure 7.28 shows that **both pattern are practically identical**. They both are composed by crossing lines at 60º in the same orientation and have hexagonal geometry, so both are isotropic. The only difference is the location of the horizontal elements. In the diagrid system, the horizontal beams meet the diagonal beams at their intersecting node, whereas in the tessellation 3.6.3.6 the horizontal elements meet the diagonals at mid height**. This results in shorter elements and therefore stiffer elements in pattern A. As the nodes have been modelled fixed, there is going to be bending moments that contribute to the panels deformation. That bending contribution to the deformation is secondary compared with the axial deformation, but it can make the difference especially since the nodes are modelled as fixed instead of pinned**. Another effect not considered here as it is a linear elastic analysis, is that the horizontal elements reduce the effective length of the diagonals providing lateral stability against buckling. It comes at the cost of having more nodes but at the same time simpler connections. Other explanation would be to consider the deviation in the performance an error from the diagrid homogenization introduced by the horizontal top and bottom horizontal elements overlapping the panels boundary.

Pattern B75*) Great Mosque of Damascus. This is the other structural grid with a similar performance to conventional diagrids. Figure 29 is the superposition of this pattern with a conventional diagrid and it shows **that pattern B75* can be understood as a conventional diagrid with a varying beam depth along its elements**. It is expected that this pattern would have a similar performance as a conventional diagrids in linear elastic regime. It displays a hexagonal symmetry so its structural behaviour is isotropic too.

This research is based on the stiffness-based design approach, and since it only uses the modulus of elasticity in the y-direction and the shear modulus as material parameters, those are the mechanical properties chosen to assess their relative performance. **In real buildings there are out-of-plane, second order and non-linear effects, and specially horizontal forces that taken into account could disrupt the performance classification obtained**. As an example, the pattern with the highest possible homogenized modulus of elasticity in the y-direction (and the smallest possible axial to bending strain energy) would be a striped pattern made of vertical lines. For a 45% saturation it would have an equivalent modulus of elasticity in the y-direction of 45%, twice as much as the conventional diagrid.

Conventional diagrid has been proven isotropic due to their hexagonal symmetry, so a good performance is also to be expected when horizontal loads are introduced in combination with the main vertical loading. **Patterns A, A*, B75* and P* are also isotropic due to their hexagonal symmetry as the conventional diagrids, so their relative performance compared to the conventional diagrid should stand even if horizontal loads are introduced in combination with the vertical loading.**

FIG 7.30. Merdeka tower[31]

In the particular case of tall buildings, the current tendency is to move away from the equilateral triangles from the conventional diagrid systems towards more lender triangles that optimize the equivalent modulus of elasticity in the x- and y-direction relationship. A clear example is the Merdeka tower[31] currently under construction and expected to be with a 664m height the world´s third tallest building. The optimum diagrid design would be based on the Michell truss, with pointy triangles at the building base and shallow triangles at the top levels.

This is mentioned to point out that there are other diagrid systems besides the equilateral conventional diagrids that are better suited in the particular cases of tall buildings and are not included in the comparison table.
The conclusion is that the response to research question is a clear yes. It possible to design structural grids inspired on historic Islamic patterns that have similar performance levels to conventional diagrids and therefore they can be used as an alternative to conventional diagrids in some cases for practical applications.

OVERVIEW APPLICABILITY

The geometric Islamic star patterns have been historically used as ornamentation elements. They have been carved, painted, cladded with tilling or ever built up in sun blockers, but historically they were never used as the building main bearing structural system. **The new applications of the geometric Islamic patterns as bearing systems introduces a knowledge gap about their in-plane structural behaviour and relative performance**. Thanks to the new computational drawing and analysis tools, this lack of previous experience is not being an impediment for architects to propose spectacular designs with some of the patterns studied in this document.

A story of success would be the several buildings designed by the Japanese architect Shigeru Ban using the best performing pattern A. Yesli Mosque. Probably the architect was not inspired by the Islamic tradition when he came with this tessellation and it is simply its high structural performance, simplicity and aesthetics that led him to use it. Nevertheless, the conclusion rom this research allow the broader public to be aware of the suitability of this solution. An example of the many buildings proposed by Shigeru Ban with this structural grid is La Seine Musicale[32] in France:

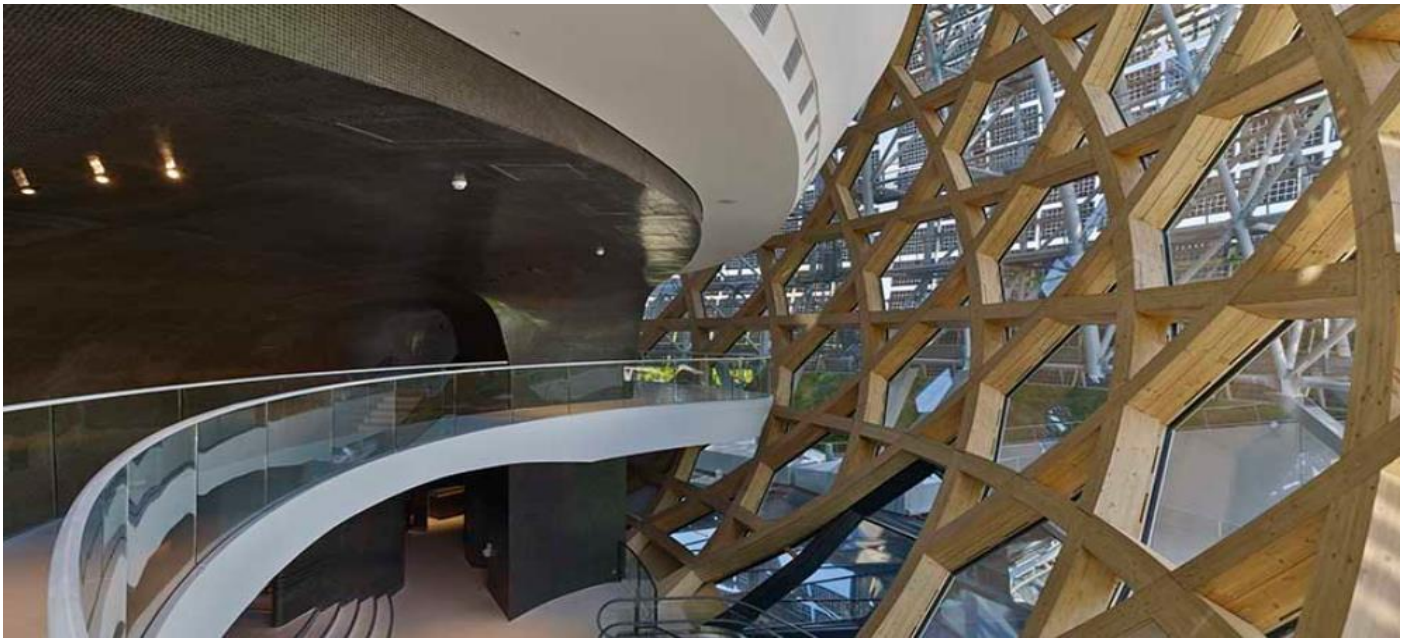

FIG 7.31. La Seine Musicale by Shigeru Ban

Unfortunately, this knowledge gap has not been successfully overcome by other architects. In the next example, Moataz Faissal Farid[33] use the pattern E. Shirvanshans Palace for his Islamic Centre structural façade. In this particular case, it is clear that the architect has been influenced by the Islamic tradition and he has used that seemed appropriate for its simplicity and aesthetics. Despite the beautiful looks of the project, this document has demonstrated that E. Shirvanshahs Palace is the worst performing pattern, it has been used with its weakest orientation that it would have benefited greatly of filling the crosses.

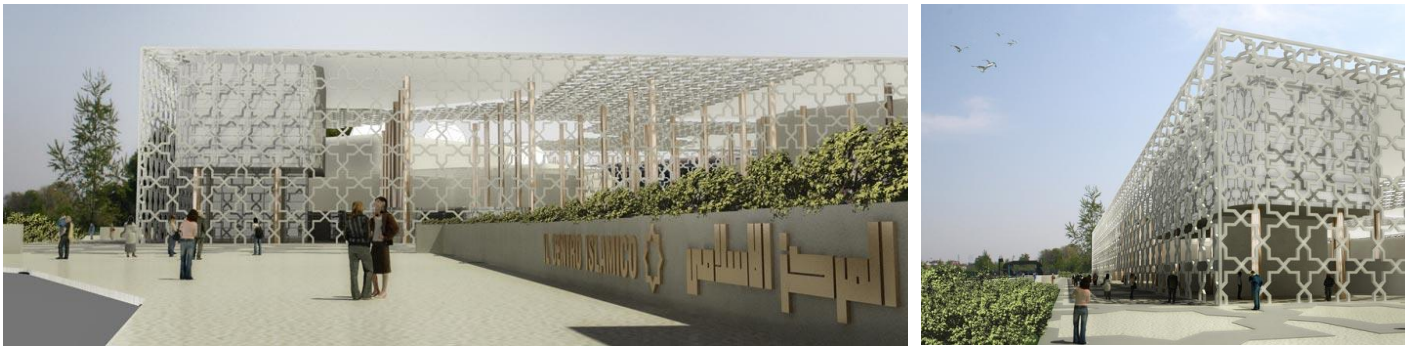

FIG 7.32.Morataz Faissal Farid proposal for a new Islamic centre

This document bridges that gap with comparative tables to identify the best performing patterns and their best orientation. In that sense, **it is considered that this research successfully achieves the goal of providing a useful tool for the decision making in the design process of bearing geometric Islamic patterns.**

SPECIAL CASES IN TALL BUILDINGS

The homogenization method used in this document has provided for each pattern the ideal homogenized mechanical properties of an infinite panel. This is the best approach to get the equivalent meta-material of a micro-scale structural grid such as carbon nanotubes, but it has some disadvantages when it is applied to large structural grids. **Its parametric implementation to objects with different geometry has an impact in the internal geometry of the used meta-material. This is especially true in the case of tall buildings, the floors constitute a series of equidistant planes that remain plane and in the same position regardless of the external geometry**. The internal geometry of the meta-material cannot freely move, warp and adapt to the external geometry due the floors constrain, introducing the effects named here squeezing and distortion. The other effect of the floors in that they introduce a series of new supports every time they touch the diagrid. Due to the floor great in-plane stiffness and limited out-of-plane stiffness, those intermediate supports prevent the nodes differential horizontal displacement in what is called a diaphragm action. Those intermediate supports can change the internal behaviour of the meta-material, making the homogenization done completely unsuitable in some particular cases.

Table 7.2 shows the results of the method accuracy assessment, applying three different patterns to the same 50-storeys prismatic building. The relative beam depth has been chosen in the cases in the middle of the of the tables range, corresponding to a homogenized modulus of elasticity in the y-direction of approximately 10% E_b. The conclusion was the pre-design tool has a higher accuracy than modelling all the bars, but it was faster and easier to implement. Table 7.3 shows the results of applying the exact same procedure to other three examples with a different geometry. **The patterns used are the same as well as their saturation and therefore their homogenized mechanical properties. The width differs but since it is a linear elastic analysis, the relative results in table 7.3 are comparable one on one with the values from table 7.2**.

The response change due to the alteration of the grid geometry could directly be observed by comparing the drifts from the model with all the beam elements and from the application of the predesign tool as the homogenization process does not take into account those effects. The intermediate supports and the distortion effects cannot be addressed using the predesign tool, however, the squeezing effect can be partly compensate by reducing the module size in the x-direction in each squeezed level.

Tower A: Yesli Mosque pattern with squeezing effect at the top. This tower is very similar to the examples used in the method accuracy assessment with the difference that the top floors have been reduced introducing the squeezing effect in that region. **This example tries to identify how effective would be to adapt the modulus size in the x-direction to compensate the squeezing effect**. The estimated error of modelling all the beam elements is +2.5%, similar to the +2.3% from table 7.2. The estimated error of the predesign tool is -9.6%, whereas it was just -0.1% in the method assessment in table 7.2. It has been observed a significant increment in the error from adapting the relative beam depth to the new definition of the module size in the x-direction. **This approach is not is advisable as the relative beam depth has more influence in the stiffness than the change of geometry from the squeezing effect.** This

Tower D: Lahore Fort Complex pattern, squeezing effect increasing throughout its height with constant distortion at each level. The squeezing effect is addressed by increasing the saturation as the perimeter decreases (smaller modulus size in the x-direction implies that the same absolute beam depth has a bigger relative beam depth). It is assumed that most of the error incurred will correspond to the great distortion effect. The error introduced by the use of the membrane elements (line 3) is -15.1% instead of the +7.3% from the method accuracy assessment in table 7.2. If the squeezing effect is assumed mostly addressed by the saturation variation, the drift difference from -15.1% to +7.3% is caused mostly by the distortion effect. In other words, tower D should have deflected 775mm (7.3% less than the membrane model that does not take into account the distortion effect) but it deflected 985mm instead. Those 210mm are cause by the distortion effect. In this particular case, for this geometry, pattern and distortion level, **the distortion effect has increased 27% the deflections in the beam model. As the predesign tool was providing 7.3% larger deflections than the expected top displacement, in this particular case the predesign tool would require a distortion factor of 1.2 to be applied to the obtained deflections with the predesign tool**. This distortion factor can easily be increased to 1.3 if it´s considered that the way the squeezing effect was addressed provided an extra 10% of stiffness as in tower A.

Tower I. Hasht Behseht pattern, squeezing effect at mid height of the tower combined with a small constant distortion and intermediate supports derived from modules bigger than then floor height. The squeezing effect is partly compensated by adapting the saturation with the module size in the x-direction corresponding to each level. The distortion introduced is much smaller than in tower D so qualitatively it is expected that the distortion effect will increase the beam model deflection below that 20%, although each pattern can respond differently. The error introduced with the use of membrane elements (line 3) is +90.9% instead of the +17.1% from the method accuracy assessment in table 7.2. As the membrane model with beam homogenized mechanical properties deflects 586mm, the beam model would be expected to deflect 485mm (17.1% less than 586mm) if the distortion effect is not considered or approximately 533m (10% more of 485mm) if the distortion effect is accounted for. However, the measured deflection in the beam model is 307mm, approximately 40% less of the expected defection if the intermediate supports were not taking place. In other words, **the intermediate supports are stiffening the pattern by introducing transversal rigid planes inside the pattern module that can greatly alter the bending to axial strain energy ratio. In this particular case, the intermediate supports reduce expected deflections approximately 40%, but it will depend on the pattern under study and the relative distance of the planes rigid planes inside the pattern. In all cases, the intermediate supports will increase the structural grid performance and not taking it into consideration at the predesign stage will lead to conservative design**s.

In conclusion, the homogenization process obtained an equivalent ideal material corresponding to a plane infinite panel that will not correspond with the built structural grid. The use of complex geometries and its application to tall buildings introduce effects not considered in the homogenization that will disrupt the expected structural performance. Those effects are minimized in the case of other shells structures such as does but can be important in the case of tall buildings. It is not advisable to take into account the squeezing effect by adapting the saturation with the change of the modulus size in the x-direction as the relative beam depth affects the overall stiffness more than the geometry change derived from the squeezing effect. The distortion effect cannot be accounted for and depends on the angle of the distortion and the pattern. However, in a representative case it has been found a required correction factor of approximately 1.2-1.3 that is in line with other uncertainty factors used in practice. Finally, the intermediate supports can have a great influence in the final drift. Its quantity depends on the pattern used and the number of diaphragms inside the module. Nevertheless, the introduction of intermediate supports is always beneficial and not considering them will always lead to more conservative solutions.

7.3.3. RQ3. FURTHER RESEARCH

Further research can be carried out on the building level of the performance of structural grids inspired in historical geometric Islamic ornamental art:

- Study cases and practical comparison of the application of tessellation 3.6.3.6. (here named pattern A. Yesli Mosque) against conventional diagrid systems in a variety of materials. One important conclusion is that this pattern can become a feasible alternative to conventional diagrids. This finding can have an impact on industry, so a more in depth assessment and further research of that specific pattern is recommended. Interest: Very high
- Further studies on the pattern size effect on the Islamic structural grid behaviour applied to tall buildings. As the module grows, the pattern can span several levels at the same time, introducing intermediate supports at the grid intersection with the floor slabs. This diaphragm effect provides a higher stiffness to the bearing system and it can alter significantly the pattern behaviour. Interest: High.
- Further studies on the squeezing and distortion effects on the Islamic structural grids behaviour. Characterization and quantification for different angles and levels of implementation. Interest: High

REFERENCES

[1] S. Nemat-Nasser and M. Hori (2013). Micromechanics: Overall Properties of Heterogeneous Materials. Amsterdam: Elsevier
[2] UN DESA (2018). 2018 Revision of World Urbanization Prospects. United Nations
[3] D. Rastorfer, J. William, LeMessurier's (1985) Super-Tall Structures: Architecture-Engineering.
[4] Moon, K. S., Connor, J. J., and Fernandez, J. E. (2007). Diagrid structural systems for tall buildings: characteristics and methodology for preliminary design. Struct. Design Tall Special Build. 16. 205–230.
[5] S. D. Taranath, N. B. Mahantesh and M. B. Patil (2014). Comparative study of pentagrid and hexagrid structural system for tall building. J. Civil Eng. Environ. Technol. 1. 10-15.
[6] G. M. Montuori, M. Fadda, G. Perrella and E. Mele (2015). Hexagrid–hexagonal tube structures for tall buildings: patterns, modeling, and design. Struct. Design Tall Special Build. 24. 912–940. DOI: 10.1002/ tal.1218
[7] G. Angelucci, and F. Mollaioli (2018). Voronoi-Like Grid Systems for Tall Buildings. Frontiers in Built Environment December 2018. DOI: 10.3389/fbuil.2018.00078
[8] N. Emami, A. Khodadadi, and P. V. Buelow, (2014). Design of shading screens inspired by Persian geometric patterns: An integrated structural and daylighting performance evaluation," in Shells. Proceedings of the IASS-SLTE Symposium
[9] N. K. Khouri (2017). Structural Grid Shell Design with Islamic Pattern Topologies. Massachusetts Institute of Technology.
[10] M. Goldsmith (1953). The tall building: the effects of scale. Master Thesis, Illinois Institute of Technology.
[11] K. S. Moon (2008). Material-saving design strategies for tall building structures. CTBUH 2008 8th World Congress, Dubai
[12] A. G. M. Michell (1904) The limits of economy of material in frame-structures, Philosophical Magazine, Vol. 8. p. 589-597.
[13] W. Prager (1978). Nearly optimal design of trusses, Computers & Structures, ISSN 0045-7949, Vol: 8. Page: 451-454
[14] G. Montuori (2015) Innovative structural solutions for tall buildings. Ph D. Thesis University of Naples Federico II
[15] A. T. Slobbe, M.A.N. Hendriks, J.G. Rots (2012) Systematic assessment of directional mesh bias with periodic boundary conditions: Applied to the crack band model. Engineer Fracture Mechanics 109. p.186-208
[16] National Programme on Technology Learning (NPTEL), Mumbai, India. Course on Composite Materials and Structures for Aerospace Engineering
[17] Y. Abdullahi, M. R. Bin Embi (2013) Evolution of Islamic geometric patterns. Frontiers of Architectural Research 2. p.243-251
[18] School of Islamic Geometric Design
[19] E. Broug (2006). Islamic Geometric Patterns. Ed Thames & Hudson
[20] E. H. Hankin (1925). The Drawing of Geometric patterns in Saracenic Art. Memoirs of the Archeological Survey of India. No. 15. Archeological Survey or India.
[21] C. S. Kaplan (2005). Islamic star patterns from polygons in contact. ISBN: 1-56881-265-5